

**T.C.
BİNGÖL UNIVERSITY
INSTITUTE OF SCIENCES**

**INHIBITION OF MILD STEEL CORROSION BY RHEUM
RIBES (IŞGIN) GREEN EXTRACTS IN 1,0 M HCl SOLUTION**

PhD THESIS

FATMA KAYA

CHEMISTRY DEPARTMENT

**SUPERVISOR
Prof. Dr. Ramazan SOLMAZ**

**2nd SUPERVISOR
Doç. Dr. İbrahim Halil GEÇİBESLER**

BİNGÖL - 2022

**T.C.
BİNGÖL UNIVERSITY
INSTITUTE OF SCIENCES**

**INHIBITION OF MILD STEEL CORROSION BY RHEUM
RIBES (IŞGIN) GREEN EXTRACTS IN 1,0 M HCl SOLUTION**

PhD THESIS

FATMA KAYA

CHEMISTRY DEPARTMENT

**SUPERVISOR
Prof. Dr. Ramazan SOLMAZ**

**2nd SUPERVISOR
Doç. Dr. İbrahim Halil GEÇİBESLER**

BİNGÖL - 2022

PREFACE

This thesis study was supported by the Bingöl University Scientific Research Projects Coordination Unit (BÜBAP) (Project NoFEF.2017.00.012) for the inhibition effect of Işgın (RR) on the corrosion of mild steel in 1 M HCl solution. I want to thank BÜBAP for their support.

Prof. Dr Ramazan SOLMAZ, who did not spare his interest and support in my thesis's planning, research, execution, and formation, deserves my eternal gratitude. I also benefited from his vast knowledge and experience and shaped my work in light of scientific foundations with his guidance and information.

I am immensely grateful to Doç.Dr.İbrahim Halil Geçibesler for all of his support during my time at Bingöl University. I appreciate how he has consistently encouraged and guided me in my studies and has always been friendly and supportive of my efforts and struggles. Throughout the thesis research, I am grateful to my distinguished teachers on the thesis monitoring committee, Prof. Dr İbrahim Yasin ERDOĞAN and Prof. Dr İskender DEMİRKOL. Furthermore, thanks to research assistant Res. Ass. Sadık VAROLGÜNEŞ for his excellent assistance in producing reinforced concrete and preparing it for testing.

I'd like to thank the Department of Chemistry at the Faculty of Arts and Sciences and the Central Laboratory staff for experimental research and characterisation measures. Special thanks to Doç.Dr. Ece ALTUNBAŞ ŞAHİN and Dr. İnan DURSUN for their help with sample characterisation and measurement. Aside from that, I'd like to thank PhD student Mrs. Yeşim DURSUN for her friendship and contributions to the characterisation measures.

I want to express my heartfelt gratitude to my esteemed family members for their moral support throughout my doctoral studies.

Fatma KAYA

Bingöl 2022

İÇİNDEKİLER

PREFACE	i
TABLE OF CONTENTS	ii
LIST OF ABBREVIATIONS	vi
LIST OF FIGURES	vii
LIST OF TABLES	xv
ÖZET	xvii
ABSTRACT.....	xviii
1. INTRODUCTION	1
1.1. Definition	1
1.2. Corrosion Forms, Recognition, and Protection	1
1.2.1. Pitting Corrosion	2
1.3. Fundamental Electrochemical Concepts	5
1.3.1. Reactions in Electrochemical Systems	5
1.3.2. The Law of Faraday	7
1.3.3. The Electrode Potential Concept	7
1.3.4. The Galvanic Cell	8
1.3.5. Reference Electrodes	11
1.3.6. Electrochemical Series	13
1.3.7. Polarization	15
1.3.8. Electrolytic Conductance	19
1.4. Copper and Steel	20
1.4.1. Material	20
1.4.2. Characteristics of general corrosion	21
1.4.3. Atmospheric Corrosion	22
1.4.4. Corrosion in Water	25
1.5. Corrosion Protection	25
1.6. Corrosive Environments and Their Characteristics	25
1.6.1. Corrosive Environment Characteristics	26

1.6.3. Acidity/Alkalinity.....	26
1.7. Steel Corrosion In Concrete	27
1.8. Corrosion Control and Prevention	30
1.8.1. Corrosion Inhibitor	31
1.9. <i>Rheum Ribes</i> (Işgın).....	33
2. LITERATURE REVIEW.....	36
3. MATERIALS AND METHODS	51
3.1. Copper	51
3.1.1. Preparation of Electrodes	51
3.1.2. Preparation of RR Extracts	51
3.1.3. Test Solutions	52
3.1.4. Electrochemical Measurements	22
3.1.5. Characterization of the Metal Surface	52
3.2. Mild Steel	53
3.2.1. Working Electrode Preparation	53
3.2.2. Plant Material Extraction	53
3.2.3. Electrolyte Preparation	54
3.2.4. Electrochemical Testing	54
3.2.5. The Synergistic Inhibitory Effect of KI.....	55
3.2.6. Surface Characterization Studies	55
3.2.7. Surface Inhibitor Film Persistence.....	56
3.3. Reinforced Concrete	56
3.3.1. Preparation of Concrete	56
4. RESULTS AND DISCUSSIONS	59
4.1. Corrosion Protection Ability of <i>Rheum Ribes</i> (Işgın) Extracts on Copper....	59
4.1.1. Variation of Open Circuit Potential with Exposure Time.....	59
4.1.2. Electrochemical Impedance Spectroscopy.....	60
4.1.3. Linear Polarization Resistance	63
4.1.4. Potentiodynamic Polarization Curves.....	64
4.1.5. Surface Characterization Studies.....	66
4.2. Adsorption And Corrosion Inhibition Capability of <i>Rheum Ribes</i> (Işgın) Root Extract For Mild Steel Protection.....	69
4.2.1. Variation of Open Circuit Potential with Exposure Time.....	69

4.2.2. Electrochemical Impedance Spectroscopy.....	70
4.2.3. Linear Polarization Resistance	75
4.2.4. Potentiodynamic Polarization Curves.....	76
4.2.5. The Synergistic Inhibitory Effect of KI.....	80
4.2.6. Studies of Surface Characterization.....	83
4.2.7. Mechanism of Adsorption and Inhibition Process.....	89
4.2.8. Stability of Surface Inhibitor Film.....	91
4.2.9. A Summary Literature Survey on Root Extracts of Plants.....	95
4.3. Adsorption And Corrosion Inhibition Capability of <i>Rheum Ribes</i> (Işgin)	
Leaf Extract For Mild Steel Protection.....	97
4.3.1. Variation of Open Circuit Potential with Exposure Time.....	97
4.3.2. Electrochemical Impedance Spectroscopy.....	98
4.2.3. Linear Polarization Resistance	101
4.3.4. Potentiodynamic Polarization Curves.....	102
4.3.5. The Synergistic Inhibitory Effect of KI.....	104
4.3.6. Studies of Surface Characterization.....	107
4.3.7. Mechanism of Adsorption and Inhibition Process.....	112
4.3.8. Stability of Surface Inhibitor Film.....	114
4.4. Adsorption And Corrosion Inhibition Capability of <i>Rheum Ribes</i> (Işgin)	
Flower Extract For Mild Steel Protection.....	118
4.4.1. Variation of Open Circuit Potential with Exposure Time.....	118
4.4.2. Electrochemical Impedance Spectroscopy.....	119
4.4.3. Linear Polarization Resistance	122
4.4.4. Potentiodynamic Polarization Curves.....	123
4.4.5. The Synergistic Inhibitory Effect of KI.....	126
4.4.6. Studies of Surface Characterization.....	127
4.4.7. Mechanism of Adsorption and Inhibition Process.....	134
4.4.8. Stability of Surface Inhibitor Film.....	134
4.4.9. The effect of Exposure Time on Protection Capability of RR	
Flower Extract	137
4.4.10. Determination of Excess Surface Charge.....	139
4.5. Corrosion Inhibition Capability of <i>Rheum Ribes</i> (Işgin) Flower Extract For	
Steel Rebar Protection In Reinforced Concrete.....	141

5. CONCLUSIONS AND SUGGESTIONS	145
REFERENCES	148
BIBLIOGRAPHY	162

LIST OF ABBREVIATIONS

RR	: Rheum Ribes
RR root	: Rheum Ribes Roots
RR leaf	: Rheum Ribes Leaf
RR flower	: Rheum Ribes flower
EIS	: Electrochemical Impedance Spectroscopy
LPR	: Linear Polarization Resistance
PP	: Potentiodynamic polarization
E_{ocp}	: Open Circuit Potential
MS	: Mild Steel
KI	: Potassium Iodide
AC	: Alternating Current
DC	: Direct Current
EECD	: Electrical Equivalent Circuit Diagram
<i>CPE</i>	: Constant Phase Element
R	: Resistance
E_{corr}	: Corrosion Potential
i_{corr}	: Corrosion Current Density
ΔG^0_{ads}	: Standard free energy of adsorption
K_{ads}	: Adsorption equilibrium constant
t	: Time
R_p	: Polarization resistance
R_{ct}	: Charge transfer resistance
R_d	: Double layer resistance
R_f	: Film resistance
R_a	: Accumulation resistance
R_L	: Inductive resistance
η	: Inhibition efficiency
α	: Slope of Bode plots

LIST OF FIGURES

Figure 1.1.	Macroscopic and microscopic forms of localized corrosion (Url-3, 2022)	3
Figure 1.2.	Variations in the cross-sectional shape of pits. (a) Narrow and deep. (b) Elliptical. (c) Wide and shallow. (d) Subsurface. (e) Undercutting. (f) Shapes are determined by microstructural orientation (Davis, 2000)	4
Figure 1.3.	Schematic of an active corrosion pit on metal in a chloride solution (Ahmad, 2006)	5
Figure 1.4.	An electrochemical cell with arrows indicating current flow direction (Mattsson, 1996)	6
Figure 1.5.	A metal (Me) has formed an electrical double layer in an aqueous solution containing metal ions, Me^{n+} (Mattsson, 1996)	8
Figure 1.6.	Figure 1.6. Typical galvanic cell (Ahmad, 2006)	9
Figure 1.7.	Half cells connected by a liquid junction (Mattsson, 1996)	10
Figure 1.8.	Components of typical commercial reference electrode: (a) electrical connection, (b) metal–metal salt electrode, (c) filling solution that maintains electrode interface equilibrium, (d) glass or polymeric electrode body, (e) porous frit (Kelly, 2002)	11
Figure 1.9.	Determination of electrode potential using a reference electrode (Mattsson, 1996)	13
Figure 1.10.	The anodic and cathodic polarisation curves; E = electrode potential, i = current density and η = polarisation (Mattsson, 1996)	16
Figure 1.11.	Overpotential curves for two simultaneous electrode reactions at an electrode surface; E = electrode potential, i = current density (Mattsson, 1996)	17
Figure 1.12.	Represents polarisation(η) as a function of current density(i). The continuous line denotes total polarisation, while the logarithm denotes complete polarisation and i_o = exchange current density (Mattsson, 1996)	18

Figure 1.13.	A. An electrical analogue of an electrode; R = electrolyte resistance, CD = double layer capacitance, L = inductance, R_1 and R_2 = resistances. Impedance spectra for various electrode types (B-D); R = resistive part, X = reactive part; arrows indicate increased frequency (ω) (Mattsson, 1996)	18
Figure 1.14.	Electric current is transported through an electrolyte (Mattsson, 1996)..	19
Figure 1.15.	Cast iron structures: A, white cast iron; cementite (Fe, C) matrix with pearlite precipitates; B, grey cast iron; pearlite or ferrite matrix graphite flakes; C, spheroidal cast iron; pearlite or ferrite matrix graphite nodules; D, malleable iron; irregular graphite grains in a pearlite or ferrite matrix (Mattsson, 1996)	22
Figure 1.16.	Fe-H, O potential-pH diagram at 25°C; 1 o 6 M dissolved Fe (Mattsson, 1996)	22
Figure 1.17.	Corrosion cells, sulfate nest, active in the atmospheric corrosion of steel (Mattsson, 1996)	22
Figure 1.18.	Corrosion depth (P) as a function of exposure time (t) on atmospheric corrosion of steel: e, Millheim, Ruhr; 0, Cuxhaven; A, Olpe (Mattsson, 1996)	24
Figure 1.19.	The same results are shown in Figure 1.18 as a bilogarithmic diagram of corrosion depth (P) and exposure time (r) (Mattsson, 1996)	24
Figure 1.20.	The pH of a few common environments	27
Figure 1.21.	Environments exhibit a wide range of oxidising/reducing behaviour (Davis, 2000)	27
Figure 1.22.	Active/passive cell concrete structures on steel (Mattsson, 1996)	28
Figure 1.23.	The steel corrosion process in concrete (Broomfield, 2011)	29
Figure 1.24.	. Rheum Ribes images (Url-5, 2021)	34
Figure 2.1.	Corrosion causes by metals and alloys.....	36
Figure 2.2.	Nyquist plots for different concentrations of pomegranate bark extract in 1 M HCl.....	41
Figure 2.3.	Physical adsorption scheme of protonated inhibitor in HCl medium on the metal surface	43
Figure 2.4.	Green corrosion inhibitors in groups.....	45
Figure 3.1.	Substances in a mixture	57

Figure 3.2.	4 x 4 x 16 cm prismatic specimens	57
Figure 3.3.	Reinforced concrete used in testing	58
Figure 4.1.	The change of open circuit potential of Cu with immersion time in 1 M HCl (●) and containing 1000 ppm RR flower (○), RR leaf (◆), and RR root (☆) solutions	60
Figure 4.2.	The Nyquist (a), log Z-log f (b), and phase angle-log f (c) (Bode) plots of Cu obtained in 1 M HCl solution without (●) and with the addition of 1000 ppm RR flower (○), RR leaf (◆) and RR root (☆) solutions after 1-hour exposure.....	62
Figure 4.3.	Polarization curves of Cu were obtained in 1 M HCl solution without (●) and with the addition of 1000 ppm RR flower (○), RR leaf (◆), and RR root (☆) solutions after 1-hour exposure	64
Figure 4.4.	SEM images of Cu surface after exposure to 1 M HCl solution in the presence of 1000 ppm RR flower (b), RR leaf (b), and RR root (c)	66
Figure 4.5.	EDX spectrums and elemental composition of Cu surface after exposure to 1 M HCl solution in the presence of 1000 ppm RR flower (b), RR leaf (b), and RR root (c)	67
Figure 4.6.	Contact angles of Cu surface after exposing to 1 M HCl solution in the absence and presence of 1000 ppm RR flower	68
Figure 4.7.	The variation of open circuit potential of MS with immersion time in 1 M HCl solution (●) and containing 100 (☆), 250 (+) 500 (◆) 1000 (○), and 2000 (*) ppm RR root extracts.....	69
Figure 4.8.	The Nyquist (a) and log Z-log f (Bode) (b) plots of MS obtained in 1 M HCl solution (●) and containing 100 (*), 250 (☆), 500 (◆) and 1000 (○) ppm RR root extracts. Solid lines show corresponding fitting curves. The inset on Fig. 3a shows the related electrical equivalent circuit diagram.....	72
Figure 4.9.	Polarization curves of MS obtained in 1 M HCl solution (●) and containing 100 (*), 250 (☆), 500 (◆) and 1000 (○) ppm RR root extracts.....	78
Figure 4.10.	The variation of Eocp of MS with immersion time (a); potentiodynamic polarization (b), Nyquist (c) and log Z-log f (Bode)	81

(d) plots of MS obtained in 1 M HCl solution in the absence (●) and containing 1000 ppm RR root (○), 1000 ppm RR root+1000 ppm KI (★); EECDS proposed for the MS/solution interface in 1 M HCl and 1 M HCl+1000 ppm RR root (c'), 1 M HCl+1000 ppm RR root+1000 ppm KI (c'').....

Figure 4.11. SEM images of MS taken after exposure to 1 M HCl (a and b), 1 M HCl+1000 ppm RR root (c) and 1 M HCl+1000 ppm RR root+1000 ppm KI (d) (The insets on c and d show 5 000x magnified images of the same surfaces); 3D dimensional AFM images of MS after exposure to 1 M HCl+1000 ppm RR root (e) and 1 M HCl+1000 ppm RR root+1000 ppm KI (f)..... 84

Figure 4.12. EDX spectrum of the MS surface, the distribution of some elements on the metal surface (EDX-mapping images) and cross-sectional analyses of some elements on the surface of MS after exposure to 1 M HCl solution in the presence of 1000 ppm RR root for 1 hour..... 86

Figure 4.13. EDX spectrum of the MS surface, the distribution of some elements on the metal surface (EDX-mapping images) and cross-sectional analyses of some elements on the surface of MS after exposure to 1 M HCl solution in the presence of 1000 ppm RR root+1000 ppm KI..... 87

Figure 4.14. Contact angle images of the MS surface after exposure to 1 M HCl, 1 M HCl + 1000 ppm RR root and 1 M HCl + 1000 ppm RR root + 1000 ppm KI solutions for 1 hours..... 88

Figure 4.15. Langmuir adsorption plot of MS obtained in 1 M HCl solution with the addition of various concentrations of RR root extract..... 89

Figure 4.16. Schematic presentation of interactions between organic molecules of extract and metal surface..... 91

Figure 4.17. The variation of anodic and the cathodic current densities as a function of time under constant +100 mV anodic (a) and -100 mV cathodic (b) overpotentials conducted in 1 M HCl solution (●) and containing 1000 ppm RR root (○), 1000 ppm RR root+1000 ppm KI (★) 92

Figure 4.18. Anodic (a) and cathodic (b) CVs of MS obtained in the test solutions (1: 1 M HCl, 2: 1 M HCl+1000 ppm RR root, 3: 1 M HCl+1000 ppm 94

	RR root+1000 ppm KI); Anodic CV-time plots of MS obtained in 1 M HCl (c), 1 M HCl+1000 ppm RR root €, 1 M HCl+1000 ppm RR root+1000 ppm KI (g); Cathodic CV-time plots of MS obtained in 1 M HCl (d), 1 M HCl+1000 ppm RR root (f), 1 M HCl+1000 ppm RR root+1000 ppm KI (h).....	
Figure 4.19.	The variation of open circuit potential of MS with immersion time in 1 M HCl solution (●) and containing 100 (☆), 250 (+) 500 (◆) 1000 (○) and 2000 (*) ppm RR leaf extracts.....	97
Figure 4.20.	The Nyquist (a) and log Z-log f (Bode) (b) plots of MS obtained in 1 M HCl solution (●) and containing 100 (*), 250 (☆), 500 (◆) and 1000 (○) ppm RR leaf extracts. Solid lines shows corresponding fitting curves. The insets on Fig. 3a show the related EECDs.....	99
Figure 4.21.	Polarization curves of MS obtained in 1 M HCl solution (●) and containing 100 (*), 250 (☆), 500 (◆) and 1000 (○) ppm RR leaf extracts.....	103
Figure 4.22.	The variation of Eocp of MS with immersion time (a); potentiodynamic polarization (b), Nyquist (c) and log Z-log f (Bode) (d) plots of MS obtained in 1 M HCl solution in the absence (●) and containing 1000 ppm RR leaf (○), 1000 ppm RR leaf+1000 ppm KI (★); EECDs proposed for the MS/solution interface in 1 M HCl and 1 M HCl+1000 ppm RR leaf (c'), 1 M HCl+1000 ppm RR leaf+1000 ppm KI (c'').....	105
Figure 4.23.	SEM images of MS taken after exposure to 1 M HCl (a and b), 1 M HCl+1000 ppm RR leaf (c) and 1 M HCl+1000 ppm RR leaf+1000 ppm KI (d) (The insets on c and d show 5 000x magnified images of the same surfaces); 3D dimensional AFM images of MS after exposure to 1 M HCl+1000 ppm RR leaf (e) and 1 M HCl+1000 ppm RR leaf+1000 ppm KI (f).....	108
Figure 4.24.	EDX spectrum of the MS surface, the distribution of some elements on the metal surface (EDX-mapping images) and cross-sectional analyses of some elements on the surface of MS after exposure to 1 M HCl solution in the presence of 1000 ppm RR leaf for 1 hour.....	109

Figure 4.25.	EDX spectrum of the MS surface, the distribution of some elements on the metal surface (EDX-mapping images) and cross-sectional analyses of some elements on the surface of MS after exposure to 1 M HCl solution in the presence of 1000 ppm RR leaf+1000 ppm KI.....	110
Figure 4.26.	Contact angle images of the MS surface after exposure to 1 M HCl, 1 M HCl + 1000 ppm RR leaf and 1 M HCl + 1000 ppm RR leaf + 1000 ppm KI solutions for 1 hours.....	112
Figure 4.27.	Langmuir adsorption plot of MS obtained in 1 M HCl solution with the addition of various concentrations of RR leaf extract	113
Figure 4.28.	The variation of anodic and the cathodic current densities as a function of time under constant +100 mV anodic (a) and -100 mV cathodic (b) overpotentials conducted in 1 M HCl solution (●) and containing 1000 ppm RR leaf (○), 1000 ppm RR leaf+1000 ppm KI (★)	115
Figure 4.29.	Anodic (a) and cathodic (b) CVs of MS obtained in the test solutions (1: 1 M HCl, 2: 1 M HCl+1000 ppm RR leaf, 3: 1 M HCl+1000 ppm RR leaf+1000 ppm KI); Anodic CV-time plots of MS obtained in 1 M HCl (c), 1 M HCl+1000 ppm RR leaf (e), 1 M HCl+1000 ppm RR leaf+1000 ppm KI (g); Cathodic CV-time plots of MS obtained in 1 M HCl (d), 1 M HCl+1000 ppm RR leaf (f), 1 M HCl+1000 ppm RR leaf+1000 ppm KI (h)	116
Figure 4.30.	The variation of Eocp of MS with immersion time in 1 M HCl solution (●) and containing 100 (☆), 250 (+) 500 (◆) 1000 (○) and 2000 (*) ppm RR flower extracts	118
Figure 4.31.	The Nyquist (a) and log Z-log f (Bode) (b) plots of MS obtained in 1 M HCl solution (●) and containing 100 (*), 250 (☆), 500 (◆) and 1000 (○) ppm RR flower extracts. Solid lines shows corresponding fitting curves. The insets on Fig. 3a show the related EECs	120
Figure 4.32.	Polarization curves of MS obtained in 1 M HCl solution (●) and containing 100 (*), 250 (☆), 500 (◆) and 1000 (○) ppm RR flower extracts.....	124
Figure 4.33.	The variation of Eocp of MS with immersion time (a); potentiodynamic polarization (b), Nyquist (c) and log Z-log f (Bode)	

	(d) plots of MS obtained in 1 M HCl solution in the absence (●) and containing 1000 ppm RR flower (○), 1000 ppm RR flower+1000 ppm KI (★); EECDs proposed for the MS/solution interface in 1 M HCl and 1 M HCl+1000 ppm RR flower (c'), 1 M HCl+1000 ppm RR flower+1000 ppm KI (c'')	126
Figure 4.34.	SEM images of MS taken after exposure to 1 M HCl (a and b), 1 M HCl+1000 ppm RR flower (c) and 1 M HCl+1000 ppm RR flower+1000 ppm KI (d) (The insets on c and d show 5 000x magnified images of the same surfaces); 3D dimensional AFM images of MS after exposure to 1 M HCl+1000 ppm RR flower (e) and 1 M HCl+1000 ppm RR flower+1000 ppm KI (f)	128
Figure 4.35.	EDX spectrum of the MS surface, the distribution of some elements on the metal surface (EDX-mapping images) and cross-sectional analyses of some elements on the surface of MS after exposure to 1 M HCl solution in the presence of 1000 ppm RR flower for 1 hour	129
Figure 4.36.	EDX spectrum of the MS surface, the distribution of some elements on the metal surface (EDX-mapping images) and cross-sectional analyses of some elements on the surface of MS after exposure to 1 M HCl solution in the presence of 1000 ppm RR flower+1000 ppm KI	130
Figure 4.37.	Contact angle images of the MS surface after exposure to 1 M HCl, 1 M HCl + 1000 ppm RR flower and 1 M HCl + 1000 ppm RR flower + 1000 ppm KI solutions for 1 hours	132
Figure 4.38.	Langmuir adsorption plot of MS obtained in 1 M HCl solution with the addition of various concentrations of RR flower extract	133
Figure 4.39.	The variation of anodic and the cathodic current densities as a function of time under constant +100 mV anodic (a) and -100 mV cathodic (b) overpotentials conducted in 1 M HCl solution (●) and containing 1000 ppm RR flower (○), 1000 ppm RR flower+1000 ppm KI (★)	134
Figure 4.40.	Anodic (a) and cathodic (b) CVs of MS obtained in the test solutions (1: 1 M HCl, 2: 1 M HCl+1000 ppm RR flower, 3: 1 M HCl+1000 ppm RR flower+1000 ppm KI); Anodic CV-time plots of MS obtained in 1 M HCl (c), 1 M HCl+1000 ppm RR flower (e), 1 M HCl+1000	

	ppm RR flower+1000 ppm KI (g); Cathodic CV-time plots of MS obtained in 1 M HCl (d), 1 M HCl+1000 ppm RR flower (f), 1 M HCl+1000 ppm RR flower+1000 ppm KI (h)	136
Figure 4.41.	. Nyquist (a, c) and Bode (b, d) plots of MS obtained in 1 M HCl solution without and with the inhibitor after 1 hour (●) and 6 hours (○) immersion; Polarization curves (e) of MS obtained in 1000 ppm RR flower extract containing 1 M HCl solution after 1 hour (●) and 6 hours (○) immersion	138
Figure 4.42.	R _p vs. applied potential plot in 1 M HCl solution containing 1000 ppm RR flower extract	140
Figure 4.43.	Nyquist (a) and log Z-log f (Bode) (b) plots of SR, embedded in reinforced concrete without inhibitor, obtained in 3.5 % NaCl solution after various exposure times (6 hours (●), 24 hours (*), 72 hours (☆), 120 hours (◆) and 168 hours (○))	142
Figure 4.44.	SEM and 3D AFM images of surface of SR embedded in reinforced concrete without (a and c) and with 1000 ppm RR flower (b and d) were obtained in 3.5 % NaCl solution after 168 hours exposure	144

LIST OF TABLES

Table 1.1.	Electrode potentials on the hydrogen scale for some common reference electrodes at 25°C	12
Table 1.2.	The electrochemical series at 25°C	14
Table 1.3.	A galvanic series of some metals in seawater at 20°C	14
Table 4.1.	Electrochemical parameters obtained from LPR measurements in 1 M HCl solution in the absence and presence of 1000 ppm RR flower, RR leaf, and RR root at 298 K	63
Table 4.2.	Electrochemical data derived from polarization measurements obtained in 1 M HCl solution in the absence and presence of 1000 ppm RR flower, RR leaf, and RR root at 298 K	65
Table 4.3.	Electrochemical parameters of MS were determined from EIS data obtained in 1 M HCl solution without and with various concentrations of RR root extract and KI added RR root extract at 298 K.....	73
Table 4.4.	Electrochemical data of MS determined from LPR measurements obtained in 1 M HCl solution in the absence and presence of various concentrations of RR root extract without and with KI edition at 298 K.....	76
Table 4.5.	Electrochemical parameters of MS determined from PP measurements obtained in 1 M HCl solution in the absence and presence of various concentrations of RR root extract and KI added RR root at 298 K	78
Table 4.6.	Fitting results of EIS data and electrochemical parameters determined from EIS measurements for MS obtained 1 M HCl solution in the absence and presence of various concentrations of RR leaf without and with KI edition at 298 K.....	100
Table 4.7.	Electrochemical data of MS determined from LPR measurements obtained in 1 M HCl solution in the absence and presence of various concentrations of RR leaf extract without and with KI edition at 298 K	102
Table 4.8.	Electrochemical parameters of MS determined from PP measurements	

	obtained in 1 M HCl solution in the absence and presence of various concentrations of RR leaf extract and KI added RR leaf at 298 K	103
Table 4.9.	Fitting results of EIS data and electrochemical parameters determined from EIS measurements for MS obtained 1 M HCl solution in the absence and presence of various concentrations of RR flower without and with KI edition at 298 K.....	122
Table 4.10.	Electrochemical data of MS determined from LPR measurements obtained in 1 M HCl solution in the absence and presence of various concentrations of RR flower extract without and with KI edition at 298 K	122
Table 4.11.	Electrochemical parameters of MS determined from PP measurements obtained in 1 M HCl solution in the absence and presence of various concentrations of RR flower extract and KI added RR flower at 298	125
Table 4.12.	Table 4.12. Fitting results of EIS data and electrochemical parameters determined from EIS measurements for MS obtained in 1 M HCl solution with and without RR flower extract at 298 K after 6 h exposure.....	139
Table 4.13.	LPR data obtained in 3.5% NaCl solution after 168 hours of exposure at 298 K for SR embedded in reinforced concrete without RR flower and containing 1000 ppm RR flower extract.....	139
Table 4.14.	LPR data obtained in 3.5% NaCl solution after 168 hours of exposure at 298 K for SR embedded in reinforced concrete without RR flower and containing 1000 ppm RR flower extract.....	143

IŞGININ (RR) YUMUŞAK ÇELİĞİN 1 M HCl ÇÖZELTİSİNDEKİ KOROZYONUNA İNHİBİSYON ETKİSİ

ÖZET

Bu çalışmada, *Rheum Ribes* (Işgın) (RR) bitkisinin çiçek (RR çiçek), yaprak (RR yaprak) ve kök (RR kök) ekstraktları hazırlanmış ve asidik ortamda yumuşak çelik korozyonuna koruyucu etkileri araştırılmıştır. Ayrıca, en iyi performansı gösteren özütün bakır ve betonarme yapıya gömülmüş inşaat (donate) çeliğinin korozyonuna inhibitör etkisi de incelenmiştir. RR'nin farklı bölgerlerinden elde edilen özütler farklı RR derişimlerinde 1 M HCl çözeltisinde çözülmüştür. Özütlerin inhibisyon etkileri açık devre potansiyelinin zamanla değişimi (E_{ocp-t}), lineer polarizasyon direnci (LPR), elektrokimyasal empedans spektroskopisi (EIS) ve potansiyodinamik polarizasyon (PP) ölçümleri ile incelenmiştir. Metal yüzeyinde oluşan filmin kararlılığı kronoamperometri (CA) ve döngüsel voltametri (CV) teknikleri ile araştırılmıştır. Korozif bir ortama maruz bırakıldıktan sonra metallerin yüzeyleri taramalı elektron mikroskobu (SEM), enerji dağılımlı X-ışını spektroskopisi (EDX), atomik kuvvet mikroskobu (AFM) ve temas açısı ölçümleri kullanılarak incelenmiştir.

Elde edilen bulgular, özüt moleküllerinin metal yüzeyinde sıkı tutunmuş, homojen dağılmış ve koruyucu filmler oluşturduğunu ve korozyona karşı koruma sağladıklarını göstermiştir. Ekstrakt derişiminin ve daldırma süresinin artması ile inhibisyon etkisi artmıştır. Özütlerin koruyucu performansı RR çiçek > RR yaprak > RR kök şeklinde değiştiği belirlenmiştir. İnhibitörlü çözeltilerde iyodür iyonlarının varlığı, genellikle sinerjistik etki ile koruma etkinliğini arttırmıştır. 1000 ppm özüt derişiminde; ortama 1000 ppm KI eklendiğinde RR kök ekstraktının koruma etkisi %84,5'ten %89,1'e, RR yaprak ekstraktının koruma etkisi ise %89'dan %93,1'e yükselmiştir. Ancak, tek başına %94,6 inhibisyon sağlayan RR çiçeği içeren ortama KI eklenmesi sinerjistik etki oluşturmamıştır. Bu özütün yumuşak çeliğin korozyonuna inhibisyon etkisi 6 saat daldırma sonunda %98,3'e yükselmiştir. Özüt molekülleri metal yüzeyine fiziksel ve kimyasal etkileşimler ile adsorbe olmuştur. Yüzeyde oluşan özüt filmlerinin son derece kararlı olduğu belirlenmiştir. Ancak, ekstraktların bakırın korozyonuna inhibisyon etkilerinin yumuşak çelik ile kıyaslandığında daha düşük olduğu belirlenmiştir. RR kök özütünün, 1 M HCl çözeltisinde bakırın korozyonuna neredeyse etki etmediği belirlenmiştir. Özütlerin koruyucu performans sıralaması yumuşak çelik ile aynıdır. Son olarak, RR çiçek özütü betonarme yapılara ilave edilerek inşaat (donate) çeliğinin korozyonuna inhibisyon etkisi %3,5 NaCl çözeltisinde incelenmiştir. Sonuçlar, RR çiçeğinin, çelik için iyi bir korozyon inhibitörü olduğunu göstermiştir. 168 saat sonra bile %84,0 gibi çok yüksek bir koruma etkisi göstermiştir.

Anahtar Kelimeler: *Rheum Ribes* (Işgın), doğal bitki özütleri, korozyon inhibitörü, betonarme korozyonu.

INHIBITION OF MILD STEEL CORROSION BY RHEUM RIBES (IŞGIN) GREEN EXTRACTS IN 1,0 M HCl SOLUTION

ABSTRACT

In this study, flower (RR flower), leaf (RR leaf), and root (RR root) extracts of *Rheum Ribes* (Işgin) (RR) were prepared, and their protective effects on mild steel corrosion in an acidic medium were investigated. Additionally, the extracts were applied as corrosion inhibitor at a specific concentration for copper and steel rebar embedded in reinforced concrete. Excerpts from various plant parts were dissolved in a 1 M HCl solution with various RR extract concentrations. Open circuit potential (E_{ocp-t}), linear polarization resistance (LPR), electrochemical impedance spectroscopy (EIS), and potentiodynamic polarization (PP) measurements were performed to investigate protection ability of the extracts. The stability of surface film was evaluated using chronoamperometry (CA) and cyclic voltammetry (CV) studies. After being exposed to a corrosive medium, the surfaces of metals were examined using scanning electron microscopy (SEM), energy dispersive X-ray spectroscopy (EDX), atomic force microscopy (AFM) and contact angle measurements.

The results demonstrated that the extract molecules formed adherent, homogenously distributed and protective films on metal surface and provide protection ability against to corrosion. Increasing the concentration of RR green extracts and the immersion time resulted in a strong inhibition effect against corrosive attacks on the alloy's surface. The protective performance of the extracts were in the order of RR flower > RR leaf > RR root. The presence of iodide ions in the inhibited solutions generally provided better protection ability via a synergistic inhibition effect. At 1000 ppm extract concentration; the protection efficiency of RR root extract increased from 84.5% to 89.1%, protection efficiency of RR leaf extract increased from 89% to 93.1% after the addition of 1000 ppm KI to the inhibited solution. But, there was not a synergism between iodide ions and RR flower, which had 94.6% inhibition efficiency individually. The inhibition efficiency of this extract on mild steel corrosion increased to 98.3% after 6 hours exposure. The extract molecules adsorbed to metal surface via physical and chemical interactions. The surface extract films were very stable. Despite this, the inhibition efficiencies of the extracts on copper were lower with respect to mild steel. RR root extract was almost incapable of protecting copper from corrosive ions in 1 M HCl solution. The order of inhibitor properties of the extracts were the same as mild steel. Lastly, the inhibition effect of the RR flower extract on the breakdown of steel rebar by adding to the reinforced concrete structures was investigated in 3.5% NaCl solution. The results indicated that RR flower is a good corrosion inhibitor for steel rebar embedded in reinforced concrete. Even after 168 hours, it still offered a very high protection efficiency of 84.0%.

Keywords: *Rheum Ribes* (Işgin), mild steel, natural plant extracts, corrosion inhibitor, reinforced concrete corrosion.

1. INTRODUCTION

1.1. Definition

Corrosion, in its broadest sense, now refers to the breakdown of materials caused by chemical or physical reactions with their surroundings. Materials are the raw components used to manufacture tools, machinery, and other products. Metals, polymers, and ceramics are a few examples. Corrosion between solids can also occur, but it is more common in a liquid or gaseous environment.

1.2. Corrosion Forms, Recognition, and Protection

Corrosion is a major industrial setback that causes material weakness and significant economic losses worldwide (Pérez-Miranda et al., 2020). Recent highlights of Global Corrosion Awareness Day include an estimated US\$ 2.5 trillion in annual corrosion costs worldwide (3 to 4 % of the GDP of compounds will affect the corrosion process. Reactive, unstable metals undergo electrochemical reactions in industrialised countries) (Url-1, 2021; Url-2, 2021). Corrosion generally refers to processes in which metals react with non-metallic components, resulting in various environmental chemicals. These environments form more stable elements and decrease their energy (Verma et al., 2020; Kusumastuti et al., 2017).

Corrosion manifests itself in a variety of ways. Typically, classification is based on one of three factors:

- Corrosion can be classified as "wet" or "dry." The first necessitates the presence of fluid or humidity, whereas dry corroding typically involves a high-temperature gas interaction.
- Corrosion mechanism involves electrical or chemical direct reactions.
- Corroded metal appearance: corrosion, in which metals corrode at the same rate across the entire surface, is either uniform and affects only small areas, or it is not uniform and affects only small areas (Davis, 2000).

Metal corrosion in aqueous environments is an electrochemical process typically involving two or more partial reactions occurring on the metal or alloy surface at or near microstructural features (Hinton et al., 1995). The corrosion reaction can be delayed or stopped if the film is deposited as a highly insoluble and impermeable film in close contact with the metal surface. The corrosive attack rate is unaffected if the film is dissolved or not precipitated on the surface; however, if corrosion products cover only a portion of the character, motion in uncoated areas may be accelerated, and pits may form (Burns, 1953).

U. R. Evans, Uhlig, and Mars Fontana have contributed substantially to the contemporary understanding of corrosion (Ahmad, 2016). Evans utilised his classical electrochemical theory to provide a contemporary understanding of the causes and management of corrosion. Uhlig contributed significantly to investigating metal and alloy passivity, pitting corrosion, stress corrosion, cracking, and hydrogen embrittlement. Mars Fontana investigated the mechanism of water and harsh chemicals, as well as the stresses on metal alloys, in great detail. He created corrosive attack methods, alloys, inhibitors, coatings, and electrolysis protection systems to prevent breakdowns in manufacturing plant systems. Fontana distinguished eight distinct types of corrosion, all of which are interconnected. These are the eight types of corrosion: (1) uniform or general attack; (2) galvanic or two-metal corrosion; (3) crevice corrosion; (4) pitting; (5) intergranular corrosion; (6) selective leaching or parting; (7) erosion-corrosion; and (8) stress corrosion. This language provided a common language and guidelines for scientists and engineers. (Fontana, 1986; McCafferty 2010; Frankel, 2016).

1.2.1. Pitting Corrosion

Pitting is a type of corrosion that results in sharply defined pits when it occurs in a concentrated area. They can be small or large in diameter, but in most cases, they are small. Holes on the surface can be isolated or closely connected, giving the appearance of the raw surface. Pitting can occur in any metal or alloy engineering. Pitting occurs when the remaining surface of a metal is anodised or when highly localised corrodent changes, such as notches, cause accelerated localised attacks on metal contacts. Pitting is a type of insidious corrosion. Perforation can fail, as well as a low weight loss on the metal.

Furthermore, pits are typically small and go unnoticed. A small number of isolated wells are easily overlooked on a generally uncorroded surface. Visual tests cannot detect a large number of very small pits on a generally uncorroded surface, and they may overestimate their potential harm. Corrosion products frequently mask small or moderate general corrosion in holes.

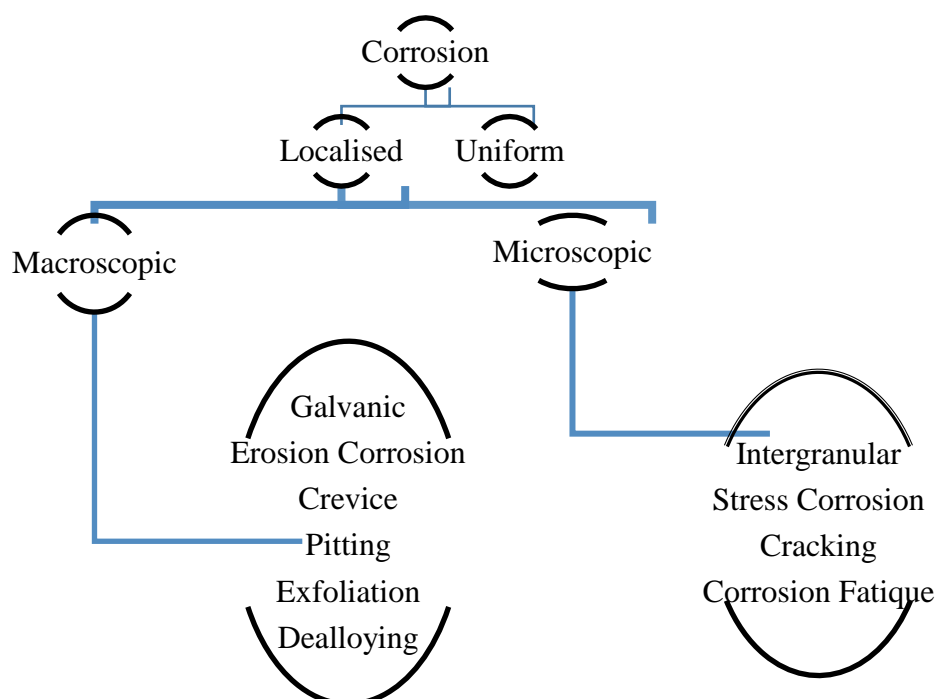


Figure 1.1. Macroscopic and microscopic forms of localized corrosion (Url-3, 2022)

Local metal surface inhomogeneity, local liability loss, mechanical or chemical rupture of the protective coating oxide, relatively distant cathode galvanic corrosion, formation of a metal ion or oxygen concentration cell under a solid depot, and physical presence are some of the causes of pitting. The reasonable rate is proportional to the aggressiveness of the corrodent at the pitting site and the electrical conductivity of the corrodent solution. When combined with a specific metal, some ions increase the likelihood of pitting and accelerate the attack once it has begun. Pitting is typically associated with combinations of the metal and environment where the corrosion rates are relatively low. Pits are frequently spread over the surface and change locations in relatively mild corrodents with low-alloy carbon steels. Individual wells become virtually indistinguishable when they merge, resulting in a roughened surface but a generally even reduction in transverse section. If the initial carbon

steel pits are not combined in this manner, rapid metal penetration and minor general corrosion will occur at the pit sites.

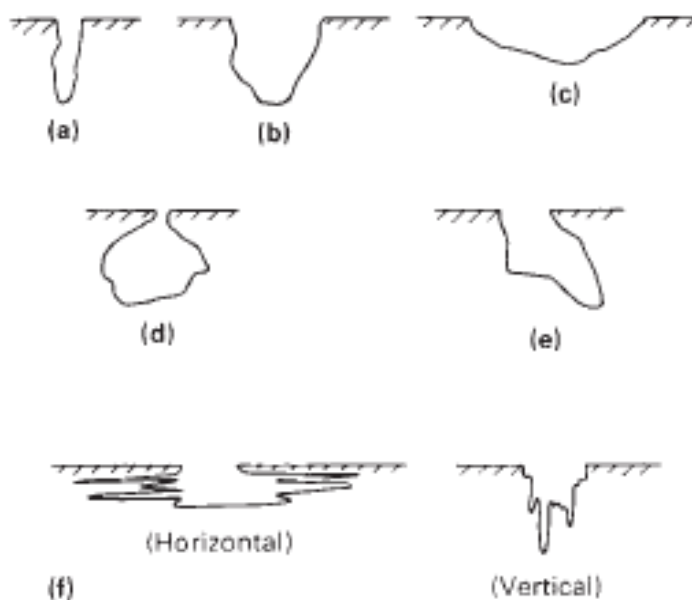


Figure 1.2. Variations in the cross-sectional shape of pits. (a) Narrow and deep. (b) Elliptical. (c) Wide and shallow. (d) Subsurface. (e) Undercutting. (f) Shapes are determined by microstructural orientation (Davis, 2000)

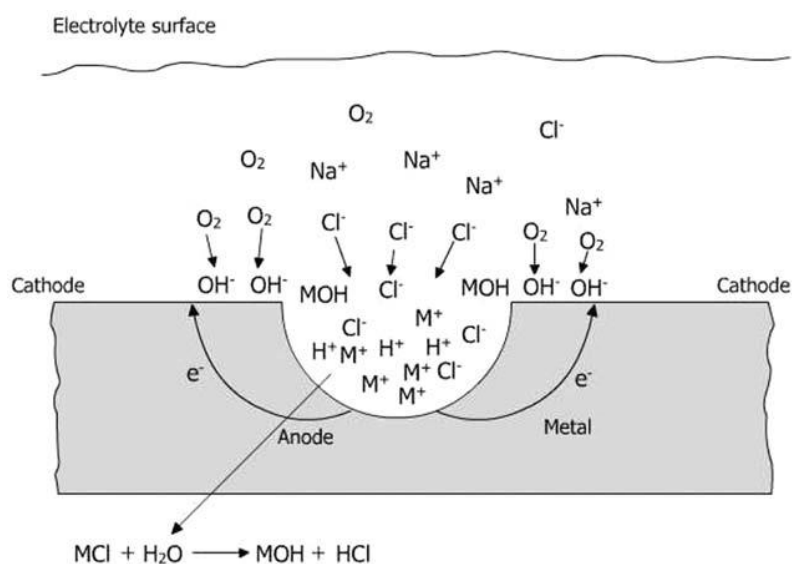


Figure 1.3. Schematic of an active corrosion pit on metal in a chloride solution (Ahmad, 2006)

Pitting takes place in the most frequently used metals and alloys. Iron buried in the soil corrodes with shallow pits, but deep cavities form in carbohydrate stones exposed to

hydrochloric acid or steel immersed in seawater. Aluminium pits are in chloride-ion-containing waters, and aluminium cups are in polluted waters. Despite its high corrosion resistance, stainless steels are more prone to pitting than many other metals. Although high-alloy chromium-nickel and molybdenum stainless steels are more pitting-resistant, they are not immune to all service conditions.

The following practices are suggested for reducing or minimising pitting corrosion: Reduce the concentrations of environmental aggressors such as chloride, temperature, acidity, and oxidants. Change the system design to avoid crevices and deposit formation, circulate to avoid stagnant solutions, and ensure proper drainage. Choosing materials with known pH service resistance and monitoring chloride concentration and temperature. Increased media velocity, as well as a cathode or anodic Protection, are used to remove solid deposits from exposed metal surfaces. Use an effective chemical inhibitor to increase resistance to localised attacks. Local corrosion is reduced by eliminating oxygen concentration cell mechanisms, and aerated environments are deaerated (Mattsson, 1996; Davis, 2000).

1.3. Fundamental Electrochemical Concepts

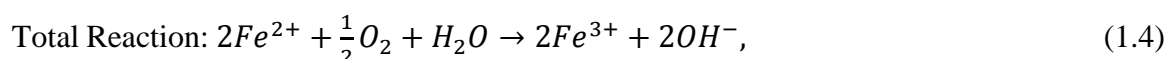
1.3.1. Reactions in Electrochemical Systems

An electrochemical reaction is characterised by the fact that it takes place with donating or receiving of electrons. Such a reaction can be schematically represented:



Where Red is a reducing agent (electron donor), Ox is an oxidising agent (electron acceptor), and n is the total number of electrons in the reaction (e⁻). We call response oxidation when electrons are emitted, i.e. when it moves to the left. It is a reduction if it occurs with electron consumption, i.e. it moves to the right. A redox pair is a combination of a reducing agent and an oxidising agent, as indicated by the formula, and the reaction is a redox reaction.

In any substantial percentage, charged particles could perhaps exist free in a solution. As a result, the electrons released during an oxidation process must be devoured throughout a simultaneous reduction reaction. In solution, oxidising and reducing agents, such as:



A further potential outcome is the chemical change in an electrolytic system (Figure 1.4). An ordinary electrochemical cell comprises two electrodes connected by an electrolyte. The electrodes are composed of an electron conductor, such as a metal in contact with an electrolyte. The electrolyte is typically an aqueous solution that conducts electricity. Ions transport current through the electrolyte; this is a defining characteristic. The anode conducts a positive current into the electrolyte. The cathode is the other electrode through which the electric current exits the electrolyte. Electric current flows through the surface of an electrode in either direction; there is always an electrochemical reaction.

In contrast, the cathode reaction is always a reduction reaction. An electrolytic cell is an electrochemical cell in which an external source forces the current flow. A galvanic cell is an electrochemical cell that can generate an electric current (Mattsson, 1996).

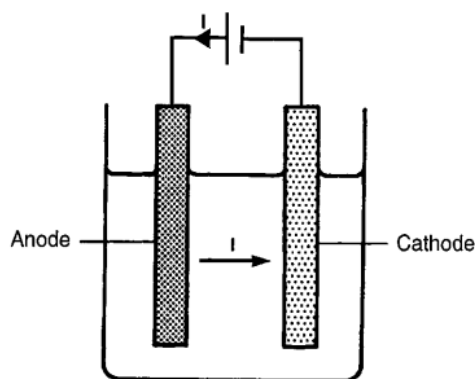


Figure 1.4. An electrochemical cell with arrows indicating current flow direction (Mattsson, 1996)

1.3.2. The Law of Faraday

As a result, current entry and exit from an electrolyte are always associated with electrode reactions, manifesting as changes in the electrode materials or the environment. The amounts converted during electrode reactions are proportional to the current flowing through the electrode surface. Faraday's law clearly states that a conversion that includes one mole of electrons (e^-) requires 96 500 coulombs (ampere-seconds), or 26.8 Ah (ampere-hours). The optimised conditions for a designated reaction rate provide sufficient carrying through the electrode's surface. The remainder of the current is absorbed by other electrode reactions running concurrently at the electrolyte interface (Mattsson, 1996).

1.3.3. The Electrode Potential Concept

When a piece of metal, Me, is immersed in an aqueous solution containing metal ions, Me^{n+} , electrode reactions occur at the metal's surface until equilibrium is reached:



These reactions usually form an electrical double layer at the interface (Figure 1.5). As either a result of the general appearance of this electrostatic interaction, the metal object now has a different electric potential, known as the Galvani potential (ϕ_1), than the solution (ϕ_2). The difference in Galvani potential, $\phi_1 - \phi_2$, cannot be directly calculated. Still, its relative importance can be determined by comparing it to the difference in Galvani potential of a so-called reference electrode. The electrode potential, denoted by the symbol E , is a relative value that can be measured (Mattsson, 1996.).

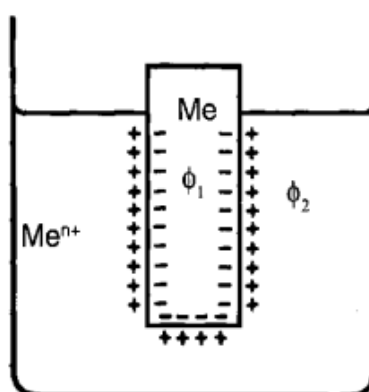


Figure 1.5. A metal (Me) has formed an electrical double layer in an aqueous solution containing metal ions, Me^{n+} (Mattsson, 1996)

There is a relationship between the electrode potential (equilibrium potential) and the activity of the metal ion, i.e. the 'effective' metal ion concentration in the solution when the system is in equilibrium. The Nernst equation describes this relationship:

$$E = E^{\circ} + \frac{0.0001983.T}{n} \cdot \log_{10} a_{\text{Me}^{n+}} \quad (1.6)$$

Where E° is the standard electrode potential, a constant characteristic of the electrode reaction, T is the absolute temperature, and $a_{\text{Me}^{n+}}$ is the metal ion activity, i.e. the 'effective' metal ion concentration, which is frequently replaced by the metal ion concentration for approximate calculations. Similar conditions apply when an inert metal (a non-reacting metal such as platinum or gold) is surrounded by a redox pair-containing solution. Reactions occur according to the following formula until equilibrium is reached:



These reactions form an electrical double layer in the surface zone, where the inert metal is in contact with the solution (see Figure 1.5). The redox potential of the emulsion is the electrode potential in this case. The mixture has a high redox potential, indicating it is highly oxidising. The relationship between the redox potential and the activities of Ox and

Red is analogous to the relationship between metal in contact with a solution containing metal ions. This relationship is also given by the Nernst equation, which is written as follows:

$$E = E^\circ + \frac{0.0001983.T}{n} \cdot \log_{10} \frac{a_{\text{Ox}}}{a_{\text{Red}}} . \quad (1.8)$$

The Nernst equation for Me/Me^{n+} is a subset of this equation, where $a_{\text{Red}} = a_{\text{Me}} = 1$

1.3.4. The Galvanic Cell

A galvanic cell is an electrochemical cell that can generate an electric current. An electric current will flow from one electrode (positive pole) to the other if the electrodes of such a galvanic cell are coupled via the external metal conductor (negative pole). On the other hand, the electrolyte's current flows in the opposite direction, as shown in Figure 1.6. As a result, the positive side serves as the cathode, and the negative pole serves as the anode (Ahmad, 2006.).

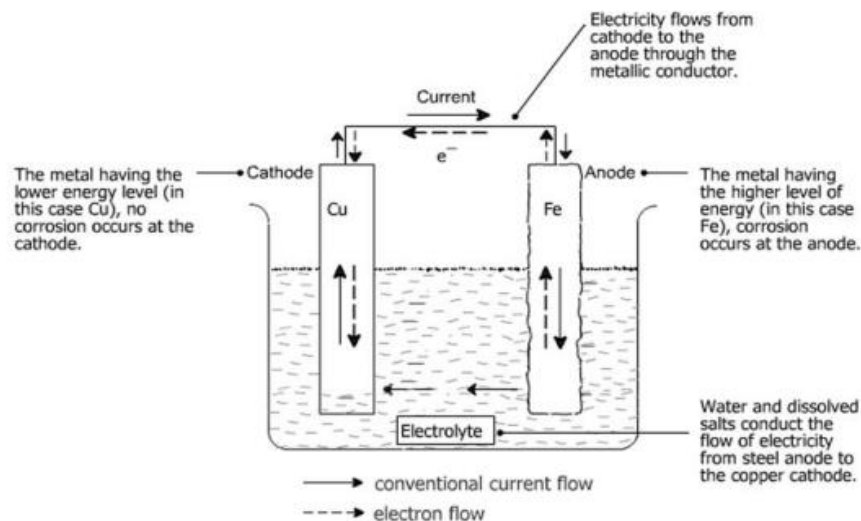


Figure 1.6. Typical galvanic cell (Ahmad, 2006)

The terminal voltage is the electrical potential difference between the electrodes that can be measured with a voltmeter. The electromotive force, or e.m.f., is the terminal voltage measured when the galvanic cell is not producing current. When a metal conductor

connects the electrodes, the electromotive force is a measure of the driving force of the chemical reaction that will occur in the cell. The electromotive power (ΔE) can be calculated using the electrode potentials (E_1 and E_2) of the cell's electrodes:

$$\Delta E = E_1 - E_2 \quad (1.9)$$

There are three types of galvanic cells: thermo-galvanic (electrodes made of the same material but with different concentrations of the substances involved in the reactions) and bimetallic (electrodes made of other materials but with varying concentrations of the substances involved in the reactions). Concentration cells have electrodes made of the same material as the reactions but different concentrations of the substances involved. A half cell is a name for each electrode and surrounding electrolyte. The two halves of a galvanic cell can be in contact with the same or different electrolytes, as shown above. In the latter case, the electrolytes may be separated using a membrane, which may, for example, allow ion exchange, i.e. current flow. A liquid junction can sometimes connect two half-cells, as shown in Figure 1.7 (Mattsson, 1996). The electrolyte in the liquid junction is possibly absorbed in a thickening agent, such as an agar-agar gel. Following international practice, a galvanic cell with a liquid junction is written schematically, as shown in the following example, with the positive pole on the right:

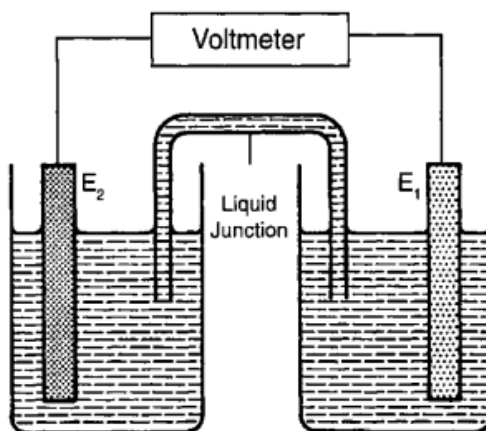


Figure 1.7. Half cells connected by a liquid junction (Mattsson, 1996)

1.3.5. Reference Electrodes

The hydrogen reaction was chosen as the reaction to which zero volts were assigned many years ago. The gold standard for reference electrodes is a hydrogen electrode immersed in a neutral pH solution saturated with hydrogen gas at room temperature. The value is zero because the reaction is in equilibrium with the other reactant in a 1 M solution of the ion of interest (H^+). This device is known as the normal hydrogen electrode (SHE) (NHE). Therefore, the $V(SHE)$ or V notation is employed when discussing voltages at other electrodes (NHE). An ideal reference electrode (RE) would have a value independent of the concentration of any other species in the solution of interest, be in thermodynamic equilibrium, be readily available at a low cost, and be straightforward to maintain. Although the NHE electrode produces no voltage, it has several significant disadvantages in practice. A constant supply of hydrogen gas is one of the most important requirements. Fortunately, more practical RE has been developed and made available for purchase (Kelly, 2002).

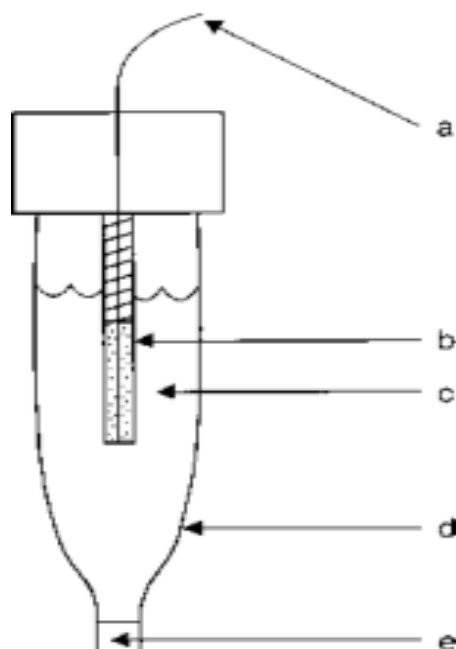


Figure 1.8. Components of typical commercial reference electrode: (a) electrical connection, (b) metal-metal salt electrode, (c) filling solution that maintains electrode interface equilibrium, (d) glass or polymeric electrode body, (e) porous frit (Kelly, 2002)

The following are some examples of reference electrodes:

- The calomel electrode, which is made up of mercury in contact with a solution of mercury (I) chloride (calomel) and potassium chloride at a specific concentration, such as 0,1 M, 1 M, or saturated solution (SeE),
- The copper/copper sulfate electrode is constructed of copper and has been in contact with a saturated copper sulfate solution (Cu/CuSO₄).

Table 1.1. Electrode potentials on the hydrogen scale for some common reference electrodes at 25°C

	Designation	E_H (V)
Standard hydrogen electrode	H ₂ (1 atm) H ⁺ ($a = 1$)	0
Calomel electrode (saturated)	Hg Hg ₂ Cl ₂ , KCl (saturated)	+ 0.244
Calomel electrode (1 M)	Hg Hg ₂ Cl ₂ , KCl (1 M)	+ 0.283
Calomel electrode (0.1M)	Hg Hg ₂ Cl ₂ , KCl (0.1 M)	+ 0.336
Silver/silver chloride electrode (0.1 M)	Ag AgCl, KCl (0.1 M)	+ 0.288
Copper/copper sulphate electrode (saturated)	Cu CuSO ₄ (saturated)	+ 0.318
Manganese dioxide electrode	MnO ₂ Mn ₂ O ₃ , NaOH(0.5 M)	+ 0.405

Experimentally determining the Galvani voltage differential, the total value of an electrode's electrode potential, is difficult. In most instances, you will have to settle for an approximation. The test electrode, i.e., whose electrode potential is to be determined, is connected to a so-called reference electrode via an electrolyte, a liquid junction (Figure 1.7). It comprises a half-cell with a constant and reproducible electrode potential. A high-impedance voltmeter assesses the resulting electrochemical cell's electromotive force (ΔE). The monitoring is implemented to ensure that the current flow is kept as low as reasonably achievable (Mattsson, 1996).

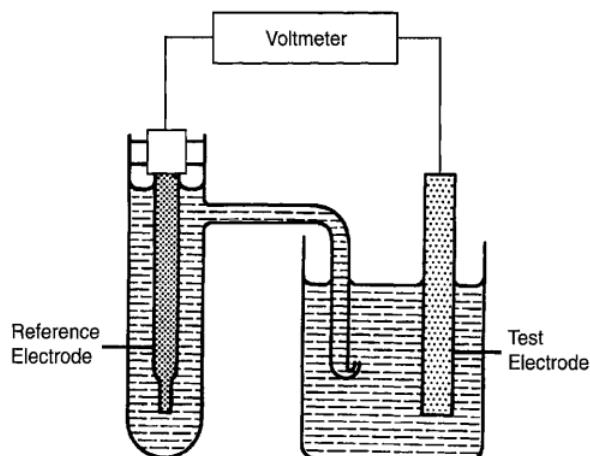


Figure 1.9. Determination of electrode potential using a reference electrode(Mattsson, 1996)

$$E = E_{\text{test}} - E_{\text{ref}} \quad (1.11)$$

$$E_{\text{test}} = \Delta E + E_{\text{ref}} \quad (1.12)$$

The test electrode's electrode potential is calculated by adding the recorded electromotive force, ΔE , and a constant equal to the reference electrode's electrode potential. The latter is notoriously difficult to determine, so in practice, the working electrode's possibility concerning the reference electrode, ΔE , must suffice. It is impossible to provide a definitive answer without knowing which electrode will serve as the reference (Mattsson, 1996).

1.3.6. Electrochemical Series

Each electrode reaction has a predetermined potential. The electrode potential occurs when all the substances involved in the electrode reaction have activity = 1. The electrochemical series (Table 2) is created by organising the electrode reactions in conjunction with the relevant predicted values(Mattsson, 1996).

Table 1.2. The electrochemical series at 25°C

Electrode reaction	Standard electrode potential, E_H (V)
$\text{Au}^3 + 3\text{e}^- \rightleftharpoons \text{Au}$	+ 1.42
$\text{Cr}_2\text{O}_7^{2-} + 14\text{H}^+ + 6\text{e}^- \rightleftharpoons 2\text{Cr}^{3+} + 7\text{H}_2\text{O}$	+ 1.36
$\text{Cl}_2 + 2\text{e}^- \rightleftharpoons 2\text{Cl}^-$	+ 1.36
$\text{O}_2 + 4\text{H}^+ + 4\text{e}^- \rightleftharpoons 2\text{H}_2\text{O}$	+ 1.23
$\text{Ag}^+ + \text{e}^- \rightleftharpoons \text{Ag}$	+ 0.80
$\text{Cu}^+ + \text{e}^- \rightleftharpoons \text{Cu}$	+ 0.52
$\text{Cu}^{2+} + 2\text{e}^- \rightleftharpoons \text{Cu}$	+ 0.34
$\text{H}^+ + \text{e}^- \rightleftharpoons \frac{1}{2}\text{H}_2$	0
$\text{Pb}^{2+} + 2\text{e}^- \rightleftharpoons \text{Pb}$	- 0.13
$\text{Sn}^{2+} + 2\text{e}^- \rightleftharpoons \text{Sn}$	- 0.14
$\text{Ni}^{2+} + 2\text{e}^- \rightleftharpoons \text{Ni}$	- 0.23
$\text{Co}^{2+} + 2\text{e}^- \rightleftharpoons \text{Co}$	- 0.28
$\text{Cd}^{2+} + 2\text{e}^- \rightleftharpoons \text{Cd}$	- 0.40
$\text{Fe}^{2+} + 2\text{e}^- \rightleftharpoons \text{Fe}$	- 0.41
$\text{Cr}^{3+} + 3\text{e}^- \rightleftharpoons \text{Cr}$	- 0.74
$\text{Zn}^{2+} + 2\text{e}^- \rightleftharpoons \text{Zn}$	- 0.76
$\text{Mn}^{2+} + 2\text{e}^- \rightleftharpoons \text{Mn}$	- 1.03
$\text{Ti}^{2+} + 2\text{e}^- \rightleftharpoons \text{Ti}$	- 1.63
$\text{Al}^{3+} + 3\text{e}^- \rightleftharpoons \text{Al}$	- 1.71
$\text{Mg}^{2+} + 2\text{e}^- \rightleftharpoons \text{Mg}$	- 2.38
$\text{Na}^+ + \text{e}^- \rightleftharpoons \text{Na}$	- 2.71
$\text{Ca}^{2+} + 2\text{e}^- \rightleftharpoons \text{Ca}$	- 2.76
$\text{K}^+ + \text{e}^- \rightleftharpoons \text{K}$	- 2.92
$\text{Li}^+ + \text{e}^- \rightleftharpoons \text{Li}$	- 3.05

Table 1.3. A galvanic series of some metals in seawater at 20°C

	Metal	Electrode potential, E_H (V)
<div style="display: flex; flex-direction: column; align-items: center;"> <div style="margin-bottom: 10px;">↑</div> <div style="margin-bottom: 10px;">More noble metals</div> <div style="margin-bottom: 10px;">↓</div> <div style="margin-bottom: 10px;">Less noble metals</div> <div style="margin-bottom: 10px;">↓</div> </div>	Gold	+ 0.42
	Silver	+ 0.19
	Stainless steel (18/8) in the passive state	+ 0.09
	Copper	+ 0.02
	Tin	- 0.26
	Stainless steel (18/8) in the active state	- 0.29
	Lead	- 0.31
	Steel	- 0.46
	Cadmium	- 0.49
	Aluminium	- 0.51
	Galvanised steel	- 0.81
	Zinc	- 0.86
	Magnesium	- 1.36

A noble metal is a metal that has a relatively high standard potential, such as copper. On the other hand, a base metal corresponds to a low common potential, such as sodium or magnesium. It should be noted that the electrochemical series only applies to oxide-free metal surfaces and activities for which standard possibilities are valid. In practice, oxide films frequently cover metal surfaces. Besides, their actions can diverge dramatically when

metal ions combine with other constituents to form so-called complexions. As a result of these factors, the measured potentials may be out of order with the electrochemical series. A galvanic series is created when metals exposed to a given electrolyte, such as seawater, are arranged according to measured electrode potentials. Only the electrolyte under consideration, i.e. the electrolyte in which the measurements were taken, is correct (Mattsson, 1996).

1.3.7. Polarization

According to the formula, both oxidations of metal atoms to metal ions and reduction of metal ions to metal atoms occur at the metal's surface when it is exposed to an aqueous solution containing an ion of that metal:



Since an electron exchange took place, the rates of the two reactions could be calculated utilising two different current densities (current density = current strength per unit of surface area) \leftarrow_i and \rightarrow_i . At equilibrium, the current exchange density (E_o) $\leftarrow_i = \rightarrow_i = i_o$, if no other electrode reactions occur at the electrode surface (E_o). The Nernst equation can calculate the electrode potential, also known as the equilibrium potential. Whenever a net current, I , is applied to the surface, it indicates that $\leftarrow_i \neq \rightarrow_i$. The applied net current density will be the difference between \leftarrow_i and \rightarrow_i in reality. While a current is applied to the electrode surface, the electrode potential changes and takes on the value E_i . Polarisation refers to the state of the electrode. Polarisation is a change in electrode potential and is usually denoted by the Greek letter η .

$$\eta = E_i - E_o \quad (1.14)$$

The polarisation is divided into two major components:

- Concentration polarisation is caused by the concentration difference between the layer of electrolyte closest to the electrode surface, i.e. the diffusion boundary layer, and the bulk of the electrolyte.

- Activation polarisation as a result of electrode reaction retardation. Anode polarisation is always positive, while cathode polarisation is always negative (Figure 1.10).

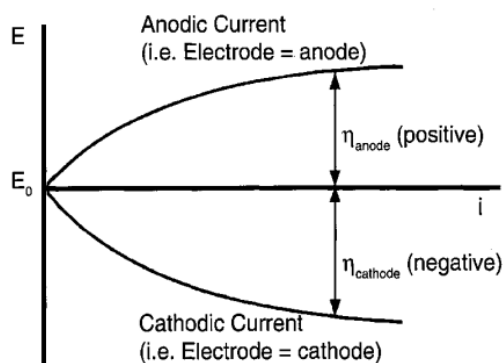


Figure 1.10. The anodic and cathodic polarisation curves; E = electrode potential, i = current density and η = polarisation (Mattsson, 1996)

As the current drawn from the cell increases, polarisation decreases the terminal voltage of a galvanic cell. The polarisation created by passing current from an external entity through an electrolytic cell necessitates a higher applied voltage. Consequently, if polarisation can be attributed to a specific electrode reaction, it is overpotential. The overpotential is the difference between the electrode potential with applied current and the equilibrium potential for the electrode reaction in question. Hydrogen overpotential, for example, occurs during the electrolytic evolution of hydrogen as follows:



Oxygen overpotential emerges throughout oxygen production via electrolysis, according to:



However, two or more electrode reactions can happen simultaneously at an electrode. A cathode reaction with an equilibrium potential of E_{01} , for example, and an anode reaction with an equilibrium potential of E_{02} , can occur at the same time (Fig. 10). Since there is no

net current flowing across the surface of the electrode, the anodic and cathodic current densities are equal (mix). The electrode exhibits a "mixed potential" (E_{mix}), which is the point where the anodic and cathodic overpotential curves intersect. The electrode potential change that occurs when current is applied to such an electrode is also regarded as polarisation. At the same electrode, two or more electrode reactions, such as a cathode reaction with an equilibrium potential of E_{01} and an anode reaction with an equilibrium potential of E_{02} , are common simultaneously (Fig. 1.11). Therefore no net current is applied to the electrode surface; the anodic and cathodic current densities are the same (i_{mix}). The electrode exhibits a so-called mixed potential (E_{mix}), which corresponds to the point of intersection of the anodic and cathodic overpotential curves. Polarisation refers to the change in electrode potential when current is applied to such an electrode (Mattsson, 1996).

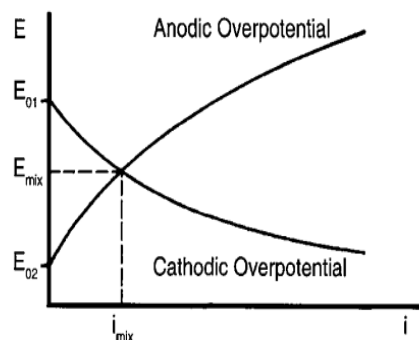


Figure 1. 11. Overpotential curves for two simultaneous electrode reactions at an electrode surface; E = electrode potential, i = current density (Mattsson, 1996)

Activation polarisation is proportional to current density at low polarisation values. At higher polarisation values ($> ca\ 30-50\ mV$), there is a linear relationship between activation polarisation and the logarithm of current density. This relationship is described by the Tafel equation:

$$\ln i = a + b \cdot \log_{10} i \quad (1.17)$$

As a result, polarisation curves are typically drawn as a function of $\log_{10} i$, yielding straight lines known as Tafel lines. At low current densities, concentration polarisation is often negligible. Still, at high current densities, it can be dominant (Figure 1.12). Traditional polarisation curves are recorded using direct current, and steady-state conditions are

expected. The electrode is then converted to a resistance known as the polarisation resistance, which varies with current density (Mattsson, 1996).

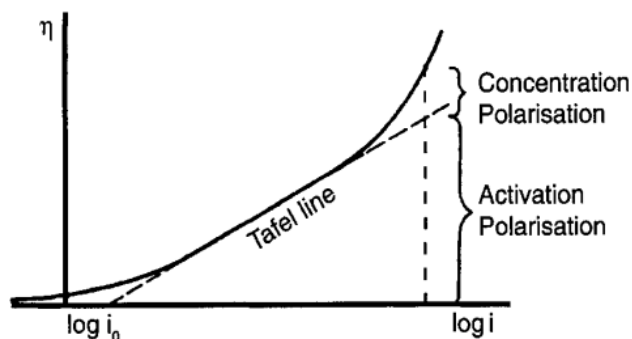


Figure 1.12. Represents polarisation(η) as a function of current density(i). The continuous line denotes total polarisation, while the logarithm denotes complete polarisation and $i_o =$ exchange current density (Mattsson, 1996)

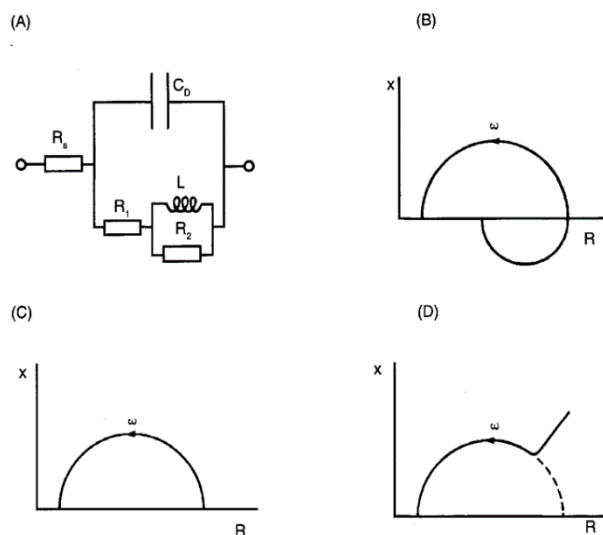


Figure 1.13. A. An electrical analogue of an electrode; $R =$ electrolyte resistance, $CD =$ double layer capacitance, $L =$ inductance, R_1 and $R_2 =$ resistances. Impedance spectra for various electrode types (B-D); $R =$ resistive part, $X =$ reactive part; arrows indicate increased frequency (ω) (Mattsson, 1996)

In the meantime, an alternating current is applied, and the electrode resembles a more complex electrical model with polarisation impedance and resistive, capacitive, and inductive components. Figure 1.12 portrays an example of an electrical model of this category. Measuring the (A.C.) impedance of an alternating current electrode would provide information about the electrode processes and the information obtained by measuring direct current polarisation. This method is known as electrochemical impedance spectroscopy (EIS). Figure 1.13 shows B-D examples of impedance spectra obtained by

varying the frequency of the alternating current (ω) for various types of electrodes. The internal relationships between the different electrode impedance components determine the shape of the curve, which reveals the rate-determining step(s) of the electrode process (Mattsson, 1996).

1.3.8. Electrolytic Conductance

Current is transported in an electrolyte solution by the movement of ions, anions (negatively charged), and cations (positively charged).

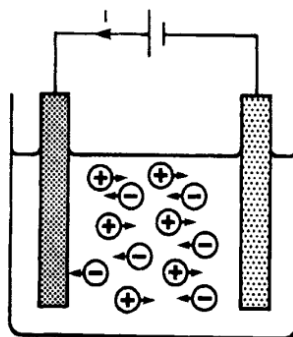


Figure 1.14. Electric current is transported through an electrolyte (Mattsson, 1996)

Anions migrate against the current while cations migrate with it. The anions and cations in the solution are always electro-neutral, which means they balance each other. Ohm's law governs current transport through an electrolyte solution:

$$U = IR \quad (1.18)$$

Where I is the current in amperes, U is the potential difference between the electrodes, and R is the electrolyte resistance in ohms. Further:

$$\frac{1}{R} = L \quad (1.19)$$

L is the conductance of the electrolyte in ohm^{-1} , and the following formula is used to calculate the volume of a liquid with rectangular surfaces:

$$L = K \frac{q}{l} = \frac{q}{pl} \quad (1.20)$$

q is the cross-sectional area of the liquid in cm^2 , l is its length in cm , K is the specific conductance or conductivity in $\text{ohm}^{-1} \text{cm}^{-1}$, and p is the typical resistance in ohm-cm . Ionic compounds contribute to current transport through the liquid electrolyte in various ways. Consequently, ions with vastly different mobilities or high ionic conductivity are observed. The percentage of current carried by an ionic species in an electrolyte solution is represented by its transport number. Even though current transport is distributed differently among the various ions in solution, the current rarely results in significant changes in the electrolyte's bulk concentration because fluid movement permits rapid equalisation.

On the other hand, current transport can cause significant changes in concentration in a thin solution film (10^{-1} - 10^{-5} cm thick) close to the electrode surfaces, i.e. in a so-called diffusion boundary layer, where convection is difficult. For example, the pH near the electrode surface will significantly differ from the pH in the bulk of the solution. Another consequence is concentration polarisation (Mattsson, 1996).

1.4. Copper and Steel

1.4.1. Material

Steel is a material composed primarily of iron, containing between 0.2% and 2.1% carbon by weight. Carbon is frequently incorporated into iron alloys. Other alloys are manganese, chromium, vanadium, and tungsten. The amount of alloys in a material's structure determines its hardness, tensile strength, and flexibility. Steel with a higher carbon content becomes harder and more durable than iron.

Nonetheless, this alloy becomes softer than iron. The electrochemical theory of corrosion can be represented by galvanic cells on the surface of a metal. The metal ions mixed with the solution in the anodic region of a metal's exterior are in equilibrium with the reaction occurring in the cathodic area. The subsequent electrochemical change occurs in the anodic region (Erbil, 1985).

Carbon steels are typically comprised of micro-alloyed steels and carbon-manganese steels. Carbon-manganese steels frequently have manganese contents of up to 1.50 / 0; the dividing line with low-alloyed steel is diffuse. When the entire range of alloying substance exceeds 5%, the steel is called high-alloyed steel. There are two types of cast iron: grey cast iron and white cast iron (Figure 1.15). Grey cast iron is distinguished by a graphite phase that can take the form of flakes or spheres. A grade of cementite distinct white cast iron (Fe_3C). Moldable iron first solidifies to white cast iron before being heat-treated to form irregular graphite grains. There is also cast iron alloyed with nickel or silicon. Steel and cast iron are frequently used for structures due to their low cost and high strength: buildings, bridges, pylons, and cars in the air; ships and offshore platforms in the water; and water and gas pipes, as well as gasoline and oil tanks in the ground (Mattsson, 1996).

1.4.2. Characteristics of General Corrosion

Rusting refers to the corrosion of steel, cast iron, and corrosion products.

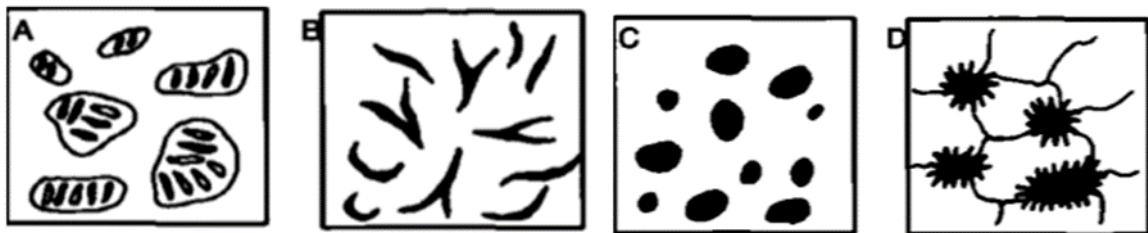


Figure 1.15. Cast iron structures: A, white cast iron; cementite (Fe, C) matrix with pearlite precipitates; B, grey cast iron; pearlite or ferrite matrix graphite flakes; C, spheroidal cast iron; pearlite or ferrite matrix graphite nodules; D, malleable iron; irregular graphite grains in a pearlite or ferrite matrix (Mattsson, 1996)

Carbon steel constructions of numerous forms (Figure 1.16): A, white cast iron; carbides (Fe, C) data frame with pearlite crystals; B, grey cast iron; carbon black flakes in a pearlite or ferrite matrix; C, spherically symmetric cast iron; graphite nodules in a pearlite or ferrite matrix; D, malleable iron; infrequent grains of graphite in a pearlite or ferrite matrix. The potential-pH graph for the system Fe-H, O (Figure 1.16) captures the corrosion potentials of steel and cast iron under diverse environmental conditions. In aqueous solutions, it is clear that the metal is susceptible. Passivation is possible at relatively high pH values, according to the stability domains for Fe, O, and F, O. (8- 11). However, there is a risk of

corrosion at extremely high pH levels. In general, small quantities of alloying additives do not affect corrosion characteristics (Mattsson, 1996).

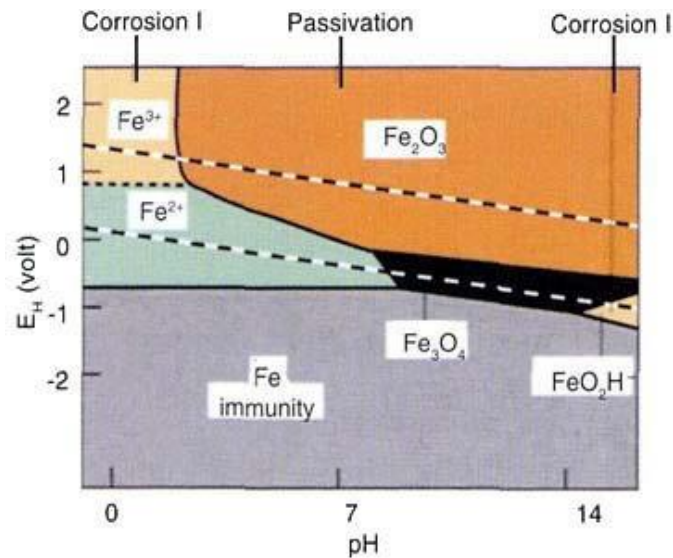


Figure 1.16. Fe-H, O potential-pH diagram at 25°C; 1 to 6 M dissolved Fe (Mattsson, 1996)

1.4.3. Atmospheric Corrosion

Steel rusts in the open air, and the resulting rust coating is composed of a porous, loosely adhering outer layer of crystalline α - and γ - $FeOOH$ and a dense, more tightly clinging inner layer of amorphous and crystalline $FeOOH$.

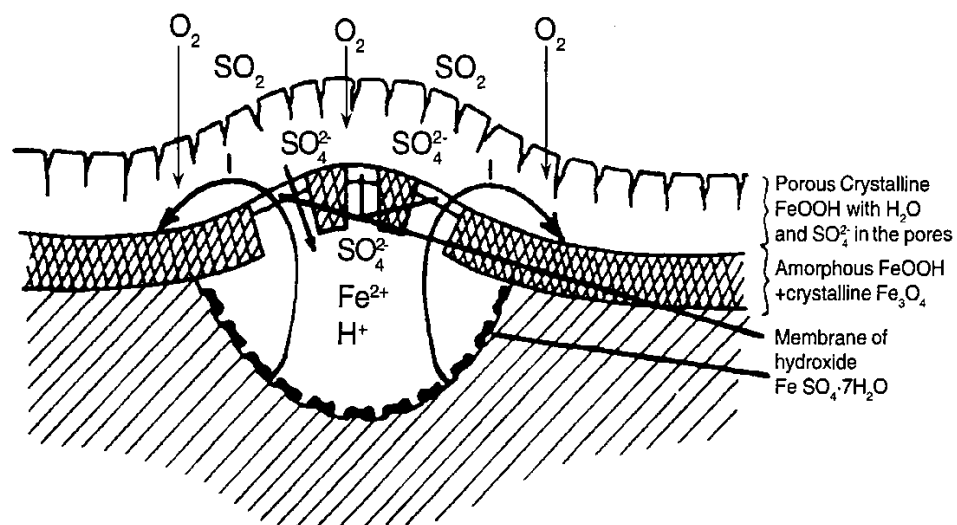


Figure 1.17. Corrosion cells, sulfate nest, active in the atmospheric corrosion of steel (Mattsson, 1996)

Corrosion cell, also known as sulfate nest, is active in the atmospheric corrosion of steel. This rust coating, Fe₃O₄, does not protect against future attacks adequately. Decay happens as a consequence of the action of corrosion cells, where the anodes are located in sulfate nests, which are small pits rich in sulfate. The surrounding area serves as a cathode. The following formula summarises the reactions that are currently occurring:

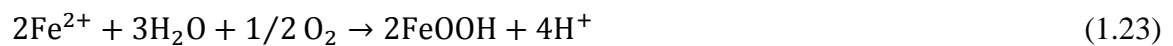
At the cathode:



At the anode:



In the rust:



In most cases, the rise in depth of penetration (P) with time (t) follows a power law:

$$P = kt^n \quad (1.24)$$

where k and n are constants. This formula can be expressed differently.

$$\log P = \log k + n \log t \quad (1.25)$$

Figure 1.18 conveys the time functions of pit depth in three different types of atmospheres. Straight lines represent the same curves in a bilogarithmic diagram (Figure 1.18). At steady-state conditions, the corrosion rates for steel in various types of atmospheres are as follows:

rural atmosphere	5-10 μm / year
marine atmosphere	10-30 μm / year

urban atmosphere 10-30 μm / year
 industrial atmosphere 30-60 μm / year

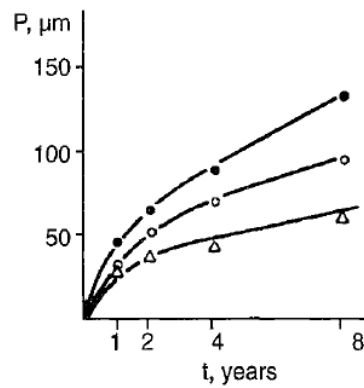


Figure 1.18. Corrosion depth (P) as a function of exposure time (t) on atmospheric corrosion of steel: e, Millheim, Ruhr; 0, Cuxhaven; A, Olpe (Mattsson, 1996)

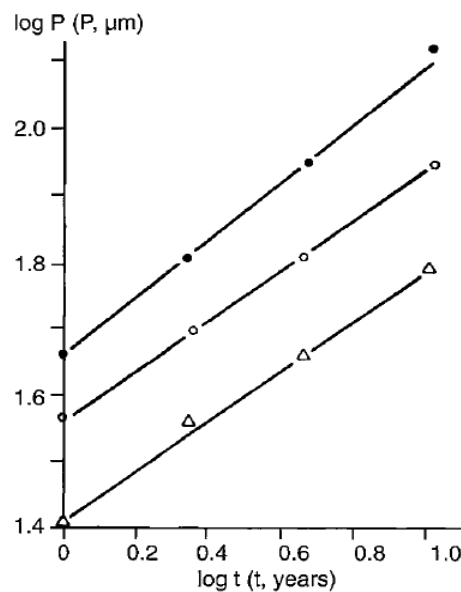


Figure 1.19. The same results are shown in Figure 1.18 as a bilogarithmic diagram of corrosion depth (P) and exposure time (t) (Mattsson, 1996)

Steel will not rust indoors if the relative humidity is less than 60%. Nevertheless, a specific type of severe atmosphere corrosion can occur after a PVC fire. Once PVC (polyvinyl chloride) burns, hydrogen chloride (HCl) is manufactured, which is gaseous and easily dispersed to surrounding areas. Moisture vapour produces hydrochloric acid, which attacks metal surfaces quickly, such as nail heads in walls, machines, electrical equipment, or stored goods. Following a PVC fire, it is critical to investigate the diffusion of hydrochloric

acid in the establishments and take cleaning and protection measures where pollution exceeds a certain limit, which is typically $10 \mu\text{g Cl}^-$ per cm^2 for steel and $20 \mu\text{g Cl}^-$ per cm^2 for more rigid structures (Mattsson, 1996).

1.4.4. Corrosion in Water

The cathode reaction, i.e. the supply of oxygen, is primarily responsible for steel corrosion in water. Still, the pH value of the water and its ability to precipitate protective calcium carbonate is also important. The corrosion rate is negligible in closed heating systems, where the dissolved oxygen content of the water is quickly depleted by corrosion. Uniform corrosion occurs at a $50\text{-}150 \mu\text{m /year}$ rate in the sea or freshwater with high oxygen content. Furthermore, localised corrosion can occur much faster, for example, in the splash zone at sea level, beneath fouling organisms, at crevices, or where the flow velocity of the water is high. Even in anaerobic conditions, microorganisms can accelerate corrosion in steel. Cast iron structures are frequently less corrosive than steel structures due in part to their larger dimensions and higher corrosion tolerance. Graphitic corrosion can, moreover, attack cast iron (Mattsson, 1996).

1.5. Corrosion Protection

Steel and cast iron corrosion rates are pretty high in aggressive conditions. Over far too rust allotment recompense for low resistance to corrosion in certain scenarios. Notwithstanding, a few more forms of Protection against corrosion are usually superior, including anti-rust painting, plastic coating, such as with sheet metal for building purposes, metal coatings, such as zinc, aluminium, aluminium-zinc, or nickel, dry-air storage, the addition of corrosion inhibitor to the corrosive environment, or cathodic Protection of constructions in aqueous environments (Davis, 2000).

1.6. Corrosive Environments and Their Characteristics

Corrosive environments are classified broadly as atmospheric, underground /soil, water, acidic, alkaline, and combinations. The fact that there are significant variables complicates matters further. The presence of important variables, such as pH, temperature, and the

presence of biological organisms, adds to the complexity and can significantly alter the material's response in a given environment. Consider the dynamic interactions of various components that make up the chemistry of the atmospheres in which automobiles are driven. The combination of natural habitats (rain, snow, humidity, marine environments, etc.) and harmful artificial environmental contributions (road salts, atmospheric pollutants and emissions, and acid rain) creates a particularly aggressive corrosive environment for automobiles (Davis, 2000).

1.6.1. Corrosive Environment Characteristics

Numerous environmental characteristics or variables influence corrosion behaviour, including The pH scale measures the degree of acidity or alkalinity. Depending on the electrochemical potential, the relative degree of oxidising or reducing conditions, the E environmental temperature, the presence of harmful and beneficial species, the velocity/fluid flow rate, and the concentration of ecological corrosio (Davis, 2000).

1.6.2. Acidity/Alkalinity

Common environments contain a wide range of acidic and alkaline conditions. As shown in Fig. 1, settings can range from strong acids with low pHs to neutral backgrounds with pH 7 to strong alkalis with sodium hydroxide and calcium hydroxide at pH 14. The pH of a few common acids and alkalis is as follows:

Solutions	pH
Hydrochloric acid (1 <i>N</i>)	0.1
Sulfuric acid (1 <i>N</i>)	0.3
Boric acid (0.1 <i>N</i>)	5.2
Sodium bicarbonate (0.1 <i>N</i>)	11.6
Ammonium hydroxide (1 <i>N</i>)	11.6
Sodium hydroxide (1 <i>N</i>)	14

Strong acids with low pH values are hydrochloric acid and sulfuric acid. Boric acid and sodium bicarbonate represent a weak acid and a weak alkaline solution. Sodium hydroxide produces a highly alkaline solution with a high pH. In conjunction with its oxidising/reducing properties, the acidity or alkalinity of an environment is critical to the corrosion behaviour of various materials (Davis, 2000).

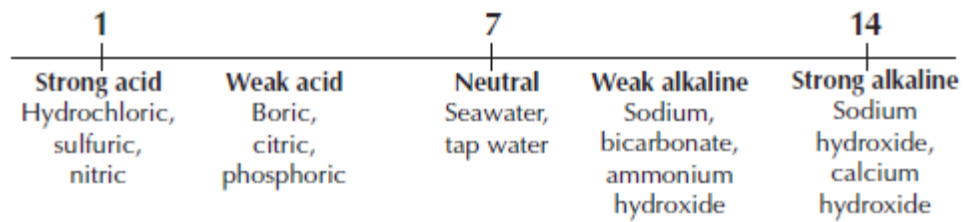


Figure 1.20. The pH of a few common environments

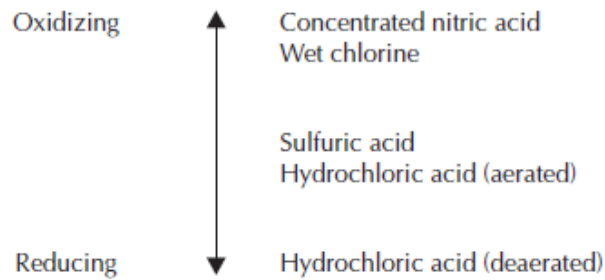


Figure 1.21. Environments exhibit a wide range of oxidising/reducing behaviour (Davis, 2000)

1.7. Steel Corrosion In Concrete

Steel ingrained in concrete is well protected from corrosion as long as the concrete has low porosity, is free of cracks, and the concrete layer over the steel is thick enough. A thickness of 20 mm is usually recommended. A passivating layer forms on the steel surface that comes into contact with alkaline concrete. On the other hand, the protective layer can be harmed if the concrete becomes carbonated due to a reaction with carbon dioxide in the air, resulting in a pH drop. Chloride from the environment, such as seawater, or added during the casting process can be harmful. Unless the steel is directly exposed, like in a crack in the concrete or a piece that isn't embedded, an active steel surface and a passive steel substrate in the cementitious materials could form an active-passive cell (Figure 1.22).

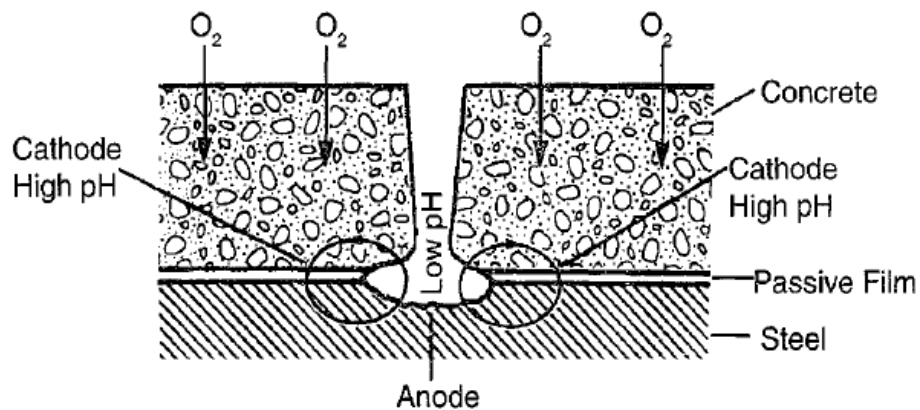


Figure 1.22. Active/passive cell concrete structures on steel (Mattsson, 1996)

Within that circumstance, the activated surface serves as the anode and is attacked locally, although the passivated steel surface functions as the cathode. Even an active-passive cell's intervention could occasionally result in the punctures of the water mains concrete cover. Several other instances of corrosion of steel reinforcements in concrete balconies, bridges, and other concrete structures exist. It is suggested that the moisture content of the cement mixture be restricted throughout arrange for the material to have fairly low permeability. In the broad sense, the waterkement percentage of concrete should not surpass 0.6, yet when encoding piping, it should always be kept below 0.5. Aesthetic compression is also preferable and can be accomplished by pulsating the blending. Infusion should be used to repair large cracks in open areas. On the other hand, fractures with a width of less than 0.1 mm are normally proven acceptable(Mattsson, 1996).

Reinforced concrete ranks high among building materials in terms of durability, adaptability, and popularity. Steel is an excellent material for the interior of tunnels and the construction of pipelines, in addition to its more obvious applications, such as the construction of buildings and bridges (Bardal, 2003). Extreme conditions, such as those found on oil rigs in the North Sea or the desert, can withstand this composite. But occasionally, it fails to deliver the promised durability and low maintenance. Deterioration can happen for several different reasons, such as wrong expectations, bad design or construction, or environmental factors that are worse than expected.

Consequently, numerous manufactured objects exhibit signs of corrosion-related damage. The difficulties of curing concrete in hot, drying environments add to corrosion control challenges, resulting in very short reinforced concrete structure lifespans. Corrosion of mild or high-strength ferritic reinforcing steels is possible because concrete is porous, and oxygen and moisture can penetrate its pores and microcracks. High calcium, sodium, and potassium hydroxide concentrations inhibit corrosion by maintaining a pH between 12.5 and 13.5. The solution's high alkalinity inhibits rapid deterioration and passivates the steel. Resulting in dense, self-maintaining gamma ferric oxide that prevents further corrosion. The concrete itself will frequently be the target of an assault when reinforcing concrete is being used. However, two chemicals can reach the steel beneath the concrete without first dissolving the concrete. Carbon dioxide and chlorides are the most common atmospherically borne species that can easily permeate concrete without causing significant damage. Then promote steel corrosion by removing the passive oxide layer created and maintained by the concrete pore water's alkalinity (Broomfield, 2011).

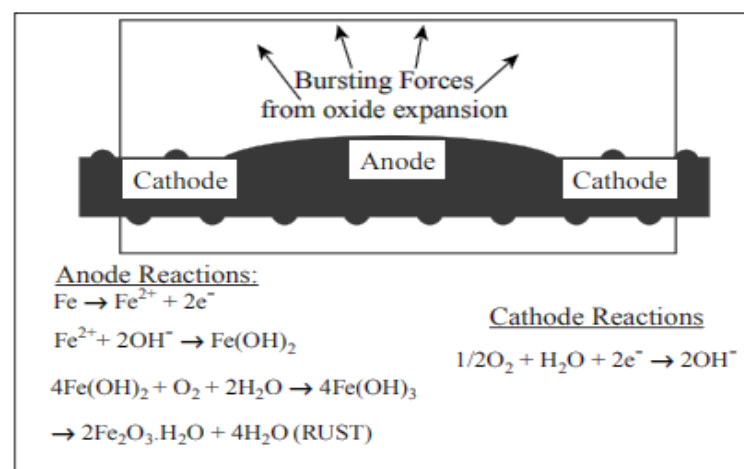


Figure 1.23. The steel corrosion process in concrete (Broomfield, 2011)

The electrochemical corrosion mechanism shared by carbonation- and chloride-induced corrosion is visualised in Figure 1.23. The separation of anodes and cathodes is critical to understanding, measuring, and controlling steel corrosion in concrete. Steel corrosion in concrete is fundamentally an aqueous mechanism with very poor transport of corrosion products away from the anodic site. It further causes a large amount of corrosion product to form, as well as cracking and spalling of the concrete and delaminations running parallel

to the plane of the reinforcing steel. Ferrous ions can remain in solution or diffuse away and deposit elsewhere in the concrete's pores and microcracks if there is not enough oxygen at the anodic site, causing significant section loss without the usual concrete cracking and spalling warning signs (Broomfield, 2011).

1.8. Corrosion Control and Prevention

Corrosion control and prevention is an important aspect of metal science, and it is supported by several disciplines, such as metallurgy, electrochemistry, physics, and chemical engineering. Additionally, vigorous methods such as acid pickling and unnecessary scale washing are widely used in industries to remove impurities (Solmaz, 2014) (Singh et al., 2011), (Assassi-Sorkhabi et al., 2004). Acids are the most common solutions for these systems, with HCl, H₂SO₄, and HNO₃ being relatively common examples (Singh et al., 2011).

The major corrosion-reduction methods currently used are material selection, design, cathodic safety, coatings, and inhibitors (Liu et al., 2017). Corrosion inhibitors are one solution to prevent corrosion. In conjunction with the focus on the corrosion awareness organisation, the report highlighted that the global market for corrosion inhibitors was \$7.2 billion in 2019 and is expected to reach \$9.6 billion by 2026. (url-1.4; Hossain, et al. 2020). It is frequently difficult to avoid corrosion in specific cases. Still, ideally, inhibitors are introduced to the industry to reduce the intensity of corrosion, which minimises potential changes in the properties of metal parts when placed in a corrosive environment. As a result, stopping corrosive reactions is critical to reduce the economy's increased demand for natural resources and to reduce the number of toxic materials produced and released into the environment during these reactions. (Verma et al., 2020; Kalla et al., 2016; Oloruntoba et al., 2017; Liu et al., 2017).

1.8.1. Corrosion Inhibitor

A corrosion inhibitor is a substance that binds to a metal surface and acts as a barrier to developing corrosive reactions. The primary characteristics of inhibitors are anodic, cathodic, mixed, and volatile corrosion inhibitors. Anodic inhibitors also add oxygen to the

metal surface, forming a thin film. They reduce the material's potential for corrosion by oxidising corrosive elements with a less reactive surface layer. Cathodic inhibitors slow cathodic reactions or reduce the diffusion of reducing elements to the metal surface such as hydrogen or oxygen. Cathodic poisons, such as arsenic and selenium ions, also slow the reaction, as do oxygen scavengers and sulfite ions, inhibiting oxygen diffusion.

Corrosion inhibitors are classified as either inorganic or organic. Inorganic corrosion inhibitors work by the corrosion of metals and forming a protective oxide film on the metal surface or a poorly soluble metal salt. However, their concentrations in the corrosive environment must be constantly monitored because of their oxidising properties. Most have toxic qualities, making them extremely harmful to humans and the environment. Some metal salts, such as those in the lanthanide group, are quite costly.

Organic compounds used as corrosion inhibitors are generally adsorbed on the metal surface, forming a barrier between the metal and corrosive media. According to the literature, molecules containing P, N, S, and O atoms and molecules with double or triple bonds are better adsorbed on the metal surface and, thus, more effective inhibitors (Oloruntoba et al., 2017; Assassi-Sorkhabi et al., 2004). Studies on the use of environmentally friendly molecules are being conducted in this field because most organic inhibitors are toxic and negatively affect people and the environment (Hojat Jafari et al., 2019; R. Kusumastuti et al., 2017). Natural plant extracts have recently become popular for this purpose (Seyedmojtaba Ghoreishiamiri et al. 2020; Akhil Saxena et al.2017). Natural plant extracts or active ingredients are natural and have no adverse effects on humans or the environment. It is natural, and its prices are lower than synthetic corrosion inhibitors. For this reason, it is extremely important to concentrate studies on these plants. Natural products are both healthy and economical; for this purpose, chemicals are the most important use potential for the future (Ehteram A. Noor. 2011; M.A. Quraishib et al., 2010).

Mixed inhibitors are compounds that form a film or store residue on the metal surface to reduce cathodic and anodic reactions. Examples include sodium silicate and phosphate, used in domestic water softener salts to prevent rust [url-1.3]. The most crucial component of corrosion inhibitors is determining the chemical stability of metals. Three major concerns should be considered when determining the likelihood of a successful corrosion

inhibitor. In this regard, the proposed inhibitor should be used correctly and over time. Finally, understanding how the inhibitor interacts with the metal during the reaction and how metal corrosion can be avoided is critical (Ghoreishiamiri et al., 2020; Al Zubaidy et al., 2012). Most corrosion inhibitors are organic, with one or more polar groups; O, N, P, S atoms, and π - electrons, and inorganic combinations such as nitrite, nitrate, chromate, dichromate, and phosphate. (Hossain, et al., 2020). Furthermore, organic inhibitors reduce corrosion via adsorption, whereas inorganic inhibitors prevent corrosion by reacting to anodised or cathodic process components (Tamalmani et al., 2020).

Previously, inorganic salts and organic compounds used as corrosion inhibitors in the industry were ineffective because they were costly, harmful, and created health and environmental risks in the case of severe productivity to delay the corrosion rate. Recent research has shown that organic inhibitors extract metal from their surroundings via adsorption and film formation. Adsorption centres are organic compounds with a high electron density and heteroatoms such as phosphorus, sulfur, nitrogen, oxygen, or those with multiple bonds that are as effective as corrosion inhibitors (Döner et al., 2011; Jafari et al., 2019). Several π - bonds, functional groups such as-OR,-COOH,-S.R., R_2 , and heteroatoms such as N, S, and O are found in many organic compounds in natural product extracts. The close coordination of the heteroatomic metal and the lone electron pair results in the absorption of inhibitor molecules on the metal surface. (Verma, et al., 2020 ; Kusumastuti, et al., 2017; Sethuraman et al., 2017; Ashassi-Sorkhabi, et al., 2004; Oloruntoba et al., 2017; Singh et al., 2011; Jafari et al., 2019).

Green inhibitors are typically biodegradable, contain no hazardous metals, and cause zero or negligible human and environmental toxicity.(Verma, et al., 2020; Sethuraman et al., 2017; Kalla et al., 2016; Oloruntoba et al., 2017; Haldhar et al., 2018). Extracts are obtained from various parts of plants, and these natural sources include a wide range of chemical compositions, such as aromatic rings, carbonyl, carboxylic, amine, and hydroxyl. These compounds are effective acidic media inhibitors that slow down the corrosion of metals and alloys. These plant extracts are also widely available due to the abundance of plant resources. (Oloruntoba et al., 2017; Haldhar et al., 2018). Plant or green corrosion inhibitors could sometimes replace synthetic organic and inorganic inhibitors. The

mechanism of action of green corrosion inhibitors relies on the active ingredient's structure, and as a result, many researchers have developed hypotheses to explain this phenomenon.

Numerous researchers have identified various plants as green corrosion inhibitors with high acidic medium inhibition efficiency. Reduce the efficiency of these plants from the highest to the lowest efficiency values: *Sida cordifolia* exhibit an inhibition efficiency of 98.83 % at 500 mg/L (Saxena et al., 2018), *Butea monosperma* displays an inhibition efficiency of 98 % at 500 mg / L (Saxena, et al., 2017), *Murraya koenigii* demonstrates an inhibition efficiency of 96 % at 600 mg / L (Quraishi et al., 2010), *Cuscuta reflexa* reveals an inhibition efficiency of 95 % at 500 mg / L (Saxena, et al., 2018), Radish fruits prove an inhibition efficiency of 79 % at 100,000 mg / L (Noor, 2011), and *Kola nitida* indicates an inhibition efficiency of 78 % at 1200 mg / L (Njoku et al., 2016) respectively.

1.9. *Rheum Ribes* (Işgın)

Işgın (R.R.) is found in several countries as well as the Eastern Anatolia region of Türkiye (Ağrı, Bingöl, Elazığ, Hakkari, Kars, Van, and Sivas) (Saxena, et al., 2018). It flourishes best on rocky and mountainous terrain. It is common for individuals to consume the plant in its fresh state. This plant has a sour flavour, helps to strengthen the stomach, prevents vomiting, and causes constipation (Njoku et al., 2016). In addition to using the underground parts to treat haemorrhoids and diabetes, this plant is also used in various parts of the country to aid digestion (Tosun et al., 2003). Due to its low pH value, R.R. is eaten by peeling and has a sour taste. Young roots and stems of R.R. are used as measles and smallpox preventative and anti-fungal agents. Its roots have anti-inflammatory properties in addition to curing diabetes, ulcers, and stomach ailments (Tosun et al., 2003). The antibacterial properties of R.R. anthraquinones (Aygün et al., 2020) are highlighted. This plant is extraordinarily rich in vitamin C. 5.59 % dry matter, 0.63 % total ash, 1.3 % protein, 3.75 g/g iron, 1.13 g/g zinc, 0.5 g/g copper, 0.423 g/g manganese, 0.255 g/g vitamin A, 0.614 g/g vitamin E, and 98.6 g/g selenium (Kalkan et al., 2020 ; Khiveh et al., 2017). RR, as previously stated, is a safe and natural plant that can be used to protect metals. R.R. has been documented by numerous researchers for a variety of effective applications, beginning with the biological synthesis of silver nanoparticles. Antimicrobial applications in wound healing, medical engineering, and electronic applications (Aygün et al., 2020)

have produced silver nanoparticles that are robust, environmentally friendly, and cost-effective. Second, research on food packaging shows that RR-containing film inhibits the growth of important human and food pathogens (Kalkan et.al, 2020). Third, R.R. Effects on Dysentery in Children, according to the findings of the study, R. R Syrup, in addition to standard antibiotic treatment, has a significant effect on the relief of fever and diarrhoea in Shigella Dysentery and is prescribed as an additional medicine for the disease (Khiveh et al., 2017).

R.R. can potentially lower glucose concentration and high cholesterol in people with diabetes due to its renoprotective impacts, as evidenced by biochemical and histopathological observations. It is also concluded that R.R. extract has a significant anti-hyperglycemic effect following treatment (Shokri et al., 2014).



Figure 1.24. Rheum Ribes images (Url-5, 2021)

According to the research, the antioxidant significance of R. Ribes is one of the most widely used medicinal and edible medicinal plants. As a result, R. Ribes may have assisted people in protecting themselves from lipid peroxidation and free radical damage, and their extracts are likely to produce healthy food products and additives (Öztürk et al., 2007).

The inhibitory effects of the extracts from various R.R. parts on copper corrosion in 1 M HCl solution were investigated. Several electrochemical techniques were used to accomplish this. Following exposure to corrosive R.R. extracts, the metal's surface was examined with the help of SEM, EDX, and contact angle measurements. Based on the information gathered, it was determined which area of this plant would best protect the

copper. The full extract will focus on the next research stage, and its protective properties will be improved by adjusting a few parameters. The extraction of the Rheum Ribes plant and its corrosion resistance when immersed in 1 M HCl of mild steel were investigated using electrochemical methods, gravimetric measurements, electrochemical impedance spectroscopy, and potentiodynamic polarisation.

Furthermore, the effects of structural inhibitor parameters on inhibiting the efficacy of their adsorption system on the surface of alloys have been investigated, as well as correlations with experimental results with quantum chemical parameters.

2. LITERATURE REVIEW

Corrosion, also renowned as chemical change, is a natural process that occurs in metals and alloys over time and helps them become thermodynamically stronger. Corrosion can occur for a variety of natural and artificial reasons. Corrosion is commonly used to describe the severe deterioration of metal properties caused by their interaction with environmental factors. It is well known that corrosion is detrimental both to the environment and to living things. Causes of deterioration vary between metals and alloys. Surface deterioration of metals and alloys can be caused by various variables, including acids, bases, moisture, salts, chemicals, climatic and environmental temperature fluctuations, and hazardous gases.

Furthermore, the colonies formed by the creatures living on mild steel aid in the rapid and permanent progression of corrosion on the alloy. Acids are used in industry for various purposes, including cleaning, metal dissolution, production, and purification. Acids used at multiple stages weaken metals and alloys and damage metals' ion structures through chemical attacks on their surfaces. The destructions they cause in their internal system damage their stability and make them susceptible to corrosion. (Salleh, S.Z. et al., 2021).

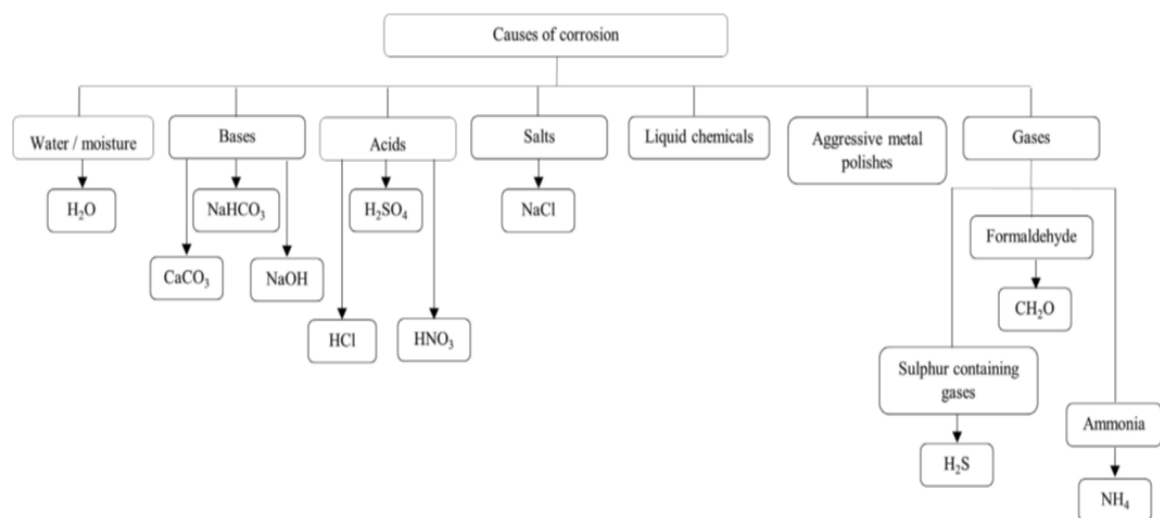


Figure 2.1. Corrosion causes by metals and alloys (Salleh, S.Z. et al., 2021)

Electrochemical processes are widely believed to account for the vast majority of corrosion. The reduction of oxygen and the oxidation of hydrogen are the fundamental chemical reactions in the beginning stages of decomposition and its progression. The internal structure of the metal, its constituents, defects in its formation, the number of impurities, its reaction to environmental conditions, interactions with liquids, and reaction with oxygen are the factors that have the greatest impact on corrosion (Marzorati, S. et al.,2018; Aslam, R. et al.,2022).

Corrosion and its Socioeconomic Consequences, according to R. Aslam, are as follows: Corrosion degrades metallic and nonmetallic compounds over time due to their reaction to environmental conditions and interconnections with living and nonliving substances in their surroundings. (Rahimi, F.A. et al.,2020).Purified metals are in an unstable and high-energy state for various reasons; as a result, they constantly interact with their environment to eliminate this state and return to their stable condition by releasing energy. Even though numerous metals are susceptible to corrosion, iron and steel corrosion account for the vast majority of this loss. If the pipe is corroded, fluid or gas leaks may occur. Loss of structural integrity caused by corrosion is even more disastrous. Consequently, alloy deterioration is a significant financial and technical problem that necessitates ongoing research into potential solutions (Aslam, R. et al.,2022)

The weight loss strategy is the most common and straightforward approach for determining corrosion rates in inhibition testing. The mass of a piece of metal or alloy is measured before it is degraded, weighed, and cleaned of reaction residues. Once more, the group of the disassembled component is determined and also figured out how bad things are getting, and calculations are done. When corrosion rates are obtained with and without the inhibitor, the level of effectiveness of the inhibitor can be determined by comparing the two (Papavinasam, S.2000). Because flaws in the analyzed metal sample could have such a large impact on the results, error bars must be presented. Consequently, it is crucial to guarantee the accuracy of the measurement (Salleh, S.Z. et al., 2021).

The anti-decomposition effect can be investigated using gravimetric analysis, voltammetric investigation, and interfacial evaluation.GCIs derived from plant extracts are typically evaluated using conventional techniques such as measuring weight loss

(WLM). These evaluations are the basis for developing hypotheses regarding the underlying inhibition mechanism. In addition, cutting-edge methods for measuring electrochemical processes, including potentiodynamic polarization (PDP) and electrochemical impedance spectroscopy (EIS), are discussed (Marsoul et al., 2020; Gromboni et al., 2021). In contrast to these more immediate measurements, the conventional gravimetric method reveals abundant findings (Adam et al., 2015). Electrochemical processes performed on the kinetics of deterioration rate constants within the existence of an inhibitor can yield a substantial amount of information regarding the inhibition mechanism.

On the other hand, constant prevailing measurement on a metallic exterior cannot be obtained without first measuring the open-circuit potential (EOCP) (Faiz et al., 2020). The magnitude trend of the results suggests that they are reasonable and could be used to support the level of reticence efficiency, despite the theoretical differences between these methods. Regularly, redox reactions are used to assess the performance of protective coatings regarding time. It is possible to use it to calculate other properties in addition to providing information regarding the material's resistance to corrosion (Stern, M. 1957). Electrochemical impedance spectroscopy is a widely used technique employed in electrochemistry (EIS). EIS is used to evaluate how a low alternating current voltage at different frequencies affects the chemical reaction. The understanding of electrochemistry from a mechanical perspective.

PDP measurements are typically performed at predetermined immersion times and temperatures, with and without various inhibitor concentrations. This measurement uses a three-electrode cell with a working electrode, a counter electrode, and a reference electrode (Popoola, 2019). Depending on the task, various dielectric substances might be employed as electrodes (Hamdy and El-Gendy, 2013). (Hamdy and El-Gendy, 2013). An existing reaction resulting from surface ability will be used to test the efficacy of GCIs in removing rust. Several adjustments can be used to evaluate GCI's effectiveness, such as curve contour and the position of oxidation and reduction or anodic power density densities. By changing the GCI intensity, atmospheric test conditions, and plant parts used, it is possible to investigate the various effects of GCIs on the corrosion inhibition efficiency of metals (Salleh, S.Z. et al., 2021)(Salleh, S.Z. et al., 2021). Potentiodynamic

polarization measurements are a destructive monitoring technique that can be performed by constructing a cell containing the metal under investigation and its surrounding environment. The outer face of the sample must be prepared before conducting any experiments to ensure that the initial point of measurement is distinct and reliable. The current-voltage diagram reveals the open-circuit possibility, positive electrode, oxide layer neighbourhood, and air transformation responses.

Statistical analysis is necessary for comparing data found in the meaningful research literature. Linear polarization resistance is an additional highly precise method for determining electrochemical properties. In a three-electrode setup, the polarization of the material is used to estimate the corrosion rate (Stern, M. 1958). In most cases, the polarization is on the order of 10 mV when measured in comparison to the open circuit potential of the material (OCP). The slope of a graph of potential versus current as the potential is varied, and the power between the working and counter electrodes can be used to quantify the charge transport resistance of a particular material. As a reaction mechanism, the corrosion rate of the material is applied to construct a schematic diagram out of circuit boards. On the other hand, EIS spectra can be generated in a matter of minutes, whereas exposure tests can take several weeks to complete. The most difficult challenges are related to data interpretation, as modelling the metal solution interface necessitates the building projects of a transmission line (Salleh, S.Z. et al., 2021).

Moreover, using polarization curves, the PDP method can also be utilized to determine inhibition efficiency (IE%), wear percentage (V_{COR}), corrosion current density (i_{COR}), and redox potential (E_{COR}) (Olakolegan et al., 2020). This calculation was performed in the study by Olakolegan et al. (Pal and Das, 2020). Using equations (4) and (5) from (Şahin et al., 2020), it is possible to calculate V_{COR} and IE% from PDP measurements:

$$\text{Corrosion rate. } (V_{COR}, g/m^2) = \frac{(i_{COR}) \times t \times M}{F} \quad (2.1)$$

$$\text{Inhibition efficiency. } (IE_{PDP} \%) = \frac{(i_{COR})_a - (i_{COR})_p}{(i_{COR})_a} \times 100 \quad (2.2)$$

Where $iCOR$ is the electron flow intensity ($A\text{m}^{-2}$), M is the molar mass of the substrate (gmol^{-1}), F is the Faraday constant ($C\text{mol}^{-1}$), t is the interaction time (s), $(iCOR)_a$ is the flow deterioration density without the impediment ($A\text{m}^{-2}$), and $(iCOR)_p$ is the concentration of corrosion rate with the impediment ($A\text{m}^{-2}$). Additional analyses can be performed using the potentiodynamic polarization to determine the inhibitory activity and other oxidation variables.

EIS is frequently used to determine how much current flows and how much resistance exists on the surface of a metal when an inhibitor is present and when it is not. EIS experiments are the most effective way to determine how quickly corrosion occurs (Alvarez et al., 2018). (Alvarez et al., 2018). EIS could be used to ascertain a system's input resistance, also known as the recurrence of changeable prospects (Miralrio and Espinoza Vazquez, 2020). Randle's equivalent circuit loop of current solution (R_s), charge transport tension (R_{ct}), and double-layer capacitance clarifies the characterization of the electrochemical performance of a material engrossed in an acidic solution (C_{dl}). The outcomes of an EIS evaluation are usually represented using a Nyquist plot, with the fundamental element of the amplitude mapped across the X-axis and the fictional aspect obtained by plotting along the Y-axis (Thomas et al., 2020). Evaluating the I.E. and using the EIS measurement and Equation 6:

$$\text{Inhibition. efficiency. } (IE_{EIS}\%) = \frac{R_a - R_b}{R_a} \times 100 \quad (2.3)$$

R_a is the electron transport opposition in the utter lack of a suppressor, while R_b is the charge transfer tension whenever an active ingredient is prevalent.

Marsoul et al. (2020) are scientists who worked in the field of metal corrosion and used the EIS for their research and observations. They investigated the feasibility of pomegranate bark extract (*Punica granatum* L) as a mild steel GCI in an HCl solution. Figure 2 depicts the Nyquist plots of different percentages of pomegranate bark extract in 1 M HCl formed using the EIS method. Figure 2 illustrates that a single loop capacitive is acquired for any pomegranate bark composition. These results recommended that a charge transfer process determines the percentage during which mild steel denatures at an extreme pH (Tan et al., 2020a). Moreover, a greater distance with a maximum density of

H.A. might well be related to increased interfacial tension on the ground of mild steel by sourced adsorbates (Marsoul et al., 2020)

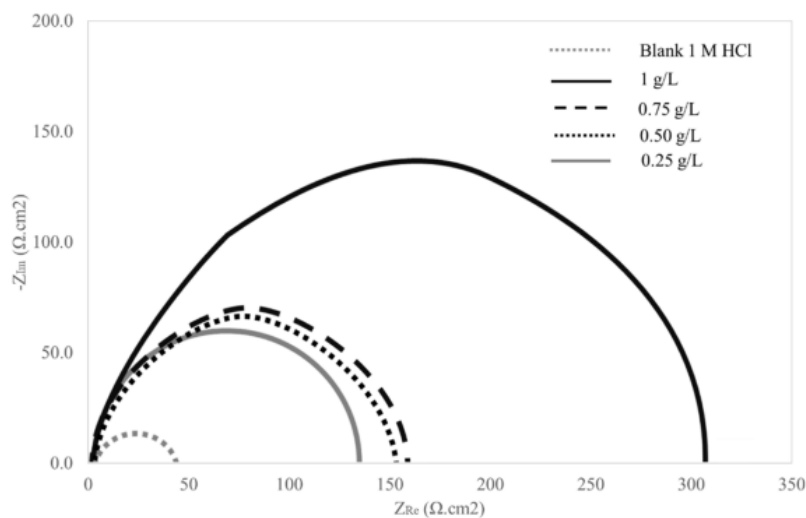


Figure 2.2. Nyquist plots for different concentrations of pomegranate bark extract in 1 M HCl (Marsoul et al., 2020)

Scanning electron microscopy (SEM), atomic force microscopy (AFM), and X-ray photoelectron spectroscopy are the most frequently employed techniques for evaluating the surface topography of unprotected and affected chemical substrates with or without inhibitors (XPS).

Due to the attack of a corrosive medium, the surface of an exposed object lacking an inhibitor typically has a rough texture. In contrast, the exposed surface containing an inhibitor is relatively smoother than the exposed surface without an inhibitor. An adsorptive film is suggested to be applied to the metal's smooth surface. Specifically, Da Rocha et al. (2012) submit that forming an adsorptive film of phenolic compounds from grape pomace extract on carbon steel inhibits HCl (Da Rocha et al.,2012). Raghavendra compared the metal surfaces after adding and not adding the green sections to see how they affected the metal and alloys.SEM images supported his conclusion about the effectiveness of the inhibitory activity exerted by multiple GCIs on the carbon surface of rebar(Raghavendra, 2018)

Investigating the adsorption isotherm is necessary for comprehending the corrosion process. Adsorption isotherms (Zhu, Y.et al., 2017) help to learn equilibrium inhibitor concentrations for adsorbed and bulk inhibitors. Adsorption isotherms are crucial for

determining specimen engagement. Absorption spectra can help you better understand the relationship between the protective agent and the metal or alloy outer layer. According to researchers, the interaction of the functional groups of the raw materials with the alloy to be protected is the first step in the process by which biomolecules impede metal corrosion. Before acknowledging corrosion protection mechanisms, it is necessary to understand the adsorption characteristics of biological substances on the material's surface. The topography, homogeneity, physiochemical nature, charge transmission within the compound, aggressive form of media, and natural binding site chemical nature of the base metal all impact binding. The sequence boundary connections establish ion or neutral molecule adsorption on bare metals in solution. (Salleh, S.Z. et al., 2021). Based on the types of forces present, two kinds of adsorption can be distinguished:

(a) Chemical penetration: The formation of chemical bonds that bind a thin coating of particles and molecules to the surface is referred to as this kind of interaction. The consequences of this type of adsorption are essentially permanent.

b) Physical adsorption: This type of adsorption has comparable energy levels to condensation. Electrostatic and van der Waals adsorption processes generate significantly less heat of adsorption than chemisorption. In the case of physisorption, interactions between the ions or dipoles of the inhibitor and the charged metal surface include both coulombic and other types. In this situation, adsorption occurs rapidly; however, the adsorbing species are easily removed from the surface by washing. Species with only weakly grouped atoms, such as π -electrons in aromatic rings, multiple bonds, or unpaired electrons in functional groups containing oxygen, nitrogen, sulfur, or phosphorus, frequently donate electrons to the empty orbital of transition metals. This process is called electron donation. In most instances, the corrosion inhibition performance of a group of organic substances with the same sequence homology but different heteroatoms will appear as follows: The first element is phosphorus, followed by sulfur, nitrogen, and oxygen (Salleh, S.Z. et al., 2021).

The inhibition mechanism is currently the focus of research as part of an effort to provide evidence supporting the dependability of I.E. for GCIs derived from plant extracts. On metal substrates, Adsorption mechanisms for GCI can be broken down into three

categories: physisorption, chemisorption, or a combination of the two, also referred to as a mixed-type adsorption inhibitor. Physisorption refers to the attachment of molecules to solid surfaces, whereas chemisorption involves chemical reactions (Faisal et al., 2018). Physisorption is the attachment of molecules to solid surfaces, whereas chemisorption involves chemical reactions (Faisal et al., 2018). Mixed inhibitors provide the greatest coverage because they inhibit cathodic and anodic reactions (Brycki et al., 2018).

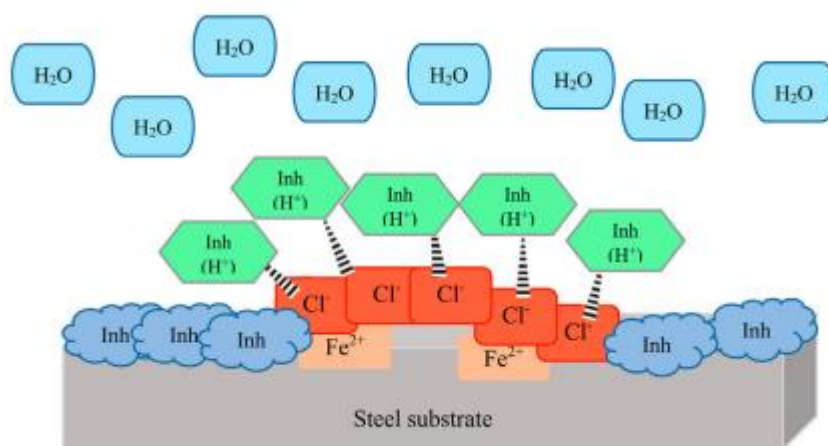


Figure 2.3. Physical adsorption scheme of protonated inhibitor in HCl medium on the metal surface (Hanini et al., 2019).

Corrosion inhibitors are substances that bind to the surface of metals and prevent the formation of corrosive reactions. The primary characteristics of corrosion inhibitors are anodic, cathodic, mixed, and volatile. Additionally, anodic inhibitors add oxygen to the surface of the metal, forming a thin film. They reduce the material's corrosion potential by oxidizing corrosive elements with a less reactive surface layer. Cathodic inhibitors slow cathodic reactions or reduce the diffusion of reducing elements, such as hydrogen or oxygen, to the metal surface. Cathodic poisons, such as arsenic and selenium ions, oxygen scavengers, and sulfite ions, which inhibit oxygen diffusion, also slow the reaction. Both cathodic and anodic reactions can be inhibited using a substance known as a mixed inhibitor. Sodium silicate and phosphate are two examples of salts used to eliminate rust in residential water softeners. Volatile corrosion inhibitors, implications transmitted to the corrosion site in an enclosed environment, form a thin protective layer at active metal sites. Boilers use vaporized condenser tubes to transport corrosion-preventive substances like morpholine and hydrazine. [Url. 3]. The essential feature of

corrosion inhibitors is determining the chemical stability of metals. The effectiveness of a corrosion inhibitor depends on three primary factors. Under these conditions, the proposed inhibitor should be used appropriately and gradually. How will the efficacy of the corrosion inhibitor be assessed once the procedure has begun? It is critical to understand how the inhibitor interacts with the metal during the reaction to prevent metal corrosion[(Ghoreishiamiri et al., 2020),(Al Zubaidy et al., 2012)].

Corrosion inhibitors, such as inorganic salts and organic compounds, were previously used to slow the industry's corrosion rate. Still, they were ineffective due to their high costs, negative effects, and potential risks to human health and the environment under extreme production conditions. Recent research has revealed that organic inhibitors can remove metal from their environments through adsorption and film formation. Corrosion inhibitors that are also adsorption centres contain heteroatoms such as phosphorus, sulfur, nitrogen, and oxygen and have a high electron density [(Doner et al., 2011),(Jafari et al., 2019)]. Numerous -bonds, functional groups such as -OR, -COOH, -S.R., and R₂, and heteroatoms such as N, S, and O are present in the numerous organic compounds in natural product extracts. Inhibitor molecules are absorbed on the metal surface due to the close coordination between the heteroatomic metal and the lone electron pair. (Oloruntoba et al., 2017); (Singh et al., 2011); (Jafari et al., 2019); (Verma, Quraishi, & Ebenso, 2020); (Kusumastuti, Pramana, & Soedarsono, 2017); (Sethuraman et al., 2017); (Ashassi-Sorkhabi, Majidi and Seyyedi, 2004)

Corrosion of ferrous metals and alloys is a natural occurrence; however, it threatens human health and the environment. Corrosion inhibition of corrosion through the inhibitor treatment process is used to address this issue effectively. Plant-derived corrosion inhibitors are natural. Conventional corrosion inhibitors are an option that has been extensively discussed in published works. The findings confirmed the use of plant extracts in treating various high, I.E. metal corrosion. Plant extracts contain links between, I.E. and GCI's heteroatoms and π -electrons. Multiple theoretical and experimental approaches have confirmed the efficacy of plant extracts as eco-friendly corrosion inhibitors. (Salleh, S.Z. et al., 2021).

According to a great number of studies, various plant extracts have been used in manufacturing settings worldwide to prevent corrosion (Shehata et al., 2018). Many plant parts suitable for extraction of corrosion inhibition have been the subject of extensive research. Organic green corrosion inhibitors (OGCIs) and inorganic green corrosion inhibitors (IGCIs) are the two types of GCIs, as shown in Figure 2.4 (El Ibrahim et al., 2020).

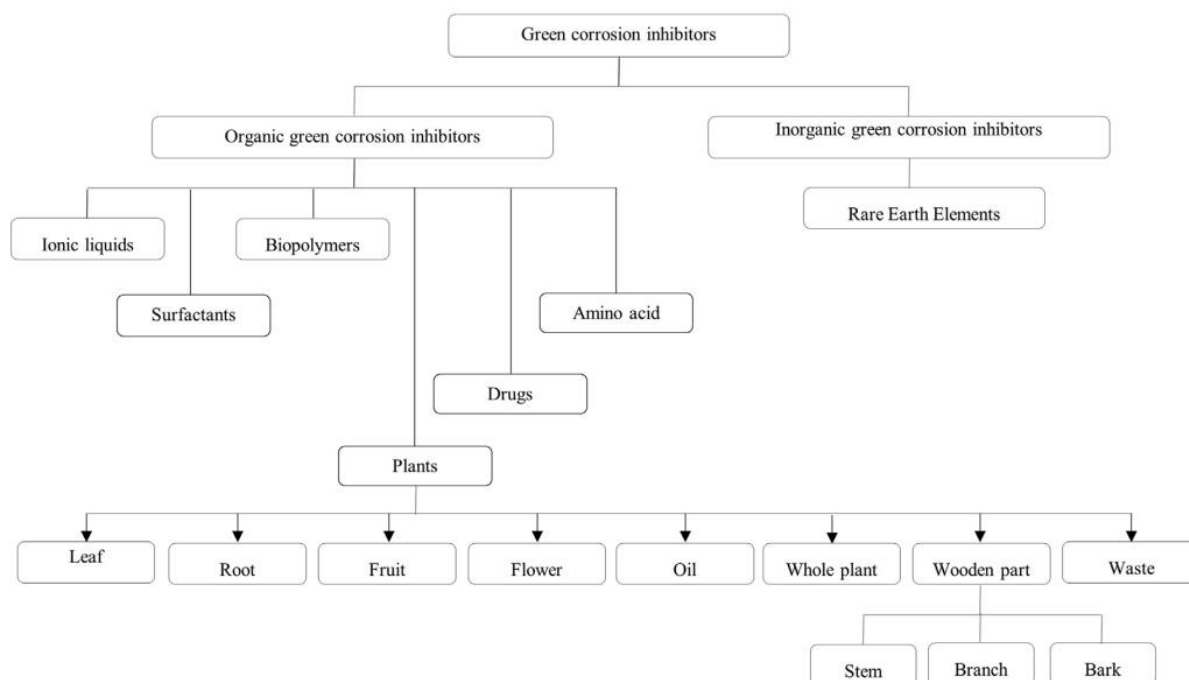


Figure 2.4. Green corrosion inhibitors in groups(Salleh, S.Z. et al., 2021)

Green corrosion inhibitors are typically biodegradable, free of toxic metals, and cause zero or negligible toxicity to humans and the environment[(Verma, Quraishi, and Ebenso, 2020),(Sethuraman et al., 2017),(Kalla et al., 2016) (Oloruntoba et al., 2017), (Haldhar et al., 2018)]. Extracts are derived from various plant parts containing different chemical compounds, including aromatic rings, carbonyl, carboxylic, amine, and hydroxyl. These compounds are efficient corrosion inhibitors for metals and alloys in acidic environments. Due to the abundance of plant resources, these plant extracts are readily available [(Oloruntoba et al., 2017), (Haldhar et al., 2018)]. In certain instances, plant-based or environmentally-friendly corrosion inhibitors could replace synthetic organic and inorganic inhibitors. The mechanism of action of green corrosion inhibitors depends on the structure of the active ingredient, and as a result, many researchers have developed hypotheses to explain this phenomenon.

Researchers have identified various plants as green corrosion inhibitors with high acidic medium inhibition efficiency. Reduce the efficiency of these plants from the most efficient to the least efficient: *Sida cordifolia* has an inhibition efficiency of 98.83% at 500 mg/L (Saxena et al., 2018), *Butea monosperma* has an inhibition efficiency of 98% at 500 mg / L [(Saxena, Prasad and Haldhar, 2017)], *Murraya koenigii* has an inhibition efficiency of 96% at 600 mg / L [(Quraishi et al., 2010)].

Wild Rheum ribes grows in Turkey (Tosun and Akyüz Kizilay, 2003). This plant is also known as "Işgın," "Uşgun," and "Ucgun" (Aygün et al., 2020). Some plant species are used in the medical industry, while others are grown for their aesthetic value. The plant contains abundant cancer-fighting vitamins C, A, B1, B2, E, and K. These are all used in treating cancer. The R.R. plant is also a member of the Polygonaceae family, which is known to contain antioxidants [(Aygün et al., 2020), (Ragasa et al., 2017)]. Components of Rheum Ribes include long-chain hydrocarbons, in particular long-chain n-alkanes (80.81%), as well as a high number of unsaturated fatty acids (66%) (n-eicosane (27.08%), palmitic acid (9.9%), n-tetracosane (7.34%)), linoleic acid (6.56%), and the main components of ethyl linoleate (Ragasa et al., 2017).

Numerous researchers have demonstrated the usefulness of R.R. for various significant applications. The researchers began by determining the function of R.R. in the biological synthesis of silver nanoparticles. This research resulted in the production of silver nanoparticles that were robust, environmentally friendly, and contained cost-effective antimicrobial components for use in wound healing, medical engineering, and electronic applications (Aygün et al., 2020). Second, studies on the effects of RR-containing films on the growth of significant human and food-borne pathogens have been published (Kalkan, Ota, and Engin, 2020). This investigation concerned food packaging. Third, R.R. Effects on Children with Dysentery, according to the research, R. R. Syrup, in addition to the standard antibiotic treatment, has a significant effect on the relief of fever and diarrhoea in Shigella Dysentery and is prescribed as an additional treatment for the disease. Also, this is because R. R. Syrup significantly relieves fever and diarrhoea associated with Shigella dysentery (Khiveh et al., 2017).

Biochemical and histopathological results of the study have shown that R.R. can be used to lower plasma glucose and cholesterol levels. These findings are due to R.R. having renoprotective effects on diabetes. We can also conclude that R.R. extract has a significant hypoglycemic effect following treatment (Shokri et al., 2014). According to the research, *R. ribes* is one of the world's most widely employed medicinal and edible plants. It also plays an important role in antioxidant defence. As a result, *R. ribes* may have protected people from lipid peroxidation and free radical damage, and the extracts of these plants are likely to be used to produce healthy food products and additives (Oztürk et al., 2007).

Numerous proposals for new synthetic organic compounds have been proposed over the past two decades. Some of these compounds show promise as corrosion inhibitors; DMEA, TETA, and sodium benzoate all performed well in long-term exposure trials on concrete, reliably elevating the chloride concentration at which corrosion may commence. In contrast, only alkaline solutions were used for short-term testing of the newly proposed compounds. Long-term studies on concrete must be conducted to evaluate whether or not the inhibitor is effective (Bolzoni et al. 2022)..

There are several reports in the scientific literature about the effectiveness of various polyesters used as corrosion inhibitors for rebar. In an alkaline environment, polyglycerol azealate (PGAZ) and 4-1-4- methoxyphenyl cyclohexylhene 9-oxodecanoate (MPOD) is employed to prevent corrosion of the rebar alkaline environment, polyglycerol area late (PGAZ) and 4-1-4- methoxyphenyl cyclohexylhene 9-oxodecanoate (MPOD) are employed to prevent corrosion of the rebar. Polyesters were produced, and their corrosion-prevention abilities against rebar in an alkaline solution of 0.5 mol/L chlorides were tested at 10, 100, and 1000 ppm. Test results on the efficacy of these macromolecules MPOD were found to have maximum effectiveness of 72% in its inhibition. In comparison, PGAZ was found to have a minimum efficiency of 58%, mostly due to their different levels of aromaticity (Bolzoni et al. 2022)

Polyacrylamide (PAM), an additional promising polymeric inhibitor, was investigated by Zhi et al. [47] for its capacity to prevent corrosion in carbon steel. The chloride concentration in the alkaline solution ranged from 0.01 mol/L to the point when corrosion

began. The critical chloride concentration increased from 0.03 mol/L in the reference solution to 0.1 mol/L at the maximum inhibitor concentration (0.15 wt%). PAM molecules can connect to the steel outer surface to the acryl-amino functional group (CONH₂) (Bolzoni et al.2022).

There is a potential that nitrate could serve as an adequate substitute. Although the researchers share the trait of an anodic inhibitor with nitrite, their impact appears to be delayed. In most articles indicating a favourable effect of calcium nitrate, the chloride content at the rebar level is never given, casting doubt on the veracity of the results claimed. The observed increase in chloride concentration appeared modest, despite the inhibitor's significant addition. In addition, as a fixed accelerator, the asserted long-term efficacy may be related to reduced chloride diffusion(Bolzoni et al.2022).

Researchers led by Hu et al.looked at the efficacy of organic core-shell corrosion inhibitors (CSCI) in preventing the corrosion of rebars when exposed to an alkaline solution as part of their investigation. They chose a di-block copolymer of polyethylene oxide and polystyrene for the CSCI (PEO113-b-PS1171). The capsules contained BTA at a concentration of 1.05 g/L as an inhibitor. The radius of the shell is estimated to be 400 nm. At a concentration of around 2.27 10⁻³ wt%, BTA-containing CSCI improved rebar corrosion resistance by more than 93%. Both empty and BTA-containing CSCI adsorbed chlorides efficiently on the reinforcing surface. Moreover, when BTA was liberated from BTA-containing CSCI, [Fe(BTA)₃]⁺ complexes were formed at corrosion sites(Hu et al.2021).

Jiang et al. studied DNA's ability to prevent steel rebar corrosion in acidic environments. DNA-based corrosion inhibitors coat steel with a thick, durable film to prevent rust and other damage. The randomly selected oligonucleotides ranged from 20 to 80 nucleotides. DNA inhibits alkaline solutions containing 0.01 to 0.1 mol/L NaCl. Maximum efficiency was found at 0.0025% DNA. DNA adsorption on steel's surface inhibited cathodic corrosion. DNA adsorbs preferentially on the steel surface where the corrosion reaction is active during the middle and late stages of corrosion, limiting the anodic reaction. DNA is a mixed inhibitor (Jiang et al.2017.)

Carbon steel rebars were protected against rust and corrosion in a chloride-rich mortar using *Opuntia ficus-indica* (OFI) mucilage. Moulds were made from a 1:3 mixture of Ordinary Portland Cement and silica sand. W/C=0.8. There was 4 to 8% Nopal, also known as OFI, in the mix. Its amino acids and long-chain carbohydrates serve as anti-rust and deterioration coatings. The specimens were subjected to a wet-dry cycle containing 3.5% NaCl. According to the study, adding 8% Nopal slime to chloride-contaminated effectively prevented steel corrosion. Slime not only makes things more watertight, but it also makes them impervious to harmful substances. In order to achieve the reported efficiency, a high inhibitor dosage of 8% by weight of cement was implemented (Martinez et al. 2016).

Benjamin Valdez Salas and his colleagues used neem as a novel and environmentally friendly carbon steel inhibitor in reinforced concrete (the leaf extract of *Azadirachta indica*). In a simulated chloride environment, they compared the efficiency of the green extract against corrosion to that of three inorganic commercial inhibitors. The objective was to determine the efficacy of the green extract. They examined the efficiency of the Neem inhibitor under various situations, such as temperature, droop, weight change, air content, compressive strength, and chloride ion penetration. After 182 days of testing, it was shown that the green extract did not impact the structural stability of the concrete, but it did provide 95% effective protection against chloride conditions. The testing session lasted for 182 days (Salas B V et al. 2021.)

Nayem Hossain and his colleagues conducted another investigation to obtain a deeper comprehension of the role that natural inhibitors play. In an acidic environment, Hossain utilized *Terminalia arjuna* as a corrosion inhibitor for mild steel. Hossain determined the origin of the inhibition using Fourier-transform infrared spectroscopy and scanning electron microscopy of the surface. They identified the effectiveness of the *Terminalia arjuna* extract after three days of testing. Leaves have a maximum corrosion efficiency of 64.1% in the more concentrated inhibited solution. In green inhibitor solutions, weak C-O, C=C, and N-H bands may prevent low corrosion of mild steel samples. The microstructure of mild steel samples in a green solution indicates a modest corrosion effect (Hossain N, et al.2022.)

The development of GCIs derived from plant extracts is one of the areas of corrosion inhibition that has received the most attention. Many studies on the use of plant extracts in corrosion prevention are published each year. The increasing number of publications on this topic demonstrates that it is crucial to find a better solution for corrosion problems by employing plant extracts as a corrosion inhibitor. We decided to use R.R. as a corrosion inhibitor for mild steel in reinforced concrete based on the growing evidence indicating that GCIs derived from plant extracts have significant potential for combating corrosion.

Using electrochemical, microscopic, potentiodynamic, and spectroscopic methods, the ability of Rheum Ribes (Isgın) to adsorb and inhibit corrosion on a mild steel surface using a 1 M HCl solution was investigated. Additionally, the inhibition mechanism was examined. The R.R. appears to be adsorbed by the metal interface, as evidenced by the results and experimental values. Furthermore, the film forms a protective layer evenly distributed across the surface of the metal. Applying a green molecule film to the surface of mild steel has been shown to protect against corrosion.

The inhibitor inhibits both the cathodic and anodic reactions. The anodizing or cathodic response mechanisms are unaffected by the formation of the R.R. film layer on the alloy's exterior surface. Electrostatic interactions at the alloy's interface uniformly absorb and disperse R.R. molecules, which function exceptionally well as inhibitors.

3. MATERIALS AND METHODS

3.1. Copper

3.1.1. Preparation of Electrodes

The working electrode was made of Cu with a purity of 99.98-99.99%. The cylindrical copper rods were prepared by embedding them in polyester and leaving out only the lower end of the measurement. The electrode's total surface area in contact with the solution was 0.0707 cm². The Cu electrodes were cleaned with sandpaper, the last of which was a 2000 grid, using a sanding machine before the measurements. After washing with pure water and absolute ethanol, they were immersed in an ultrasonic bath for a set amount of time before being immersed in the test solutions without waiting. A Pt sheet with a total surface area of 2 cm² was utilized as an auxiliary electrode. The reference electrode was Ag/AgCl (3 M KCl).

3.1.2. Preparation of R.R. Extracts

This study made use of R.R. from the Bingöl region. The extraction procedure has previously been described in detail [31]. After collecting the R.R. taxon grown in its natural habitats, the leaf, flower, and root parts were separated and dried on unprinted papers in a sunny place. The dried plant parts were ground to 30 mesh particle size by scraping with a laboratory-type mill. Each ground plant organ was weighed 100 g and extracted with 2 L methanol. As a result of the extraction process, it was filtered and separated from the extract pulp part. The remaining pulp was extracted with the same amount of methanol two more times. The methanol in the extract solution obtained as a result of the extraction process was removed with the help of a rotary evaporator at temperatures not exceeding 40°C under low pressure. The dry extract from the evaporation process was taken into an amber-coloured bottle and stored in the refrigerator at +4 °C.

3.1.3. Test Solutions

The corrosion tests were performed in 1 M HCl and 1000 ppm extracts containing 1 M HCl solutions. Dilution of 1 M H.C. HCl solution produced an analytical grade HCl solution (97%). 1000 mg dried R.R. extracts were dissolved in pure water and diluted to 1 L in a 1 L flask with distilled water. The temperature of corrosive solutions was kept at 298 K in a water bath during the tests. The experimental set-up was opened to the atmosphere, and the solutions were not stirred during the experiments.

3.1.4. Electrochemical Measurements

The electrochemical behaviour of Cu was investigated using computer-controlled CHI 660D and CHI6096 A.C. Electrochemical Analyzers. Pt and Ag/AgCl electrodes were used as counter and reference electrodes. Initially, the working electrodes were immersed in 1 M HCl in the absence and presence of the extracts for 1 hour, and the change in E_{ocp} was plotted against the immersion time. Regarding this exposure time, EIS data were collected in the frequency range from 100 kHz to 0.003 Hz. The amplitude was 10 mV from peak to peak. Upon completion of these tests, LPR experiments were carried out at 0.001 V s^{-1} , ranging from -10 mV more negatively to +10 mV more positively versus E_{ocp} , and an i - E plot was obtained. Polarisation resistance was discovered in the formation of these lines. Finally, polarisation plots from E_{ocp} to anodic potentials were obtained in the same system at a scan rate of 1 mV s^{-1} .

3.1.5. Characterization of the Metal Surface

Cu was left in the 1 M HCl solution for 1 hour without and with each extract added. The metal was removed, cleaned thoroughly with purified water, dried, and stored in a desiccator until measurements were taken. A Jeol model (JEOL 6510) SEM was used to examine their surface structure and appearance. EDX measurements were used to determine the chemical composition of the surface. While to assess the consistency of hydrophobic or hydrophilic characters and the guest, the orientation of the molecules at the surface contact angle measurements were taken [32, 33]. The sessile water drop theory was used in these experiments.

3.2. Mild Steel

3.2.1. Working Electrode Preparation

The samples for the M.S. were prepared by cutting a cylindrical rod to a length of approximately 4 centimetres. C (1.720), O (0.115), Al (0.173), Si (0.133), P (0.052), Cr (0.057), Mn (0.704), Ni (0.115), Cu (0.144), Mo (0.204), Sn (0.126), and Fe make up the chemical composition (*wt%*) of the MS sample (remainder). The samples were placed in a polyester block, excluding its bottom surface, which had a surface area of 0.785 cm² after being connected with copper wire for electrical conductivity. Scales and oxides were manually removed before using the working electrode with varying grades of sandpaper to achieve a grade 2000 open surface area. The sample was washed with distilled water, vigorously washed with ethanol, and then washed again with distilled water before being dried with filter paper. For each test, a freshly sanded electrode was immersed in ethanol for three minutes, cleaned with ultrasonic waves, and then immersed in the test solution.

3.2.2. Plant Material Extraction

The R.R. plant was discovered in the Turkish province of Bingöl. It was taken to the lab and dried on blank papers in dark, damp rooms without the sun's light. The dried herb samples were ground in a laboratory-style mill. In a glass extractor flask, 100 g of the powdered herb sample was mixed with 2 L of methanol. The extraction process was carried out in a lab for three days. Following the extraction process, the active ingredients that went into the organic phase were separated from the plant pulp using filter paper. The extraction was repeated twice under the same conditions, and the pulp residue was mixed with the R.R. root extracts. The methanol solvent in the R.R. root extract was removed using a rotary evaporator at temperatures no higher than 40°C and low pressure. Dry R.R. root extract with a 7.8% yield was placed in an amber sample bottle and wrapped in aluminium foil after evaporation. The dried R.R. root extract was stored at +4°C for future research (Kaya et al., 2018).

3.2.3. Electrolyte Preparation

A 1 M solution of HCl containing six different concentrations of R.R. root extract with or without adding K.I. was used as the corrosive medium. The HCl used in this Preparation had a reagent grade of 97% (Sigma Aldrick), and a 1 M test solution was made by combining it with distilled water. In the test solution, the concentration of R.R. root extract ranged from 100 to 2,000 ppm. Each of the test solutions was prepared with plant extracts that were completely dissolved, resulting in a completely uniform mixture. Moreover, to improve the R.R. root extract's stability and protective capacity, 1000 ppm of K.I. was added to 1000 ppm of plant extract mixed with 1 M HCl, and the tests were repeated to account for these new conditions.

Electrochemistry experiments were carried out in a climate-controlled room, but the solution was never stirred. The temperature of the solutions was kept constant throughout the investigation by a thermostat set to 298 K. Each experiment was repeated three times to ensure that the results could be reliably reproduced (Haldhar *et al.*, 2018).

3.2.4. Electrochemical Testing

The polarization properties of various metallic materials vary depending on the material's content's open circuit potential, disintegration, and passivation. These electrochemical parameters calculate a material's corrosion factors (Url-2, 2022). Electrochemical techniques are a simple and low-cost method for determining a material's electrochemical properties. These techniques detect metal corrosion by examining the response of energy absorption products to regulated electrochemical interruptions.

The electrochemical measurements were performed using a computer-controlled CHI 660D or CHI 6096E A.C. Electrochemical Analyzer. A three-electrode electrochemical cell was used in these tests. A platinum sheet (2 cm² total surface area) and an Ag/AgCl electrode were auxiliary and referenced electrodes (3 M KCl). An Ag/AgCl electrode was designated for each potential value. The MS electrode was immersed in corrosive solutions for one hour before electrochemical measurements to establish steady-state open circuit potential (E_{ocp}) conditions (Solmaz, 2014a). The change in potential with

time ($E_{ocp}-t$) was recorded for 3600 s. The electrochemical impedance spectroscopy (EIS), linear polarization resistance (LPR), and potentiodynamic polarization (P.P.) measurements were then monitored.

The EIS measurements were carried out at E_{ocp} , frequencies ranging from 100 kHz to 0.01 Hz with a perturbation amplitude of 0.005 V peak-to-peak. The EIS data were analyzed using licensed ZView software by fitting experimental data to suggested electrical equivalent circuit diagrams (EECD). LPR measurements were performed by measuring the electrode potential at ± 0.010 V around E_{ocp} using cathodic potentials as a starting point. The scanning rate was 0.001 V s^{-1} . Upon completion of the LPR measurements, P.P. measurements were taken from the cathodic potentials to the anodic domain with 1 mV s^{-1} potential scan rate.

3.2.5. The Synergistic Inhibitory Effect of KI

A 1 M HCl solution with 1000 ppm of R.R. root was mixed with 1000 ppm of K.I. to stabilize the surface inhibitor film and boost its protection. $E_{ocp}-t$, EIS, LPR, and P.P. studies were performed to determine how well the surface inhibitor film blocked iodide ions and how electrochemically stable it was when iodide ions were present. We examined the surface of the M.S. electrode after it had been in an inhibited solution with iodide ions for 1 hour, employing SEM, EDX, AFM, and contact angle measurements. The stability of the film formed on the M.S. surface was also evaluated, and results were compared of HCl solutions with and without K.I.

3.2.6. Surface Characterization Studies

MS surface was characterized with SEM, EDX, AFM, and contact angle measurements after 1 hour of exposure to a 1 M HCl solution with and without an inhibitor at 298 K. The MS surface was cleaned before being immersed in the solutions described above. After being removed from the solutions, its surface was washed with water and dried with N_2 gas. SEM (JEOL 6510) and AFM were used to examine the metal's surface (Nanoteknoloji Park System XE-100). EDX measurements were used to determine the surface's chemical composition and the film's distribution by looking at the distribution of

specific elements (EDX mapping images) and the cross-sectional structure of the surface (JEOL 6510). While to determine whether the exterior area was hydrophobic or hydrophilic, contact angle measurements were taken (Biolin Scientific, Theta Lite). The theory of water drops that stay put was used in these tests (Seddiket al., 2020; Dehghani et al., 2019; Asadi et al., 2019).

3.2.7. Surface Inhibitor Film Persistence

The stability of the inhibitor film that formed on the metal's surface was determined using electrochemical methods such as chronoamperometry (C.A.) and cyclic voltammetry (CV). The working electrode was exposed for one hour to 1000 ppm R.R. root or 1000 ppm K.I added to 1000 ppm R.R. root solutions containing 1 M HCl. Once the Eocp attained a state of functional equilibrium, the experiments could begin. Similar studies were conducted without additives compared to the R.R. root or K.I. plant extract experiments. The system was exposed to +100 mV anodic or -100 mV cathodic constant overpotentials (vs E_{ocp}) for 3600 s during the C.A. measurements, and the current densities were plotted against time. Cyclic voltammograms of anodic or cathodic potentials were conducted by scanning the potential from E_{ocp} to +100 mV anodic or -100 mV cathodic potentials (vs E_{ocp}). Ten whole segments were used at a scan rate of 0.010 V s⁻¹. The experiments were carried out at 298 K, and the solutions were not mixed during the tests.

3.3. Reinforced Concrete

3.3.1. Preparation of Reinforced Concrete

Initially, the mixture was dry-mixed by hand in a 3 dm³ mixer, and then water was added, and the combination was machine-mixed for 2.5 minutes. Following this, the mortar was hand-mixed for 15 seconds so that no cement remained on the mortar container's wall and then machine-mixed for 45 seconds before being poured into the moulds. 1300 grams of sand, 304 grams of cement, and 201 grams of water were added to a mixture to account for the loss. Concrete with a 20 MPa strength was produced by combining a concrete mix and reinforcing bars.



Figure 3.1. Substances in a mixture

In the study, it was required to determine the rusting percentages of the reinforced concrete. Firstly 4x4x16 cm prismatic specimens were cast for this purpose (Figure 1). The samples were kept in the curing process to be durable for 7 days. The mortar rounds were poured simultaneously to achieve optimal properties. For each level of maturation, three samples were run. Moulds are fabricated using stainless steel. Each of the prism-shaped moulds depicted in Figure 3.1 contains three distinct compartments. Following the 7-days curing period, measurements were performed.



Figure 3.2. 4 x 4 x 16 cm prismatic specimens



Figure 3.3. Reinforced concrete used in testing

4. RESULTS AND DISCUSSIONS

The corrosion inhibition effect of three parts of the RR plant was initially studied for copper and MS. Then, detailed studies were performed for the metal, which is protected better by applying the extracts.

4. 1. Corrosion Protection Ability of *Rheum Ribes* (Işgin) Extracts on Copper

4.1.1. Variation of Open Circuit Potential with Exposure Time

Changes at the metal/solution interface and the initiation and continuation of copper corrosion could all cause E_{ocp-t} variation. These lines could also reveal details about the reaction mechanism or the dominance of anodic or cathodic processes. Before conducting electrochemical measurements, a stable steady-state open circuit condition is also required. As a result, the change in E_{ocp} of Cu during test solution exposure was initially recorded for 1 h. Figure 4.1 shows a graphical representation of this information.

Figure 4.1 shows that the potential of Cu sharply shifts to more negative potentials during the first 80 seconds. This behaviour is responsible for copper dissolution. After about a half-hour, the potential shifts to the positive side and nearly remains constant. Copper passivation is caused by $CuCl_{(k)}$ and other copper corrosion products (Kosec *et al.*, 2007). The addition of the extracts abruptly causes the metal's E_{ocp} to shift into passive regions. This result shows that the molecules of extracts form a surface-protective film that serves as a fundamental physical barrier and prevents the corrosion of Cu by mainly influencing the anodic mechanism after adding the isolate E_{ocp} of the metal shifts to passive regions sharply (Sedik *et al.*, 2020). The potential changes depend on the type of extract, with RRF having the most tolerant and stable potential. These differences could be explained by the difference in the chemical composition of each part of the plant. The potential approaches steady-state conditions in all cases, making electrochemical measurements possible.

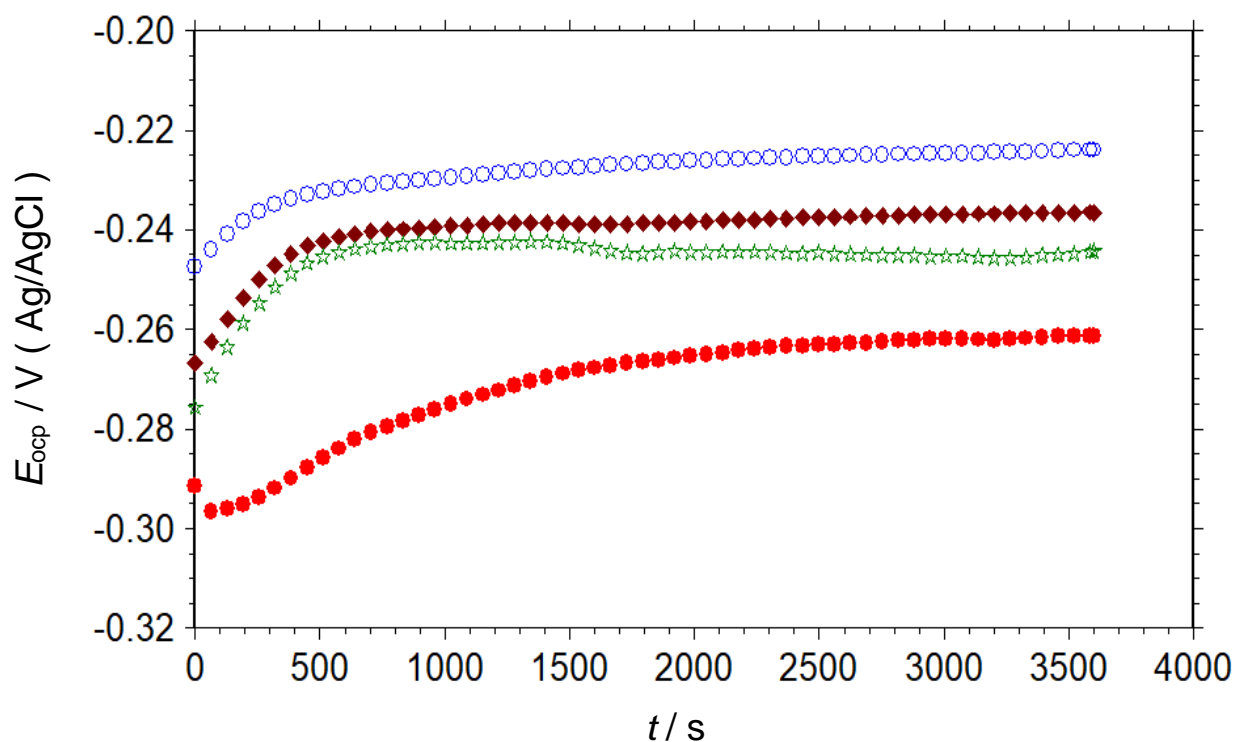
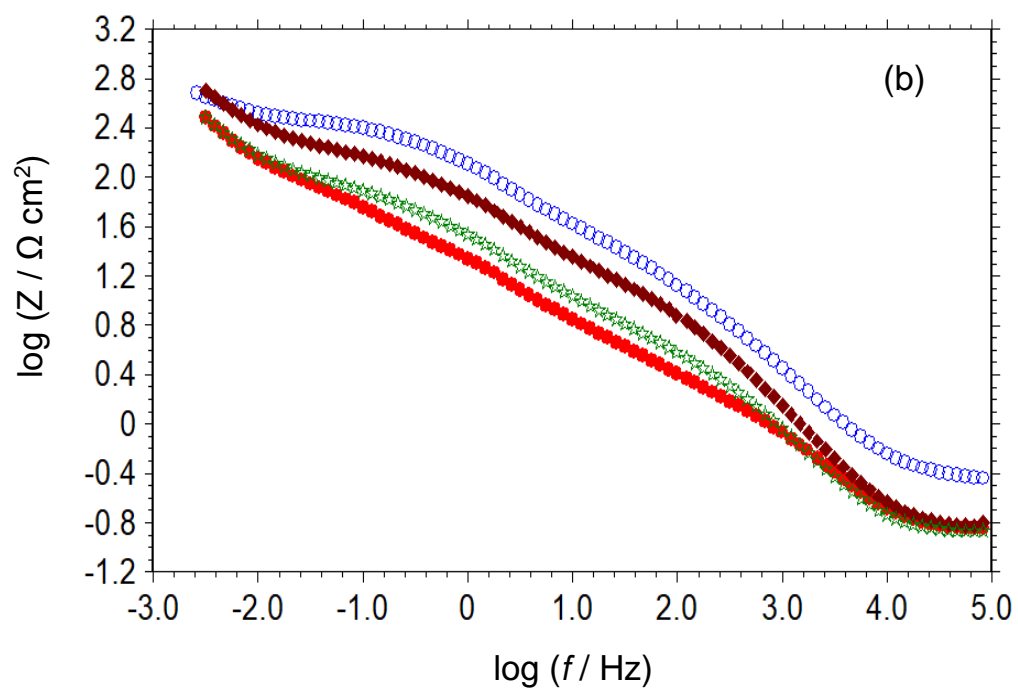
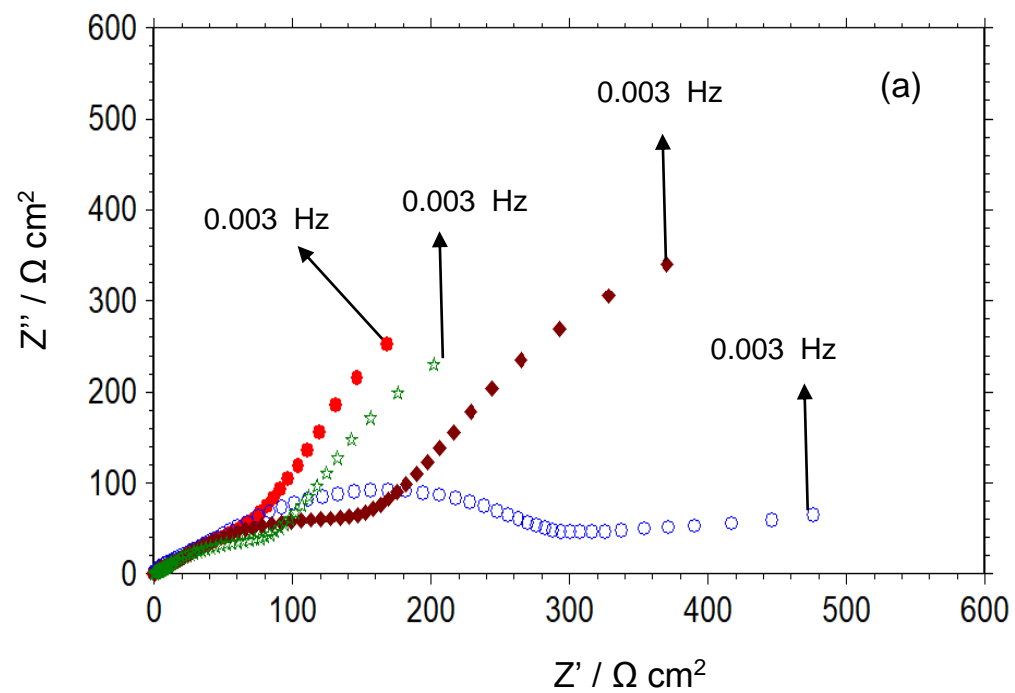


Figure 4.1. The change of open circuit potential of Cu with immersion time in 1 M HCl (●) and containing 1000 ppm RR flower (○), RR leaf (◆), and RR root (☆) solutions

4.1.2. Electrochemical Impedance Spectroscopy

EIS is one of the most effective electrochemical methods available today for studying the behaviour of metal/solution interfaces because it allows for resistance measurement without polarising the surface. In the behaviour of the film-modified metal surface/solution interface, the EIS technique was employed. Figure 4.2 shows related Nyquist and Bode plots of Cu obtained in acidic solutions containing RRF, RRL, and RRR extract. Even though the Nyquist curves (Figure 4.2a) only define two loops, the Bode plots (Figures 4.2b and c) show that three-time constants appeared. When the graphs obtained in uninhibited HCl solution were examined, the high-frequency loop at high frequencies could be attributed to charge transfer and double layer resistance (Rajkumar and Sethuraman, 2016). The resistance of copper chloride species formed on the surface could be assigned to the second middle-frequency one. At low frequencies, a straight line appeared, generally defined as Warburg impedance (Qiang *et al.*, 2018); this is due to the diffusion resistance of corrosive ions such as CuCl_2^- at the metal/solution interface.



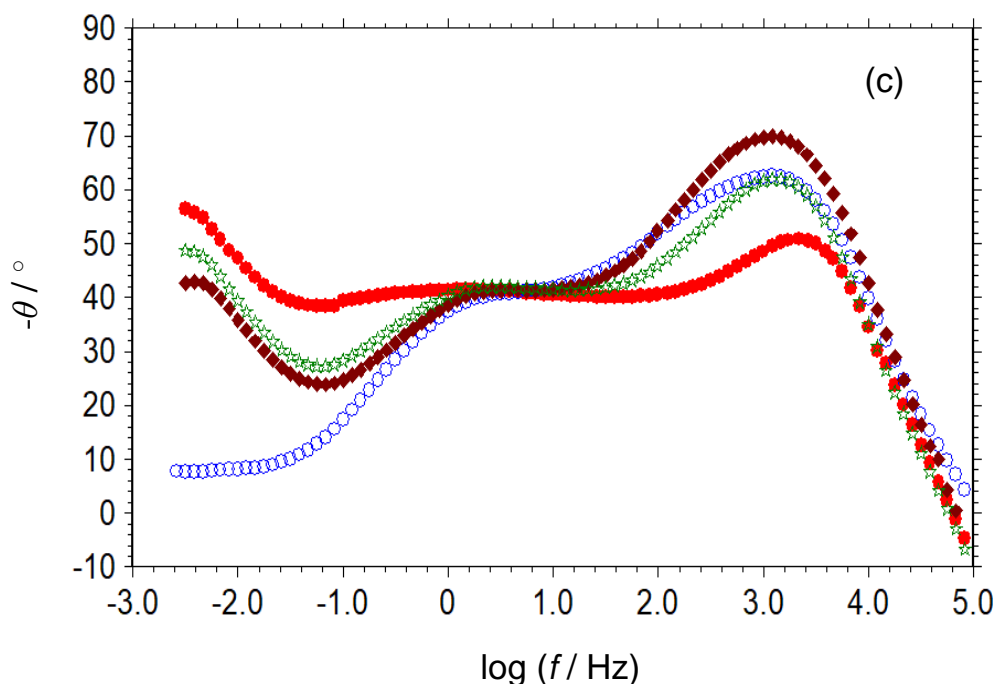


Figure 4.2. The Nyquist (a), $\log Z$ - $\log f$ (b), and phase angle- $\log f$ (c) (Bode) plots of Cu obtained in 1 M HCl solution without (\bullet) and with the addition of 1000 ppm RR flower (\circ), RR leaf (\blacklozenge) and RR root (\star) solutions after 1-hour exposure.

The general behaviour of Cu did not change when the RR extracts were added to a 1 M HCl solution, indicating that the extracts inhibit Cu corrosion without changing the mechanism (Seddik *et al.*, 2020). However, the total number of high and middle-frequency loops increased in the order RRF > RRL > RRR. The increased charge transfer and film resistance suggest that the extract molecules form a protective organic film over the Cu surface [39] and protect Cu from acidic corrosion. High and low frequencies are explained in the same way as 1 M HCl. The middle time constant corresponds to film resistance and could be assigned to film formation at the surface and copper products under the film or film pores. In the presence of the extracts, the angle of the low-frequency line related to the Warburg impedance decreases, reaching its lowest value in the case of RRF. Results could be attributed to forming a compact and adherent film at the surface, which prevents corrosive ions from diffusing (Qiang *et al.*, 2018). Polarization resistance was defined as the total resistance of charge transfer resistance, double layer resistance, film resistance, and resistance to corrosive species accumulation at the surface (R_p). Figure 4.2 shows that the extracts of RRF and RRL inhibit the corrosion rate of Cu and protect it from corrosion. However, the RRR extract could not adequately protect the metal in this acidic solution.

Therefore, it cannot be advised to use this extract. Further research, on the other hand, is required to improve the protection efficiency of RRF or RRL. In the next stage, we intend to strengthen the protection efficiency by incorporating a suitable organic molecule or KI to create a synergy between the extract molecules and the additive. The extracts' protection ability will also be tested in an H₂SO₄ solution because the surface is cleaner in this acid, and more molecules are expected to be adsorbed over the surface and perform better protection. The data presented here are preliminary data from this project. Other studies, such as extract concentration, exposure time, type of corrosive media, and synergistic effect of KI to increase protection efficiency, as well as data analyses by a licensed fitting program, are still going on and will be reported in another study.

4.1.3. Linear Polarization Resistance

The LPR technique was also used to investigate the extracts' corrosion resistance. Current-potential curves were obtained in 1 M HCl solution in the absence and presence of 1000 ppm of each plant extracts for this purpose. Table 4.1 shows the R_p values, and inhibition efficiencies (η) used to generate the data.

Table 4.1. Electrochemical parameters obtained from LPR measurements in 1 M HCl solution in the absence and presence of 1000 ppm R flower, RR leaf, and RR root at 298K

<i>Inhibitor</i>	R_p (Ω cm ²)	η %
1 M HCl	107	
RRF	57.4	60.3
RRL	195	45.1
RRR	112	4.7

The slopes of the $E-i$ curves were used to calculate R_p values, while the following equation was used to calculate η values:

$$\eta = \left(\frac{R'_p - R_p}{R'_p} \right) \times 100 \quad (4.1)$$

In this equation, R'_p and R_p Cu's polarisation resistances in 1 M HCl solution with and without RR extracts, respectively. The LPR results are in perfect accordance with the EIS

data, as shown in Table 4.1. Although RRF and RRL could protect the Cu in 1 M HCl solution, RRR almost does not change the corrosion rate of the metal in these conditions and thus cannot be used as a corrosion inhibitor. RRF provides the best protection capability. The best inhibitor (RRF), whose protection ability will be increased by more than 90% in the following section, will be the subject of additional research, as was previously stated.

The ability of RRF and RRL to protect the metal surface could be attributed to the formation of a protective film of extract molecules on the metal surface. Further research into the adsorbed molecules and protection mechanism is ongoing and will be reported later.

4.1.4. Potentiodynamic Polarization

Semi-logarithmic anodic current potential curves of Cu obtained in 1 M HCl in the absence and presence of the extracts are shown in Figure 4.3.

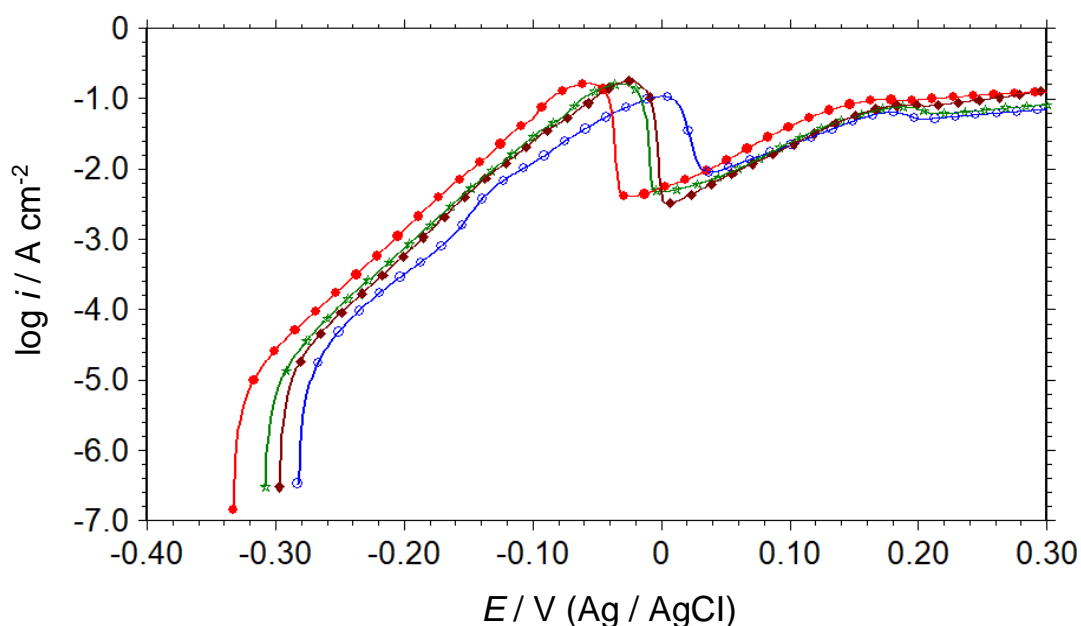


Figure 4.3. Polarization curves of Cu were obtained in 1 M HCl solution without (●) and with the addition of 1000 ppm RR flower (○), RR leaf (◆), and RR root (☆) solutions after 1-hour exposure

As is seen in Figure 4.3, E_{ocp} of Cu in 1 M HCl without the extracts was -0.333 V. When the potential of the metal increases in these conditions, the current density increases sharply due to the dissolution of Cu (Rajkumar and Sethuraman 2016; Qiang *et al.*, 2018).



$\text{CuCl}_{(s)}$ deposits on the surface and diminishes the dissolution rate when the concentration of copper ions on the surface reaches its resolution constant. A passivation peak appears around -0.056 V due to $\text{CuCl}_{(s)}$ formation on the surface[38, 39]. Around -0.03 V , full passivation occurs. Because the $\text{CuCl}_{(s)}$ is not stable at the surface, the current density remains high. By increasing the potential scan to more positive potentials, the current density increases again, resulting in the formation of soluble cuprous complex CuCl_2^- (Qiang *et al.*, 2018; Liao *et al.*, 2011a; Liao *et al.*, 2011b):



The E_{ocp} of Cu shifts toward more positive regions when the RR extracts are added to the corrosive media, and the current densities decrease, which is greater at the RRF. These findings are consistent with the $E_{\text{ocp-t}}$ measurements. Thus, polarisation measurements show that the extracts are mixed-type corrosion inhibitors with a predominantly anodic action (Sedik *et al.*, 2020). The lines are almost parallel around the Tafel region, indicating that the extracts inhibit corrosion without affecting the dissolution mechanism and that the dissolution reaction is controlled by activation. However, as described in the EIS studies, the overall reaction mechanism is diffusion controlled. Surface extract films work by simply blocking (Sedik *et al.*, 2020).

Table 4.2. Electrochemical data derived from polarization measurements obtained in 1 M HCl solution in the absence and presence of 1000 ppm R flower, RR leaf, and RR root at 298K

Inhibitor	E_{ocp} (V)	$i_{-0.2 \text{ V}}$ ($\mu\text{A cm}^{-2}$)
1 M HCl	-0.333	1348
RRF	-0.283	318
RRL	-0.297	592
RRR	-0.308	736

Table 4.2 contains some electrochemical data derived from these curves (More details will be given in subsequent studies). The polarization data in Figure 4.3 and Table 4.2 also show that RRF provides better corrosion protection. However, RRR's protection ability is very

low, making it unsuitable for practical applications. On the other hand, RRF's protection ability needs to be improved for practical applications, and we will conduct additional studies as described above in the following studies.

4.1.5. Surface Characterization Studies

SEM images of Cu exposed to the extract containing HCl solution for 1 h are shown in Figure 4.4. Adsorption of the extract molecules results in forming compact and adherent organic films over the copper in the presence of the isolate. The formed layer is a physical barrier between the corrosive solution and the metal surface. In the case of RRF, the best film is created, which could explain the higher corrosion protection efficiency.

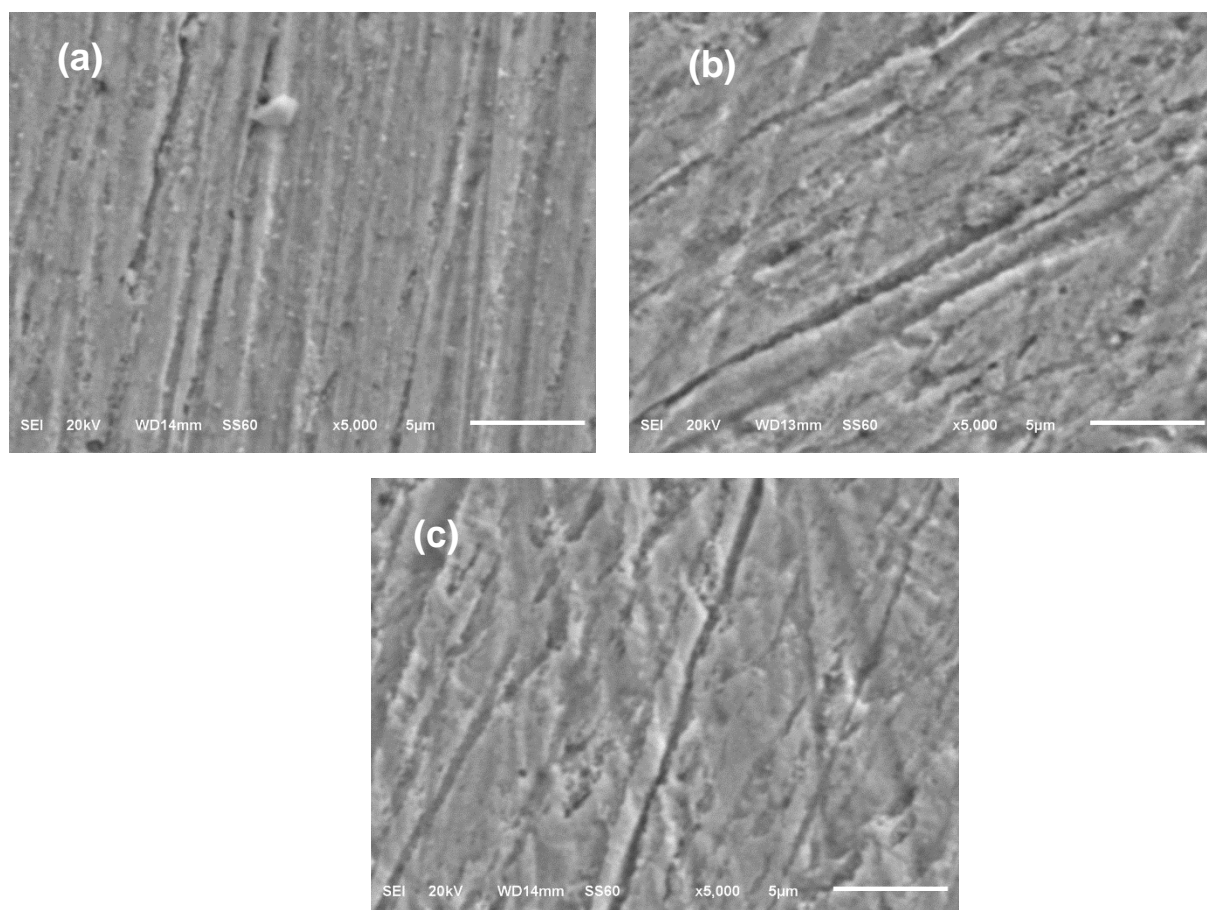


Figure 4.4. SEM images of Cu surface after exposure to 1 M HCl solution in the presence of 1000 ppm RR flower (a), RR leaf (b), and RR root (c)

EDX measurements were used to examine the chemical composition of the same surfaces. Figure 4.5 depicts the obtained data. Because Cu does not contain C, O, S, N, or P, these metals are derived from the surface film formed by the molecules of plant extract. Cl⁻

indicates the formation of CuCl_x species on the bare metal regions under the film or in the film pores. There is no linear relationship between an element's composition and inhibition efficiency, which may be due to differences in the chemical composition of different plant parts.

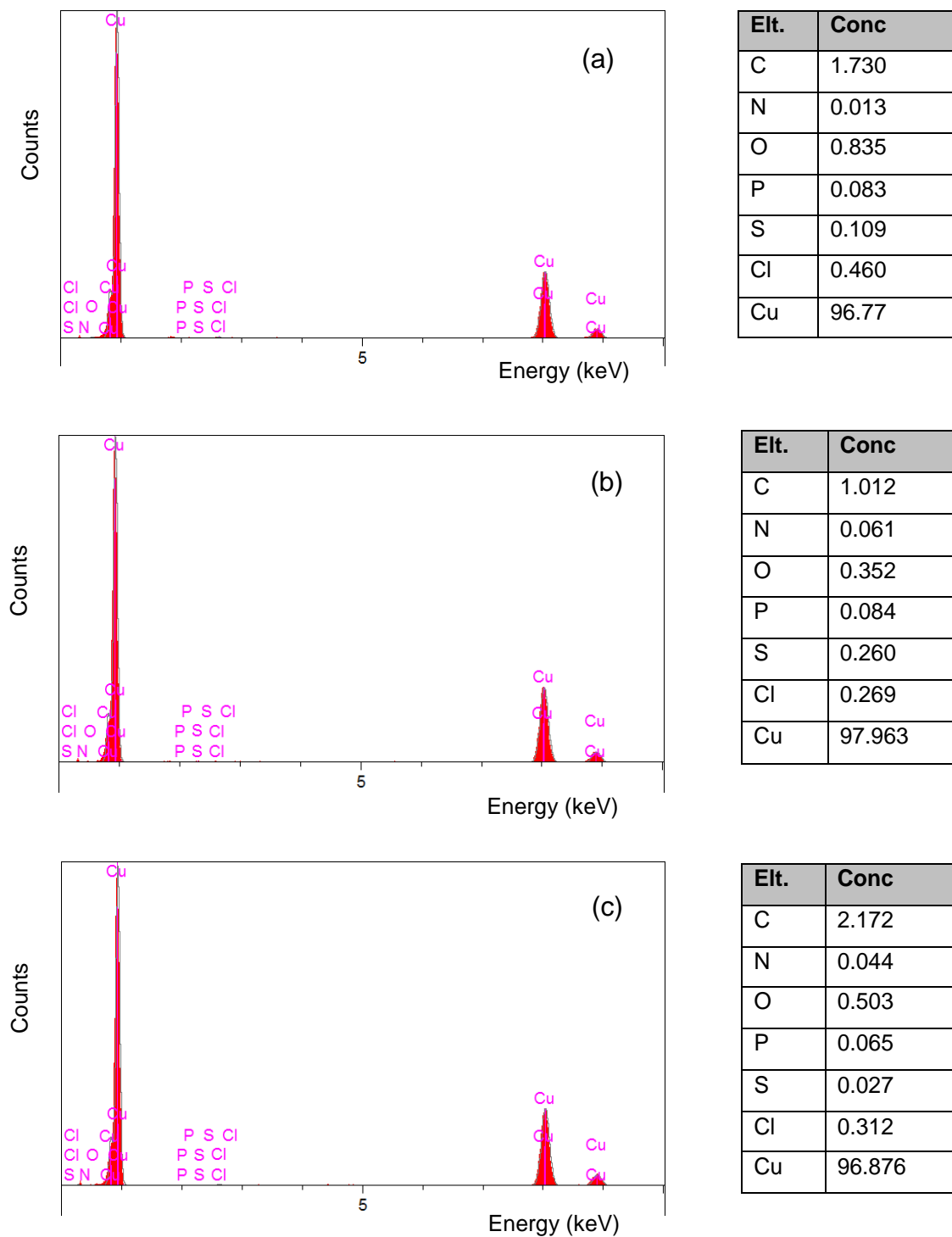


Figure 4.5. EDX spectrums and elemental composition of Cu surface after exposure to 1 M HCl solution in the presence of 1000 ppm RR flower (b), RR leaf (b), and RRroot (c)

Contact angle measurements were used to investigate the hydrophilic or hydrophobic properties of the RRF film formed on the surface, which performed better in terms of protection. The studies of the other isolates films were not completed, even though future studies will only be performed on this extract to improve its protection efficiency. Figure 4.6 demonstrates the obtained data. Since having to add RRF to the corrosive solution, the surface's contact angle increases. The observation implies that the extract molecules are oriented and adsorbed to the surface along with more electronegative sites, and the surface's hydrophobic character tends to increase.



Figure 4.6. Contact angles of Cu surface after exposing to 1 M HCl solution in the absence and presence of 1000 ppm RRflower

4.2. Adsorption and Corrosion Inhibition Capability of *Rheum Ribes* (Işgin) Root Extract for Mild Steel Protection

4.2.1. Variation of Open Circuit Potential with Exposure Time

E_{ocp} changes over time reveal information about the onset and progression of MS corrosion and whether anodic or cathodic processes are more important. It is also widely accepted that accurate electrochemical measurements require a steady-state open circuit (Sığırcık *et al.*, 2016). Initially, the change in E_{ocp} of MS while exposed to the test solutions was measured for 3600 seconds and plotted in Figure 4.7.

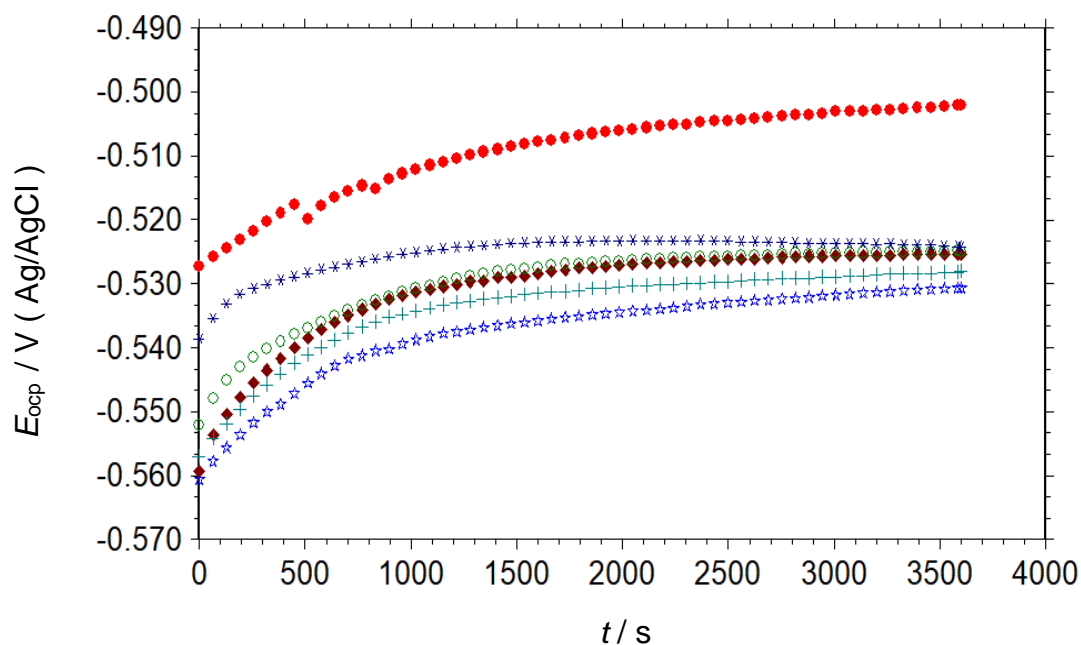


Figure 4.7. The variation of open circuit potential of MS with immersion time in 1 M HCl solution (●) and containing 100 (☆), 250 (+) 500 (◆) 1000 (○), and 2000 (*) ppm RR root extracts

Figure 4.7 indicates that MS has experienced a dramatic shift toward more favorable outcomes. The dissolution and removal of active metals such as Fe in the HCl solution, leaving only nobler metals on the surface, could cause the potential to shift to positive values. The E_{ocp} was unstable the first time it was exposed. The outcome was most likely due to the metal actively dissolving and unsafe surface corrosion products. The potential is roughly the same after 3600 s.

When RR root extract is added to the corrosive solution, the initial E_{ocp} becomes more cathodic when compared to a solution that contains no inhibitors. The plant extract molecules dominate the cathodic reaction more than the anodic reaction. The lowest concentration posed the greatest risk. The values changed from negative to positive as the extract concentration increased from 100 ppm to 2000 ppm. During the first 1000 seconds after placing the electrode in the solution, the metal's E_{ocp} rapidly moves to passive regions. Because the molecules of the extract stick to the surface of the metal in a way that depends on how much RR root extract is in the corrosive medium, the E_{ocp} reaches equilibrium faster. Changes in the E_{ocp} -t curves that no longer occur demonstrate that the inhibitor film is extremely stable in the inhibited HCl solution, particularly at high concentrations. In all cases of inhibited solutions, the potential approaches steady-state conditions, allowing electrochemical measurements. It could also be said that the extract molecules adhere to the surface of the steel and form a protective film, which primarily affects the cathodic reaction.

4.2.2. Electrochemical Impedance Spectroscopy

EIS is a highly sensitive method of characterizing that is used to determine the electrical response of electrochemical systems, such as corrosion, without destroying them. Instead of direct current (DC), EIS systems use low-amplitude alternating current (AC) voltages with a range of frequencies to cause electrochemical reactions in a working electrode and measure the response time of electrochemical systems.

The EIS utilizes AC and does not alter the metal/solution interface; therefore, it has been utilized as a potent tool to accomplish this objective (Salcı *et al.*, 2022). The term "impedance" is synonymous with "resistance," but it can also be used to classify complex circuits with nonlinear current-voltage relationships, such as those with capacitance, inductance, or mass diffusion. The best parts of this theory are combined in EIS. This is accomplished by connecting theoretical circuit elements to real electrochemical processes occurring in materials and by allowing data on current, voltage, and frequency to be altered to match analog circuit models (Url-3, Christie L.C. Ellis *et al.*, 2022).

The dynamic electrochemical behavior of an electrode undergoing electrochemical reactions, according to the EIS principle, influences a variety of things (Paul S. Nnamchi,

et al., 2018). Applying an alternating current potential to an electronic device (such as an electrochemical analyzer), measuring the AC response, and recording phase shifts and amplitude changes over a wide frequency range yield EIS data. EIS results include determining how resistant something is to polarization as well as its resistance to a solution (J. Telegdi *et al.*, 2018) (Paul S. Nnamchi, *et al.*, 2018). The value on the real axis in Nyquist plots indicates that the solution resistance (R_s) is either zero or close to the plot's root. The total resistance to polarization and solution is given by the low-frequency interception of the actual axis. As a result, the polarization resistance equals the half-diameter circle (R_p). The Bode plots show the same data as the Nyquist plots, but they show the frequency-time relationship better (Paul S. Nnamchi, *et al.*, 2018).

The interface between the MS and the solution, as well as the behavior of the surface inhibitor film, were studied using EIS. The experimental results of the Nyquist (a) and Bode (b) curves of MS after 1-hour immersion in a 1 M HCl solution with or without different concentrations of RR root extracts are shown in Figure 4.8 The tests used six different concentrations. However, due to the need for clarity, this figure only shows four concentration data points. When the curves are examined, they appear to be a depressed half-circle that begins in the high-frequency region and ends in the middle-frequency region in both environments with and without inhibitors. Following that, a second inductive loop appeared at low frequencies. The charge transfer resistance (R_{ct}) and double layer resistance (R_d) in the absence of the inhibitor, as well as all other accumulations at the metal/solution interface (R_a), such as corrosion products of inhibitor molecules and metal-organic complexes, are related to the high-frequency and middle-frequency capacitive loops. This loop additionally depicts the film resistance of adsorbed inhibitor molecules in an inhibitor-containing solution (R_f)

The total resistance was dubbed the polarization resistance ($R_p = R_{ct} + R_d + R_a$ in the absence of the inhibitor or $R_p = R_{ct} + R_d + R_f + R_a$ in the presence of the inhibitor). The low-frequency inductive loop could be used to detach or stabilize unattached or unstable products or compounds that have become stuck to the metal/solution interface or relaxation process on the metal surface. (Salcı *et al.*, 2022; Solmaz *et al.*, 2008; Qian *et al.*, 2013; Palomar-Pardavé *et al.*, 2012; Yadav *et al.*, 2012). The addition of RR root extract to a corrosive medium increases the diameter of the capillary loop, and the size of the loop is proportional to the amount of extract. The increase in R_p in this loop indicates that extract molecules are

adhering to the metal/solution interface and that the extract is a good protector (Jokar et al., 2016).

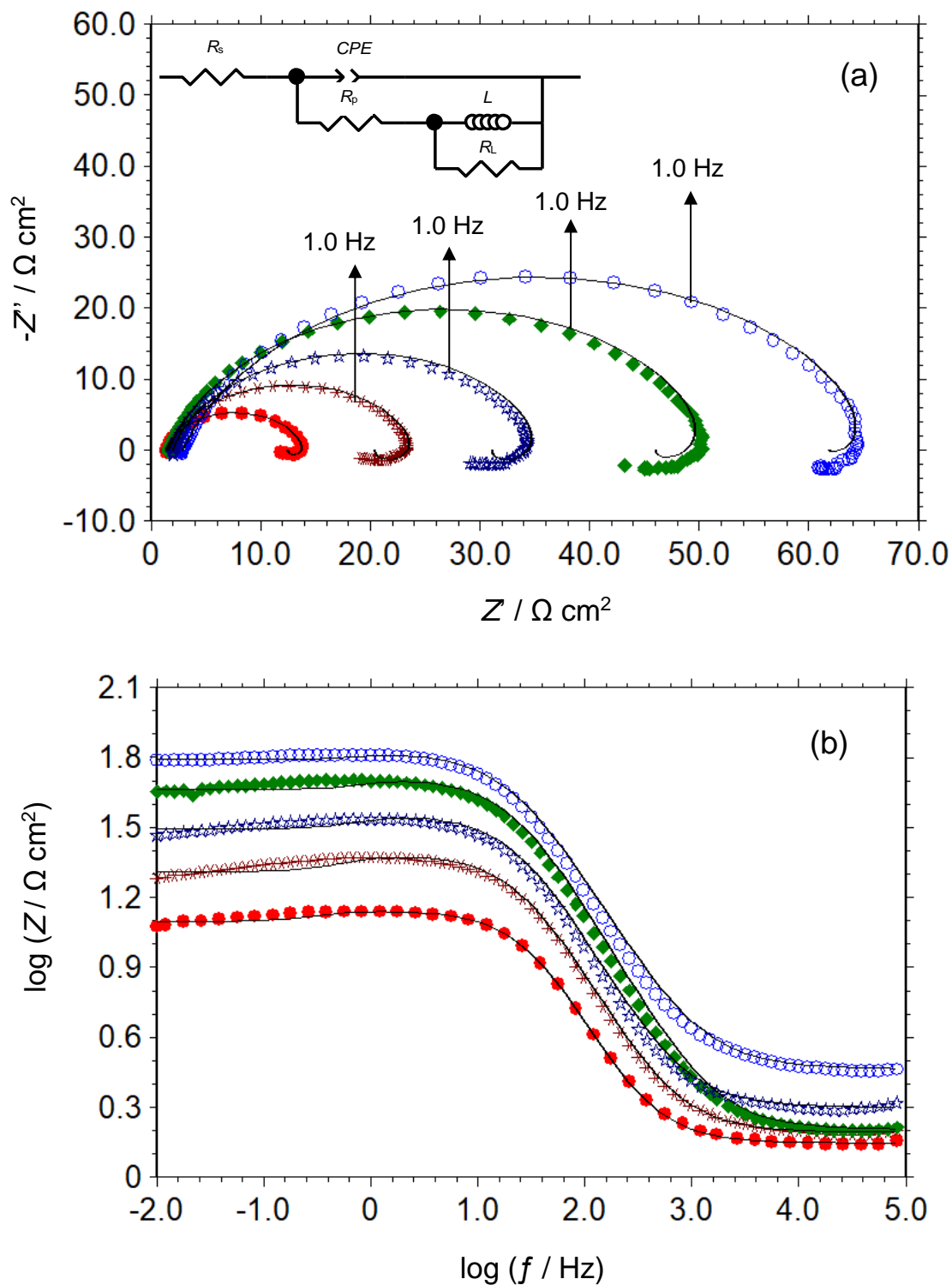


Figure 4.8. The Nyquist (a) and $\log Z$ - $\log f$ (Bode) (b) plots of MS obtained in 1 M HCl solution (\bullet) and containing 100 ($*$), 250 (\star), 500 (\blacklozenge) and 1000 (\circ) ppm RR root extracts. Solid lines show corresponding fitting curves. The inset on Fig. 3a shows the related electrical equivalent circuit diagram

Table 4.3. Electrochemical parameters of MS were determined from EIS data obtained in 1 M HCl solution without and with various concentrations of RR root extract and KI added RR root extract at 298 K

C_{inh} (ppm)	EIS						
	CPE ($10^{-6}/s^n \Omega^{-1} cm^{-2}$)	n	R_p (Ωcm^2)	L	R_L	α	η %
-----	758	0.89	10.80	4.126	1.59	-0.63	-----
100	525.3	0.86	18.9	9.18	3.89	-0.67	42.9
250	377.6	0.88	27.2	15.0	5.04	-0.69	60.3
500	283.9	0.85	44.5	21.04	6.10	-0.73	75.7
750	256.2	0.86	50.6	31.79	4.84	-0.72	78.7
1000	257.5	0.82	59.1	12.72	5.57	-0.69	81.7
2000	260.5	0.83	65.2	65.8	4.43	-0.70	82.7
1000 ppm RR root+ 1000 ppm KI	283.55	0.83	100.4	-----	-----	0.68	89.2

The behavior of real capacitive loops in the real world is not perfect, even though these loops are perfect halves of circles. This is explained by the frequency dispersion of surface inhomogeneity (Solmaz, 2014a; Anejjar *et al.*; 2013; Ehteshamzadeh *et al.*, 2009; Behpour *et al.*, 2010) and the difference in diameters between electrons and inhibitor molecules, as electrons control charge on the metal side of the metal/solution interface, whereas adsorbed molecules control charge on the solution side. Since the total charge of the negatively charged electrons and positively charged molecules that adhere to the surface should be equal, the positively charged molecules on the solution side of the double layer occupy a great deal of space and move toward the solution (Solmaz 2014b; Dehri and Özcan 2006). At frequencies in the middle of their range, the slope of the Bode curves (α) for ideal capacitors is 1 (Yadav *et al.*, 2012; Solmaz 2014b). These values, which range from -0.63 to -0.73, are found in Table 1 and were obtained using Figure 3b. The deviations from ideal behavior are caused by the non-ideal structure of the MS/solution interface (Silva *et al.*, 2021; Solmaz 2014a; Salcı *et al.*, 2022; Solmaz 2014b), which was initially identified for capacitive behavior. A differential capacitance, as opposed to an ideal capacitor (C_{dl}),

forms at the interface between the two layers as a direct consequence of this. This aspect of capacitive behavior was discussed in greater detail previously.

An electrical equivalent circuit diagram (EECD) of the Randle was suggested to be included in Figure 4.9a as an inset (Qian *et al.*, 2013). This decision was made after taking into account the findings from the previous research as well as the observations that were made. In the context of this EECD, the letters R_s stand for solution resistance, CPE for constant phase element, R_p for polarization resistance, L for inductance, and R_L for the resistance of the inductive loop. The results of the process of confirming the data obtained through the experiments to the suggested EECD were processed through a licensed fitting program called ZView Software, and Table 1 presents the outcomes of this procedure. The phase shift is expressed as a degree of deviation from ideality and is represented by the letter n in this table. CPE was used instead of C_{dl} for the fitting analysis to achieve a better fitting, which will be described in more detail below (Goulart *et al.*, 2013; Farag and Hegazy 2013; Tourabi *et al.*, 2013; El Hajjaji *et al.*, 2021);

$$Z_{CPE} = Y_0^{-1}(j\omega)^{-n} \quad (4.5)$$

Y_0 is a proportional factor, $j^2=-1$ is an imaginary number, and ω is the angular frequency expressed in rad^{-1} ($\omega = 2\pi f_{\max}$, f_{\max} is the frequency of which the imaginary component of the impedance is maximal). The following equation was used to determine the percentage corrosion inhibition efficiency (η %) of the root extract:

$$\eta\% = \left(\frac{R_p' - R_p}{R_p'} \right) \times 100 \quad (4.6)$$

Where R_p and R_p' represent the polarization resistance of the MS when it is calculated in a solution of 1 M HCl without and with inhibitor, respectively. R_p is the value that is used when the inhibitor is present.

Table 4.3 is presented all of the electrochemical data that were gathered from the EIS measurements. After the addition of RR root extract, higher R_p and η % values were obtained when the data presented in this Table and Figure 4.9 were analyzed. The

effectiveness of the protection improves as the concentration of the substance being protected rises. After 1000 ppm, however, this trend with increasing concentrations begins to level off. Because of the increased protection efficiency, it can be deduced that extract molecules have been adsorbing at the interface between the metal and the solvent to form a protective film. Higher concentrations were not applied because doing so would have been prohibitively expensive for the practical applications. The value of n is nearly constant; in the presence of a high inhibitor concentration, there is only a slight reduction in comparison to the uninhibited corrosive solution. This may be attributed to the porous structure of the surface film. Following the addition of the inhibitor, CPE values were found to be lower. These values continued to fall as the concentration of RR root extract was increased. This behavior also suggests that extract molecules are adsorbing onto the metal surface, which increases surface coverage and/or the thickness of the inhibitor film at the MS/solution interactivity and decreases capacitance (Policarpi and Spinelli, 2020; Qian *et al.*, 2013; Moradi *et al.*, 2013; Tang *et al.*, 2013; Solmaz 2014b). This is under the Helmholtz model, which is given below (Farang and Hegazy, 2013; Li *et al.*, 2012):

$$C = \frac{\varepsilon^0 \varepsilon S}{d} \quad (4.7)$$

In which " d " is the thickness of the organic film at the double layer, " S " is the area of the metal's surface, and " ε^0 " and " ε " are respectively, the vacuum and environment dielectric constants.

4.2.3. Linear Polarisation Resistance

LPR is an additional electrochemical analytical method that can be used to determine the resistance of electrochemical processes that occur in the metal/solution. This technique involves scanning the potential of the electrode around E_{ocp} between very low cathodic and anodic overpotentials; as a result, there is little polarization on the surface. We were able to determine the R_p of the metal based on the slope of the current-potential curves that we obtained using the equation provided below:

$$R_p = \frac{SdE}{dI} \quad (4.8)$$

In this context, " S " refers to the surface area of the electrode, " E " stands for potential, and " I " stands for current.

R_p of MS obtained in 1 M HCl solution with and without various concentrations of RR root extracts was calculated using LPR measurements. Table 2 shows the outcomes of these calculations. The corresponding η % values were calculated using equation 2 and are shown in the same Table. The data in Table 2 demonstrate unequivocally that the incorporation of the extract increases resistance due to the formation of a protective barrier on the metal's surface, resulting in a significant reduction in the rate at which MS corrodes. It has been discovered that increasing the concentration of the extract increases its protective capacity, and these findings are very consistent with the impedance data obtained at each concentration.

Table 4.4. Electrochemical data of MS determined from LPR measurements obtained in 1 M HCl solution in the absence and presence of various concentrations of RR root extract without and with KI edition at 298 K

C (mM)	R_p (Ω cm ²)	η %
-----	12.35	-----
100	20.3	39.2
250	31.2	60.4
500	48.3	74.4
750	64.1	80.7
1000	69.2	82.2
2000	73.0	83.1
1000 ppm KI	18.2	32.1
1000 ppm RR root+	116.2	89.4
1000 ppm KI		

4.2.4. Potentiodynamic Polarization Curves

Potentiodynamic polarization (PP) is one of the most common methods for measuring DC electrochemical corrosion. The PPs in the test electrode has a wide range of potential,

which generates a sufficient current on the metal surface, mostly oxidizing or reducing the reaction. The potential for each measured point is shown as a function of current density (i) (or $\log i$) to obtain the polarization curve. A polarization curve can be used to determine the metal's corrosion kinetic parameters, such as its corrosion potential (E_{corr}), corrosion current density (i_{corr}), anodic (β_a) or cathodic (β_c), Tafel slopes, weight loss (WL), and so on, under the given conditions. The advantage of this method is that the rate of corrosion and the efficacy of corrosion protection can be determined quickly and locally (J. Telegdi et al.).

Semi-logarithmic PP curves of MS were obtained in a 1 M HCl solution with and without varying concentrations of RR root extract. The results of these experiments are depicted graphically in Figure 4.9. Table 4.7 shows the corrosion parameters derived from these curves, which can also be found in the previous section where they were described. The percentage was calculated using the following equation based on the current density values ($\eta\%$):

$$\% \eta = \left(\frac{i - i'}{i} \right) \times 100 \quad (4.9)$$

" i_{corr} " and " i'_{corr} " are corrosion current densities of MS calculated in 1 M HCl solution without and with extract, respectively. These values were obtained by extrapolating anodic current-potential curves' linear region (around the Tafel region) to their corrosion potential. Theoretically, the values of " WL " were figured out using the equation below (Solmaz 2014a);

$$W = \frac{i_{\text{corr}} \times t \times M}{F} \times 10,000 \quad (4.10)$$

In this equation, " i_{corr} " as described above and its unit was A cm^{-2} , " t " is the corrosion time (s), " M " is the equivalent molar weight of Fe (g mol^{-1}), " F " is Faraday constant (96500 C mol^{-1}), and " $10,000$ " was a constant to convert the unit cm^2 to m^2 .

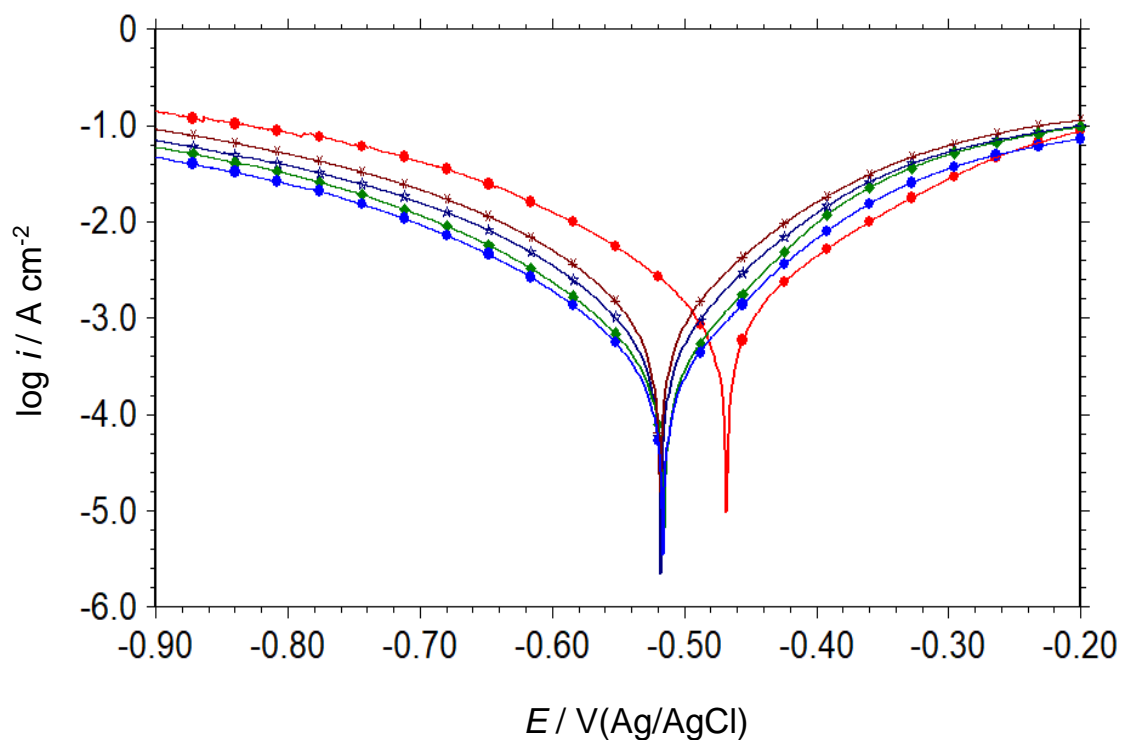


Figure 4.9. Polarization curves of MS obtained in 1 M HCl solution (●) and containing 100 (*), 250 (☆), 500 (◆) and 1000 (○) ppm RR root extracts

Table 4.5. Electrochemical parameters of MS were determined from PP measurements obtained in 1 M HCl solution in the absence and presence of various concentrations of RR root extract, and KI added RR root at 298 K

C_{inh} (ppm)	E_{corr} (V)	i_{corr} (mA cm ⁻²)	β_a (mV dec ⁻¹)	β_c (mV dec ⁻¹)	WL (g m ⁻² h ⁻¹)	η %
----	-0.468	1.1401	118	120	11.88	----
100	-0.518	0.6930	106	121	9.20	39.2
250	-0.518	0.4154	79	116	5.51	63.6
500	-0.515	0.2480	71	118	3.29	78.2
750	-0.518	0.1908	69	114	2.53	83.3
1000	-0.516	0.1768	70	119	2.35	84.5
2000	-0.513	0.1603	67	122	2.13	85.9
1000 ppm RR root+1000 ppm KI	-0.477	0.1240	123	138	1.65	89.1

The E_{corr} of MS in corrosive solution without inhibitors is -0.468 V concerning the Ag/AgCl reference electrode, as shown in Figure 4.9. Beginning with E_{corr} and progressing to anodic or cathodic overpotentials, anodic and cathodic current densities increase, and these reactions are governed by activation. When a corrosive medium is treated with RR root extract, the corrosive medium gains more cathodic potentials, and both the anodic and cathodic current densities decrease. As a result, the extract is a mixed-type corrosion inhibitor that primarily inhibits the reaction of cathodic hydrogen evolution (Policarpi and Spinelli, 2020). The RR root extract, in particular, slows the rate of anodic metal dissolution and the rate of cathodic hydrogen gas evolution.

As the inhibitor concentration increases, the current density decreases, and the effectiveness of the inhibition increases, as shown in Figure 4.9 and Table 4.7. Consequently, the inhibitor may function by forming a surface film of adsorbed inhibitors that acts as a barrier between the metal and the corrosive medium. The rate at the metal corrodes slows down whenever there is a reduction in the density of the current caused by corrosion. The η % has dropped by 85.9% after this time, implying that adding plant extract to a corrosive environment prevents the metal from dissolving and any potential economic losses. The protection is enhanced at higher concentrations, but after 1000 ppm, it does not change significantly.

The cathodic curves in the Tafel region of the uninhibited and inhibited solutions were nearly identical, and the β_c values in Table 4.7 are too close together, implying that the RR root extract slows the rate of cathodic hydrogen evolution without changing the way the reaction works. This result is possible because the surface inhibitor film obstructs light. As a result, the inhibitor is effective if it covers the metal's surface. The surface coverage ($1-\theta$) is nearly full when the concentration is 1000 ppm. Corrosion occurs only on exposed metal parts or through holes in the surface film (Solmaz 2014a). More research into closing these pores or tightening the film may improve its ability to protect. Iodide ions were added to the solution stopped in the previous section. Adding RR root extract, on the other hand, contains the flow of anodic current and reduces β_a by almost 50%. Moreover, the extract alters the way the anodic reaction occurs, preventing it from happening. More investigation is required to comprehend the mechanism fully.

The findings of the experiments conducted by PP are consistent with those obtained by EIS and LPR. All the electrochemical tests demonstrated that the extract's protective ability improved with increasing concentration, but this improvement was minimal at higher concentrations, and 1000 ppm was sufficient. Since more molecules can adhere to the surface when the concentration is high, the surface is better covered. Consequently, more in-depth studies were conducted at 1000 ppm RR root extract, considering the cost of the protection method.

4.2.5. The Synergistic Inhibitory Effect of KI

In acidic solutions, chloride ions typically form a bridge between positively charged metal surfaces and positively charged inhibitor molecules, facilitating the adsorption of inhibitor molecules (Jokar *et al.*, 2016). However, iodide ions are more polarizable than chloride ions and are expected to behave better for this action (Wan *et al.*, 2022; Oulabbas *et al.*, 2022). To increase the inhibition efficacy and stability of the surface inhibitor film, 1000 ppm KI was added to a 1 M HCl solution containing 1000 ppm of RR root extract. The results of repeated E_{ocp-t} , EIS, LPR, and PP analyses for conditions containing equivalent iodide ions are depicted in Figure 4.10.

Figure 4.10a shows how the E_{ocp} of MS changes when 1000 ppm KI is added to a solution that has been inhibited. Furthermore, this is compared to HCl solutions that have neither been inhibited nor not been inhibited. The general trend of iodide ions in the electrolyte is the same as that observed in a 1 M HCl solution containing 1000 ppm of RR root. However, the E_{ocp} shifted toward more positive values than the uninhibited corrosive solution. The steady-state E_{ocp} value observed for this solution was -0.479 V, which was -0.502 V for 1 M HCl and -0.525 V for 1 M HCl+1000 ppm RR root+1000 ppm KI solutions. These findings suggest that iodide ions added to the solution have better surface coverage (Jokar *et al.*, 2016) or a tighter film, resulting in a better physical barrier at the MS/solution interface.

The PP curves of MS in a 1 M HCl solution with 1000 ppm RR root + 1000 ppm KI are shown in Fig. 4.10b. The curves of MS taken in HCl solutions with and without inhibitors are shown on the same graph so they can be compared. This curve was used to calculate the corrosion parameters shown in Table 4.7. When KI is added to a corrosive medium

containing RR root extract, E_{corr} shifts toward more anodic potentials, and the corrosion current density decreases compared to the absence of KI. The plant extract acts as a mixed-type, mostly anodic corrosion inhibitor when iodide ions are present. MS's level of protection in this situation is 90%. In this case, the β_a and β_c values of MS are very close to those found in a 1 M HCl solution. So, when iodide ions are present, the extract prevents MS from corroding without changing the anodic or cathodic reaction mechanisms.

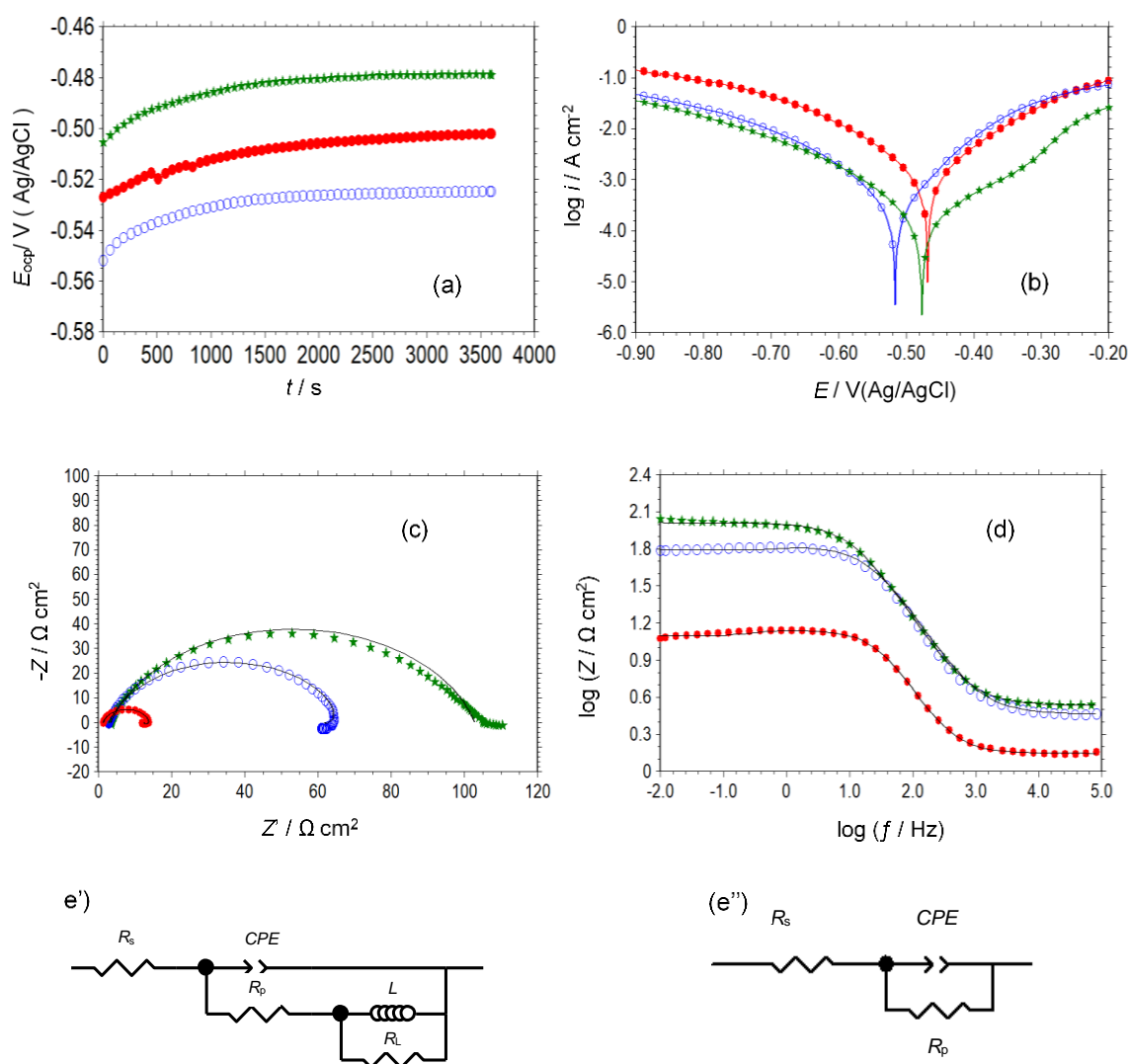


Figure 4.10. The variation of E_{ocp} of MS with immersion time (a); potentiodynamic polarization (b), Nyquist (c), and $\log Z''$ - $\log f$ (Bode) (d) plots of MS obtained in 1 M HCl solution in the absence (●) and containing 1000 ppm RR root (○), 1000 ppm RR root+1000 ppm KI (★); EECDs proposed for the MS/solution interface in 1 M HCl and 1 M HCl+1000 ppm RR root (c'), 1 M HCl+1000 ppm RR root+1000 ppm KI (c'')

Figure 4.10b and 4c portray the Nyquist and Bode plots of MS obtained in a solution of 1 M HCl+1000 ppm RR root+1000 ppm KI. The MS curves obtained in a 1 M HCl solution in the absence and presence of 1000 ppm RR root extract are plotted on the same graph. The EECDs shown in Figure 4.10e' and e'' were used to fit these curves, and the resulting electrochemical data are shown in Table 4.3. The MS plots obtained in iodide-free solutions are displayed on the same figures for comparison. The low-frequency inductive loop vanished in the presence of 1000 ppm KI in the inhibited solution, leaving only a single time constant in the Bode curve. The absence of a low-inductive loop indicates a more stable and compact film at the metal's surface, which may provide improved corrosion resistance. Only one capacitive loop was observed in this medium, indicating that the reaction is activation controlled in the presence of iodide ions (Palomar-Pardavé *et al.*, 2012). Iodide ions aid in extract molecules' adsorption and help stabilize the surface film. Adding KI improves the corrosion resistance and inhibition of the RR root extract.

LPR measurements for the MS electrode were carried out in a 1 M HCl solution inhibited with 1000 ppm KI, and the results are shown in Table 4.4. The same experiments were carried out with 1000 ppm KI in a 1 M HCl solution to compare and investigate the potential synergy between the halogen ions and the extract molecules. Table 4.4 shows that adding KI to 1 M HCl increases resistance, indicating enhanced iodide ion adsorption. However, adding 1000 ppm KI to 1000 ppm RR root extract containing 1 M HCl increases corrosion resistance, which is consistent with EIS results. The protection level reaches 90%, which is sufficient for practical applications.

Two types of adsorption (Aulabbas *et al.*, 2022; Aramaki *et al.*, 1987) mediated the synergistic inhibition effect of halogen ions in acidic solutions: (i) the competitive adsorption of halogen ions and charged organic molecules and (ii) the co-adsorption of halogen ions and charged organic molecules. Halogen ions and charged organic molecules adsorb on separate metal surface sites in (i). Co-adsorption occurs when one molecule adsorbs to the metal surface first, followed by another molecule adsorbing through the first. The following synergistic factor (s) (Khadom *et al.*, 2022; Li *et al.*, 2020) define this process:

$$s = \frac{1-I_{1+2}}{1-I'_{1+2}} \quad (4.11)$$

" I_1 " is the inhibition efficiency of the KI, " I_2 " is the inhibition efficiency of the RR root, and " $I_{1+2} = (I_1 + I_2) - (I_1 I_2)$ " is the inhibition efficiency of the RR root+KI.

If $s=1$, there are no interactions between the halogen ions and the inhibitor molecules, so both types of molecules are adsorbed on the metal surface separately. Competitive adsorption occurs if $s < 1$. Co-adsorption of halogen ions and organic molecules occurs when $s > 1$. This factor was determined to be 1.14 by using the values from Table 4.4. Accordingly, the increased protection ability results from the co-adsorption of iodide ions and charged organic molecules (Oulabbas *et al.*, 2022). Extract molecules may also be adsorbed directly to the metal surface via active adsorption centres such as N, S, and O atoms or multiple bonds. The mechanism of inhibition will be discussed in depth in the following sections.

4.2.6. Studies of Surface Characterization

SEM, AFM, EDX, and contact angle measurements were performed on the MS surface following exposure to inhibited solutions in the absence and presence of KI. Figure 4.11 shows SEM images of the MS surface after 1 hour of exposure to 1 M HCl, 1 M HCl+1000 ppm RR root, and 1 M HCl+1000 ppm RR root+1000 ppm KI are shown.

The MS surface deteriorated considerably due to excessive metal breakdown, as seen in Fig. 4.11a and the enlarged version of the figure in Fig. 4.11b. Pitting corrosion was seen in the steel in this medium, as expected, and the metal damage was not uniform. The surface was significantly altered, and pits and fractures disappeared after adding 1000 ppm RR root extract to a corrosive media (Fig. 4.11c). The molecules of the RR root extract appear to cover and protect the steel's surface. A higher quality, more compact, and virtually equally distributed surface coating formed when 1000 ppm KI was added to an inhibited solution (Fig. 4.11d).

The AFM technique could explore the structures of organic films at the nano- or micro-scale. AFM was used to analyze the design of RR root film produced in 1 M HCl solution in the absence and presence of equivalent KI quantity. Figs. 4.11e and f show 3D dimensional AFM pictures. The AFM data are remarkably similar to the SEM results. Figure 5e displays the appearance of the organic film on the surface. Adding KI to the RR

root-inhibited acidic media results in an improvement in the quality of the surface film and the formation of a more uniform film (Fig. 4.11f). This coating is a barrier between the metal and the corrosive medium and considerably prevents MS deterioration (Jokar et al., 2016).

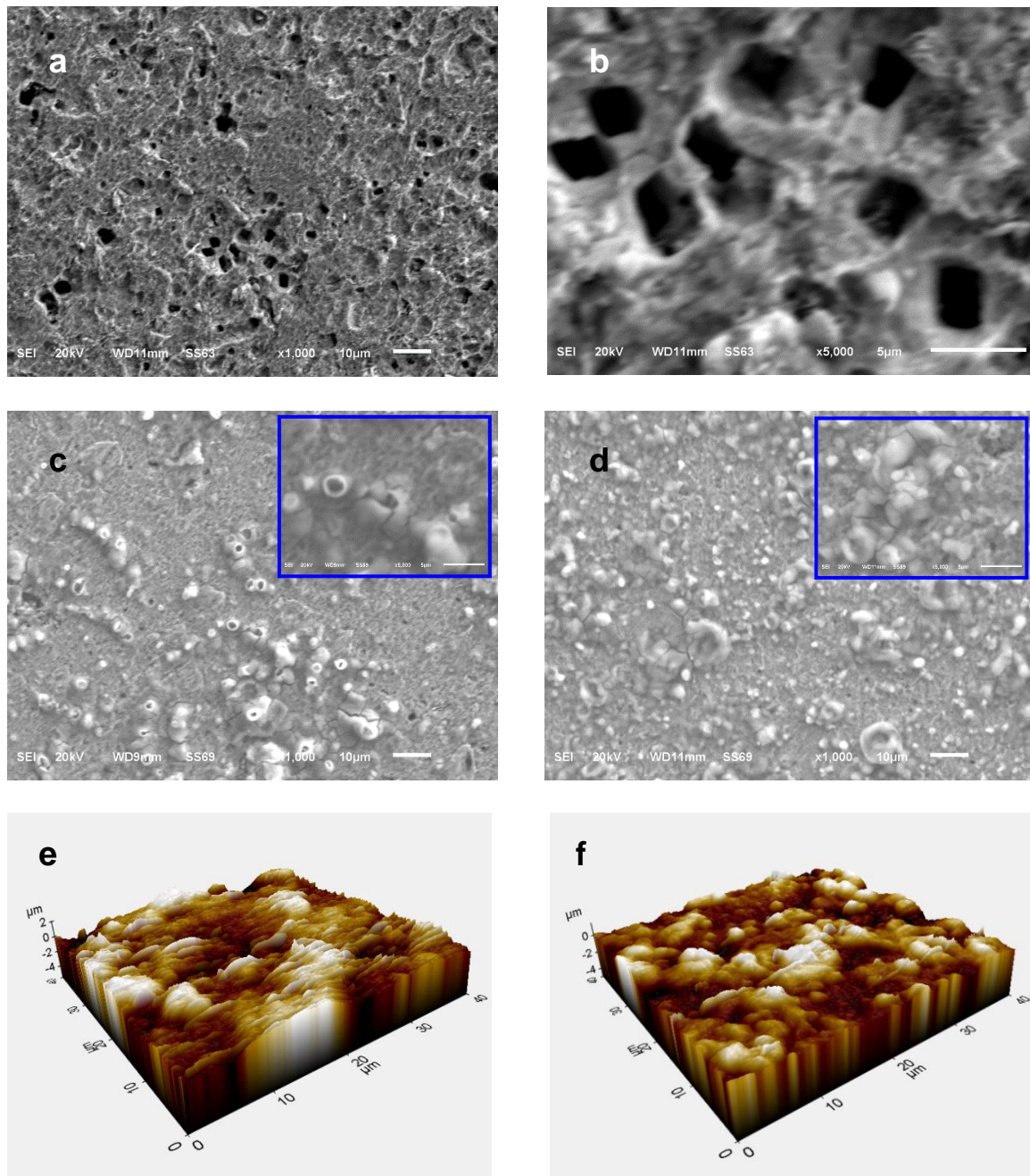


Figure 4.11. SEM images of MS taken after exposure to 1 M HCl (a and b), 1 M HCl+1000 ppm RR root (c) and 1 M HCl+1000 ppm RR root+1000 ppm KI (d) (The insets on c and d show 5 000x magnified images of the same surfaces); 3D dimensional AFM images of MS after exposure to 1 M HCl+1000 ppm RR root (e) and 1 M HCl+1000 ppm RR root+1000 ppm KI (f)

The chemical makeup of the MS sample utilized in this investigation was analyzed and discussed in the experiment. The metal has 1.720% and 0.115% O (the other elements are given in the experiment). EDX was used to evaluate the chemical composition of the inhibited surfaces and the distribution of the extracted film on the steel surface. Figures 4.12 and 4.13 show the EDX spectra of the MS surface, the distribution of some elements on the metal (EDX-mapping images), and cross-sectional analysis of some elements on the MS surface after exposure to 1 M HCl solution in the presence of 1000 ppm RR root and 1000 ppm RR root+1000 ppm KI. The EDX spectra presented in Figures 4.12 and 4.13 demonstrate the presence of a thick coating on the steel. The gathered data indicate the production of a surface layer consisting of hetero compounds, including C, N, O, and S, which are considered active adsorption sites. Cl is also found in two cases. Since the MS contains lower concentrations of C and O (1.720% and 0.115% O, section 2.1), RR root extract molecules should possess a higher concentration of these elements.

Additionally, the presence of N and S components, absent in MS, lends weight to this hypothesis. The presence of Cl results from the adsorption of chloride ions from a 1 M HCl solution and the formation of adsorbed species or corrosion products such as FeCl_{ads} or FeCl_2 under the film or in exposed areas. In the presence or absence of KI, the quantities C, N, O, and S detected on the surface of MS do not have a linear relationship (Figures 4.12 and 4.13). Different ratios or concentrations of extract molecules adsorb on the metal surface in the presence or absence of KI.

In contrast, the addition of KI causes a reduction in the quantity of these components, which may indicate that fewer molecules are adsorbed and that the surface develops a coating that is thinner but more protective as a result of the process. After adding KI to the inhibited HCl solution, the I element shows in the EDX spectrum. Additional tests demonstrate this element's adsorption, which increases extract molecule adsorption on the steel surface. A cross-sectional study reveals the presence of a homogeneous surface coating, which is improved in the fact of KI.

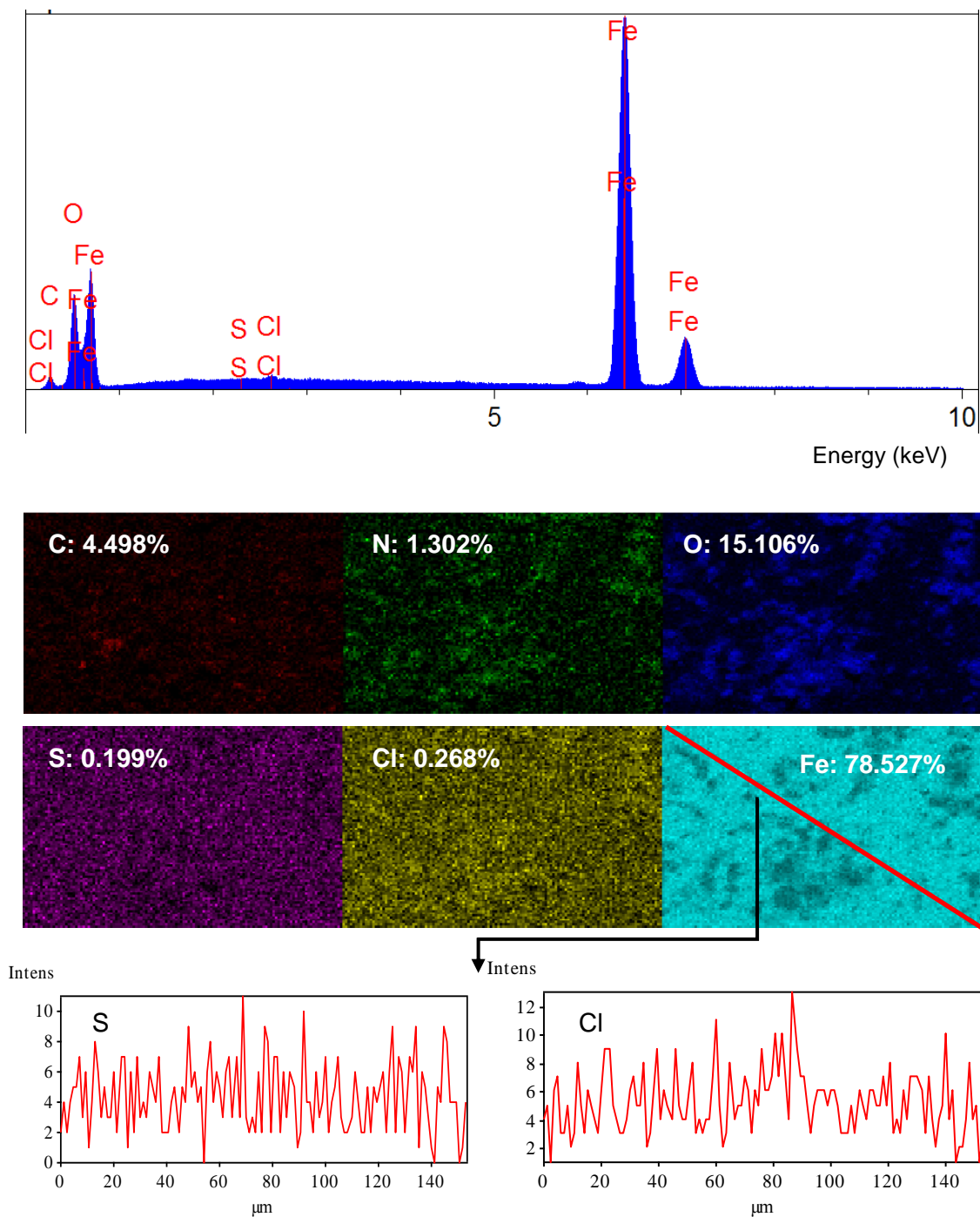


Figure. 4.12. EDX spectrum of the MS surface, the distribution of some elements on the metal surface (EDX-mapping images) and cross-sectional analyses of some elements on the surface of MS after exposure to 1 M HCl solution in the presence of 1000 ppm RR root for 1 hour

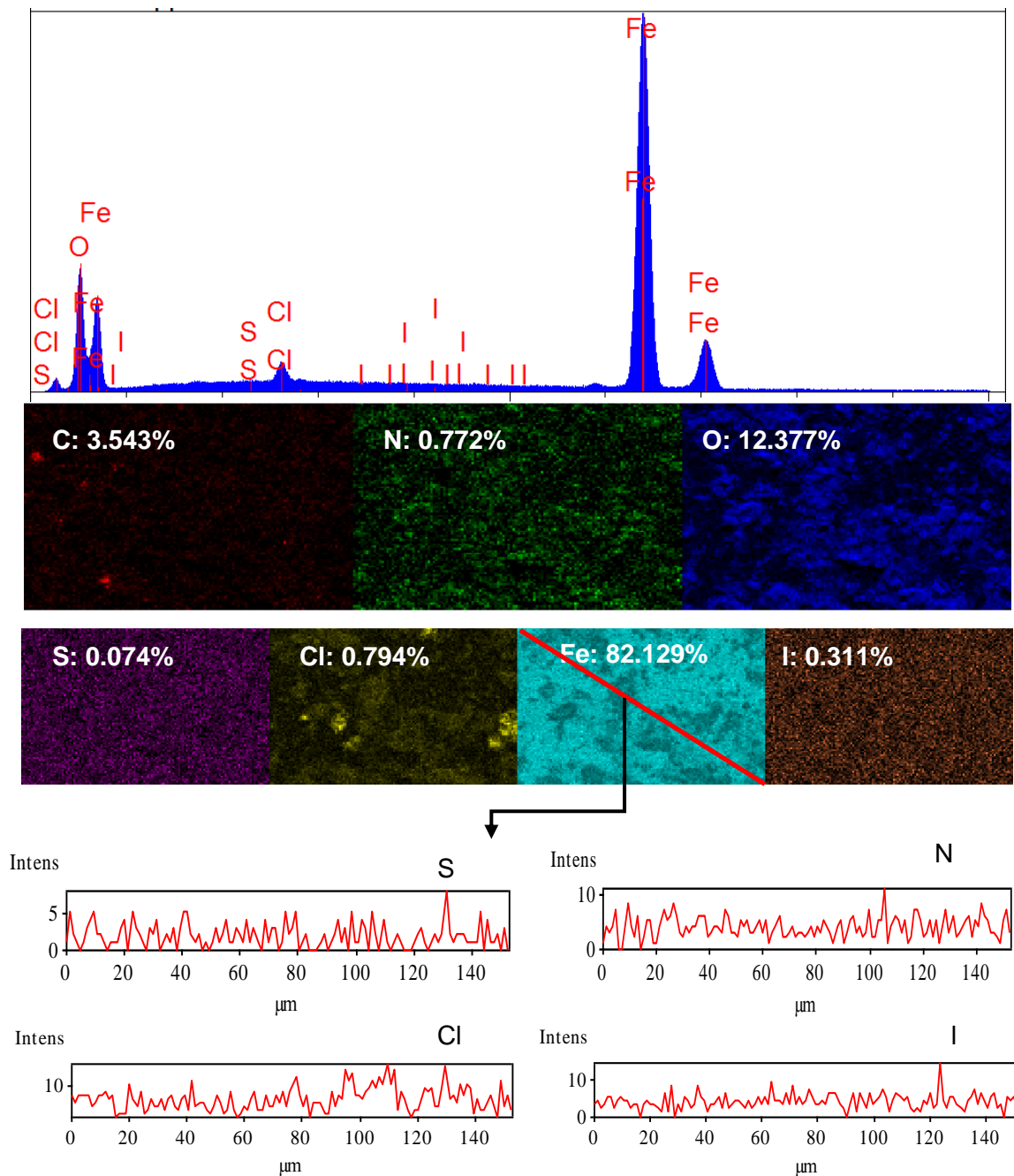


Figure 4.13. EDX spectrum of the MS surface, the distribution of some elements on the metal surface (EDX-mapping images) and cross-sectional analyses of some elements on the surface of MS after exposure to 1 M HCl solution in the presence of 1000 ppm RR root+1000 ppm KI

Surface properties, such as hydrophilic or hydrophobic features, provide critical information on the orientation of adsorbed molecules and the interaction of corrosive species with the surface or their passage through the film. One potential way to attain this goal is to measure contact angles (Moradi and Attar, 2014; Singh *et al.*, 2015; Zhnag *et al.*, 2016). Contact angle images of the MS surface after 1 hour of exposure to a 1 M HCl solution with and without the addition of 1000 ppm RR root and 1000 ppm RR root+1000 ppm KI are shown in Figure 4.14.

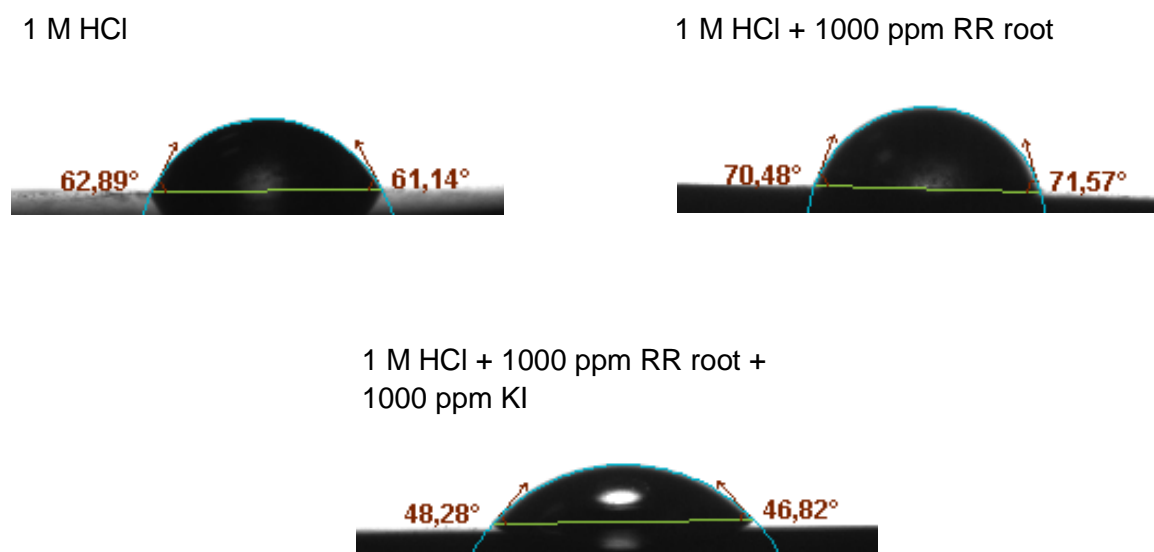


Figure 4.14. Contact angle images of the MS surface after exposure to 1 M HCl, 1 M HCl + 1000 ppm RR root and 1 M HCl + 1000 ppm RR root + 1000 ppm KI solutions for 1 hour

In the unconstrained solution, the average contact angle of the steel is 62.01°. In the presence of the RR root extract, the average contact angle rises to 71.03°. This value is less than 90°, indicating that the film is hydrophilic. The contact angles produced a considerable change in angles, showing that the molecule adsorbed by the steel surface formed a less hydrophilic coating than the unmanaged solution. When iodide ions are introduced to an inhibited solution, the contact angle reduces to an average of 47.55°. This finding could be explained by a change in the orientation of the molecules and the coating of the surface with negatively charged iodide and chloride ions, specifically on the exposed surface sites harbouring the inhibitor molecules.

4.2.7. Mechanism of Adsorption and Inhibition Process

Organic compounds decrease corrosion by clinging to metallic surfaces; Their absorption capacity is primarily responsible for their protective function. Adsorption is affected by the metal's surface charge structure, the chemical structure of organic molecules, the presence of active adsorption centres such as N, S, O, or multiple bonds, the kind and concentration of molecules, and so on. Adsorption isotherms can be used to investigate the interactions of adsorbed molecules with one another and the metal surface. The surface coverage values (θ , $\theta = \eta\%/100$) for each concentration of RR root extract were calculated and used to assess the extract's ideal isotherm. Several models were tried for this purpose, with the Langmuir adsorption isotherm providing the greatest fit, as shown in Figure 4.15.

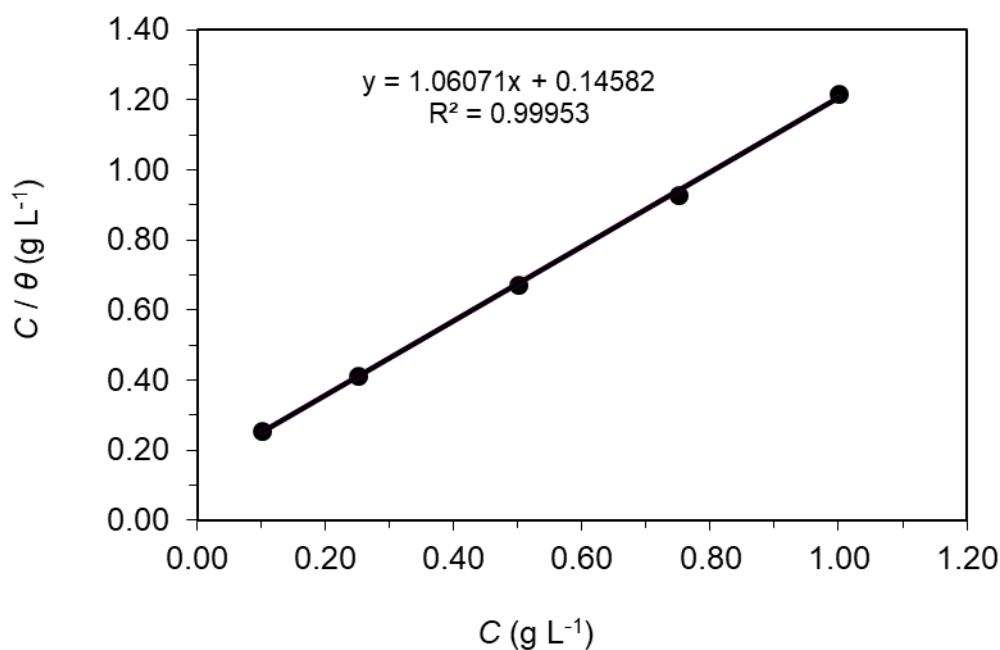


Figure 4.15 Langmuir adsorption plot of MS obtained in 1 M HCl solution with the addition of various concentrations of RR root extract

The following equation describes this isotherm:

$$\frac{C_{(inh)}}{\theta} = \frac{1}{K_{(ads)}} + C_{(inh)} \quad (4.12)$$

The unit of C in this equation is g L^{-1} (Policarpi and Spinelli, 2020), and the equilibrium constant for the adsorption-desorption process is K_{ads} .

This assumption is supported by the fact that the correlation coefficient constant, R^2 , is fairly high (0.99953) and close to 1. Therefore, we hypothesize that RR root extract molecules adsorb on specific sites of the metal and produce a uniform monolayer coating (Shahmoradi *et al.*, 2021; Oulabbas *et al.*, 2022). The slope of this plot is 1.08, which indicates that the molecules occupy 1.06 sites of the MS surface instead of 1 (Fan *et al.*, 2011). The value of K_{ads} was derived from Eq. (4.12), and Fig. 9 is 6.86 L g^{-1} , indicating a good adsorption ability and stability of the extract molecules on the metal surface (Policarpi and Spinelli, 2020). The value of K_{ads} demonstrates that the extract molecules have a high capacity for adsorption on the metal surface. This information also indicates that the adsorption of extract molecules is preferable to their desorption (Goulart *et al.*, 2013).

The standard free energy of adsorption ($\Delta G^{\circ}_{\text{ads}}$) computed using the following equation can reveal the kind of adsorption (Jokar *et al.*, 2016).

$$\Delta G^{\circ}_{\text{ads}} = -RT \ln(C_{\text{H}_2\text{O}} K_{\text{ads}}) \quad (4.13)$$

whereby $C_{\text{H}_2\text{O}} = 1000 \text{ g L}^{-1}$ is present in the solution at a concentration of 1000 g L^{-1} (Odewunmi *et al.*, 2015; Pham *et al.*, 2022). By applying this equation, we could determine that the value of $\Delta G^{\circ}_{\text{ads}}$ is equal to $-21.9 \text{ kJ mol}^{-1}$. The value of $\Delta G^{\circ}_{\text{ads}}$ is negative, suggesting that the molecules of RR root extract self-adsorb onto the MS surface since all organic inhibitors are self-adsorbed on the metal surface in this case.

Suppose the numerical value of $\Delta G^{\circ}_{\text{ads}}$ is larger than -40 kJ mol^{-1} . In that case, the chemical adsorption process is dominant, whereas the physical adsorption process is assumed to be dominant if the value is less than -20 kJ mol^{-1} (Hajjaji *et al.*, 2021). If the value of $\Delta G^{\circ}_{\text{ads}}$ falls between these two extremes, two distinct adsorption processes may occur. However, we must emphasize that the adsorption of organic molecules on the surface of the metal cannot be classified as totally chemical or purely physical because, in most circumstances, a combination of the two processes occurs (Solmaz 2014a). The $\Delta G^{\circ}_{\text{ads}}$ value of RR root extract is midway between these two values but is more closely

related to a value of -20 kJ mol^{-1} . As a result, RR root extract adsorption occurs due to chemical and physical interactions, with the first interactions primacy.

The initial step in the adsorption of organic molecules is their physical interactions with the electrode surface. Physical interactions occur directly between molecules and surfaces via weak interactions such as dipole-dipole. In addition to physisorption, further chemical reactions are also possible (Figure 4.16, a and b). Charge sharing occurs between metal d orbitals and free electron pairs of adsorption active centers, such as N, S, and O atoms, as well as electrons of double or triple bonds in organic molecules, to produce chemical interaction (Figure 16, a and b) (Haldhar et al., 2021).

In highly acidic solutions, many organic compounds can be found in equilibrium with their protonated analogues. Iodide ions and positively charged inhibitor chemicals interact synergistically, as explained in Section 4.2.4. Iodide and chloride ions that are more polarizable adsorb on the metal's surface, making the solution site of the double layer negative. These species are then capable of adsorbing protonated inhibitor molecules. Halogen ions, in particular, operate as linking bridges (Figure 16, b, and c). Fig. 10 illustrates these relationships graphically. Physical interactions between extract molecule components are always possible.

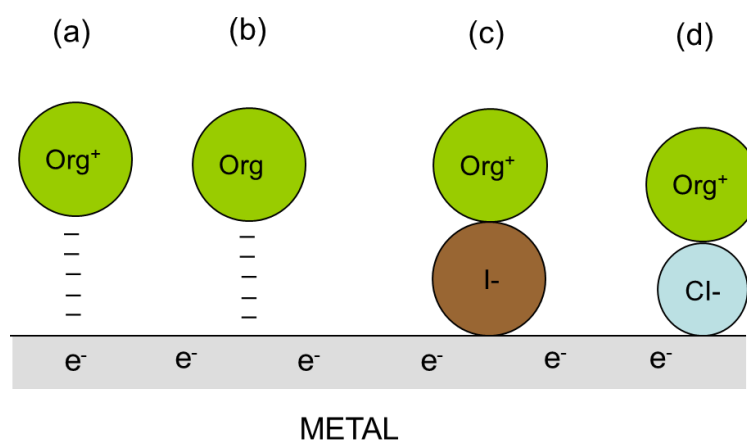


Figure 4.16. Schematic presentation of interactions between organic molecules of extract and metal surface

4.2.8. Stability of Surface Inhibitor Film

As explained in previous sections, organic molecules operate as corrosion inhibitors by adsorbing and producing a surface organic coating. The electrochemical stability of this film is necessary for practical applications, as most organic inhibitors lose their ability to protect the metal surface upon removing the protective coating. Consequently, CA and CV techniques were used to investigate the durability of the surface film generated on MS.

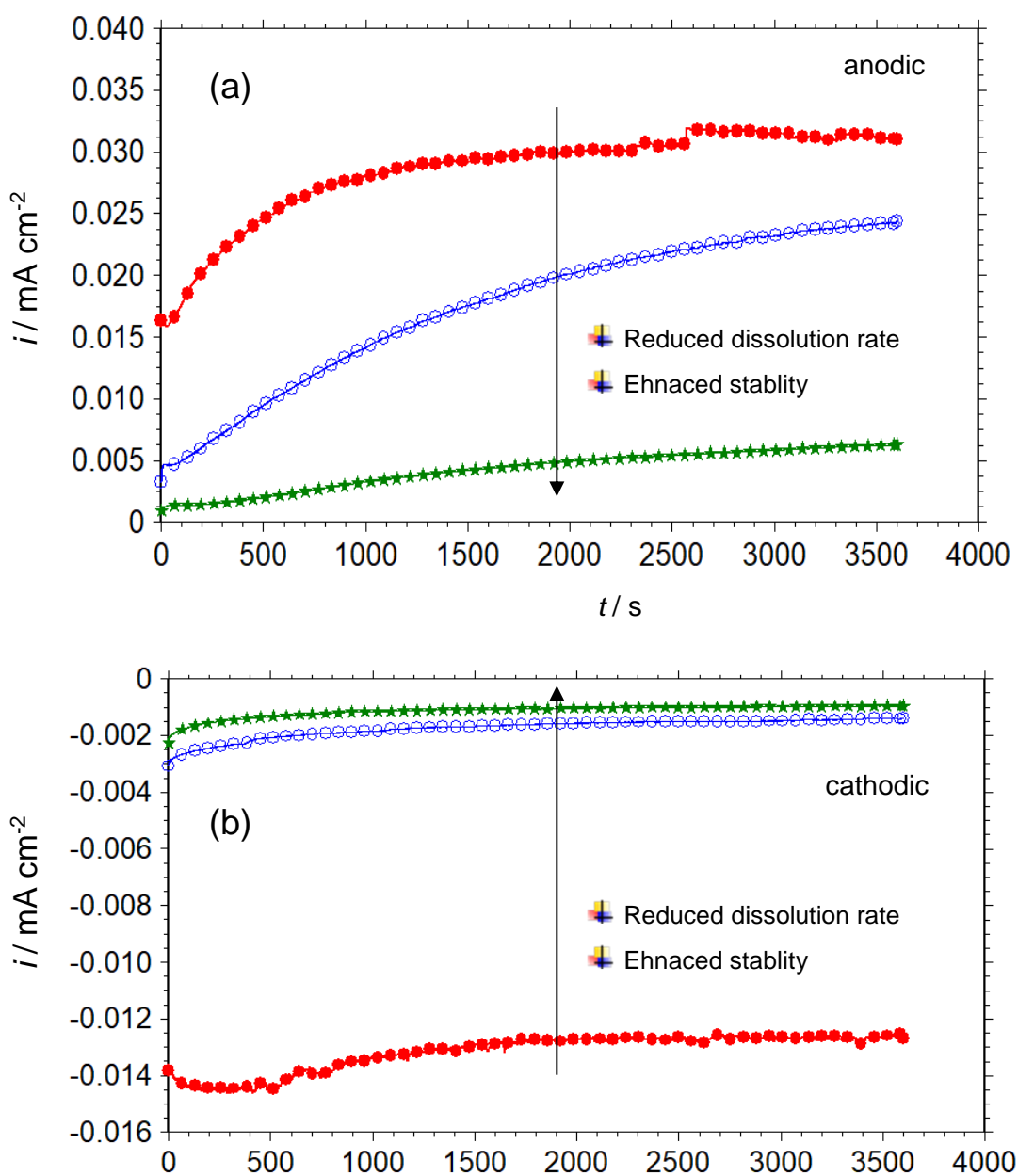


Figure 4.17. The variation of anodic and the cathodic current densities as a function of time under constant +100 mV anodic (a) and -100 mV cathodic (b) overpotentials conducted in 1 M HCl solution (●) and containing 1000 ppm RR root (○), 1000 ppm RR root+1000 ppm KI (★)

Figure 4.17 shows the fluctuation of anodic and cathodic current densities as a function of operation time under constant +100 mV anodic or -100 mV cathodic potentials obtained in 1 M HCl solution and containing 1000 ppm RR root or 1000 ppm RR root+1000 ppm KI can be shown. These results were achieved in an electrolyte containing 1000 ppm RR root.

The anodic current density recorded in a solution containing 1 M HCl showed a rapid increase as electrolysis began. Then it becomes almost constant after 1000 seconds, as shown in Figure 4.17a. This pattern continues until the electrolysis is complete. The abrupt increase in current density observed could be attributed to the excessive dissolution of MS in this aggressive solution. After the rate of disintegration has stabilized, the current remains constant despite periodic fluctuations. Under these conditions, the cathodic current density usually always remains constant, despite rare variations produced by the production of surplus hydrogen gas and the formation of gas bubbles on the electrode surface (Figure 4.17b)

Due to the adsorption of inhibitor molecules on the metal surface, adding 1000 ppm RR root extract to the corrosive solution decreases early anodic or cathodic current densities. Nevertheless, the anodic current density continuously increases during electrolysis. This observation suggests that the RR root extract film is not individually stable. The rise in current density results from the excessive dissolution of metal beneath the coating, which removes or degrades it from the surface. This film, however, is extremely stable under cathodic overpotentials; the cathodic current density is extremely low and more durable than that reported in 1 M HCl.

Following the incorporation of 1000 ppm KI into the inhibited solution, there was a discernible shift in the behaviour of the surface film. Initial anodic and cathodic current densities are both lower and rather stable throughout the electrolysis period, indicating a highly long-lasting surface coating (Sığırcık *et al.*, 2016). This observation suggests that the surface coating is an effective barrier against anodic metal dissolution and cathodic hydrogen evolution processes. In this state, the film adheres tightly to the MS surface and does not detach from it.

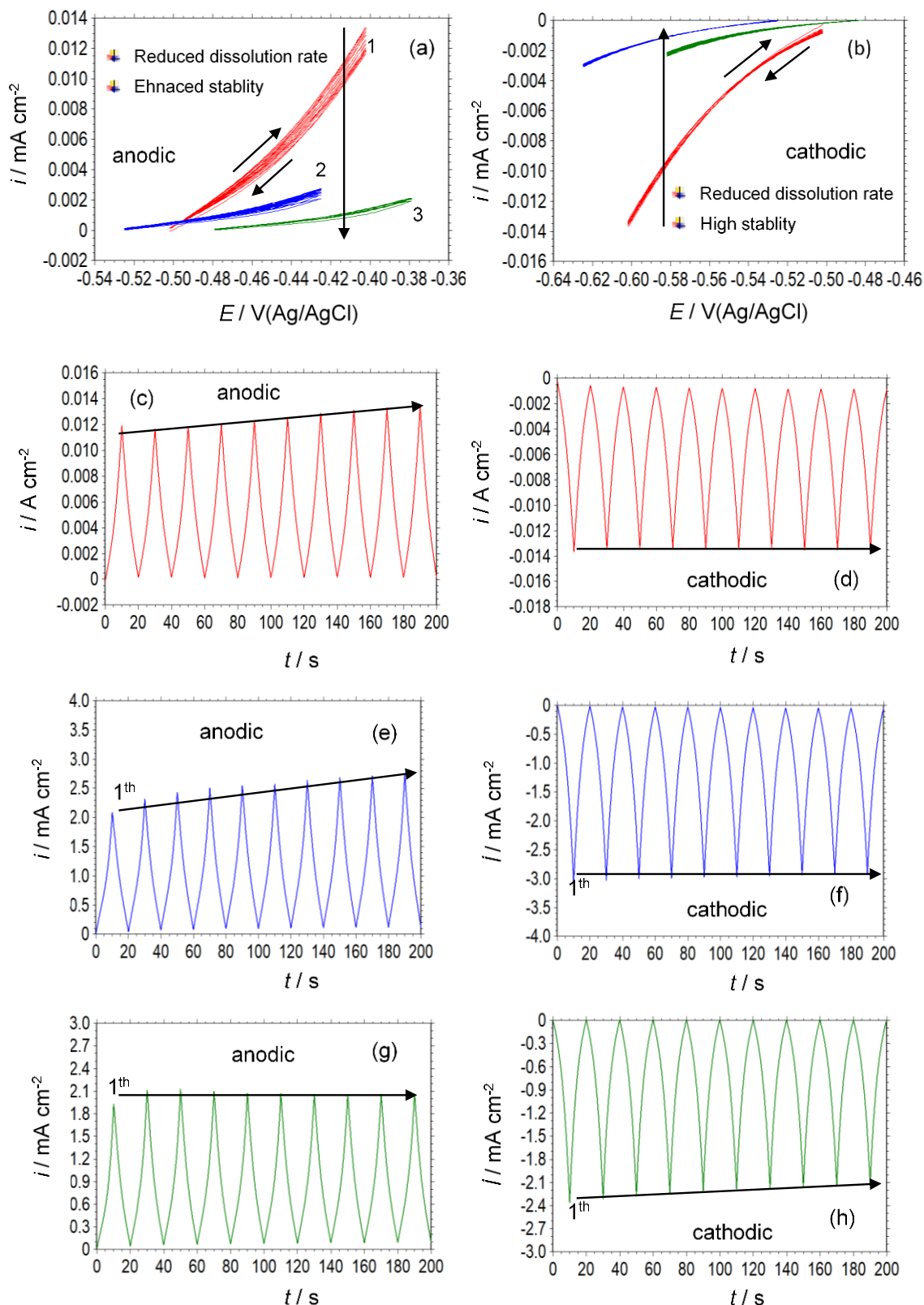


Figure 4.18. Anodic (a) and cathodic (b) CVs of MS obtained in the test solutions (1: 1 M HCl, 2: 1 M HCl+1000 ppm RR root, 3: 1 M HCl+1000 ppm RR root+1000 ppm KI); Anodic CV-time plots of MS obtained in 1 M HCl (c), 1 M HCl+1000 ppm RR root (e), 1 M HCl+1000 ppm RR root+1000 ppm KI (g); Cathodic CV-time plots of MS obtained in 1 M HCl (d), 1 M HCl+1000 ppm RR root (f), 1 M HCl+1000 ppm RR root+1000 ppm KI (h)

The CV approach was also used to test the film's stability under various dynamic situations. The anodic and cathodic CVs and CV-time plots of MS in 1 M HCl, 1 M HCl+1000 ppm RR root, and 1 M HCl+1000 ppm RR root+1000 ppm KI. Voltamograms were recorded between E_{ocp} and 100 mV anodic or cathodic overpotentials. There were 20 segments (10 complete cycles) applied. The obtained data and information can be found in Figure 4.18.

CA and CV outcomes are extremely compatible. The anodic current density increases somewhat as the number of cycles increases due to the active dissolving of the metal, as indicated by the anodic CVs (Figure 4.18a) and anodic CV-time plots (Figure 4.18c) of MS generated in the absence of an inhibitor. In the presence of 1000 ppm RR root extract, a similar pattern was seen with lower current density (Figure 4.18a and e). However, after adding 1000 ppm KI to the inhibited solution, the CV (Figure 4.18a) and CV-time (Figure 4.18g) curves showed highly consistent anodic current densities, showing that the film on the MS surface is also very stable under anodic potential scan. In 1 M HCl and 1000 ppm RR root solutions containing HCl, the MS cathodic current density is essentially constant (Figure 4.18b, d and f). However, the inhibited solution has a lower current density than the uninhibited solution. In the presence of iodide ions, however, there was greater stability and lower cathodic current density, and the cathodic current density declined as the number of cycling increased (Figure 4.18h).

4.2.9. A Summary Literature Survey on Root Extracts of Plants

Recently, many plant extracts have been studied as natural corrosion inhibitors for protecting metals. For example, at 500 mg/L, *Sida cordifolia* has an inhibition efficiency of 98.83% (Saxena *et al.*, 2018a). *Butea monosperma* restricts at 500 mg/L with a 98% efficiency L (Saxena *et al.*, 2017), *Cuscuta reflexa* hinders at 500 mg/L with a 95% efficiency (Saxena *et al.*, Haldhar, 2018b), *Murraya koenigii* impedes at 600 mg/L with a 96% efficiency (Quraishi *et al.*, 2010), *Radish fruits* inhibit at 100,000 mg/L with a 79% efficiency (Noor, 2011), and *Kola nitida* prevents at 1200 mg/L with a 78% efficiency (Njoku *et al.*, 2016) have been reported.

Ji *et al.* (2016) reported an inhibition effect of *Argemone mexicana* root extracts for MS protection; they also discovered that the extracts protect MS from corrosion; this protection

was found to increase with the concentration of the isolate in the corrosive solution. The adsorption of this extract follows the Langmuir isotherm onto the MS surface. Adsorption of the plant parts, primarily mediated by chemical interactions, slows both the anodic and cathodic reactions on the steel surface. The researcher rated this root extract's ability to provide protection at 94% effective. Joyce *et al.* (Joycee et al.) investigated the efficacy of *beetroot* extracts for multiple sclerosis in a medium simulating oil well water. The calculated efficiency of the combination of *beetroot molecules* and Zn^{2+} is 94%. Researchers used a strain of *Rhizobium leguminosarum* isolated from the legume root nodule of *Vigna mungo* to protect against MS at acidic pHs (Padmavathy et al., 2021). Leaf and root extracts of *Solanum tuberosum* (*Potato*) prevent stainless steel corrosion in an H_2SO_4 medium (Ogunmodede *et al.*, 2022). The plant extracts' inhibition effect enables a success rate of 60.8%. The molecules of the plant part adsorb on the metal via physical interactions governed by the Langmuir isotherm. It was discovered by Žbulj *et al.* that the extract from the *dandelion* root was an effective corrosion inhibitor for carbon steel when exposed to brine (Žbulj *et al.*, 2022). *Biebersteinia multifida* root extracts inhibit the corrosion of low carbon steel by 92.8% after two hours in a 1000 ppm HCl solution (Khayatkashani *et al.*, 2022). Olakolegan and colleagues (Olakolegan et al., 2022) discovered that the Udi plant's roots could prevent Al corrosion in H_2SO_4 and NaCl solutions. Flavanoids, tannis, and Keller killani were identified as the extract's active ingredients, and their presence was attributed to the inhibitor's efficacy.

4.3. Adsorption and Corrosion Inhibition Capability of *Rheum Ribes* (Işgin) Leaf Extract for Mild Steel Protection

4.3.1. Variation of Open Circuit Potential with Exposure Time

The change in E_{ocp} of MS in un inhibited and inhibited 1 M HCl solution was recorded for 3600 seconds and the data obtained are given in Figure 4.19.

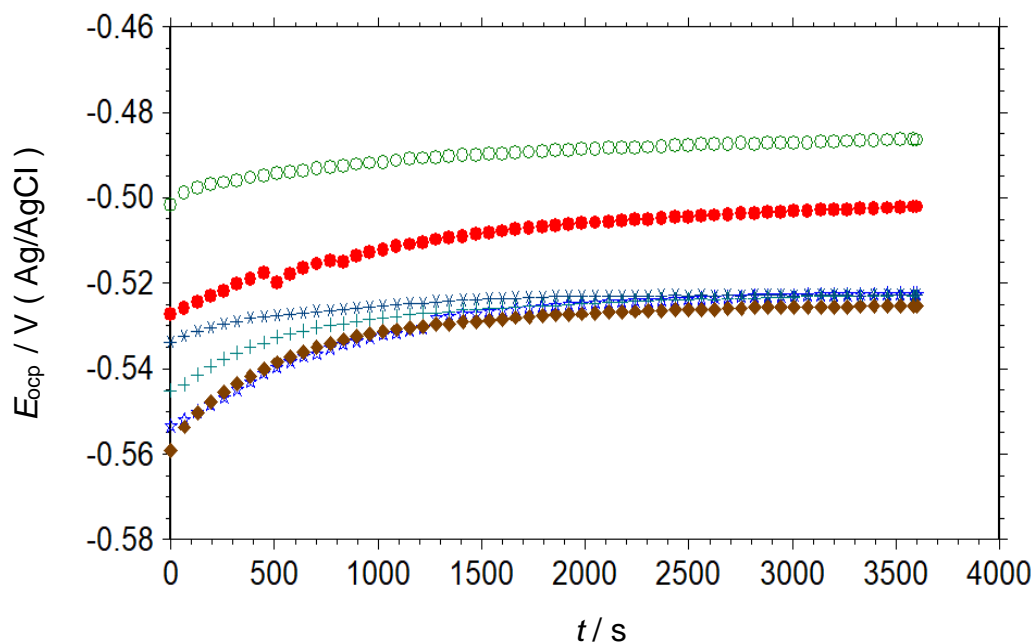


Figure 4.19. The variation of open circuit potential of MS with immersion time in 1 M HCl solution (●) and containing 100 (☆), 250 (+) 500 (◆) 1000 (○) and 2000 (*) ppm RR leaf extracts

The behavior of MS in the uninhibited solution will not be discussed since these explanations were already highlighted in previous chapters. When RR leaf extract is added to the corrosive solution, the initial E_{ocp} becomes more cathodic when compared to a solution that contains no inhibitors. This means that the extract molecules dominate the cathodic reaction more than the anodic reaction. The lowest concentration posed the greatest risk. The values changed from negative to positive as the extract concentration increased from 100 ppm to 1000 ppm. When the concentration of the extract increased further, the potential of the electrodes moves to more cathodic potentials again. During the first 1000 seconds after placing the electrode in the solution, the metal's E_{ocp} rapidly moves to passive regions. Because the molecules of the extract stick to the surface of the metal in a way that depends on how much RR leaf extract is in the corrosive medium, the E_{ocp} reaches equilibrium faster. Changes in the E_{ocp} - t curves that no longer occur demonstrate

that the inhibitor film is extremely stable in the inhibited HCl solution, particularly at high concentrations. The high potential stability indicates that the extract molecules adhere to the surface of the steel and form a durable and protective film. The film primarily affects the cathodic reaction.

4.3.2. Electrochemical Impedance Spectroscopy

The experimental results of the Nyquist (a) and Bode (b) curves of MS after 1-hour immersion in a 1 M HCl solution with or without different concentrations of RR leaf extracts are shown in Figure 4.20. When the curves are examined, they appear to be a depressed half-circle that begins in the high-frequency region and ends in the middle-frequency region in both environments with and without inhibitors. Following that, a second inductive loop appeared at low frequencies, in low concentrations. At high extract concentrations, the low-frequency inductive loop disappears and only one capacitive loop appears. This observation indicates that at high inhibitor concentrations a dense and adherent film forms on the steel surface, which blocks the corrosive ions sufficiently.

The meanings of each loop were already discussed in section 4.2. The addition of RR leaf extract to a corrosive medium increases the diameter of the capacitive loop, and the size of the loop is proportional to the amount of extract. The increase in R_p in this loop indicates that extract molecules are adhering to the metal/solution interface and that the extract is a good protector (Jokar et al., 2016). The disappearance of low-frequency inductive loop indicates formation of protective loop, adhered to the metal strongly.

These values, which range from -0.63 to -0.73, are found in Table 4.6 and were obtained using Figure 4.20b. The deviations from ideal behavior are caused by the non-ideal structure of the MS/solution interface (Silva *et al.*, 2021; Solmaz 2014a; Salcı *et al.*, 2022; Solmaz 2014b), which was initially identified for capacitive behavior. A differential capacitance, as opposed to an ideal capacitor (C_{dl}), forms at the interface between the two layers as a direct consequence of this. This aspect of capacitive behavior was discussed in greater detail previously.

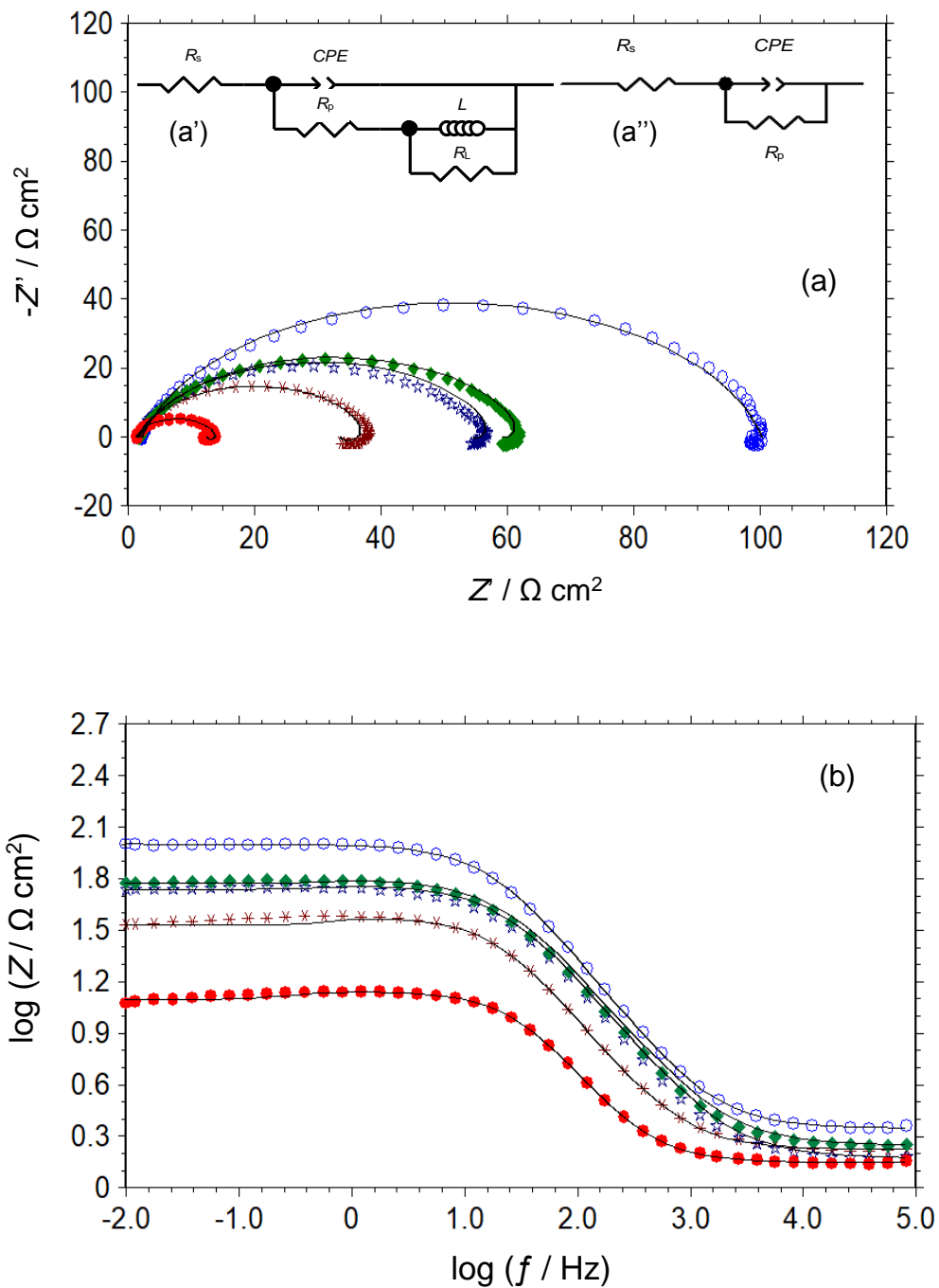


Figure 4.20. The Nyquist (a) and log Z -log f (Bode) (b) plots of MS obtained in 1 M HCl solution (●) and containing 100 (*), 250 (☆), 500 (◆) and 1000 (○) ppm RR leaf extracts. Solid lines shows corresponding fitting curves. The insets on Fig. 3a show the related EECDS

Table 4.6. Fitting results of EIS data and electrochemical parameters determined from EIS measurements for MS obtained 1 M HCl solution in the absence and presence of various concentrations of RR leaf without and with KI edition at 298 K

C_{inh} (ppm)	EIS						
	CPE ($10^{-6}/s^n \Omega^{-1} cm^{-2}$)	n	R_p (Ωcm^2)	L	R_L	α	$\eta \%$
-----	758	0.89	10.80	4.126	1.59	-0.63	-----
100	415.0	0.86	32.1	15.26	4.66	-0.70	66.4
250	281.8	0.83	53.4	47.27	3.98	-0.72	79.8
500	276.6	0.82	57.7	32.76	4.25	-0.70	81.3
750	228.2	0.84	72.1	-----	-----	-0.72	85.0
1000	184.5	0.85	98.1	-----	-----	-0.73	89.0
2000	185.5	0.84	84.3	-----	-----	-0.69	87.2
	CPE	n_1	R_1	CPE_2	n_2	R_2	
1000 ppm RR leaf+ 1000 ppm KI	283.55	0.85	93.0	7974.0	0.51	64.3	93.1

EECDs were suggested to be included in Figure 4.20a as an inset (Qian *et al.*, 2013). This decision was made after taking into account the findings from the previous research as well as the observations that were made. In the context of this EECD, the letters R_s , CPE , R_p , L , R_L values have been previously defined. The results of the process of confirming the data obtained through the experiments to the suggested EECD were processed through a licensed fitting program called ZView Software, and Table 4.6 presents the outcomes of this procedure. The phase shift is expressed as a degree of deviation from ideality and is represented by the letter n in this table. CPE was used instead of C_{dl} for the fitting analysis to achieve a better fitting.

Table 4.6 is presented all of the electrochemical data that were gathered from the EIS measurements. After the addition of RR leaf extract, higher R_p and $\eta \%$ values were obtained when the data presented in this Table and Figure 4.20 were analyzed. The effectiveness of the protection improves as the concentration of the substance being

protected rises. After 1000 ppm, the R_p and protection efficiency reduces, which may be due to the oramation of unstable surface film sor metal-organic complexes on the surface. The best extract concentration is 1000 pmms among the tested solutions. Because of the increased protection efficiency, it can be deduced that extract molecules have been adsorbing at the interface between the metal and the solvent to form a protective film. Higher concentrations were not applied because doing so would have been prohibitively expensive for the practical applications. The value of n is nearly constant; in the presence of a high inhibitor concentration, there is only a slight reduction in comparison to the uninhibited corrosive solution. This may be attributed to the porous structure of the surface film. Following the addition of the inhibitor, CPE values were found to be lower. These values continued to fall as the concentration of RR leaf extract was increased. This behavior also suggests that extract molecules are adsorbing onto the metal surface, which increases surface coverage and/or the thickness of the inhibitor film at the MS/solution interactivity and decreases capacitance (Policarpi and Spinelli, 2020; Qian *et al.*, 2013; Moradi *et al.*, 2013; Tang *et al.*, 2013; Solmaz 2014b) according to the Helmholtz model (Farag and Hegazy, 2013; Li *et al.*, 2012).

4.3.3. Linear Polarisation Resistance

LPR is an additional electrochemical analytical method that can be used to determine the resistance of electrochemical processes that occur in the metal/solution. This technique involves scanning the potential of the electrode around E_{ocp} between very low cathodic and anodic overpotentials; as a result, there is little polarization on the surface. We were able to determine the R_p of the metal based on the slope of the current-potential curves that we obtained using the equation (4.8). R_p of MS obtained in 1 M HCl solution with and without various concentrations of RR leaf extracts was calculated using LPR measurements. Table 4.7 shows the outcomes of these calculations. The corresponding η % values were calculated using equation (4.6) and are shown in the same Table. The data in Table 4.7 demonstrate unequivocally that the incorporation of the extract increases resistance due to the formation of a protective barrier on the metal's surface, resulting in a significant reduction in the rate at which MS corrodes. It has been discovered that increasing the concentration of the extract increases its protective capacity, and these findings are very consistent with the impedance data obtained at each concentration.

Table 4.7. Electrochemical data of MS determined from LPR measurements obtained in 1 M HCl solution in the absence and presence of various concentrations of RR leaf extract without and with KI edition at 298 K

C (mM)	R_p (Ω cm ²)	η %
-----	12.35	-----
100	37.4	64.4
250	57.2	78.4
500	62.7	83.2
750	73.6	84.2
1000	107.9	88.6
2000	96.0	87.1
1000 ppm KI	18.2	32.1
1000 ppm RR leaf+	171.9	92.8
1000 ppm KI		

4.3.4. Potentiodynamic Polarization Curves

Semi-logarithmic PP curves of MS were obtained in a 1 M HCl solution with and without varying concentrations of RR leaf extract, and the results of these experiments are depicted graphically in Figure 4.21. Table 4.8 shows the corrosion parameters derived from these curves, which can also be found in the previous section where they were described. The percentage was calculated using equation (4.9). The E_{corr} of MS in corrosive solution without inhibitors is -0.468 V concerning the Ag/AgCl reference electrode, as shown in Figure 4.21. When a corrosive medium is treated with RR leaf extract, the corrosive medium gains more cathodic potentials, and both the anodic and cathodic current densities decrease. E_{corr} moves to more positive potentials when the concentration of the extract increases. As a result, the extract is a mixed-type corrosion inhibitor that primarily inhibits the reaction of cathodic hydrogen evolution (Policarpi and Spinelli, 2020). The RR leaf extract, in particular, slows both the rate of anodic metal dissolution and the rate of cathodic hydrogen gas evolution.

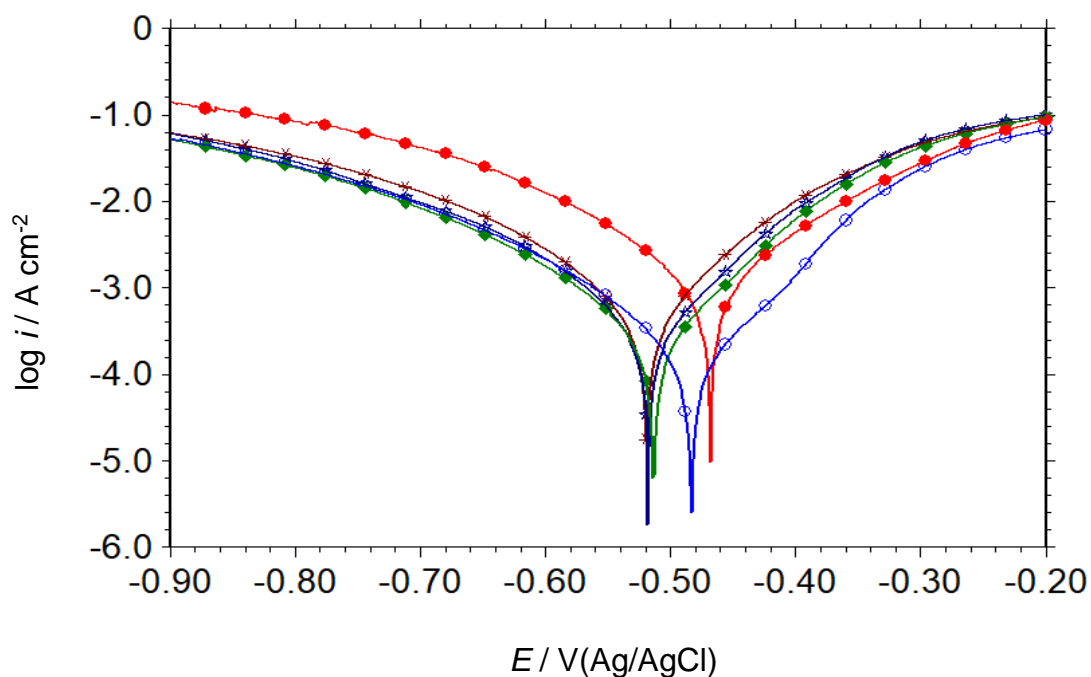


Figure 4.21. Polarization curves of MS obtained in 1 M HCl solution (●) and containing 100 (*), 250 (☆), 500 (◆) and 1000 (○) ppm RR leaf extracts

Table 4.8. Electrochemical parameters of MS determined from PP measurements obtained in 1 M HCl solution in the absence and presence of various concentrations of RR leaf extract and KI added RR leaf at 298 K

C_{inh} (ppm)	E_{corr} (V)	i_{corr} (mA cm ⁻²)	β_a (mV dec ⁻¹)	β_c (mV dec ⁻¹)	WL (g m ⁻² h ⁻¹)	η %
----	-0.468	1.1401	118	120	11.88	----
100	-0.519	0.3462	85	121	4.59	69.6
250	-0.518	0.2077	74	124	2.76	81.8
500	-0.514	0.1637	72	121	2.17	85.6
750	-0.513	0.1258	68	123	1.67	0.89
1000	-0.484	0.0929	68	119	1.23	91.8
2000	-0.516	0.1229	75	121	1.63	89.2
1000 ppm RR leaf+1000 ppm KI	-0.473	0.0578	131	143	0.77	94.9

As the inhibitor concentration increases, the current density decreases, and the effectiveness of the inhibition increases, as shown in Figure 4.21 and Table 4.8. Consequently, the inhibitor may function by forming a surface film of adsorbed inhibitors that acts as a barrier between the metal and the corrosive medium. The rate at which the metal corrodes slows down whenever there is a reduction in the density of the current caused by corrosion. The η % has dropped by 91.8% at 1000 ppm, implying that adding plant extract to a corrosive environment prevents the metal from dissolving and prevents any potential economic losses.

The cathodic curves in the Tafel region of the uninhibited and inhibited solutions were nearly identical, and the β_c values in Table 4.8 are too close together, implying that the RR leaf extract slows the rate of cathodic hydrogen evolution without changing the way the reaction works. This is possible because the surface inhibitor film obstructs light. As a result, the inhibitor is effective as long as it covers the metal's surface. The surface coverage ($1-\theta$) is nearly full when the concentration is 1000 ppm. Corrosion occurs only on exposed metal parts or through holes in the surface film (Solmaz 2014). More research into closing these pores or tightening the film may improve its ability to protect. Iodide ions were added to the solution that had been stopped in the previous section to accomplish this. Adding RR leaf extract, on the other hand, stops the flow of anodic current and reduces β_a . This means that the extract alters the way the anodic reaction occurs, preventing it from occurring. More investigation is required to fully comprehend the mechanism.

The findings of the experiments conducted by PP are consistent with those obtained by EIS and LPR. All of the electrochemical tests demonstrated that the extract's protective ability improved with increasing concentration, but this improvement was minimal at higher concentrations and 1000 ppm was sufficient. Since a greater number of molecules can adhere to the surface when the concentration is high, the surface is better covered.

4.3.5. The Synergistic Inhibitory Effect of KI

Figure 4.22a shows how the E_{ocp} of MS changes when 1000 ppm KI is added to a solution that has been inhibited. This is compared to HCl solutions that have neither been inhibited nor not been inhibited. The general trend of iodide ions in the solution is the same as that observed in a 1 M HCl solution containing 1000 ppm of RR leaf. However, the E_{ocp} shifted

toward more positive values compared to the uninhibited corrosive solution. The steady-state E_{ocp} value observed for this solution was -0.479 V, whereas it was -0.502 V for 1 M HCl and -0.525 V for 1 M HCl+1000 ppm RR leaf+1000 ppm KI solutions. These findings suggest that iodide ions added to the solution have better surface coverage (Jokar et al., 2016) or a tighter film, resulting in a better physical barrier at the MS/solution interface.

The PP curves of MS in a 1 M HCl solution with 1000 ppm RR leaf + 1000 ppm KI are shown in Fig. 4.22b. The curves of MS taken in HCl solutions with and without inhibitors are shown on the same graph so that they can be compared. This curve was used to calculate the corrosion parameters, which are shown in Table 4.8.

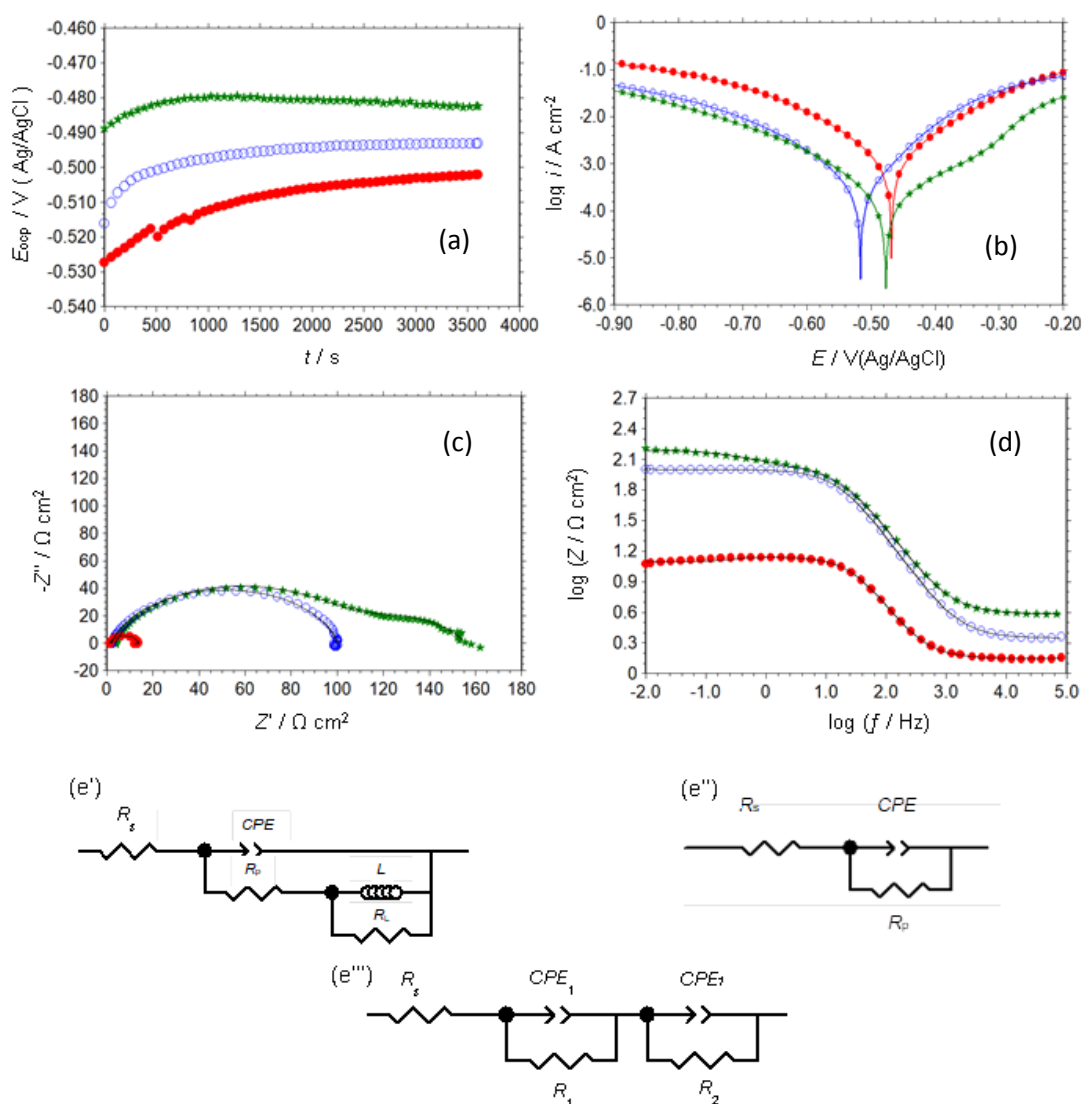


Figure 4.22. The variation of E_{ocp} of MS with immersion time (a); potentiodynamic polarization (b), Nyquist (c) and $\log Z$ - $\log f$ (Bode) (d) plots of MS obtained in 1 M HCl solution in the absence (\bullet) and containing 1000 ppm RR leaf (\circ), 1000 ppm RR leaf+1000 ppm KI (\star); EECDs proposed for the MS/solution interface in 1 M HCl and 1 M HCl+1000 ppm RR leaf (c'), 1 M HCl+1000 ppm RR leaf+1000 ppm KI (c'')

When KI is added to a corrosive medium containing RR leaf extract, E_{corr} shifts toward more anodic potentials and the corrosion current density decreases when compared to the absence of KI. When iodide ions are present, the extract acts as a mixed-type, mostly anodic corrosion inhibitor. MS's level of protection in this situation is 89.0%. In this case, the β_a and β_c values of MS are very close to those found in a 1 M HCl solution. So, when iodide ions are present, the extract prevents MS from corroding without changing the anodic or cathodic reaction mechanisms.

Figure 4.22b and 22c portray the Nyquist and Bode plots of MS obtained in a solution of 1 M HCl+1000 ppm RR leaf+1000 ppm KI. The MS curves obtained in a 1 M HCl solution in the absence and presence of 1000 ppm RR leaf extract are plotted on the same graph. The EECs shown in Figure 4.22e' and e'' were used to fit these curves, and the resulting electrochemical data are shown in Table 4.6. The MS plots obtained in iodide-free solutions are displayed on the same figures for comparison. The low-frequency inductive loop vanished in the presence of 1000 ppm KI in the inhibited solution, appearing a second capacitive loop at low frequencies and time constant in the Bode curve. The second new capacitive loop is related to the resistance of the film. The resistance significantly increased after the addition of KI to the aggressive medium. Iodide ions aid in the adsorption of extract molecules and help to stabilize the surface film. The addition of KI improves the corrosion resistance and inhibition of the RR leaf extract significantly.

LPR measurements for the MS electrode were carried out in a 1 M HCl solution inhibited with 1000 ppm KI, and the results are shown in Table 4.7. The same experiments were carried out with 1000 ppm KI in a 1 M HCl solution for comparison and to investigate any potential synergy between the halogen ions and the extract molecules. Table 4.7 shows that adding KI to 1 M HCl increases resistance, indicating enhanced iodide ion adsorption. However, adding 1000 ppm KI to 1000 ppm RR leaf extract containing 1 M HCl increases corrosion resistance, which is consistent with EIS results. The protection level reaches 92.8%, which is sufficient for practical applications.

The value of synergistic factor (s) was calculated using equation (4.11) and was determined to be 1.08 by using the values from Table 4.7. Accordingly, the increased protection ability is a result of the co-adsorption of iodide ions and charged organic molecules (Oulabbas *et al.*, 2022). Extract molecules may also be adsorbed directly to the metal surface via

adsorption active centers such as N, S, and O atoms or multiple bonds. The mechanism of inhibition will be discussed in depth in the following sections.

4.3.6. Studies of Surface Characterization

SEM, AFM, EDX, and contact angle measurements were performed on the MS surface following exposure to inhibited solutions in the absence and presence of KI. In Figure 4.23, SEM images of the MS surface after 1 hour of exposure to 1 M HCl, 1 M HCl+1000 ppm RR leaf, and 1 M HCl+1000 ppm RR leaf+1000 ppm KI are shown.

The MS surface deteriorated considerably due to excessive metal breakdown, as seen in Fig. 4.23a and the enlarged version of the same figure in Fig. 4.23b. Pitting corrosion was seen in the steel in this medium, as expected, and the metal damage was not uniform. The surface was significantly altered and pits and fractures disappeared after the addition of 1000 ppm RR leaf extract to a corrosive media (Fig. 4.23c). The molecules of the RR leaf extract appear to cover and protect the steel's surface. A higher quality, more compact, and virtually equally distributed surface coating formed when 1000 ppm KI was added to an inhibited solution (Fig. 4.23d).

The AFM technique could be used to explore the structures of organic films at the nano- or micro-scale. AFM was used to analyze the structure of RR leaf film produced in 1 M HCl solution in the absence and presence of equivalent KI quantity. Figs. 4.23e and f show 3D dimensional AFM pictures. The AFM data are remarkably similar to the SEM results. Figure 4.23 displays the appearance of the organic film on the surface. The addition of KI to the RR leaf-inhibited acidic media results in an improvement in the quality of the surface film and the formation of a film that is more uniform (Fig. 4.23f). This coating acts as a barrier between the metal and the corrosive medium and considerably prevents MS deterioration (Jokar et al., 2016).

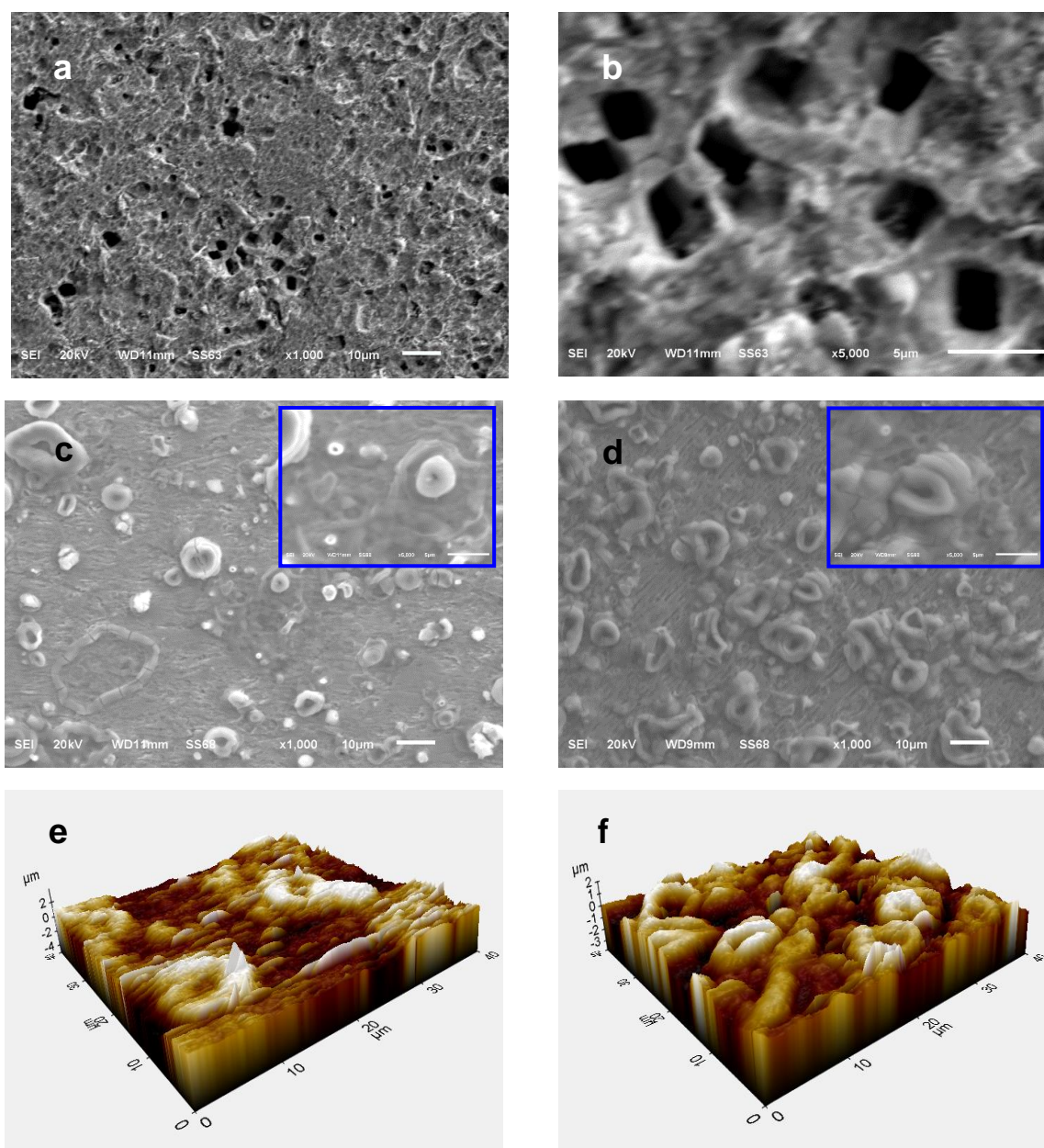


Figure 4.23. SEM images of MS taken after exposure to 1 M HCl (a and b), 1 M HCl+1000 ppm RR leaf (c) and 1 M HCl+1000 ppm RR leaf+1000 ppm KI (d) (The insets on c and d show 5 000x magnified images of the same surfaces); 3D dimensional AFM images of MS after exposure to 1 M HCl+1000 ppm RR leaf (e) and 1 M HCl+1000 ppm RR leaf+1000 ppm KI (f)

EDX was used to evaluate the chemical composition of the inhibited surfaces and the distribution of the extracted film on the surface of the steel. Figures 4.24 and 4.25 show the EDX spectra of the MS surface, the distribution of some elements on the metal (EDX-mapping images), and cross-sectional analysis of some elements on the MS surface after

exposure to 1 M HCl solution in the presence of 1000 ppm RR leaf and 1000 ppm RR leaf+1000 ppm KI.

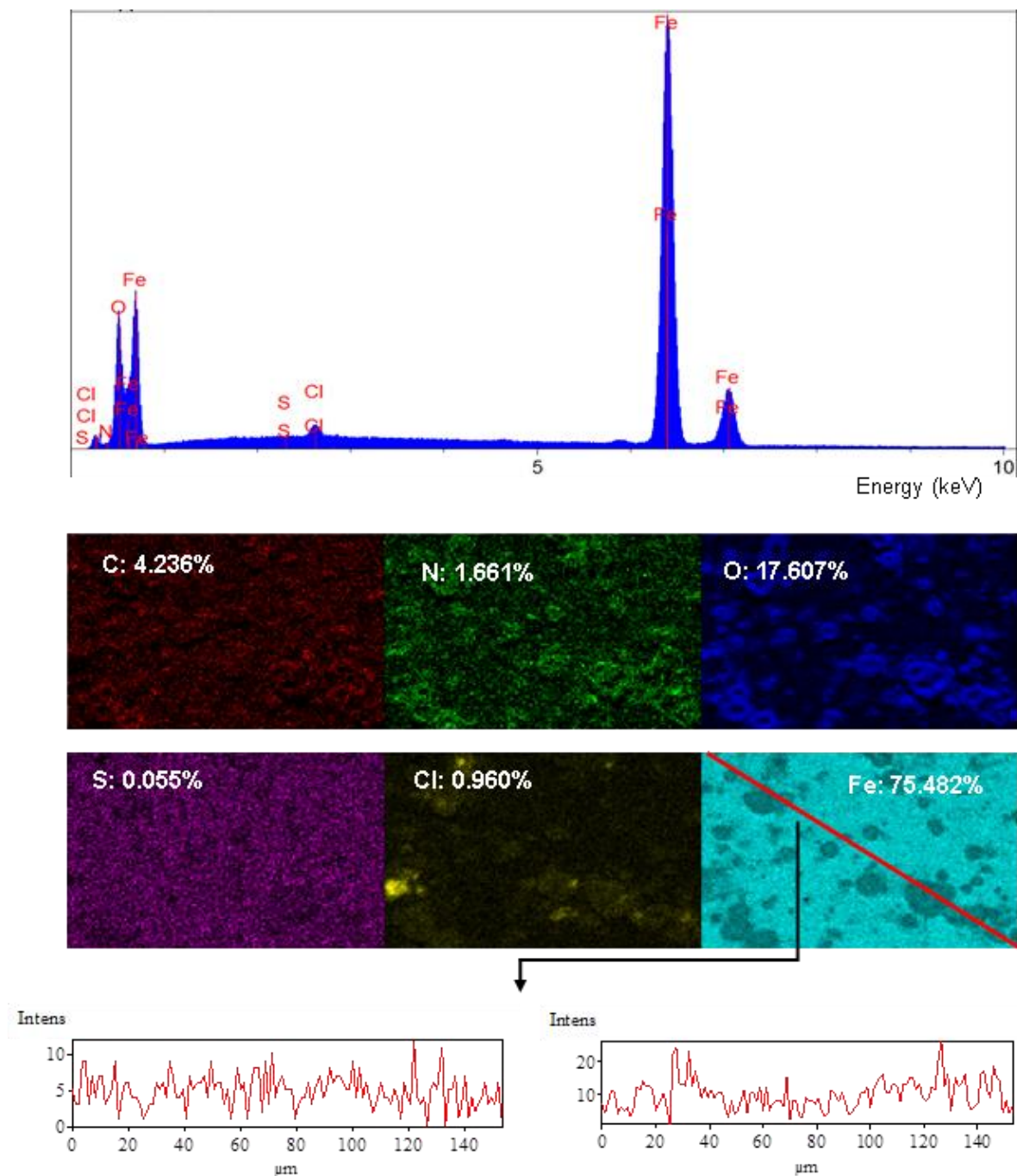


Fig. 4.24. EDX spectrum of the MS surface, the distribution of some elements on the metal surface (EDX-mapping images) and cross-sectional analyses of some elements on the surface of MS after exposure to 1 M HCl solution in the presence of 1000 ppm RR leaf for 1 hour

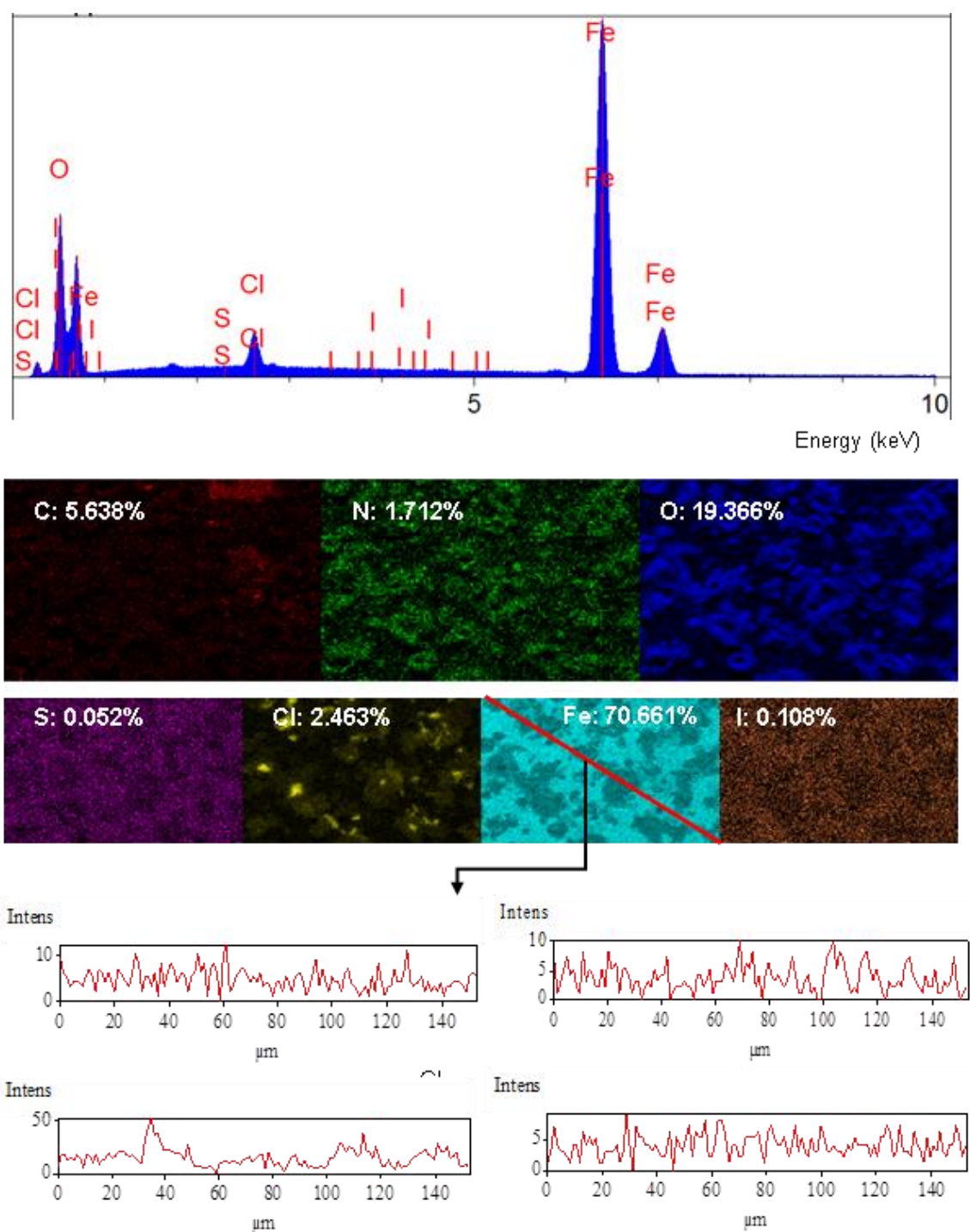


Figure 4.25. EDX spectrum of the MS surface, the distribution of some elements on the metal surface (EDX-mapping images) and cross-sectional analyses of some elements on the surface of MS after exposure to 1 M HCl solution in the presence of 1000 ppm RR leaf+1000 ppm KI

The EDX spectra presented in Figures 4.24 and 4.25 demonstrate the presence of a thick coating on the steel. The gathered data indicate the production of a surface layer consisting

of hetero compounds including C, N, O, and S, which are considered active adsorption sites. Cl is also found in two cases. Since the MS contains lower concentrations of C and O (1.720% and 0.115% O, experimental section), RR leaf extract molecules should contain a higher concentration of these elements. Additionally, the presence of N and S components, which are absent in MS, lends weight to this hypothesis. The presence of Cl results from the adsorption of chloride ions from a 1 M HCl solution and the formation of adsorbed species or corrosion products such as FeCl_{ads} or FeCl_2 under the film or in exposed areas. In the presence or absence of KI, the quantities C, N, O, and S detected on the surface of MS do not have a linear relationship (Figure 4.24 and 4.25). Different ratios or concentrations of extract molecules adsorb on the metal surface in the presence or absence of KI.

In contrast, the addition of KI causes a reduction in the quantity of these components, which may be an indication that fewer molecules are adsorbed and that the surface develops a coating that is thinner but more protective as a result of the process. After adding KI to the inhibited HCl solution, the I element shows in the EDX spectrum, and additional tests demonstrate this element's adsorption, which increases extract molecule adsorption on the steel surface. A cross-sectional study reveals the presence of a homogeneous surface coating, which is improved in the presence of KI.

Contact angle images of the MS surface after 1 hour of exposure to a 1 M HCl solution with and without the addition of 1000 ppm RR leaf and 1000 ppm RR leaf+1000 ppm KI are shown in Figure 4.26.

In the unconstrained solution, the average contact angle of the steel is 53.61° . In the presence of the RR leaf extract, the average contact angle rises to 47.55° . This value is less than 90° , indicating that the film is hydrophilic. The contact angles produced a considerable change in angles, showing that the molecule adsorbed by the steel surface formed a coating that was less hydrophilic than the unmanaged solution. When RR leaf extract and iodide ions are introduced to an inhibited solution, the contact angle reduces. This finding could be explained by a change in the orientation of the molecules and the coating of the surface with negatively charged iodide and chloride ions, specifically on the exposed surface sites harboring the inhibitor molecules.

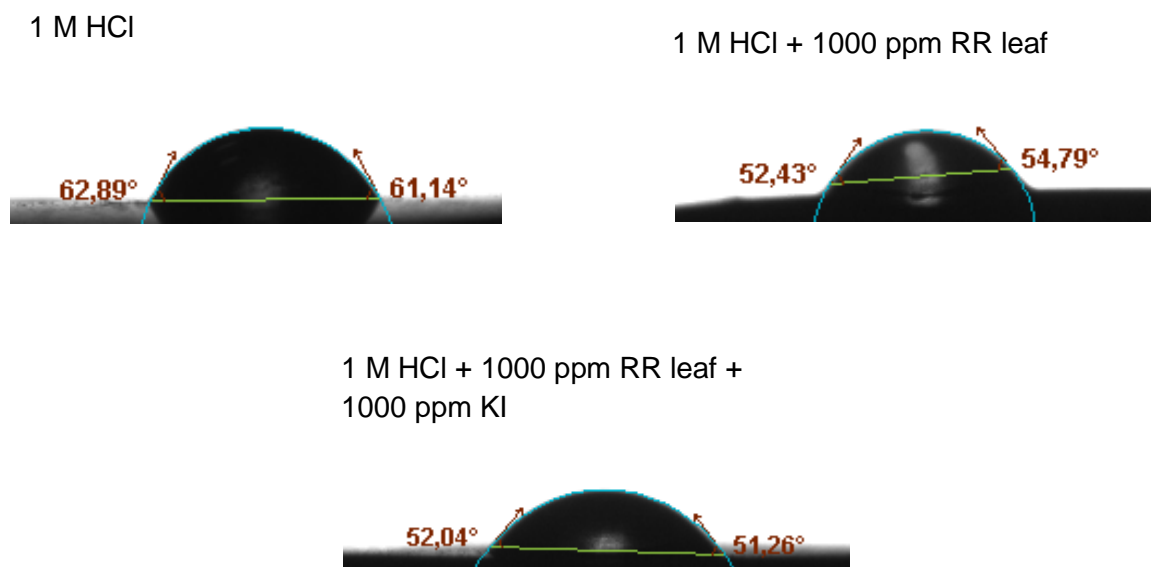


Figure 4.26. Contact angle images of the MS surface after exposure to 1 M HCl, 1 M HCl + 1000 ppm RR leaf and 1 M HCl + 1000 ppm RR leaf + 1000 ppm KI solutions for 1 hours

4.3.7. Mechanism of Adsorption and Inhibition Process

The surface coverage values (θ , $\theta = \eta\%/100$) for each concentration of RR leaf extract were calculated and used to assess the extract's ideal isotherm. Several models were tried for this purpose, with the Langmuir adsorption isotherm providing the greatest fit, as shown in Figure 4.27.

This assumption is supported by the fact that the correlation coefficient constant, R^2 , is fairly high (0.99891) and close to 1. Therefore, we hypothesize that RR leaf extract molecules adsorb on specific sites of the metal and produce a uniform monolayer coating (Shahmoradi *et al.*, 2021; Oulabbas *et al.*, 2022). The slope of this plot is 1.09, which indicates that the molecules occupy 1.09 sites of the MS surface instead of 1 (Fan *et al.*, 2011). The value of K_{ads} was derived from Eq. (4.12) and Fig. 29 is 20.07 L g^{-1} , indicating a good adsorption ability and stability of the extract molecules on the metal surface (Policarpi and Spinelli, 2020). The value of K_{ads} indicates that the extract molecules have a high capacity for adsorption on the metal surface. This information also demonstrates that the adsorption of extract molecules is preferable to their desorption (Goulart *et al.*, 2013).

Standard free energy of adsorption ($\Delta G^{\circ}_{\text{ads}}$), which is computed using equation (4.13) (Jokar *et al.*, 2016) and found to be $-24.5 \text{ kJ mol}^{-1}$. The fact that the value of $\Delta G^{\circ}_{\text{ads}}$ is negative suggests that the molecules of RR leaf extract self-adsorb onto the MS surface. This is the case since all organic inhibitors are self-adsorbed on the surface of the metal. The $\Delta G^{\circ}_{\text{ads}}$ value of RR leaf extract is midway between -20 kJ mol^{-1} . And -40 kJ mol^{-1} , but is more closely related to a value of -20 kJ mol^{-1} . As a result, RR leaf extract adsorption occurs as a result of both chemical and physical interactions, with the first interactions having primacy. As already discussed, after initial physical interactions, chemical interactions of the extract molecules and the surface are also possible. Charge sharing occurs between the d orbitals of metals and the free electron pairs of adsorption active centers, such as N, S, and O atoms, as well as the π electrons of double or triple bonds in organic molecules, to produce chemical interaction (Figure 4.16, a and b) (Haldhar *et al.*, 2021).

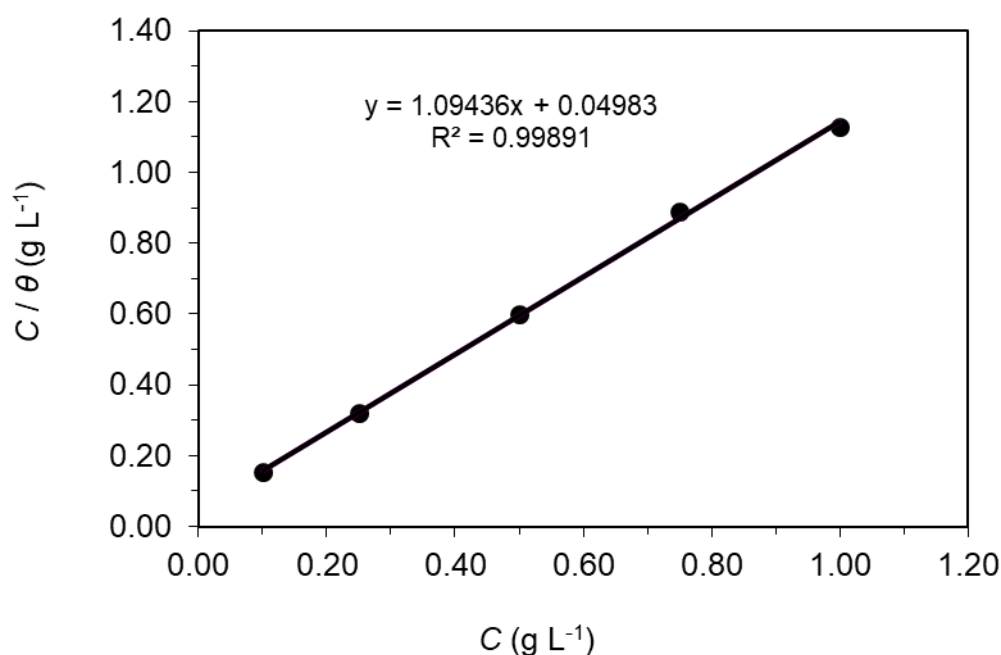


Figure 4.27. Langmuir adsorption plot of MS obtained in 1 M HCl solution with the addition of various concentrations of RR leaf extract

In highly acidic solutions, a large number of organic compounds can be found in a state of equilibrium with their protonated analogs. Iodide ions and positively charged inhibitor chemicals interact synergistically, as explained in Section 4.3.4. Iodide and chloride ions that are more polarizable adsorb on the metal's surface, making the solution site of the

double layer negative. These species are then capable of adsorbing protonated inhibitor molecules. Halogen ions, in particular, operate as linking bridges (Figure 4.16, b, and c).

4.3.8. Stability of Surface Inhibitor Film

The variation of anodic and the cathodic current densities as a function of time under constant +100 mV anodic and -100 mV cathodic overpotentials conducted in 1 M HCl solution and containing 1000 ppm RR leaf, 1000 ppm RR leaf+1000 ppm KI are given in Figure 4.28. In Figure 4.28, the fluctuation of anodic and cathodic current densities as a function of operation time under constant +100 mV anodic or -100 mV cathodic potentials obtained in 1 M HCl solution and containing 1000 ppm RR leaf or 1000 ppm RR leaf+1000 ppm KI can be shown. These results were achieved in an electrolyte containing 1000 ppm RR leaf.

The anodic current density that was recorded in a solution that contained 1 M HCl showed a rapid increase as electrolysis began, and then it becomes almost constant after 1000 seconds, as shown in Figure 4.28a. This pattern continues until the electrolysis is complete. The abrupt increase in current density observed could be attributed to the excessive dissolution of MS in this aggressive solution. After the rate of disintegration has stabilized, the current remains constant despite periodic fluctuations. Under these conditions, the cathodic current density usually always remains constant, despite periodic variations produced by the production of surplus hydrogen gas and the formation of gas bubbles on the electrode surface (Figure 4.28b)

Due to the adsorption of inhibitor molecules on the metal surface, the addition of 1000 ppm RR leaf extract to the corrosive solution decreases early anodic or cathodic current densities. Nevertheless, the anodic current density continuously increases during electrolysis. This observation suggests that the RR leaf extract film is not individually stable. The rise in current density is a result of the excessive dissolution of metal beneath the coating, which removes or degrades it from the surface. This film, however, is extremely stable under cathodic overpotentials; the cathodic current density is extremely low and more stable than that reported in 1 M HCl.

Following the incorporation of 1000 ppm KI into the inhibited solution, there was a discernible shift in the behavior of the surface film. Initial anodic and cathodic current densities are both lower and rather stable throughout the electrolysis period, indicating a highly stable surface coating (Sığircık *et al.*, 2016). This observation suggests that the surface coating acts as an effective barrier against anodic metal dissolution and cathodic hydrogen evolution processes. In this state, the film adheres tightly to the MS surface and does not detach from it.

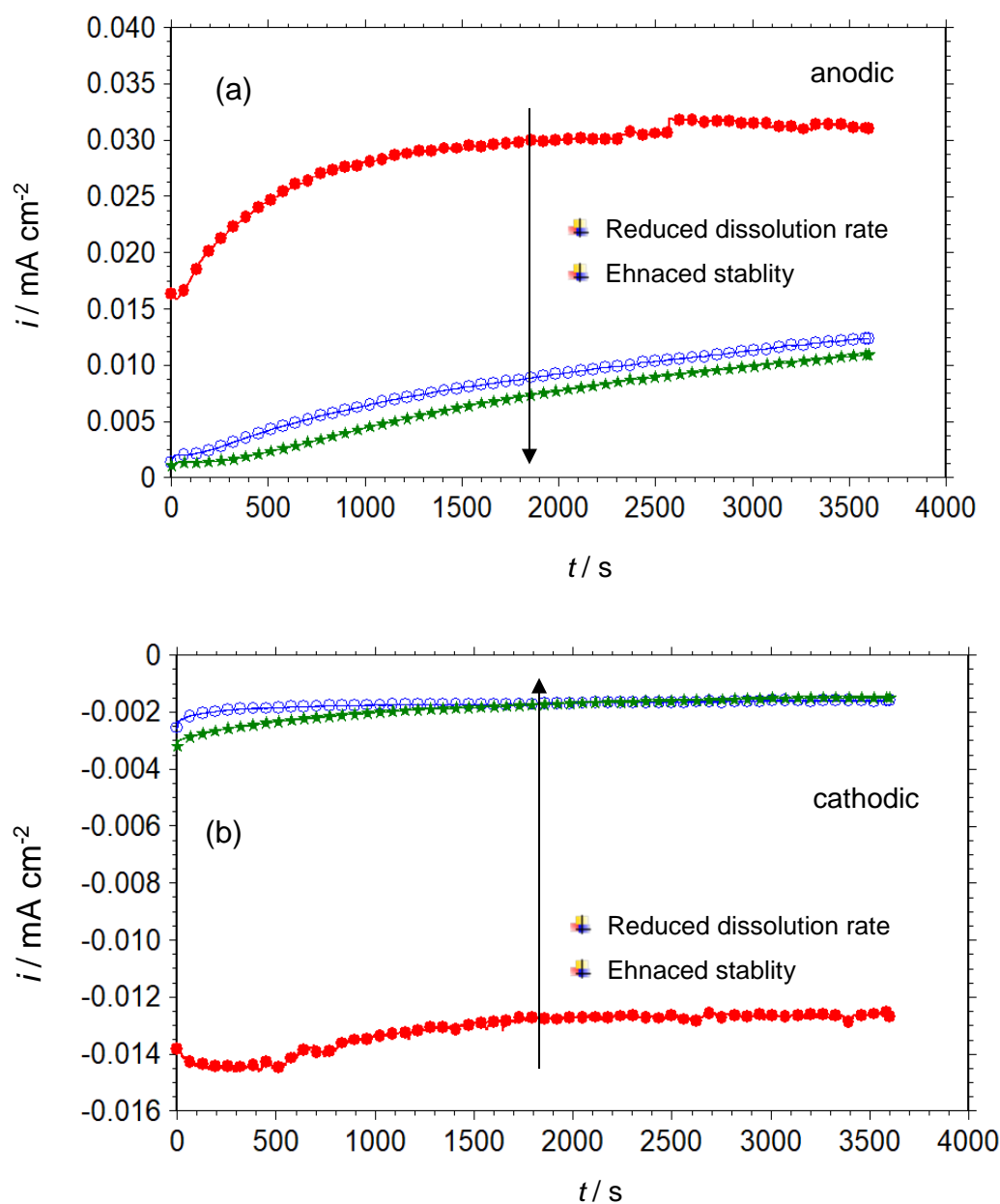


Figure 4.28. The variation of anodic and the cathodic current densities as a function of time under constant +100 mV anodic (a) and -100 mV cathodic (b) overpotentials conducted in 1 M HCl solution (●) and containing 1000 ppm RR leaf (○), 1000 ppm RR leaf+1000 ppm KI (★)

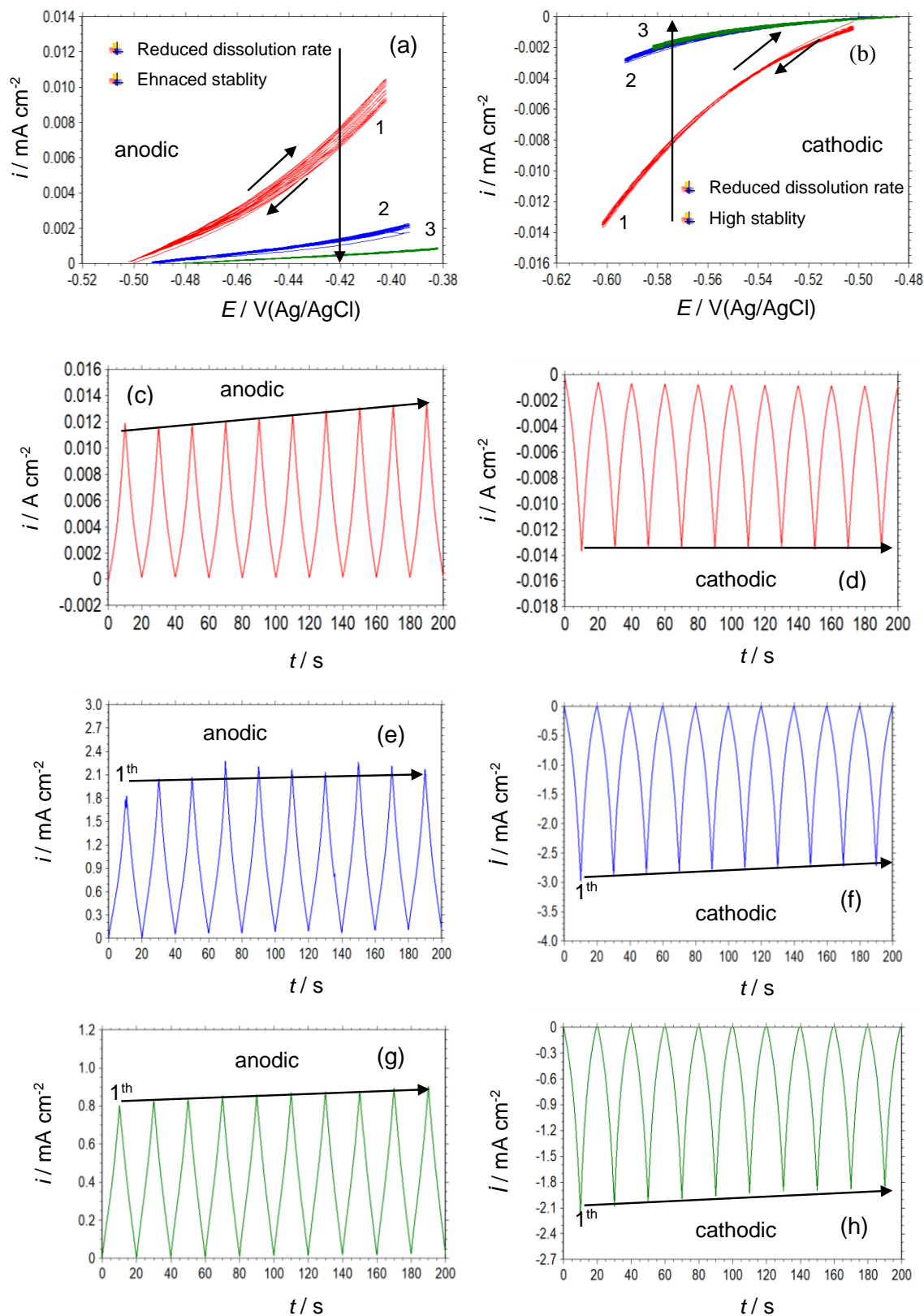


Figure 4.29. Anodic (a) and cathodic (b) CVs of MS obtained in the test solutions (1: 1 M HCl, 2: 1 M HCl+1000 ppm RR leaf, 3: 1 M HCl+1000 ppm RR leaf+1000 ppm KI); Anodic CV-time plots of MS obtained in 1 M HCl (c), 1 M HCl+1000 ppm RR leaf (e), 1 M HCl+1000 ppm RR leaf+1000 ppm KI (g); Cathodic CV-time plots of MS obtained in 1 M HCl (d), 1 M HCl+1000 ppm RR leaf (f), 1 M HCl+1000 ppm RR leaf+1000 ppm KI (h)

The CV approach was also used to test the stability of the film under a variety of dynamic situations. The anodic and cathodic CVs and CV-time plots of MS in 1 M HCl, 1 M HCl+1000 ppm RR leaf, and 1 M HCl+1000 ppm RR leaf+1000 ppm KI. The obtained data are depicted in Figure 4.29.

CA and CV outcomes are extremely compatible. The anodic current density increases somewhat as the number of cycles increases due to the active dissolving of the metal, as indicated by the anodic CVs (Figure 4.29a) and anodic CV-time plots (Figure 4. 29c) of MS generated in the absence of an inhibitor. In the presence of 1000 ppm RR leaf extract, a similar pattern was seen with lower current density (Figure 4. 29a and e). However, after adding 1000 ppm KI to the inhibited solution, the CV (Figure 4. 29a) and CV-time (Figure 4. 29g) curves showed highly consistent anodic current densities, showing that the film on the MS surface is also very stable under anodic potential scan. In 1 M HCl and 1000 ppm RR leaf solutions containing HCl, the MS cathodic current density is essentially constant (Figure 4. 29b, d and f). However, the inhibited solution has a lower current density than the uninhibited solution. In the presence of iodide ions, however, there was greater stability and lower cathodic current density, and the cathodic current density declined as the number of cycling increased (Figure 4. 29h).

4.4. Adsorption and Corrosion Inhibition Capability of *Rheum Ribes* (Işgin) Flower Extract for Mild Steel Protection

The ability of extracts from the flower of the RR plant to act as a corrosion inhibitor for MS protection in 1 M HCl solution was tested. The data are presented below, alongside the data from the other two extract parts, using the same techniques.

The data below shows that the best protection is obtained with the flower extracts. Some further studies, for example, the effect of immersion time and the determination of excess surface charge, were additionally determined and provided in this section. Also, in this part, we will apply for steel rebar (SR) embedded in reinforced concrete as a practical application in the final quote.

4.4.1. Variation of Open Circuit Potential with Exposure Time

A plot of variation in E_{ocp} of MS with exposure to 1 M HCl solution without and with various RR flower extracts was conducted for 3600 seconds. The data obtained are presented in Figure 4.30.

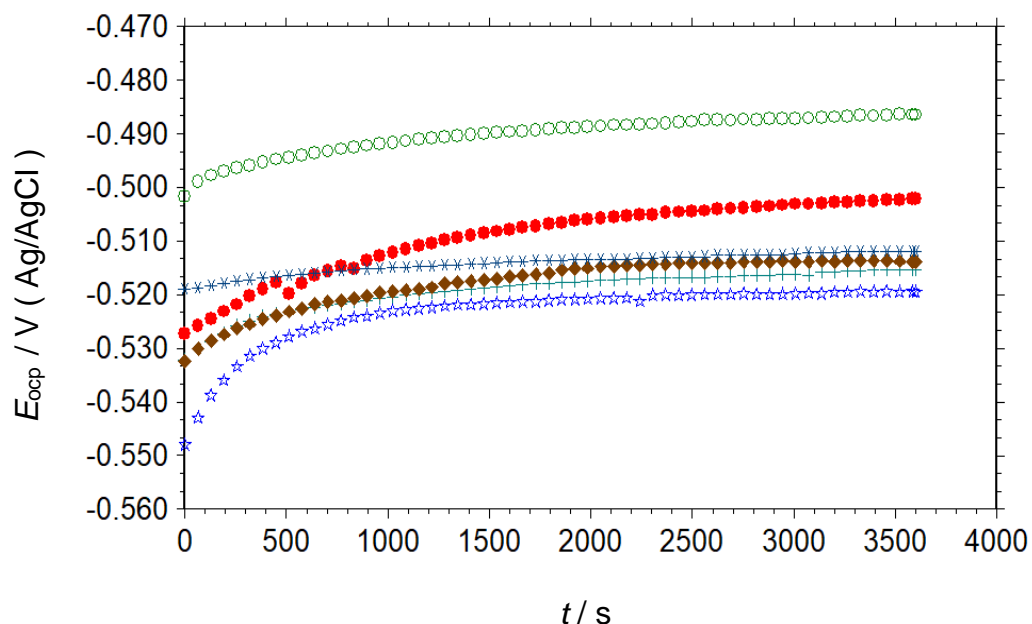


Figure 4.30. The variation of E_{ocp} of MS with immersion time in 1 M HCl solution (●) and containing 100 (☆), 250 (+), 500 (◆), 1000 (○) and 2000 (*) ppm RR flower extracts

The behaviour of MS in the uninhibited solution was highlighted in previous chapters and, therefore, will not be repeated here. The E_{ocp-t} behaviour of RR flower is very comparable with RR leaf extract. However, the surface becomes stable in a shorter exposure time when compared to the data observed for RR root or RR leaf extracts. As it is seen from Figure 4.30, with the addition of RR flower extract to 1M HCl solution, the initial E_{ocp} becomes more cathodic concerning uninhibited 1 M HCl solution. Also, this means that the extract molecules dominate the cathodic reaction more than the anodic reaction. The lowest concentration posed the greatest risk. The values changed from negative to positive as the extract concentration increased from 100 ppm to 1000 ppm. Moreover, the concentration of the extract reaches 2,000 ppm, and the potential of the electrodes shifts back to a cathodic state. During the first 1000 seconds after placing the electrode in the solution, the metal's E_{ocp} rapidly moves to passive regions. Because the molecules of the extract stick to the surface of the metal in a way that depends on how much RR flower extract is in the corrosive medium, the E_{ocp} reaches equilibrium faster. Changes in the E_{ocp-t} curves no longer occur that the inhibitor film is extremely stable in the inhibited HCl solution, particularly at 1000 ppm concentrations among the studied concentrations. The high potential stability indicates that the extract molecules adhere to the surface of the steel and form a durable and protective film. The film primarily affects the cathodic reaction.

4.4.2. Electrochemical Impedance Spectroscopy

The Nyquist (a) and Bode (b) curves of MS after 1-hour exposure to 1 M HCl solution with or without different concentrations of RR flower extracts are shown in Figure 4.31. The curves obtained for RR flower were different from the other two extracts; at concentrations higher than 250 ppm, only one time constant was observed, which indicates that this extract forms a better and tighter film with better quality forms on the metal surface. When the curves were examined, the behaviour at 100 ppm was the same for the uninhibited 1 M HCl solution. However, when the concentration increased, only one depressed half-circle appeared in the high-frequency and the middle-frequency regions

The meanings of each loop were discussed in the previous chapters and not repeated here. Adding RR flower extract to a corrosive medium increases the capillary loop's diameter, and the loop's size is proportional to the amount of plant extract. The increase in R_p in this loop indicates that extract molecules adhere to the metal/solution interface and that the

isolate is a good protector (Jokar et al., 2016). The disappearance of the low-frequency inductive loop indicates the formation of protective film adhered to the metal strongly.

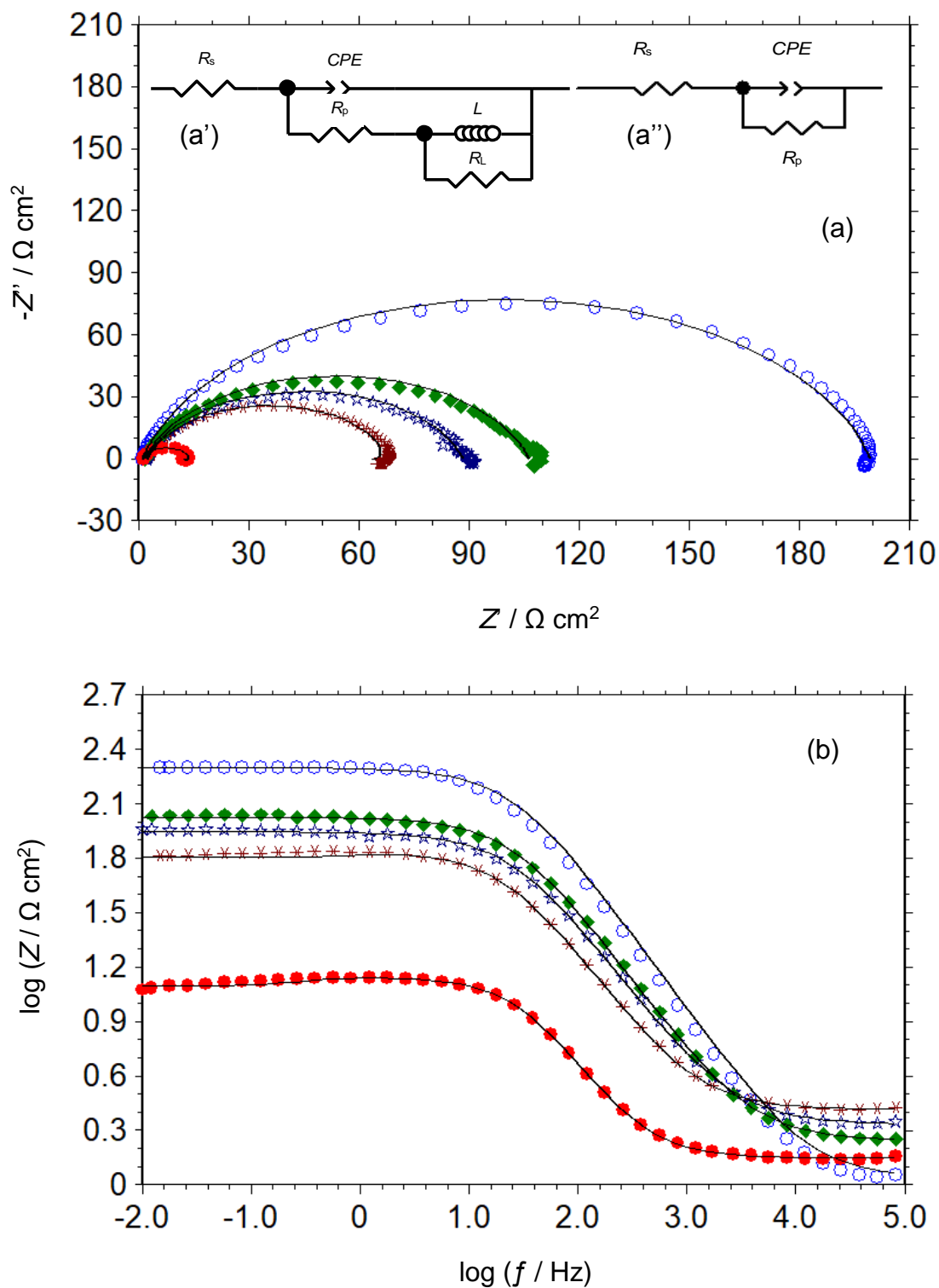


Figure 4.31. The Nyquist (a) and $\log Z$ - $\log f$ (Bode) (b) plots of MS obtained in 1 M HCl solution (●) and containing 100 (✱), 250 (☆), 500 (◆) and 1000 (○) ppm RR flower extracts. Solid lines show corresponding fitting curves. The insets on Fig. 3a show the related EECDs

These values of slopes of Bode curves were derived from Fig. 4.31b and shown in Table 4.9. These values range between -0.63 and -0.79. The deviations from ideal behaviour are caused by the non-ideal structure of the MS/solution interface (Silva *et al.*, 2021; Solmaz 2014a; Salcı *et al.*, 2022; Solmaz 2014b), which was initially identified for capacitive behaviour. A differential capacitance, as opposed to an ideal capacitor (C_{dl}), forms at the interface between the two layers as a direct consequence. This aspect of capacitive behaviour was discussed in greater detail previously. The values of slopes of Bode curves are slightly high at RR flower extracts for the other two parts, indicating better quality of the surface film.

Table 4.9. Fitting results of EIS data and electrochemical parameters determined from EIS measurements for MS obtained 1 M HCl solution in the absence and presence of various concentrations of RR flower without and with KI edition at 298 K

C_{inh} (ppm)	EIS						
	CPE ($10^{-6}/s^n \Omega^{-1} cm^{-2}$)	n	R_p (Ωcm^2)	L	R_L	α	η %
-----	758	0.89	10.80	4.126	1.59	-0.63	-----
100	231.6	0.84	61.0	18.7	5.26	-0.62	82.3
250	171.1	0.83	86.3	-----	-----	-0.70	87.5
500	133.9	0.83	104.6	-----	-----	-0.74	89.7
750	105.8	0.82	139.3	-----	-----	-0.72	92.3
1000	68.7	0.84	198.2	-----	-----	-0.79	94.6
2000	74.6	0.85	184.5	-----	-----	-0.78	94.2
	CPE	n_1	R_1	CPE_2	n_2	R_2	
1000 ppm RR flower+	233.5	0.78	68.2	12299	0.65	58.2	91.5
1000 ppm KI							

EECDs were suggested to be included in Figure 4.31a as an inset (Qian *et al.*, 2013). This decision was made after considering the findings from the previous research and the observations that were made. In the context of this EECD, the letters R_s , CPE , R_p , L , R_L

values have been previously defined. The results of confirming the data obtained through the experiments to the suggested EECD were processed through a licensed fitting program called ZView Software. Table 4.9 presents the outcomes of this procedure. The phase shift is expressed as a deviation from ideality, represented by the letter n in this Table. CPE was used instead of C_{dl} for the fitting analysis to achieve a better fitting.

After adding RR flower extract, higher R_p and η % values were obtained when the data presented in Table 4.9 and Figure 4.31 were analyzed. The effectiveness of the protection improves as the concentration of the substance being protected rises. After 1000 ppm, the R_p and protection efficiency reduce, possibly due to the formation of unstable surface film or metal-organic complexes on the surface. The best extract concentration is 1000 ppm among the tested solutions. Because of the increased protection efficiency, it can be deduced that extract molecules have been adsorbing at the interface between the metal and the solvent to form a protective film. Higher concentrations were not applied because doing so would have been prohibitively expensive for the practical applications. The value of n is nearly constant; in the presence of a high inhibitor concentration, there is only a slight reduction compared to the definitive corrosive solution. In addition, this may be attributed to the porous structure of the surface film. CPE values were found to be lower after the addition of the inhibitor. These values continued to fall as the concentration of RR flower extract was increased. The observation results express that plant isolate molecules are adsorbing onto the metal surface, increasing surface coverage and/or the thickness of the inhibitor film at the MS/solution interactivity and decreasing capacitance (Policarpi and Spinelli, 2020; Qian *et al.*, 2013; Moradi *et al.*, 2013; Tang *et al.*, 2013; Solmaz 2014b) according to the Helmholtz model (Frag and Hegazy, 2013; Li *et al.*, 2012).

4.4.3. Linear Polarisation Resistance

The R_p of the metal in 1 M HCl solution with and without various concentrations of RR flower extracts were determined based on the slope of the current-potential curves we obtained using the equation (4.8). Table 4.10 shows the outcomes of these calculations. The corresponding η % values were calculated using equation (4.6) and are shown in the same Table. The data in Table 4.10 demonstrate unequivocally that the incorporation of the extract increases resistance due to forming a protective barrier on the metal's surface, resulting in a significant reduction in the rate at which MS corrodes. It has been discovered

that increasing the concentration of the extract increases its protective capacity, and these findings are consistent with the impedance data obtained at each concentration.

Table 4.10. Electrochemical data of MS determined from LPR measurements obtained in 1 M HCl solution in the absence and presence of various concentrations of RR flower extract without and with KI edition at 298 K

C (mM)	R_p ($\Omega \text{ cm}^2$)	η %
-----	12.35	-----
100	68.7	82.0
250	107.7	88.5
500	130.7	90.6
750	146.0	91.5
1000	212.0	94.2
2000	190.1	93.5

According to the data of LPR measurements, the best protection was obtained in the RR flower extract to root or leaf extracts.

4.4.4. Potentiodynamic Polarization Curves

Semi-logarithmic PP curves of MS were obtained in a 1 M HCl solution with and without varying concentrations of RR flower extract. The results of these experiments are depicted graphically in Figure 4.32. Table 4.11 shows the corrosion parameters derived from these curves, which can also be found in the previous section where they were described. The percentage was calculated using equation (4.9). The E_{corr} of MS in corrosive solution without inhibitors is -0.468 V concerning the Ag/AgCl reference electrode, as shown in Figure 4.32. When a corrosive medium is treated with RR flower extract, the corrosive medium gains more cathodic potentials, and both the anodic and cathodic current densities decrease. E_{corr} moves to more positive potentials when the concentration of the extract increases. The value of E_{corr} does not vary with inhibitor concentration except 1000 ppm, in which this value moves to less anodic values. As a result, the extract is a mixed-type

corrosion inhibitor that primarily inhibits the reaction of cathodic hydrogen evolution (Policarpi and Spinelli, 2020). The RR flower extract, in particular, slows the rate of anodic metal dissolution and the rate of cathodic hydrogen gas evolution.

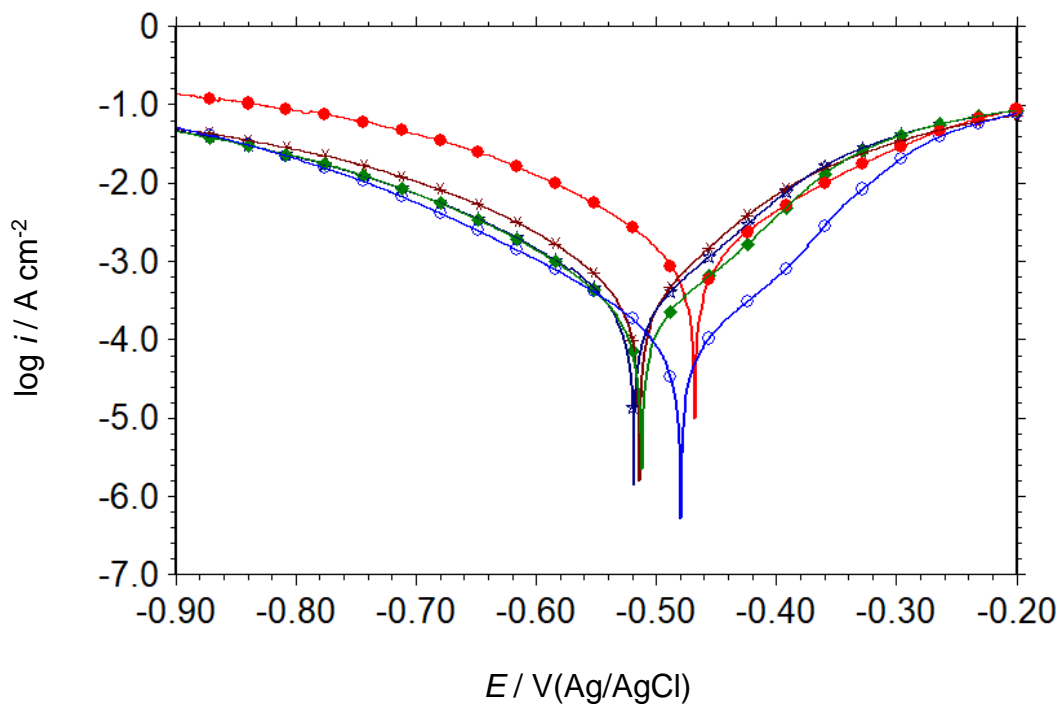


Figure 4.32. Polarization curves of MS obtained in 1 M HCl solution (●) and containing 100 (*), 250 (☆), 500 (◆) and 1000 (○) ppm RR flower extracts

As the inhibitor concentration increases, the current density decreases, and the effectiveness of the inhibition increases, as shown in Figure 4.32 and Table 4.11. Consequently, the inhibitor may function by forming a surface film of adsorbed inhibitors that acts as a barrier between the metal and the corrosive medium. Also, the rate the metal corrodes slows down whenever there is a reduction in the density of the current caused by corrosion. The η % has dropped by 94.7% at 1000 ppm, implying that adding plant extract to a corrosive environment prevents the metal from dissolving and any potential economic losses.

Table 4.11. Electrochemical parameters of MS were determined from PP measurements obtained in 1 M HCl solution in the absence and presence of various concentrations of RR flower extract, and KI added RR flower at 298 K

C_{inh} (ppm)	E_{corr} (V)	i_{corr} (mA cm ⁻²)	β_a (mV dec ⁻¹)	β_c (mV dec ⁻¹)	WL (g m ⁻² h ⁻¹)	η %
-----	-0.468	1.1401	118	120	11.88	-----
100	-0.514	0.2366	77	121	3.14	79.2
250	-0.519	0.1707	76	119	2.27	85.0
500	-0.512	0.1258	75	114	1.67	89.0
750	-0.501	0.111	66	127	1.47	90.3
1000	-0.480	0.0606	72	117	0.80	94.7
2000	-0.512	0.0820	81	121	1.09	92.8

The cathodic curves in the Tafel region of the uninhibited and inhibited solutions were nearly identical, and the β_c values in Table 4.11 are too close together, implying that the RR flower extract slows the rate of cathodic hydrogen evolution without changing the way the reaction works. Moreover, it is possible because the surface inhibitor film obstructs light. As a result, the inhibitor is effective if it covers the metal's surface. The surface coverage ($1-\theta$) is nearly full when the concentration is 1000 ppm. Corrosion occurs only on exposed metal parts or through holes in the surface film (Solmaz 2014a). More research into closing these pores or tightening the film may improve its ability to protect. Iodide ions were added to the solution stopped in the previous section. Adding RR flower extract, on the other hand, stops the flow of anodic current and reduces β_a . Also, this means that the extract alters the way the anodic reaction occurs, preventing it from happening. More investigation is required to comprehend the mechanism fully.

All the electrochemical tests demonstrated that the extract's protective ability improved with increasing concentration, reaching a maximum of 1000 ppm. Since more molecules can adhere to the surface when the concentration is high, the surface is better covered.

4.4.5. The Synergistic Inhibitory Effect of KI

Figure 4.33a shows how the E_{ocp} of MS changes when 1000 ppm KI is added to a solution that has been inhibited. The results compared to HCl solutions that have neither been inhibited nor not been inhibited. A different behaviour was observed for the KI-added inhibited solution to the previous reports in this study. The initial E_{ocp} of MS was nobler but moved to more negative potentials as the exposure time increased. The potential was unstable as only the RR flower added an acidic solution, indicating that adding KI to the inhibited solution has no positive effect. Moreover, the E_{ocp} of MS was not stable in these conditions.

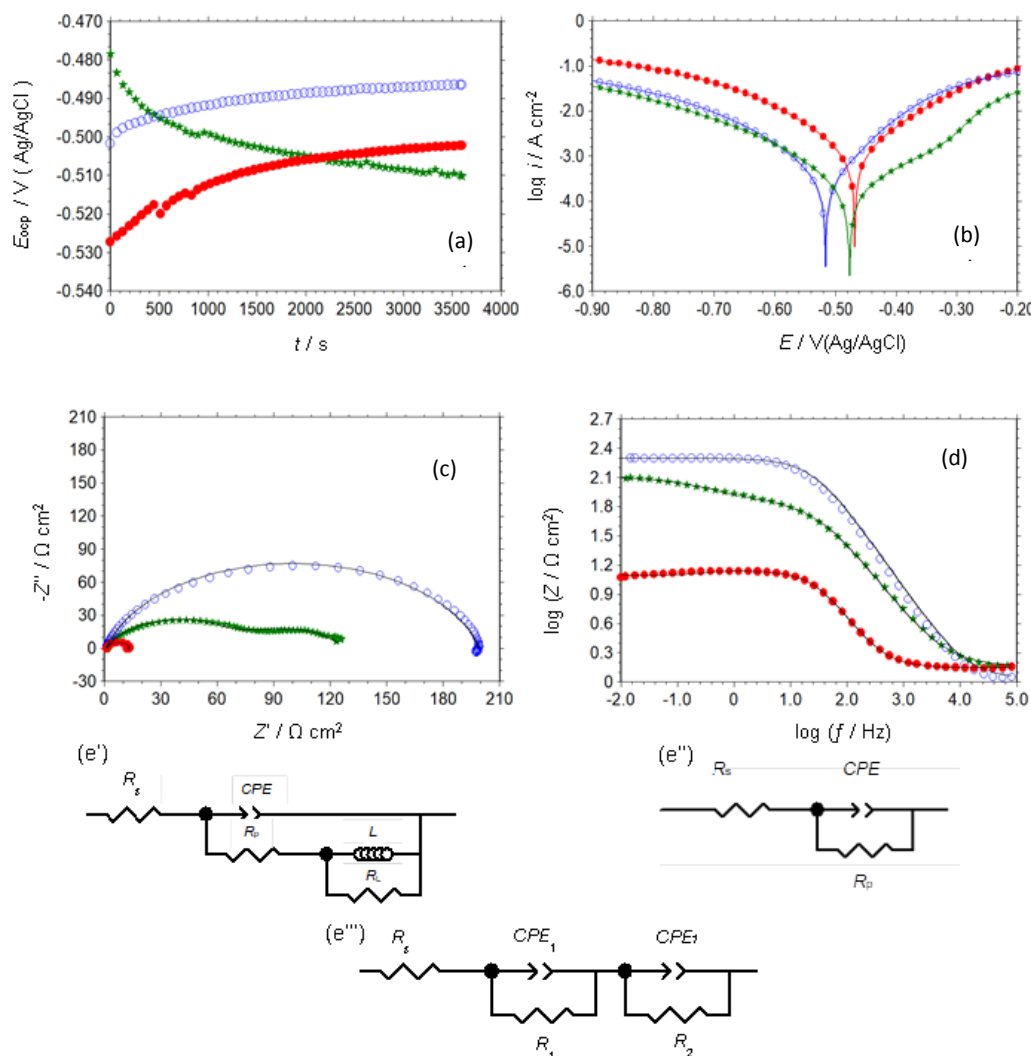


Figure 4.33. The variation of E_{ocp} of MS with immersion time (a); potentiodynamic polarization (b), Nyquist (c), and $\log Z$ - $\log f$ (Bode) (d) plots of MS obtained in 1 M HCl solution in the absence (●) and containing 1000 ppm RR flower (○), 1000 ppm RR flower+1000 ppm KI (★); EECDs proposed for the MS/solution interface in 1 M HCl and 1 M HCl+1000 ppm RR flower (c'), 1 M HCl+1000 ppm RR flower+1000 ppm KI (c'')

The PP curves (Figure 4.33a) and EIS plots (Figure 33b and c) clearly show that adding KI to the RR flower inhibited corrosive solution reduces corrosion resistance concerning the inhibited solution without KI addition. On the other hand, the protection ability is quite high. Still, we do not suggest adding KI to the inhibited solution for practical applications since the inhibitor individually performs better protection capability.

Because of the explanation above, the synergistic factor was not calculated for this system.

4.4.6. Studies of Surface Characterization

SEM, AFM, EDX, and contact angle measurements were performed on the MS surface following exposure to inhibited solutions in the absence and presence of KI. Figure 4.34 shows SEM images of the MS surface after 1 hour of exposure to 1 M HCl, 1 M HCl+1000 ppm RR flower, and 1 M HCl+1000 ppm RR flower+1000 ppm KI are shown.

The MS surface deteriorated considerably due to excessive metal breakdown, as seen in Fig. 4.34a and the enlarged version of the same figure in Fig. 4.34b. Pitting corrosion was seen in the steel in this medium, as expected, and the metal damage was not uniform. The surface was significantly altered, and pits and fractures disappeared after adding 1000 ppm RR flower extract to a corrosive media (Fig. 4.34c). The molecules of the RR flower extract appear to cover and protect the steel's surface. A higher quality, more compact, and virtually equally distributed surface coating formed when 1000 ppm KI was added to an inhibited solution (Fig. 4.34d).

AFM was used to analyze the structure of RR flower film produced in 1 M HCl solution in the absence and presence of equivalent KI quantity. Figs. 4.34e and f show 3D dimensional AFM pictures. The AFM data are remarkably similar to the SEM results. Figure 4.34e displays the appearance of the organic film on the surface. This coating is a barrier between the metal and the corrosive medium and considerably prevents MS deterioration (Jokar et al., 2016). Adding KI to the RR flower-inhibited acidic media shows a similar appearance with more particles (Fig. 4.34f). This film was not very protective, as demonstrated by the electrochemical measurements given in Figure 4.33.

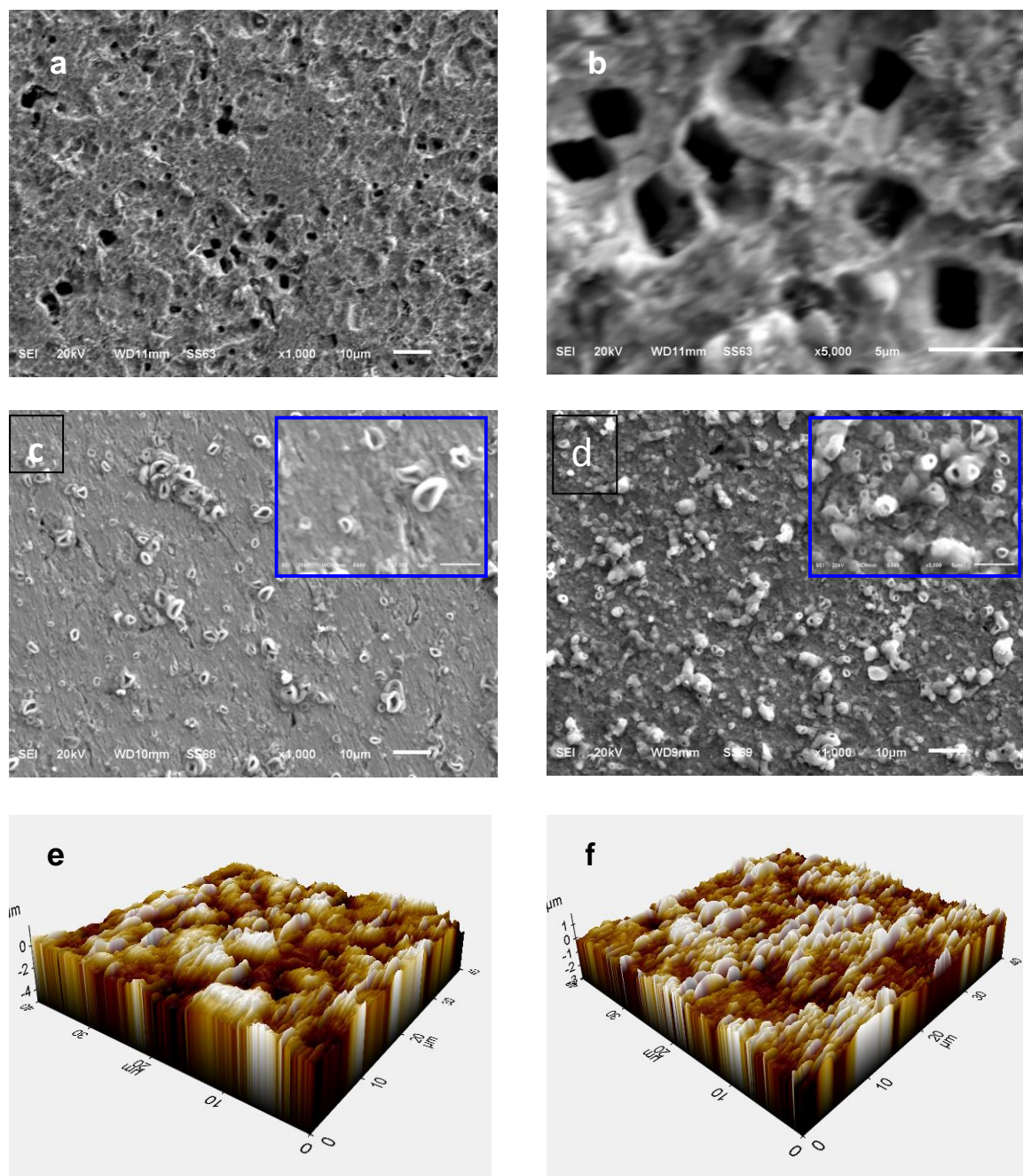


Figure 4.34. SEM images of MS taken after exposure to 1 M HCl (a and b), 1 M HCl+1000 ppm RR flower (c) and 1 M HCl+1000 ppm RR flower+1000 ppm KI (d) (The insets on c and d show 5 000x magnified images of the same surfaces); 3D dimensional AFM images of MS after exposure to 1 M HCl+1000 ppm RR flower (e) and 1 M HCl+1000 ppm RR flower+1000 ppm KI (f)

EDX was used to evaluate the inhibited surfaces' chemical composition and the extracted film's distribution on the steel surface. Figures 4.35 and 4.36 show the EDX spectra of the MS surface, the distribution of some elements on the metal (EDX-mapping images), and

cross-sectional analysis of some elements on the MS surface after exposure to 1 M HCl solution in the presence of 1000 ppm RR flower and 1000 ppm RR flower+1000 ppm KI.

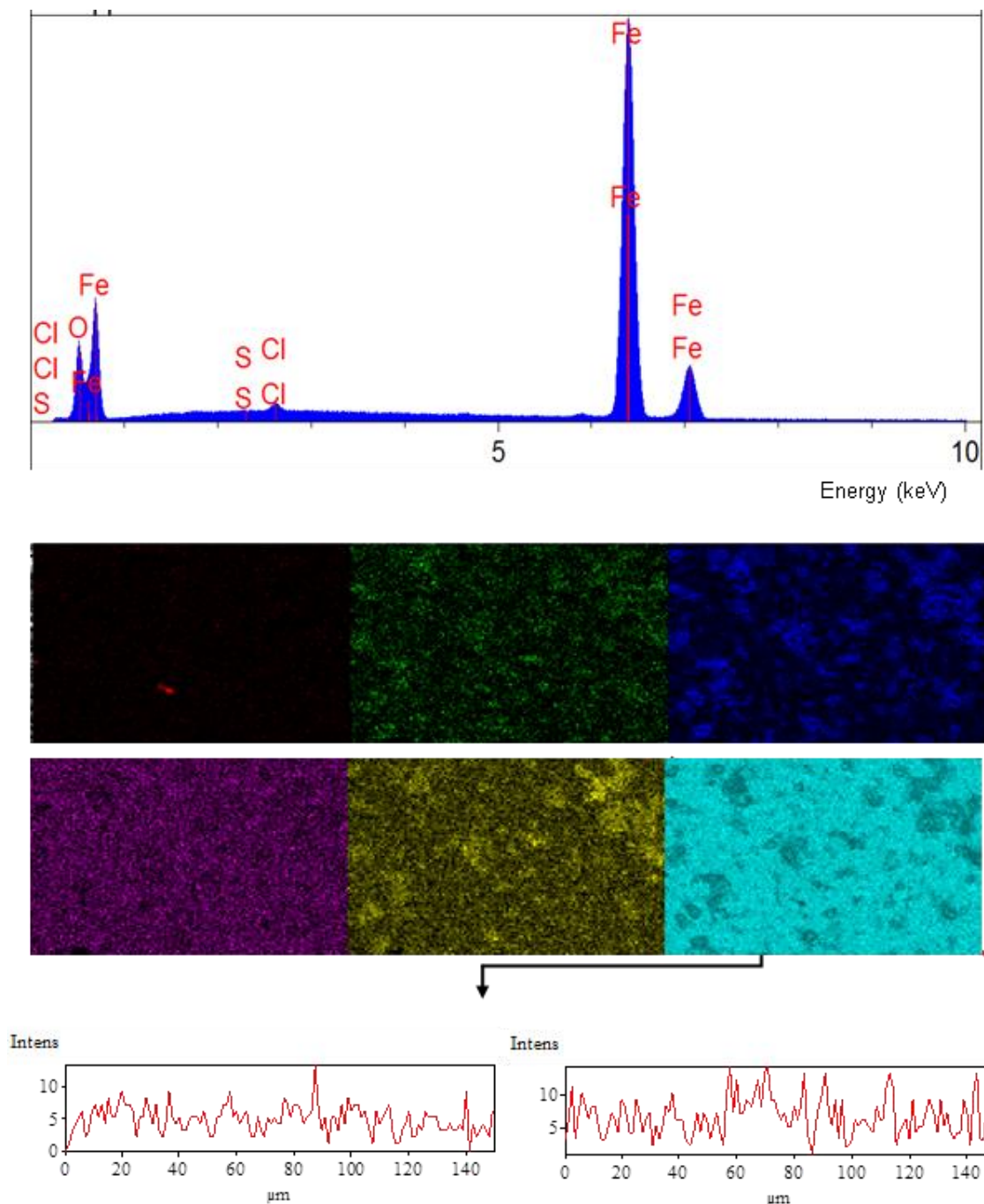


Fig. 4.35. EDX spectrum of the MS surface, the distribution of some elements on the metal surface (EDX-mapping images) and cross-sectional analyses of some elements on the surface of MS after exposure to 1 M HCl solution in the presence of 1000 ppm RR flower for 1 hour

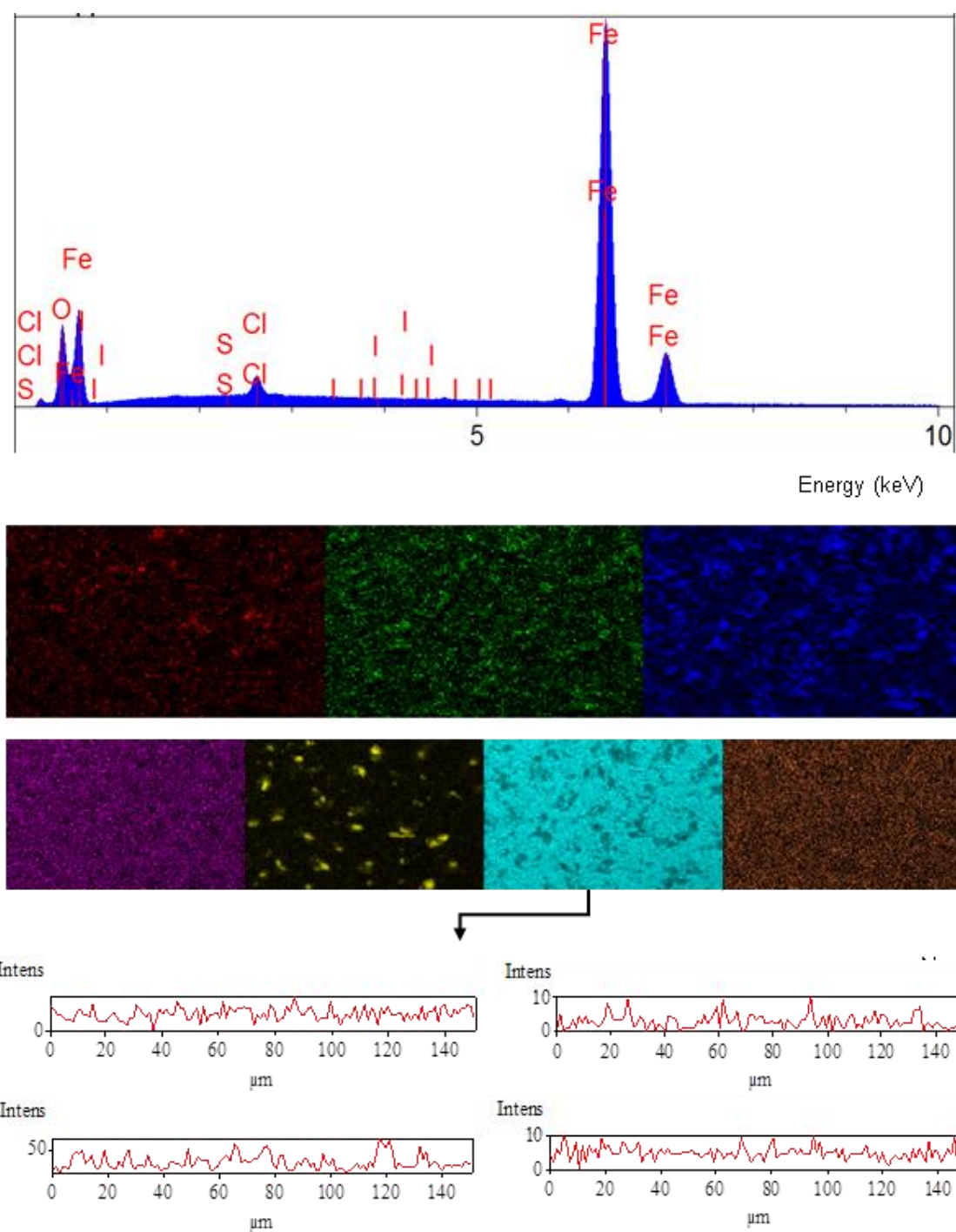


Figure 4.36. EDX spectrum of the MS surface, the distribution of some elements on the metal surface (EDX-mapping images) and cross-sectional analyses of some elements on the surface of MS after exposure to 1 M HCl solution in the presence of 1000 ppm RR flower+1000 ppm KI

The EDX spectra presented in Figures 4.36 and 4.36 demonstrate the presence of a thick coating on the steel. The gathered data indicate the production of a surface layer consisting of hetero compounds, including C, N, O, and S, which are considered active adsorption

sites. Cl is also found in two cases. Since the MS contains lower concentrations of C and O (1.720% and 0.115% O, experimental section), RR flower extract molecules should possess a higher concentration of these elements. Additionally, the presence of N and S components, absent in MS, lends weight to this hypothesis. The presence of Cl results from the adsorption of chloride ions from a 1 M HCl solution and the formation of adsorbed species or corrosion products such as FeCl_{ads} or FeCl_2 under the film or in exposed areas. In the presence or absence of KI, the quantities C, N, O, and S detected on the surface of MS do not have a linear relationship (Figures 4.35 and 4.36). Different ratios or concentrations of extract molecules adsorb on the metal surface in the presence or absence of KI.

In contrast, the addition of KI causes a reduction in the quantity of these components, which may indicate that fewer molecules are adsorbed and that the surface develops a coating that is thinner but more protective as a result of the process. After adding KI to the inhibited HCl solution, the I element shows in the EDX spectrum. Additional tests demonstrate this element's adsorption, which increases extract molecule adsorption on the steel surface. A cross-sectional study reveals the presence of a homogeneous surface coating, which is improved in the fact of KI.

Contact angle images of the MS surface after 1 hour of exposure to a 1 M HCl solution with and without adding 1000 ppm RR flower and 1000 ppm RR flower+1000 ppm KI are shown in Figure 4.37.

In the unconstrained solution, the average contact angle of the steel is 53.66° . In the presence of the RR flower extract, the average contact angle rises to 39.32° . This value is less than 90° , indicating that the film is hydrophilic. The contact angles produced a considerable change in angles, showing that the molecule adsorbed by the steel surface formed a less hydrophilic coating than the unmanaged solution. When RR flower extract and iodide ions are introduced to an inhibited solution, the contact angle reduces. This finding could be explained by a change in the orientation of the molecules and the coating of the surface with negatively charged iodide and chloride ions, specifically on the exposed surface sites harbouring the inhibitor molecules.

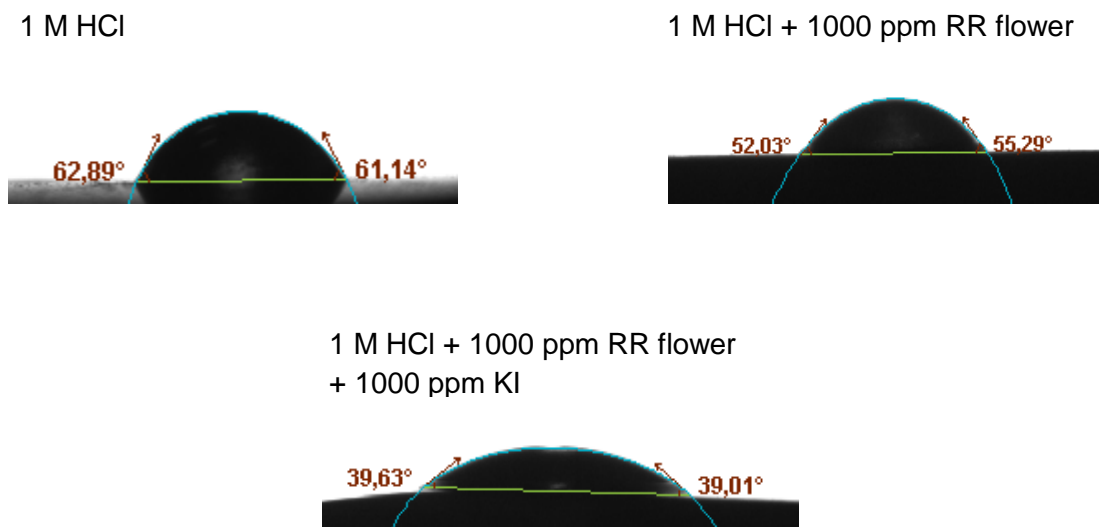


Figure 4.37. Contact angle images of the MS surface after exposure to 1 M HCl, 1 M HCl + 1000 ppm RR flower and 1 M HCl + 1000 ppm RR flower + 1000 ppm KI solutions for 1 hour

4.4.7. Mechanism of Adsorption and Inhibition Process

The surface coverage values (θ , $\theta = \eta\%/100$) for each concentration of RR flower extract were calculated and used to assess the extract's ideal isotherm. Several models were tried for this purpose, with the Langmuir adsorption isotherm providing the greatest fit, as shown in Figure 4.38.

This assumption is supported by the fact that the correlation coefficient constant, R^2 , is fairly high (0.99955) and close to 1. Therefore, we hypothesize that RR flower extract molecules adsorb on specific sites of the metal and produce a uniform monolayer coating (Shahmoradi *et al.*, 2021; Oulabbas *et al.*, 2022). The slope of this plot is 1.05, which indicates that the molecules occupy 1.05 sites of the MS surface instead of 1 (Fan *et al.*, 2011). The value of K_{ads} was derived from Eq. (4.12), and Fig. 29 is 46.27 L g^{-1} , indicating a good adsorption ability and stability of the extract molecules on the metal surface (Policarpi and Spinelli, 2020). The value of K_{ads} demonstrates that the extract molecules have a high capacity for adsorption on the metal surface. This information also indicates that the adsorption of extract molecules is preferable to their desorption (Goulart *et al.*, 2013).

Standard free energy of adsorption ($\Delta G^{\circ}_{\text{ads}}$), which is computed using equation (4.13) (Jokar *et al.*, 2016) and found to be $-26.27 \text{ kJ mol}^{-1}$. The value of $\Delta G^{\circ}_{\text{ads}}$ is negative, suggesting that the molecules of RR flower extract self-adsorb onto the MS surface. This finding shows that all organic inhibitors are self-adsorbed on the surface of the metal. The $\Delta G^{\circ}_{\text{ads}}$ value of RR flower extract is midway between -20 kJ mol^{-1} . And -40 kJ mol^{-1} is more closely related to a value of -20 kJ mol^{-1} . As a result, RR flower extract adsorption occurs as a result of both chemical and physical interactions, with the first interactions having primacy. As already discussed, chemical interactions of the extract molecules and the surface are also possible after initial physical interactions. Charge sharing between the d orbitals of metals and the free electron pairs of active adsorption centres, such as N, S, and O atoms, as well as the π electrons of double or triple bonds in organic molecules, leads to chemical interaction (Figure 4.16, a and b) (Haldhar *et al.*, 2021).

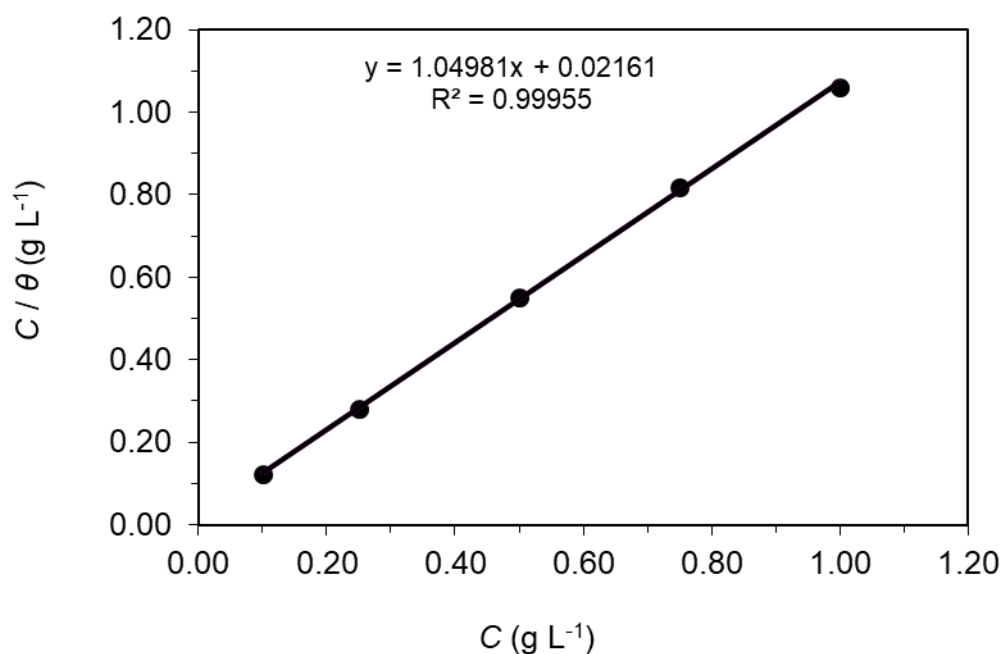


Figure 4.38. Langmuir adsorption plot of MS obtained in 1 M HCl solution with the addition of various concentrations of RR flower extract

In highly acidic solutions, many organic compounds can be found in equilibrium with their protonated analogues. Positively charged inhibitor molecules could also directly interact with the metal surface. Charge sharing between the inhibitor molecules and d orbitals of the metal is also possible.

4.4.8. Stability of Surface Inhibitor Film

The variation of anodic and the cathodic current densities as a function of time under constant +100 mV anodic and -100 mV cathodic overpotentials conducted in 1 M HCl solution containing 1000 ppm RR flower, 1000 ppm RR flower+1000 ppm KI are given in Figure 4.39.

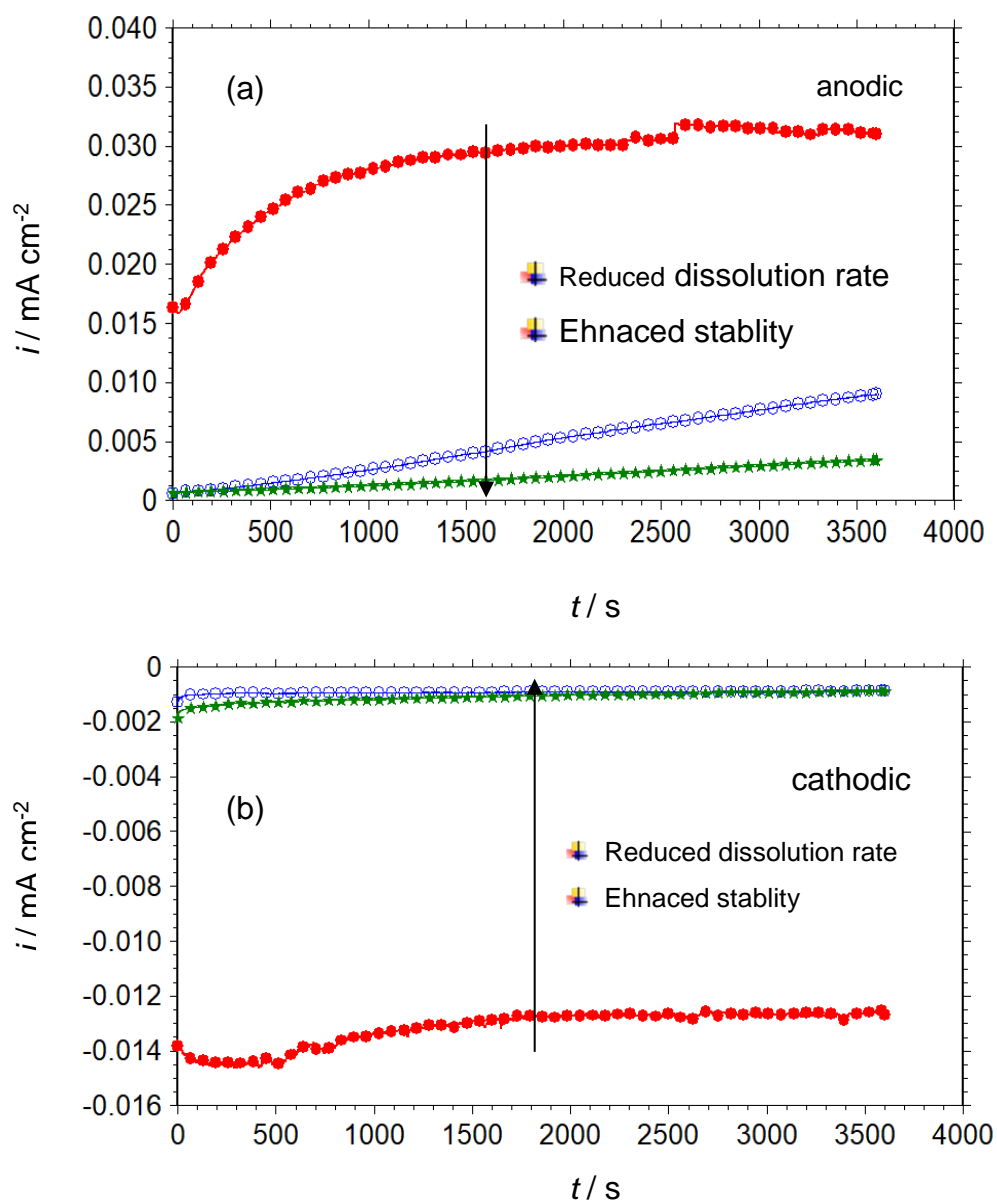


Figure 4.39. The variation of anodic and the cathodic current densities as a function of time under constant +100 mV anodic (a) and -100 mV cathodic (b) overpotentials conducted in 1 M HCl solution (●) and containing 1000 ppm RR flower (○), 1000 ppm RR flower+1000 ppm KI (★)

Figure 4.39 shows the fluctuation of anodic and cathodic current densities as a function of operation time under constant +100 mV anodic or -100 mV cathodic potentials obtained in 1 M HCl solution and containing 1000 ppm RR flower or 1000 ppm RR flower+1000 ppm KI can be shown. These results were achieved in an electrolyte containing 1000 ppm RR flower. The variations of anodic and cathodic current densities were already discussed in previous chapters and, therefore, will not be repeated here. Due to the adsorption of inhibitor molecules on the metal surface, adding 1000 ppm RR flower extract to the corrosive solution decreases early anodic or cathodic current densities. Nevertheless, the anodic current density slightly increases during electrolysis. But, the current density was quite low concerning the uninhibited solution, indicating the film's high durability under anodic potential. This film also is extremely stable under cathodic overpotentials; the cathodic current density is extremely low and more durable than that reported in 1 M HCl. Following the incorporation of 1000 ppm KI into the inhibited solution, there was a discernible shift in the behaviour of the surface film. The anodic and cathodic current densities are higher concerning the inhibited solution without KI addition.

The CV approach was also used to test the film's stability under various dynamic situations. The anodic and cathodic CVs and CV-time plots of MS in 1 M HCl, 1 M HCl+1000 ppm RR flower, and 1 M HCl+1000 ppm RR flower+1000 ppm KI. The obtained data are depicted in Figure 4.40. CA and CV outcomes are extremely compatible. The anodic and cathodic CV and CV-time plots of MS in uninhibited HCl solution were discussed in previous chapters. Moreover, when 1000 ppm KI is added to an inhibited solution, the anodic current density increases compared to an inhibited solution without KI (Figure 4.40a). In the presence of the RR flower extract, this tendency was observed. The CV-time curves (Figure 4.40g) revealed very consistent anodic current densities, indicating that the film on the MS surface is less stable than if no KI anodic potential scan was performed.

In 1 M HCl and 1000 ppm RR flower solutions containing HCl, the MS cathodic current density is essentially constant (Figure 4.40b, d and f). However, the inhibited solution without and with KI addition has lower current densities than the uninhibited solution. But, the addition of KI has no positive effect on the durability of the inhibitor film (Figure 4.40h).

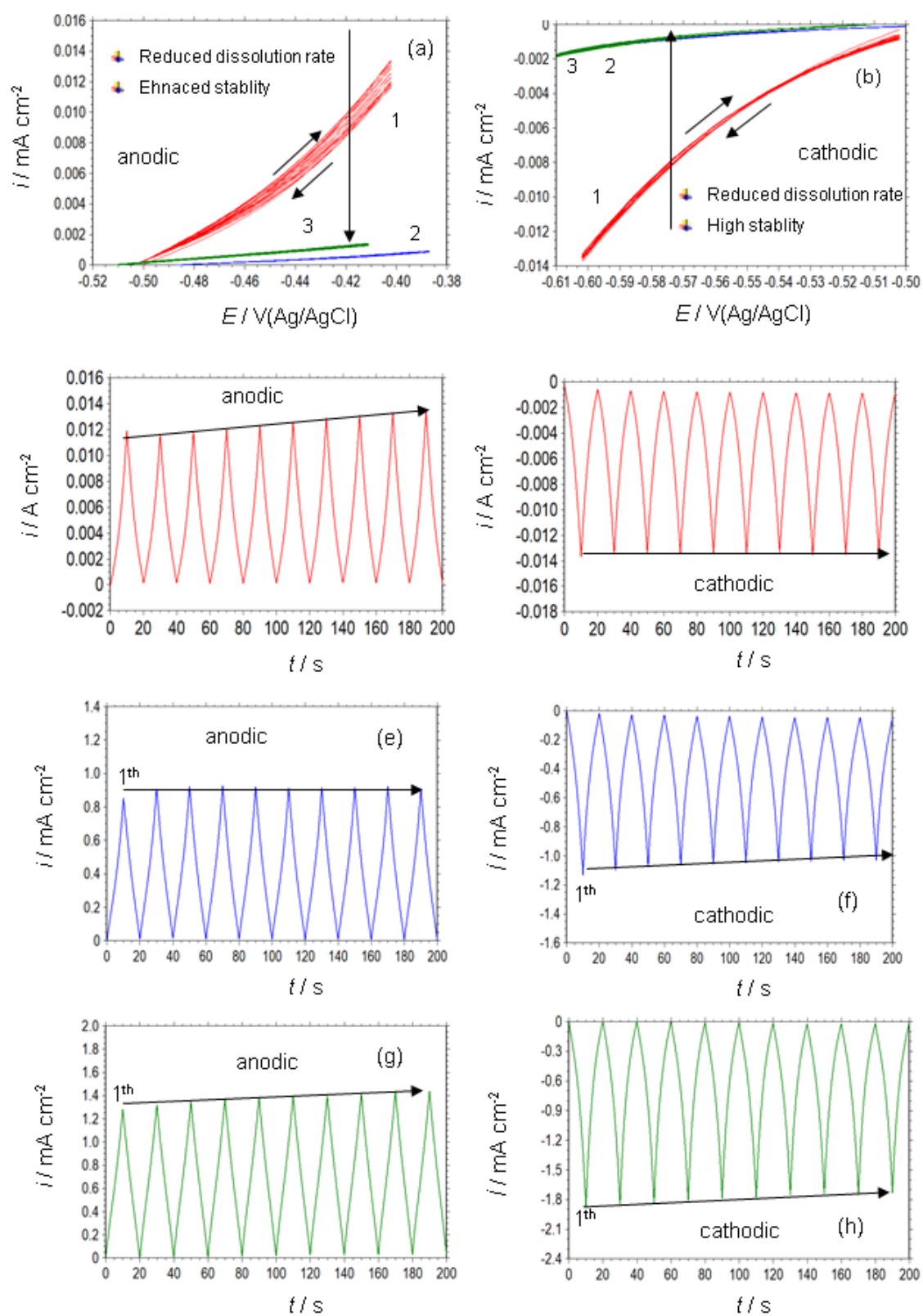


Figure 4.40. Anodic (a) and cathodic (b) CVs of MS were obtained in the test solutions (1: 1 M HCl, 2: 1 M HCl+1000 ppm RR flower, 3: 1 M HCl+1000 ppm RR flower+1000 ppm KI); Anodic CV-time plots of MS obtained in 1 M HCl (c), 1 M HCl+1000 ppm RR flower (e), 1 M HCl+1000 ppm RR flower+1000 ppm KI (g); Cathodic CV-time plots of MS obtained in 1 M HCl (d), 1 M HCl+1000 ppm RR flower (f), 1 M HCl+1000 ppm RR flower+1000 ppm KI (h)

4.4.9. The effect of Exposure Time on Protection Capability of RR Flower Extract

For practical applications, the inhibitor film is expected to have high durability with the exposure time. As reported in the earlier chapters, the RR flower has the best protection ability. Therefore, in this section, the surface film's durability and protection ability were studied for 6 hours. For his aim, the MS electrode was exposed to 1 M HCl solution in the absence and presence of 1000 ppm RR flower extract for 6 hours. Then electrochemical tests were conducted to determine corrosion rate and protection ability. The data obtained were compared with the experiments performed after 1-hour exposure. After this exposure time, the surface of MS was characterized using SEM and AFM analyses.

Nyquist and Bode plots of MS obtained in 1 M HCl solution without and with the inhibitor after 1 hour and 6 hours immersion are shown in Figure 4.41. Related electrochemical data were derived and shown in Table 4.12. The MS electrode exhibits the same behaviour after 1 hour and longer exposure time; a capacitive loop appeared at low and middle frequencies and followed an inductive loop at low frequencies. These behaviours were defined in Section 4.2. On the other hand, the resistance of MS in the uninhibited solution was reduced significantly. The MS electrode behaves very differently in the presence of the inhibitor; only one capacitive loop in Nyquist and a done-time constant in Bode plots have appeared. The finding indicates that the corrosion reaction is activation-controlled in the presence of the inhibitor. One time constant suggests a protective and tightly adhered film over the surface. The surface film provides a good physical barrier against the corrosive agents even after 4 hours. The protection ability of the extract increases to 98.3% after 6 hours.

Polarization curves (e) of MS obtained in 1000 ppm RR flower extract containing 1 M HCl solution after 1 hour and 6 hours immersion are shown in Figure 4.41 comparatively. These data are comparative with the EIS results. They indicate that a very durable and protective film forms on the surface of the metal during exposure to the inhibited solution for 6 hours.

The durability tests show that this extract could be applied for practical applications safely.

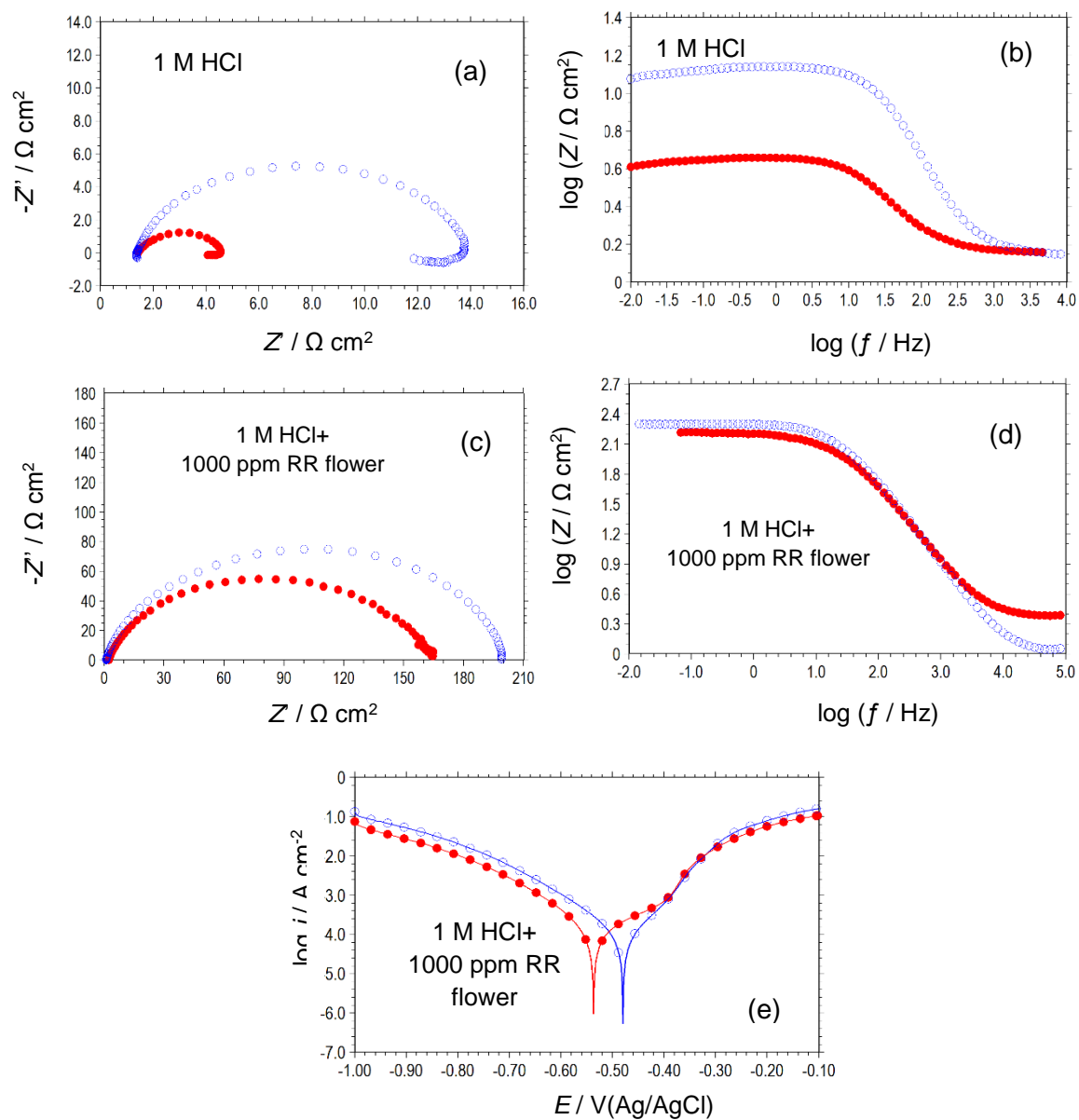


Figure 4.41. Nyquist (a, c) and Bode (b, d) plots of MS obtained in 1 M HCl solution without and with the inhibitor after 1 hour (●) and 6 hours (○) immersion; Polarization curves (e) of MS obtained in 1000 ppm RR flower extract containing 1 M HCl solution after 1 hour (●) and 6 hours (○) immersion

Table 4.12. Fitting results of EIS data and electrochemical parameters determined from EIS measurements for MS obtained in 1 M HCl solution with and without RR flower extract at 298 K after 6 h exposure

C_{inh} (ppm)	EIS						
	CPE ($10^{-6}/s^n \Omega^{-1} cm^{-2}$)	n	R_p (Ωcm^2)	L	R_L	α	η %
1 M HCl 1 hour	758	0.89	10.80	4.126	1.59	-0.63	-----
1 M HCl 6 hours	5569.9	0.83	2.71	1.12	0.43	-0.32	
1000 1 hour	68.7	0.84	198.2	-----	-----	-0.79	94.6
1000 6 hours	101.0	0.82	157.2	-----	-----	-0.72	98.3

Table 4.13. Electrochemical parameters for MS were determined from PP measurements obtained in 1 M HCl solution in the absence and presence of various concentrations of RR leaf extract at 298 K after 6 h exposure

C_{inh} (ppm)	E_{corr} (V, Ag/AgCl)	b_c (mV dec ⁻¹)	i_{corr} ($\mu A cm^{-2}$)	ν (g m ⁻² h ⁻¹)	η (%)
1 M HCl	-0.471		6136.5	81.43	-
1000	-0.537	118	155.5	2.06	98.4

4.4.10. Determination of Excess Surface Charge

A better discussion of the adsorption process of the extract could be made by determining the excess surface charge of MS in the inhibited solutions. The excess surface charge of MS was determined using the methods described in the literature (Solmaz, 2014a; Moretti *et al.*, 2013; Kardaş and Solmaz, 2006). In the described methods, the position of E_{ocp} of metal is compared concerning the related potential of zero charges (E_{pzc}) using the following equation (Solmaz 2014b):

$$E_r = E_{ocp} - E_{pzc} \quad (4.14)$$

In this equation, E_r is Antropov's rational corrosion potential (Antropov 1960). This value is defined by the electrode potential in a reduced scale, referred to as E_{pzc} of the electrode in the studied solution (Vracar and D.M. Drazic, 2002; Popova *et al.*, 2003).

EIS experiments of MS were carried out in 1 M HCl solution containing 1000 ppm RR flower extract at different overpotentials, and the obtained R_p were plotted against the applied potential. The data obtained are shown in Figure 4.42 graphically. These figures show that a maximum point appeared at -0.462 V. These potentials are called E_{pzc} of the metal (Solmaz 2014a; Solmaz 2014b). The E_{ocp} value of MS in the same conditions is shown in the figure. Using eq. (4.14), E_r is calculated as -0.025 V. Therefore, it could be said that the excess surface charge of MS was negative. Therefore, the protonated extract molecules could also directly adsorb to the metal surface

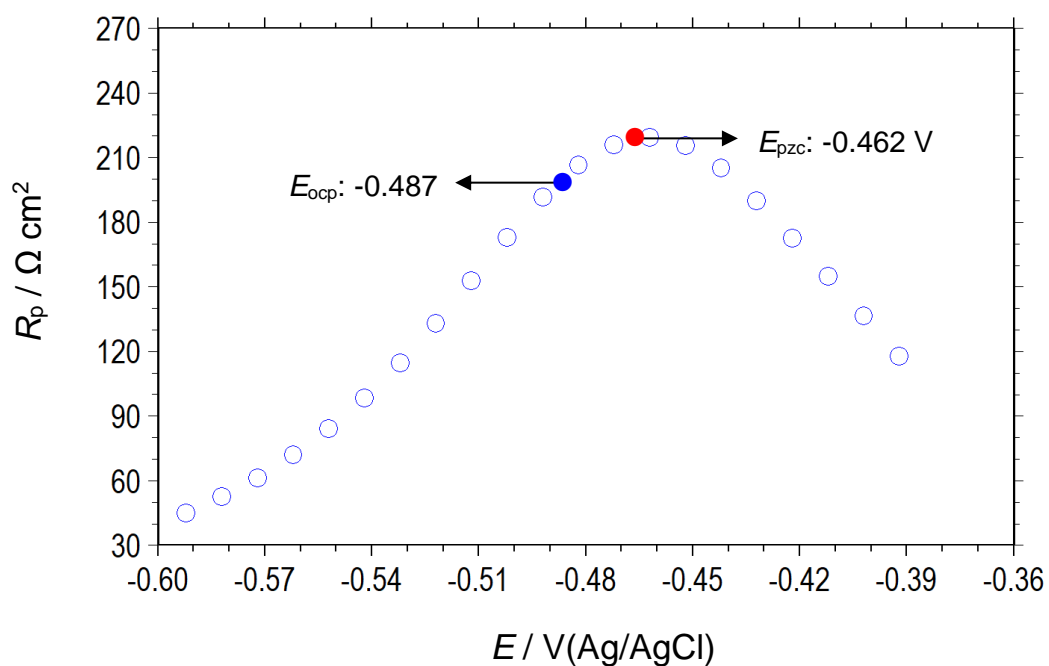


Figure 4.42. R_p vs applied potential plot in 1 M HCl solution containing 1000 ppm RR flower extract

4.5. *Rheum Ribes* (Işgin) Flower Extract's Corrosion Inhibition Capability for Steel Rebar Protection in Reinforced Concrete

One of this thesis aims is to identify the plants with high economic value and bring them into the economy, and to evaluate the unused parts of the plants used for different purposes. One of the most important components determining structures' life, quality and durability is steel rebar (SR). Corrosion of the steel used in the designs also reduces the strength and lifetime of the structure. Therefore, adding inhibitors to the concrete will increase the steel's life and form. In the previous sections, it was determined that the flower extract of the plant provided the best protection against corrosion. In this section, the inhibition effect of the flower extract on the breakdown of steel by adding to the reinforced concrete structures was investigated.

SR embedded in reinforced concrete without inhibitor and containing 1000 ppm RR flower addition was immersed into a % 3.5 NaCl solution for 168 hours. Electrochemical measurements were performed at regular intervals (6, 24, 48, 72, 96, 120, 144, and 168 hours). After 168 hours, the surface of SR was analyzed with SEM and AFM.

Nyquist and $\log Z$ - $\log f$ (Bode) (b) plots of SR, embedded in reinforced concrete without inhibitor, obtained in 3.5 % NaCl solution after various exposure times are shown in Figure 4. 43. The curves were obtained after the exposure times given above, but only some of them were provided here to show lines clearly. The solution resistance of SR embedded in the reinforced concrete is high when tempered with the data obtained in 1 M HCl solution. The solution resistance, around $30 \Omega \text{ cm}^2$ at the 6th hour, increases with the immersion time and reaches $50 \Omega \text{ cm}^2$ at the end of the 168th hour. The high solution resistance is due to the low conductivity of the electrolyte in the concrete pores. The Nyquist plot obtained after 6 hours contains two capacitive loops, one at high frequency and the other at middle frequencies. At low frequencies, a Warburg-type linear line appears. The high-frequency loop stands for charge transfer and double layer resistance, and the second for film resistance from accumulated corrosion products on the steel surface. The low-frequency line shows that the corrosion is diffusion controlled. The corrosion rate determining step is the diffusion of corrosive ions to the surface of the metal. Increasing immersion time reduces corrosion resistance, which is due to excess steel dissolution in the aggressive solution. After 72 hours, the corrosion rate does not change much.

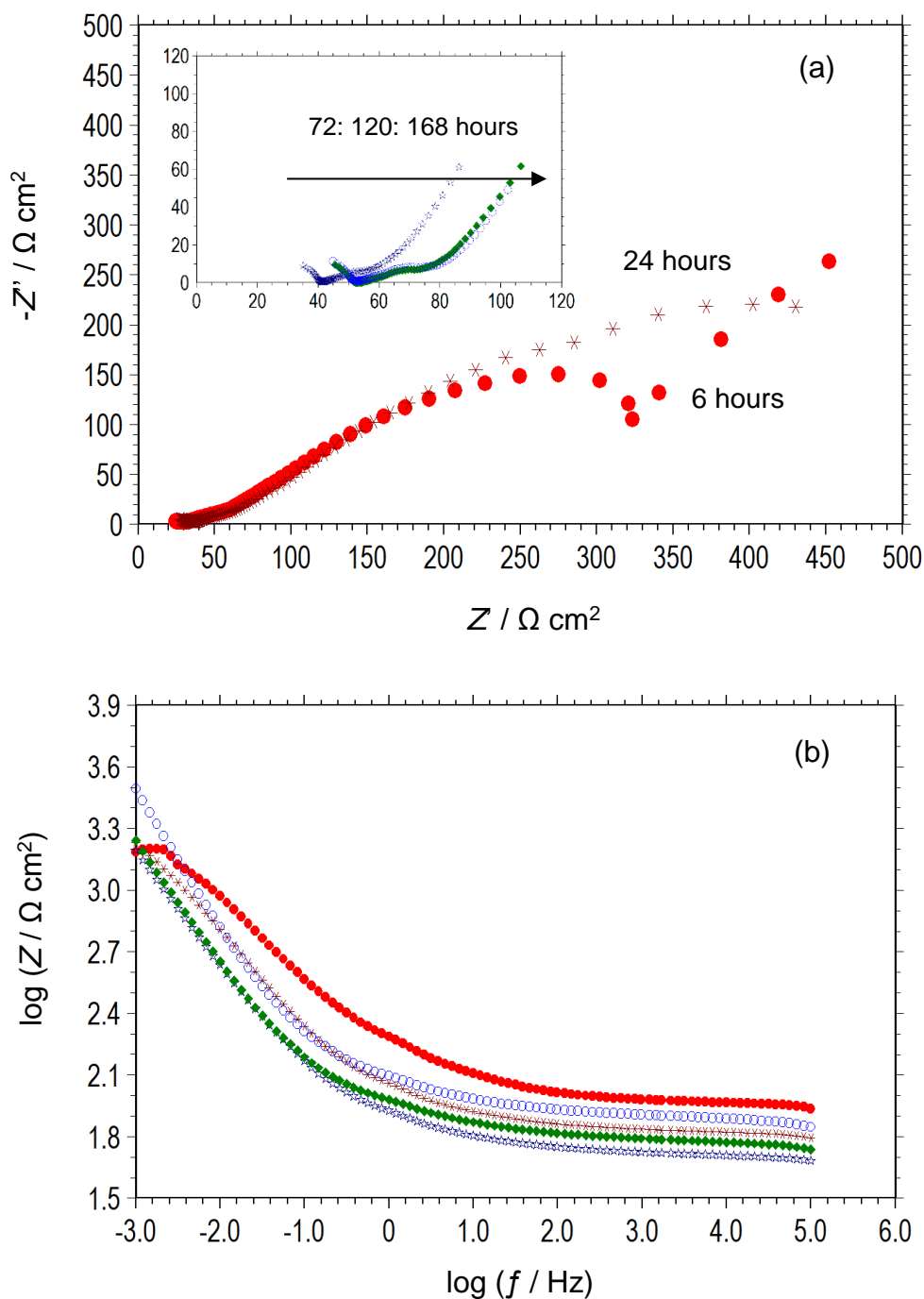


Fig. 4.43. Nyquist (a) and $\log Z$ - $\log f$ (Bode) (b) plots of SR, embedded in reinforced concrete without inhibitor, obtained in 3.5 % NaCl solution after various exposure times (6 hours (●), 24 hours (*), 72 hours (☆), 120 hours (◆) and 168 hours (○))

The Nyquist and $\log Z$ - $\log f$ (Bode) plots of SR embedded in reinforced concrete containing 1000 ppm RR flower addition are shown in Figure 4. After exposure for various lengths, these plots were obtained in a 3.5% NaCl solution. The plots' results indicate that adding

RR flower extract to the reinforced concrete does not alter the overall appearance of the plots or the patterns they follow. But, both charge transfer resistance and film resistance significantly increased. The enhanced resistance against the corrosion indicates that the RR extract molecules adsorb on the SR and provide significant protection. The low-frequency Warburg-like linear line suggests that the reaction is diffusion-controlled.

The R_p values of SR embedded in reinforced concrete without and containing 1000 ppm RR flower extract were calculated from LPR measurements, and the data obtained are shown in Table 4. 43. The extract provides a high capability of inhibition of the steel in each case. Even after 168 hours, it still offers a very high protection efficiency of 84.0%.

Table 4. 14. LPR data was obtained in 3.5% NaCl solution after 168 hours of exposure at 298 K for SR embedded in reinforced concrete without RR flower and containing 1000 ppm RR flower extract.

t (hour)	R_p (Ω cm ²)		η %
	Without inhibitor	With inhibitor	
6	167.9	601.5	72.1
24	148.0	395.7	62.6
48	74.9	261.6	71.4
72	55.1	345.8	84.1
96	54.8	308.2	82.2
120	60.5	326.0	81.4
144	79.6	339.2	76.5
168	79.3	495.3	84.0

Polarization curves of SR embedded in reinforced concrete without and containing 1000 ppm RR flower, obtained in 3.5 % NaCl solution after 168 hours of exposure, are given in Figure 4. 43. The presence of RR flower extract in the reinforced concrete moves E_{ocp} of SR to nobler potentials. It diminishes both anodic and cathodic current densities. Therefore, the inhibitor act as a mixed-type, mostly acting on an anodic reaction. The current density

of 0.0 V and 1.1 V reduced significantly, and a passive region appeared, which could be assigned to forming an adherent and protective film on the surface. This film remains on a metal surface even at high potential, suggesting that the film is very durable on the surface.

SR embedded in reinforced concrete without and with 1000 ppm RR flower were exposed to 3.5 % NaCl solution for 168 hours, and the surface of SR was analyzed with SEM and AFM. The images taken are shown in Figure 4. 44.

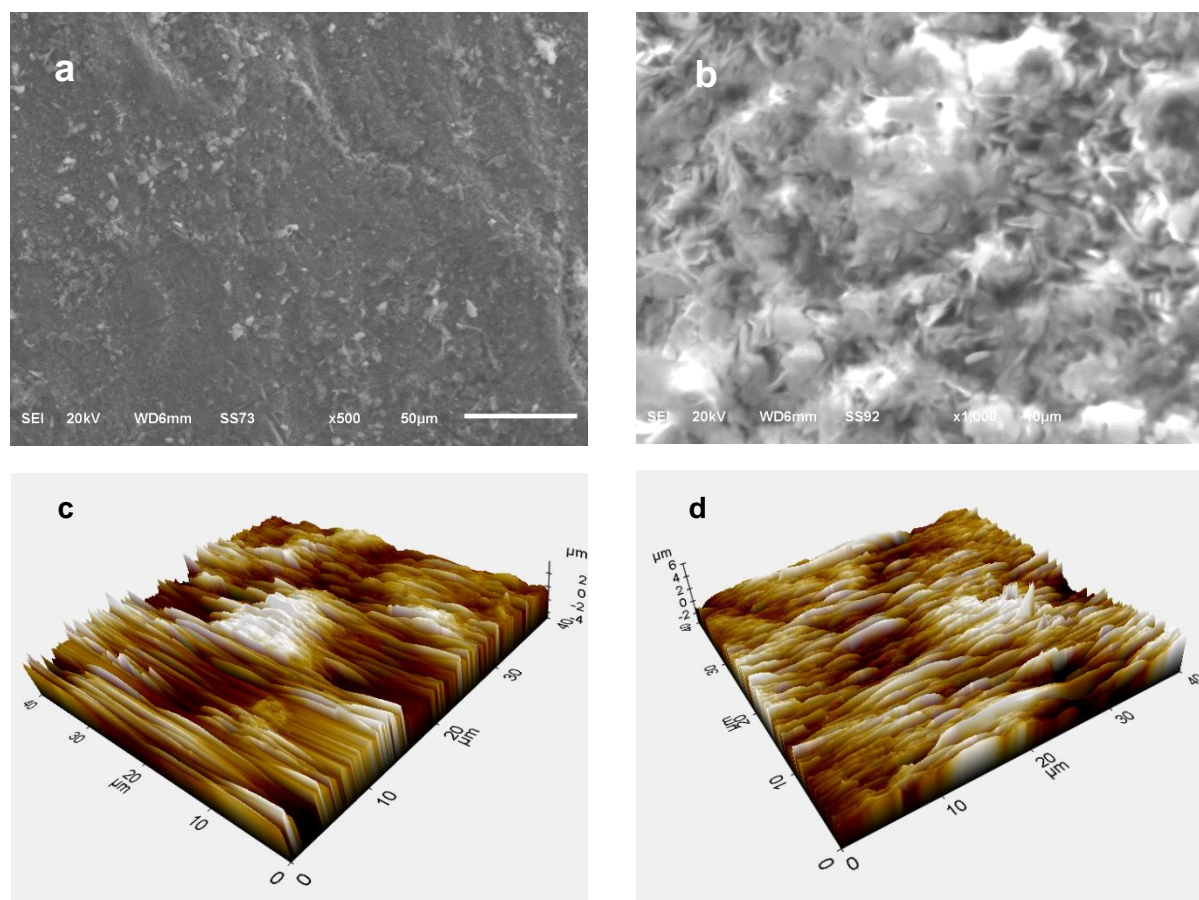


Figure 4. 44. SEM and 3D AFM images of the surface of SR embedded in reinforced concrete without (a and c) and with 1000 ppm RR flower (b and d) were obtained in 3.5 % NaCl solution after 168 hours of exposure

The steel is damaged in the absence of the inhibitor. But, a homogenous distributed and dense inhibitor film forms when RR flower extract is present in the reinforced concrete. Similar observations are seen from AFM data. This high-quality film is responsible for the high protection ability of the flower extract.

5. CONCLUSIONS AND SUGGESTIONS

A- COPPER

The extracts of different parts of ışgın, such as flower (RRF), leaf (RRL), and root (RRR), were prepared, and electrochemical techniques investigated their protective effects on copper corrosion in 1 M HCl solution. The surface of the metal after exposure to the test solutions was investigated by SEM, EDX, and contact angle measurements. The following major points could be concluded:

- 1) The effects of extracts obtained from various parts of the RR on copper behaviour in an acidic environment differed.
- 2) The extracts are adsorbed on the Cu surface and form a compact and adherent film, preventing Cu corrosion.
- 3) The RRF extract provided the best corrosion protection.
- 4) RRR extract was ineffective at protecting Cu from corrosion in 1 M HCl.
- 5) The extracts contained anodic and mixed-type corrosion inhibitors.
- 6) The addition of RRF to the corrosive solution increases the surface's hydrophobicity.
- 7) RRF has more than 60% corrosion protection efficiency, but the inhibition efficiency could be better.

B- MILD STEEL

Electrochemical, spectroscopic, microscopic, and contact angle measurements were used to investigate the adsorption and inhibitory impact of RR plant extracts on MS corrosion in 1 M HCl solution. The gathered data might be summed up as follows:

- 1) RR plant extract molecules adsorb on the surface of MS from a 1 M HCl solution and create an anticorrosion surface coating.
- 2) Its protective effectiveness increases as the extract concentration and temperature rise.

- 3) The protective performance of the extracts were in the order of RR flower > RR leaf > RR root.
- 4) The extract molecules formed adherent, homogenously distributed and protective films on metal surface and provide protection ability againt to corrosion.
- 5) When iodide ions are added to an inhibited solution, the surface inhibitor layer becomes more stable, more homogeneous, and more compact, resulting in improved protective ability and electrochemical stability.
- 6) At 1000 ppm extract concentration; the protection efficiency of RR root extract increased from 84.5% to 89.1%, protection efficieny of RR leaf extract increased from 89% to 93.1% after the addition of 1000 ppm KI to the inhibited solution. But, there was not a synergism between iodide ions and RR flower, which had 94.6% inhibition efficiency individually.
- 7) The inhibition efficiency of RR flower extract on MS corrosion increased to 98.3% after 6 hours exposure.
- 8) The RR extracta are corrosion inhibitor of mixed type with a primarily cathodic effect. In contrast, the plant dominates the anodic reaction when iodide ions are present.
- 9) The extract molecules adsorbed to metal surface via physical and chemical interactions.
- 10) In the presence of the inhibitor, the surface becomes more hydrophobic compared to the definitive solution. In contrast, hydrophilic surface characteristics increase in the presence of iodide ions.

C- STEEL REBAR

The inhibition effect of the flower extract on the breakdown of SR by adding to the reinforced concrete structures was investigated. SR embedded in reinforced concrete without inhibitor and containing 1000 ppm RR flower addition was immersed into a % 3.5 NaCl solution for 168 hours. Electrochemical measurements were performed at regular intervals. After 168 hours, the surface of SR was analyzed with SEM and AFM. The gathered data might be summed up as follows:

- 1) Adding RR flower extract to the reinforced concrete does not alter the mechanism of corrosion reaction. The low-frequency is diffusion-controlled.

- 2) Both charge transfer resistance and film resistance significantly increased.
- 3) The extract provides a high capability of inhibition of the steel. Even after 168 hours, it still offers a very high protection efficiency of 84.0%.
- 4) The inhibitor act as a mixed-type, mostly acting on an anodic reaction.
- 5) A homogenous distributed, stable and dense inhibitor film forms when RR flower extract is present in the reinforced concrete. This high-quality film is responsible for the high protection ability of the flower extract.

REFERENCES

Adam, M. R., Rahim, A. A., Shah, A. M. (2015). Synergy between iodide ions and mangrove tannins as inhibitors of mild steel corrosion. *Annals of Forest Science, Springer Nature*, 72(1), 9-15.

Advanced Multifunctional Corrosion Protective Coating Systems for Light-Weight Aircraft Alloys-Actual Trends and Challenges. <https://www.intechopen.com>, 2022. (accessed on March 21, 2022).

Ahmad, Z. (2006). *Principles of Corrosion Engineering and Corrosion Control*. (p.11-162). Burlington, USA: Elsevier Ltd.

Alaaddin, A. M., Al-Khateb, E. A., Jager A. K. (2007). Antibacterial activity of Iraqi Rheum ribes root. *Pharmaceutical Biology*, 45(9), 688-90.

Alinejad, S., Naderi, R., Mahdavian, M. (2017). Effect of inhibition synergism of zinc chloride and 2-mercaptobenzoxazole on protective performance of an eco-friendly silane coating on mild steel. *Journal of Industrial and Engineering Chemistry*, 48, 88-98.

Al Zubaidy, E. A. H. and Al Tamimi, A. (2012). Reduction of corrosion process in steel bars using inhibitors. *International Journal of Electrochemical Science*, 7(7), 6472–6488.

Andiç, S., Tunçtürk, Y., Ocak, E., Köse, Ş. (2009). Some Chemical Characteristics of Edible Wild Rhubarb Species (*Rheum Ribes L.*). *Research Journal of Agriculture and Biological Sciences*, 5(6), 973-977.

Anejjar, A., Zarrouk, A., Salghi, R., Zarrok, H., Hmamou, D. B., Hammouti, B., Elmahi, B., and Al-Deyab, S. S. (2013). Studies on the inhibitive effect of the ammonium Iron (II) sulphate on the corrosion of carbon steel in HCl solution. *Journal of Materials and Environmental Science*, 4, 583-592.

Asadi N., Ramezanzadeh, M., Bahlakeh, G., Ramezanzadeh, B. (2019). Utilizing Lemon Balm extract as an effective green corrosion inhibitor for mild steel in 1M HCl solution: A detailed experimental, molecular dynamics Monte Carlo and quantum mechanics study. *Journal of the Taiwan Institute of Chemical Engineers*, 95, 252-272.

Ashassi-Sorkhabi, H., Majidi, M. R. and Seyyedi, K. (2004). Investigation of inhibition effect of some amino acids against steel corrosion in HCl solution. *Applied Surface Science*, 225 (1–4), 176–185.

Aslam, R., Mobin, M., Zehra, S., Aslam, J. (2022). A comprehensive review of corrosion inhibitors employed to mitigate stainless steel corrosion in different environments. *Journal of Molecular Liquids*, 364, 2022.

Amin, M. A. and Ibrahim, M. M. (2011). Corrosion and corrosion control of mild steel in concentrated H₂SO₄ solutions by a newly synthesized glycine derivative. *Corrosion Science*, 53, 873–85.

Anees, A. K., Ahmed, N. A., Ahmed, N. A., Kadhim, M M., Ahmed, A. F. (2022). Combined influence of iodide ions and Xanthium Strumarium leaves extract as eco-friendly corrosion inhibitor for low-carbon steel in hydrochloric acid. *Current Research in Green and Sustainable Chemistry* , 5, 100278.

Antropov, L. I. and King, C.V. (1961). Kinetics of electrode processes and null points of metals. *The Electrochemical Society*, 108, 219.

Aramaki, K., Hagiwara, M., Nishihara, H. (1987). The synergistic effect of anions and the ammonium cation on the inhibition of iron corrosion in acid solution. *Corrosion Science*, 27(5), 487-497.

Aygün, A., Gülbağça, F., Nas, M. N., Alma, M. H., Çalimli, M.H., Ustaoglu, B., Altunoglu, Y., Baloğlu, M. C., Cellat, K. Şen, F. (2020). Biological synthesis of silver nanoparticles using Rheum ribes and evaluation of their anticarcinogenic and antimicrobial potential: A novel approach in phytonanotechnology. *Journal of Pharmaceutical and Biomedical Analysis*, 179, 113012.

Bardal, E. (2004). *Corrosion and Protection*. (p.53-131). Manchester, UK : Springer .

Bazaz, F. B. S., Khajeh, K. A. M., Shokouhei, Z. H. R. (2005). In vitro antibacterial activity of Rheum ribes extract obtained from various plant parts against clinical isolates of gram negative pathogens. *Journal of Pharmacy*, 2, 87-91.

Bedair, M. A., Soliman, S. A., Metwally, M. S. (2016). Synthesis and characterization of some nonionic surfactants as corrosion inhibitors for steel in 1.0M HCl (Experimental and Computational study). *Industrial & Engineering Chemistry*, 41, 10-22.

Behpour, M., Ghoreishi, S.M., Mohammadi, N., Soltani, N., Salavati-Niasari, M. (2010). Investigation of some Schiff base compounds containing disulfide bond as HCl corrosion inhibitors for mild steel. *Corrosion Science*, 52, 4046–4057.

Bolzoni F., Brenna, A., Ormellese, M. (2022). Recent Advances in the Use of Inhibitors to Prevent Chloride-Induced Corrosion in Reinforced Concrete. *Cement and Concrete Research*, 154, 106719.

Davis, J.R. (2000). *Corrosion: Understanding the Basics*. (p. 99-192). Ohio, USA : ASM International.

Daoudi, W., El Aatiaoui, A., Falil, N., Azzouzi, M., Berisha, A., Olasunkanmi, O., Dagdag, E., Ebenso. E., Koudad, M., Aouinti, M., Loutou, M., Adyl, O. (2022). Essential oil of *Dysphania ambrosioides* as a green corrosion inhibitor for mild steel in HCl solution. *Journal of Molecular Liquids*, 363, 11983.

Da Rocha, J.C., Ponciano Gomes, J.A.C., D'Elia, E., Gil Cruz, A.P., Cabral, L.M.C., Torres, A.G., Monteiro, M.V.C., (2012). Grape pomace extracts as green corrosion inhibitors for carbon steel in hydrochloric acid solutions, *International Journal of Electrochemical Science*, 7, 11941-11956.

De Britto Policarpi, E., Almir Spinelli, A. (2020) Application of *Hymenaea stigonocarpa* fruit shell extract as eco-friendly corrosion inhibitor for steel in sulfuric acid. *Journal of the Taiwan Institute of Chemical Engineers*, 116, 215-222.

Dehghani, A., Bahlakeh, G., Ramezanzadeh, B., Ramezanzadeh, M. (2019) Potential of Borage flower aqueous extract as an environmentally sustainable corrosion inhibitor for acid corrosion of mild steel. *Electrochemical and theoretical studies. Journal of Molecular Liquids*; 277, 895-911.

Dehri, I., Özcan, M. (2006) The effect of temperature on the corrosion of mild steel in acidic media in the presence of some sulphur-containing organic compounds. *Materials Chemistry and Physics*, 98, 316-323.

Deyab, M. (2015). Egyptian licorice extract as a green corrosion inhibitor for copper in hydrochloric acid solution. *Journal of Industrial and Engineering Chemistry*, 22, 384-389.

Dileep Kumar Yadav, M.A. Quraishi, B. M. (2012). Inhibition effect of some benzylidenes on mild steel in 1 M HCl an experimental and theoretical correlation. *Corrosion Science*, 55, 254-266.

Döner, A., Doğan, T., Dehri, I. (2014) Experimental studies of 2-pyridinecarbonitrile as corrosion inhibitor for mild steel in hydrochloric acid solution. *Corrosion Science*, 82, 125-132.

Döner, A., Solmaz, R., Özcan, M., Kardaş, G. (2011). Experimental and theoretical studies of thiazoles as corrosion inhibitors for mild steel in sulphuric acid solution. *Corrosion Science*, 53(9), 2902-2913.

Ehteshamzadeh, M., Jafari, A. H., Naderia, E., Hosseini, M. G. (2009). Effect of carbon steel microstructures and molecular structure of two new Schiff base compounds on inhibition performance in 1 M HCl solution by EIS. *Materials Chemistry and Physics*, 113(2-3), 986-993.

El Hajjaji, F., Salim, R., Ech-chihbi, E., Titi, A., Mousslim, M., Kaya, S., El Ibrahimy, B., Taleb, M. (2021). New imidazolium ionic liquids as ecofriendly corrosion inhibitors for mild steel in hydrochloric acid (1 M): Experimental and theoretical approach. *Journal of the Taiwan Institute of Chemical Engineers* 123, 346-362.

El Ibrahimy, A. J., Tahar, B. A., Chadili, M., El Issami, S., Jbara, O., Khallaayoun, A., Bazzi, L., (2018). Application of *Zizyphun Lotus*-pulpe of jujube extract as green and promising corrosion inhibitor for copper acidic medium. *Journal of Molecular Liquids*, 268, 102-113.

Erbil, M. (1985). *Korozyon*. (p. 1-100). Ankara, Türkiye: Segem.

Faisal, M., Saeed, A., Shahzad, D., Abbas, N., Ali Larik, F., Ali Channar, P., Abdul Fattah, T., Muhammad Khan, D., Aaliya Shehzadi, S. (2018). General properties and comparison of the corrosion inhibition efficiencies of the triazole derivatives for mild steel. *Corrosion Reviews*, 36, 507-545.

Faiz, M., Zahari, A., Awang, K., Hussin, H., (2020). Corrosion inhibition on mild steel in 1 M HCl solution by: *Cryptocarya nigra* extracts and three of its constituents (alkaloids). *RSC Advances*, 10, 6547-6562.

Farag, A. A., Hegazy, M. A. (2003). Synergistic inhibition effect of potassium iodide and novel Schiff bases on X65 steel corrosion in 0.5 M H₂SO₄. *Corrosion Science*, 74, 168-177.

Farhadian, A., Rahimi, A., Safaei, N., Shaabani, A., Abdouss, M., Alavi, A. (2020) A theoretical and experimental study of castor oil-based inhibitor for corrosion inhibition of mild steel in acidic medium at elevated temperatures. *Corrosion Science*, 175, 108871.

Farsak, M., Ongun, A., Kardaş, G. (2017). Anticorrosion Effect of 4-Amino-5-(4-pyridyl)-4H-1,2,4-triazole-3-thiol for Mild Steel in HCl Solution. *ChemistrySelect*, 2, 3676-3682.

Fernine, Y., Salim, R., Arrousse, N., Haldhar, R., El Hajjaji, F., Seong-Cheol, K., Touhami, M. E., Taleb, M. (2022). Anti-corrosion performance of *Ocimum basilicum* seed extract as environmental friendly inhibitors for mild steel in HCl solution: Evaluations of electrochemical, EDX, DFT and Monte Carlo. *Journal of Molecular Liquids*, 355, 118867.

Fontana, M. G. (1987). *Corrosion Engineering*. (p.1-73). Singapore: McGraw-Hill Company.

Gerengi, H., Sahin, H.İ. (2012). *Schinopsis lorentzii* Extract As a Green Corrosion Inhibitor for Low Carbon Steel in 1 M HCl Solution. *Journal of Industrial and Engineering Chemistry*, 51, 780-787.

Gerengi, H., Uygur, I., Solomon, M., Yildiz, M., Haydar, G. (2016) .Evaluation of the inhibitive effect of *Diospyros kaki* (Persimmon) leaves extract on St37 steel corrosion in acid medium. *Sustainable Chemistry and Pharmacy*, 4, 57-66.

Ghoreishiamiri, S., Raja, P.B., Ismail, M., Hidayah, N. (2020). Mechanical properties of contaminated concrete inhibited by *Areca catechu* leaf extract as a green corrosion inhibitor. *Asian Journal of Civil Engineering*, 21, 1355-1367.

Global corrosion Awareness Day. <https://www.globenewswire.com>, 2022. (accessed on February 19, 2021).

Gromboni, M. F., Sales, A., Rezende, M. A. M., Moretti, J. P., Corradini, P. G., Mascaro, L. H., (2021). Impact of agro-industrial waste on steel corrosion susceptibility in media simulating concrete pore solutions. *Journal of Cleaner Production*, 284, 124697.

Haldhar, R., Kim, S. C., Prasad, D., Bedair, M. A., Bahadur, I., Kaya, S., Dagdag, O., Guo, L. (2021). Papaver somniferum as an efficient corrosion inhibitor for iron alloy in acidic condition DFT, MC simulation, LCMS and electrochemical studies. *Journal of Molecular Structure*, 1242, 130822.

Hamzeh, S., Farokhi, F., Heydari, R., Manaffar, R. (2014). Renoprotective effect of hydroalcoholic extract of *Rheum ribes* root in diabetic female rats. *Avicenna journal of phytomedicine*, 4, 392-401.

Haldhar, R., Prasad, D., Saxena, A., Kumar, R. (2018). Experimental and Theoretical Studies of *Ficus religiosa* as Green Corrosion Inhibitor for Mild Steel in 0.5 M H₂SO₄ Solution. *Sustainable Chemistry and Pharmacy*, 9, 95-105.

Hajjaji, F. E. L., Salim, R., Ech-chihbi, E., Titi, A., Messali, M., Kaya, S., El Ibrahim, B., Taleb, M. (2021). New imidazolium ionic liquids as ecofriendly corrosion inhibitors for mild steel in hydrochloric acid (1 M): Experimental and theoretical approach. *Journal of the Taiwan Institute of Chemical Engineers*, 123, 346-62.

Hossain, N., Asaduzzaman Chowdhury, M., Kchaou, M. (2021). An overview of green corrosion inhibitors for sustainable and environment friendly industrial development. *Journal of Adhesion Science and Technology*, 35(7), 673-690.

Hongqiang, F., Shuying, L., Zongchang, Z., Hua, W., Zhicong, S., Lin, Z. (2011). Inhibition of brass corrosion in sodium chloride solutions by self-assembled silane films. *Corrosion Science*, 53, 4273-4281.

Hu, J., Zhu, Y., Hang, J., Yu, Q., Wei, J. (2021). The effect of organic core-shell corrosion inhibitors on corrosion performance of the reinforcement in simulated concrete pore solution. *Construction and Building Materials*, 267, 121011.

Iskin Otu. <http://www.iskinotu.com>. (accessed on February 21, 2021).

Jafari, H., Akbarzade, K., Danaee, I. (2019). Corrosion inhibition of carbon steel immersed in a 1 M HCl solution using benzothiazole derivatives. *Arabian Journal of Chemistry*, 12 (7), 1387-1394.

Jiang, S. B., Jiang, L. H., Wang, Z. Y., Song, S., Yan, X. (2017). Deoxyribonucleic acid as an inhibitor for chloride-induced corrosion of reinforcing steel in simulated concrete pore solutions. *Construction and Building Materials*, 150, 238-247.

Ji, G., Dwivedi, P., Sundaram, S., Prakash, R. (2016). Extract of *Argemone mexicana* roots for effective protection of mild steel in an HCl environment. *Research on Chemical Intermediates*, 42, 439-459.

Jokar, M., Farahani, T.S., Ramezanzadeh, B. (2016). Electrochemical and surface characterizations of *Morus alba pendula* leaves extract (MAPLE) as a green corrosion inhibitor for steel in 1M HCl. *Journal of the Taiwan Institute of Chemical Engineers*, 63, 436-52.

Joyce, S. C., Raja, A. S., Amalraj, A. S., Rajendran, S. (2022). Corrosion mitigation by an eco-friendly inhibitor *Beta vulgaris* (beetroot) extract on mild steel in simulated oil well water medium. *International Journal of Corrosion and Scale Inhibition*, 11, 1, 82-101.

Kalla, A., Benahmed, M., Djeddi, N. et al. (2016). Corrosion inhibition of carbon steel in 1 M H₂SO₄ solution by *Thapsia villosa* extracts. *International Journal of Industrial Chemistry*, 7(4), 419-429.

Kaya, F., Geçibesler, İ.H., Solmaz, R. (2018). Corrosion inhibition of mild steel in 1 M HCl solution by *Rheum Ribes L.* (ışgın) flower extracts. XVth International Corrosion Symposium, Hatay, Turkey, 2018, p. 287-95.

Kelly, R.G. (2003). *Electrochemical Techniques in Corrosion Science and Engineering* (p.13-15). P.E. U.S.A.: Marcel Dekker Inc.

Khaled, F. (2010). Corrosion control of copper in nitric acid solutions using some amino acids: A combined experimental and theoretical study. *Corrosion. Science*, 52, 3225-34.

Kosec, T., Milos, I., Pihlar, B. (2007). Benzotriazole as an inhibitor of brass corrosion in chloride solution. *Applied Surface Science*, 253, 8863-73.

Krishnaveni, K., Ravichandran, J. (2014). Influence of aqueous extract of leaves of *Morinda tinctoria* on copper corrosion in HCl medium. *Journal of Electroanalytical Chemistry*, 735, 24-31.

Kumar, S., Mishra, A., Pandey, A. K. (2013). Antioxidant mediated protective effect of *Parthenium hysterophorus* against oxidative damage using in vitro models. *BMC Complementary and Alternative Medicine*, 13(1), 1-9.

Kusumastuti, R., Pramana, R. I., Soedarsono, J. W. (2017). The use of morinda citrifolia as a green corrosion inhibitor for low carbon steel in 3.5% NaCl solution in AIP Conference Proceedings. *American Institute of Physics Inc.*, p. 020012.

Hossain, N., Chowdhury M. A., Rana, M., Hassan, M., Islam, S. (2022). Arjuna Leaves Extract as Green Corrosion Inhibitor for Mild Steel in HCl Solution. *Results in Engineering*, 14, 2590-1230.

Khadom, A. A., Ahmed, N., Abd, N., Ahmed, A., Kadhim, M. M., Ahmed, A. F. (2022) Combined influence of iodide ions and Xanthium Strumarium leaves extract as eco-friendly corrosion inhibitor for low-carbon steel in hydrochloric acid. *Current Research in Green and Sustainable Chemistry*, 5, 100278.

Kardaş, G., Solmaz, R. (2006). Electrochemical investigation of barbiturates as green corrosion inhibitors for mild steel protection. *Corrosion Reviews*, 24, 151-171.

Khayatkashani, M., Soltani, N., Tavakkoli, N., Nejatian, A., Ebrahimian, J., Mahdi, A. M., Salavati-Niasari, M. (2022). Insight into the corrosion inhibition of Biebersteinia multifida root extract for carbon steel in acidic medium. *Science of the Total Environment*, 836, 155527.

Li, Y., Chen, H., Tan, B., Xiang, B., Zhang, S., Luo, W., Zhang, Y., Zhang, J. (2021) Three piperazine compounds as corrosion inhibitors for copper in 0.5 M sulfuric acid medium. *Journal of the Taiwan Institute of Chemical Engineers*, 126, 231-43.

Liao, Q. Q., Yue, Z. W., Yang, D., Wang, Z. H., Li, Z. H., Ge, H. H., Li, Y.J. (2011). Self-assembled monolayer of ammonium pyrrolidine dithiocarbamate on copper detected using electrochemical methods, surface enhanced Raman scattering and quantum chemistry calculations. *Thin Solid Films*, 519, 6492-8.

Liao, Q. Q., Yue, Z. W., Yang, D., Wang, Z. H., Li, Z. H., Ge, H. H., Li, Y. J. (2011) Inhibition of copper corrosion in sodium chloride solution by the self-assembled monolayer of sodium diethyldithiocarbamate. *Corrosion. Science*, 53, 1999-2005.

Li, H., Qing, Z., Hui-Jing, L., Jin-Yi, W., Xin-Yue, W., Yan-Chao, W. (2022). Investigation of adsorption and corrosion inhibition property of Hyperoside as a novel corrosion inhibitor for Q235 steel in HCl medium. *Journal of Molecular Liquids*, 364, 120009.

Li, X., Deng, S., Fu, H (2012). Inhibition of the corrosion of steel in HCl, H₂SO₄ solutions by bamboo leaf extract. *Corrosion Science*, 62, 163-175.

Ma, H. Y., Yang, C., Chen, S. H., Jiao, Y.L., Huang, S. X., Li, D. G., Luo. J.L. (2003). Electrochemical investigation of dynamic interfacial processes at 1-octadecanethiol-modified copper electrodes in halide-containing solutions. *Electrochimica Acta*, 48, 4277-89.

Marsoul, A., Ijjaali, M., Elhajjaji, F., Taleb, M., Salim, R., Boukir, A., (2020). Phytochemical screening, total phenolic and flavonoid methanolic extract of pomegranate bark (*Punica granatum L*): evaluation of the inhibitory effect in acidic medium 1 M HCl. *Materials Today: Proceedings*, 27, 3193-3198.

Martinez, W., Torres, A., Hernandez, R., Mendoza, I Martinez, I. (2015). The inhibitive properties of nopal slime on the corrosion of steel in chloride-contaminated mortar. *Anti-Corrosion Methods and Materials*, 63, 65-71.

Marzorati,S., Verotta,L., Trasatti, S. P. (2019). Green Corrosion Inhibitors from NaturalSources and Biomass Wastes. *Molecules*, 24(1), 48.

Mattsson, E. (1996). *Basic Corrosion Technology for Scientists and Engineers*. (p. 15-66). London, UK : The Institute of Materials.

Moretti, G., Guidi, F., Fabris, F. (2013). Corrosion inhibition of the mild steel in 0.5 M HCl by 2-butyl-hexahydropyrrolo[1,2-b][1,2]oxazole. *Corrosion Science*, 76, 206-218.

Moradi, Z., Attar, M. M. (2014). An investigation on the inhibitory action of benzazole derivatives as a consequence of sulfur atom induction. *Applied Surface Science*, 317, 657-665.

Munzuroğlu, Ö., Karataş, F., Gür, N. (2000). Işgın (*Rheum ribes L.*) bitkisindeki A, E ve C vitaminleri ile selenyum düzeylerinin araştırılması. *Turkish Journal of Biology*, 24, 397-404.

Moradi, M., Duan, J., Du, X. (2013). Investigation of the effect of 4,5-dichloro-2-n-octyl-4-isothiazolin-3-one inhibition on the corrosion of carbon steel in *Bacillus sp.* inoculated artificial seawater. *Corrosion Science*, 69, 338-345.

Njoku, D.I., Ukage, I., Ikenna, O. B., Oguzie, E. E., Oguzie, K. L., Ibisi, N. (2016). Natural products for materials protection: Corrosion protection of aluminium in hydrochloric acid by *Kola nitida* extract. *Journal of Molecular Liquids*, 219, 417-424.

Nnamchi, P.S., Obayi, C.S. (2018). Characterization of Nanomaterials, Chapter 4 Electrochemical Characterization of Nanomaterials, In *Micro and Nano Technologies*. Woodhead Publishing, 103-127.

Noor, E. A. (2011). The impact of some factors on the inhibitory action of Radish seeds aqueous extract for mild steel corrosion in 1M H₂SO₄ solution. *Materials Chemistry and Physics*, 131(1–2), 160-169.

Nurudeen, A., Odewunmi, S. A., Umoren, Z. M., Gasem, S. A., Ganiyu, Q., L-Citrulline, M. (2015). An active corrosion inhibitor component of watermelon rind extract for mild steel in HCl medium. *Journal of the Taiwan Institute of Chemical Engineers*, 51, 177-185

N. Asadi, N., Ramezanzadeh, M., Bahlakeh, G., Ramezanzadeh, B. (2019). Utilizing Lemon Balm extract as an effective green corrosion inhibitor for mild steel in 1M HCl solution: A detailed experimental, molecular dynamics, Monte Carlo and quantum mechanics study. *Journal of the Taiwan Institute of Chemical Engineers*, 95, 252-272.

Oktay, M., Yıldırım, A., Bilaloğlu, B., Gülçin, V. (2007). Activity of Different Parts of Isgin (*Rheum ribes* L.). *Asian Journal of Chemistry*, 19-4, 3047-3055.

Oloruntoba, D.T., Popoola, A. P. I., Lawal, O. O. et al. (2017). Acid-acid function of *Eichhornia crassipes* roots as inhibitor for mild steel in 0.5 M H₂SO₄ solution. *Protection of Metals and Physical Chemistry of Surfaces*, 53, 150-158.

Oluwasayo, D., Olakolegan, S. S., Owoeye, E. A., Oladimeji, O. Sanya, T. (2020). Green synthesis of *Terminalia Glaucescens* Planch (Udi plant roots) extracts as green inhibitor for aluminum (6063) alloy in acidic and marine environment. *Journal of King Saud University*, 32, 1278-1285.

Ogunmodede, O. T., Olaseinde, O. A., Adewole, E., Ebitimitula, O. (2022). Duplex Stainless Steel 2101 corrosion inhibition in an acidic environment using *Solanum tuberosum* leaves and roots extract. *Egyptian Journal of Chemistry*, 8, 567-574.

Özbek, H., Ceylan, E., Kara, Ö. F., Koyuncu, M. (2002). *Rheum ribes* (Uskun) Kökü Ekstresinin Sağlıklı ve Diyabetli Farelerdeki Hipoglisemik Etkisi 14. Bitkisel İlaç Hammaddeleri Toplantısı, Bildiriler, 29-31 Mayıs, Eskisehir, 2002.

Öztürk, M., Aydoğmuş Öztürk, F., Duru, M., Topcu, G. (2007). Antioxidant activity of stem and root extracts of Rhubarb (*Rheum ribes*): An edible medicinal plant. *Food Chemistry*, 103(2), 623-630.

Pan, Y.C., Wen, Y., Xue, L. Y., Guo, X. Y., Yang, H. F. (2012). Adsorption behavior of methimazole monolayers on a copper surface and its corrosion inhibition. *The Journal of Physical Chemistry*, 116, 3532-38.

Palomar-Pardavé, M., Romero-Romo, M., Herrera-Hernández, H., Abreu-Quijano, M. A., Likhanova, V. N., Uruchurtu, J. Juárez-García, J. M. (2012). Influence of the alkyl chain length of 2 amino 5 alkyl 1,3,4 thiadiazole compounds on the corrosion inhibition of steel immersed in sulfuric acid solutions. *Corrosion Science*, 54, 231-243.

Papavinasam, S. (2011). *Uhlig's Corrosion Handbook*. (p.1169-1178) ., New Jersey, USA: John Wiley & Sons, Inc.

Pérez-Miranda, S., Zamudio-Rivera, L.S., Cisneros-Dévora, R., George-Téllez, R., Fernández, F.J. (2021). Theoretical insight and experimental elucidation of desferrioxamine B from *Bacillus* sp. AS7 as a green corrosion inhibitor. *Corrosion Engineering, Science and Technology*, 56:1, 93-101.

Pham, T. H., Lee, W. H, Jung-Gu, K. (2022). Chrysanthemum coronarium leaves extract as an eco-friendly corrosion inhibitor for aluminum anode in aluminum-air battery. *Journal of Molecular Liquids*, 347, 118269.

Popova, A., Sokolova, E., Raicheva, S., Christov, M. (2003). AC and DC study of the temperature effect on mild steel corrosion in acidic media in the presence of benzimidazole derivatives. *Corrosion Science*, 45, 33-58.

Qian, B., Wang, J., Zheng, M., Hou, B. (2013). Synergistic effect of polyaspartic acid and iodide ion on corrosion inhibition of mild steel in H₂SO₄. *Corrosion Science*, 75, 84-192.

Qiang, Y., Fu, S., Zhang, S., Chen, S. Zou, X. (2018). Designing and fabricating of single and double alkyl-chain indazole derivatives self-assembled monolayer for corrosion inhibition of copper. *Corrosion Science*, 140, 111-21.

Oulabbas, A., Abderrahmane, S., Salcı, A., Geçibesler, İ.H., Solmaz, R. (2022). Adsorption and Corrosion Inhibition of Cactus cladode Extract and Effect of KI Addition on Mild Steel in 0.5 M H₂SO₄. *Chemistry Select*, 7, e202200212 (1 of 12).

Quraishi, M.A., Singh, A., Singh, V. K., Yadav, D. K. Singh, A. K. (2010). Green approach to corrosion inhibition of mild steel in hydrochloric acid and sulphuric acid solutions by the extract of *Murraya koenigii* leaves. *Materials Chemistry and Physics*, 122(1), 114-122.

Rahal, C., Masmoudi, M., Abdelhedi, R., Sabot, R., Jeannin, M, Bouaziz, M, Refait, P. (2016). Olive leaves extract as natural corrosion inhibitor for pure copper in 0.5 M NaCl solution: A study by voltammetry around OCP. *Journal of Electroanalytical Chemistry*, 769, 53-61.

Raghavendra, N. (2019). Areca plant extracts as a green corrosion inhibitor of carbon steel metal in 3 M hydrochloric acid: gasometric, colorimetry and atomic absorption spectroscopy views. *Journal of Molecular and Engineering Materials*, 6, 1850004.

Ragasa, C., Bacar, J. Querido, M., Tan, M., Oyong, G., Brkljača, R., Urban, S. (2017). Chemical Constituents of *Rheum ribes* L. *International Journal of Pharmacognosy and Phytochemical Research*, 9, 10, 25258.

Raghavendra N. (2019). Latest exploration on Natural Corrosion Inhibitors for Industrial Important Metals in Hostile Fluid Environments: A comprehensive overview. *Journal of Bio- and Tribo-Corrosion*, 5, 54.

Rajkumar G., Sethuraman, M. G. (2016). A study of copper corrosion inhibition by selfassembled films of 3-mercapto-1H-1,2,4-triazole. *Research on Chemical Intermediates*, 42, 1809-21.

- Revie, R. W. (2008). *Corrosion and Corrosion Control*. (p. 21-649). Hoboken, New Jersey, U.S.A: John Wiley & Sons, Inc.
- Salleh, S. Z., Anasyida, A. S., Mohamad, N. M., Mardawani, M., Sarizam, M., Sharizal, A. S., Arlina, A., Pao, T. T. (2021). Plant extracts as green corrosion inhibitor for ferrous metal alloys: A review. *Journal of Cleaner Production*, 304, 127030.
- Saxena, A., Prasad, D., Haldhar, R., Singh, G., Kumar, A. (2018). Use of *Sida cordifolia* extract as green corrosion inhibitor for mild steel in 0.5 M H₂SO₄. *Journal of Environmental Chemical Engineering*, 6(1), 694-700.
- Saxena, A., Prasad, D., Haldhar, R. (2018). Investigation of corrosion inhibition effect and adsorption activities of *Cuscuta reflexa* extract for mild steel in 0.5 M H₂SO₄. *Bioelectrochemistry*, 124, 156-164.
- Sedik, A., Lerari, D., Salci, A., Athmani, S., Bachari, K., Gecibesler, İH., Solmaz, R. (2020). Dardagan Fruit extract as eco-friendly corrosion inhibitor for mild steel in 1 M HCl: Electrochemical and surface morphological studies. *Journal of the Taiwan Institute of Chemical Engineers*, 107, 189-200.
- Sethuraman, M. G., Aishwarya, V., Kamal, C., Jebakumar, T., Edison, I. (2017). Studies on Ervatanine. The anticorrosive phytoconstituent of *Ervatamia coronaria*. *Arabian Journal of Chemistry*, 10, S522-S530.
- Sethuramasamy, P., Baluchamy, T., Shen-Ming, C., Durvas, S. B., Tse-Wei, C. (2021) Sustainable approach to the antifouling and corrosion inhibitive properties of Exopolysaccharide producing *Rhizobium leguminosarum* (Legume Root Nodule Associated Bacteria) on mild steel at low pH. *International Journal of Electrochemical Science*, 16, 210373.
- Shahmoradi, A. R., Ranjbarghanei, M., Javidparvar, A. A., Guo, L. Berdimurodov, E., Ramezanzadeh, B. (2021). Theoretical and surface/electrochemical investigations of walnut fruit green husk extract as effective inhibitor for mild-steel corrosion in 1 M HCl electrolyte. *Journal of Molecular Liquids*, 338, 116550.
- Solmaz, R. (2014a). Investigation of corrosion inhibition mechanism and stability of Vitamin B1 on mild steel in 0.5 M HCl solution. *Corrosion Science*, 81, 75-84.
- Solmaz, R. (2014b). Investigation of adsorption and corrosion inhibition of mild steel in hydrochloric acid solution by 5-(4-Dimethylaminobenzylidene) rhodanine. *Corrosion Science*, 79, 169-176.

Solmaz, R., Kardas, G., Culha, M., Yazıcı, B., Erbil, M. (2008). Investigation of adsorption and inhibitive effect of 2-mercaptothiazoline on corrosion of mild steel in hydrochloric acid media, *Electrochimica Acta*, 53, 5941-5952.

Singh, A. K., Shukla, S. K., Singh, M., Quraishi, M. A. (2011). Inhibitive effect of ceftazidime on corrosion of mild steel in hydrochloric acid solution. *Materials Chemistry and Physics*, 129 (1–2), 68-76.

Singh, A., Lin, Y., Ebenso, E. E., Liu, W., Pan, J., Huang, B. (2015). Gingko biloba fruit extract as an eco-friendly corrosion inhibitor for J55 steel in CO₂ saturated 3.5 NaCl solution. *Journal of Industrial and Engineering Chemistry*, 24, 219-228.

Stern, M. (1958). A Method For Determining Corrosion Rates From Linear Polarization Data. *Corrosion*, 14, 60-64.

Stern, M. (1957). Electrochemical Polarization II. Ferrous-Ferric Electrode Kinetics on Stainless Steel. *Journal of The Electrochemical Society*, 104, 559.

Shabani-Nooshabadi, M., Hoseiny, F. S., Jafari, Y. (2015). Green approach to corrosion inhibition of copper by the extract of Calligonum comosum in strong acidic medium. *Metallurgical and Materials Transactions A*, 46, 293-9.

Shabani-Nooshabadi, M., Hoseiny, F. S., Jafari, Y. (2014). Corrosion inhibition of copper by Ephedera sacocarpa plant extract as green corrosion inhibitor in strong acidic medium. *Analytical and Bioanalytical Electro Chemistry*, 6, 341-54.

Shan, W., Tian, Z., Huikai, C., Bokai, L., Xingpeng, G. (2022). Kapok leaves extract and synergistic iodide as novel effective corrosion inhibitors for Q235 carbon steel in H₂SO₄ medium. *Industrial Crops & Products*, 178, 114649.

Salcı, A., Yuksel, H., Solmaz, R. (2022). Experimental studies on the corrosion inhibition performance of 2-(2-aminophenyl)benzimidazole for mild steel protection in 1 M HCl solution. *Journal of the Taiwan Institute of Chemical Engineers*, 134, 104349.

Sanaei, Z., Shahrabi, T., Ramezanzadeh, B., (2017). Synthesis and characterization of an effective green corrosion inhibitive hybrid pigment based on Zinc acetate-Cichorium intybus L leaves extract (ZnA-CIL.L): Electrochemical investigations on the synergistic corrosion inhibition of mild steel in aqueous chloride solutions. *Dyes and Pigments*, 139, 218-32.

Sığırcık, G., Tüken, T., Erbil, M.(2016) Assessment of the inhibition efficiency of 3,4-diaminobenzonitrile against the corrosion of steel. *Corrosion Science*, 102, 437-445.

Tang, Y., Zhang, F., Huc, S., Cao, Z., Wu, Z., Jing, W. (2013). Novel benzimidazole derivatives as corrosion inhibitors of mild steel in the acidic media. Part I: Gravimetric, electrochemical, SEM and XPS studies. *Corrosion Science*, 74, 271-282.

Tourabi, M., Nohair, K., Traisnel, M., Jama, C., Bentiss, F. (2013). Electrochemical and XPS studies of the corrosion inhibition of carbon steel in hydrochloric acid pickling solutions by 3,5-bis(2-thienylmethyl)-4-amino-1,2,4-triazole. *Corrosion Science*, 75, 123-133.

The World Corrosion Organization. <https://corrosion.org>, 2022 (accessed on September 8, 2022).

Tosun, F., Akyüz Kizilay, Ç. (2003). Anthraquinones and flavonoids from *Rheum ribes*. *Ankara Üniversitesi Eczacılık Fakültesi Dergisi*, 32(1), 31–35.

Topics by Science, Sample records for potentiodynamic polarization curves. <https://www.science.gov/topicpages/p/potentiodynamic+polarization+curves.html> (accessed on September 8, 2022).

Tourabi, M., Nohair, K., Traisnel, M., Jama, C., Bentiss, F. (2013). Electrochemical and XPS studies of the corrosion inhibition of carbon steel in hydrochloric acid pickling solutions by 3,5-bis(2-thienylmethyl)-4-amino-1,2,4-triazole. *Corrosion Science*, 75, 123-133.

Verma, C., Quraishi, M. A., Ebenso, E. E. (2020). Quinoline and its derivatives as corrosion inhibitors: A review. *Surfaces and Interfaces*, 21, 100634.

Valdez-Salas, B., Vazquez-Delgado, R., Salvador-Carlos, J., Beltran-Partida, E., Salinas-Martinez, R., Cheng, N., Curiel, Alvarez, M. (2021) Azadirachta indica Leaf Extract as Green Corrosion Inhibitor for Reinforced Concrete Structures: Corrosion Effectiveness against Commercial Corrosion Inhibitors and Concrete Integrity. *Materials*, 14(12), 3326.

Vinicius, M., Silva, L. D., Policarpi, D. B. E., Spinelli, A. (2021). Syzygium cumini leaf extract as an eco-friendly corrosion inhibitor for carbon steel in acidic medium. *Journal of the Taiwan Institute of Chemical Engineers*, 129, 342-349.

Vracar, Lj., Drazic, D. M. (2002). Adsorption and corrosion inhibitive properties of some organic molecules on iron electrode in sulfuric acid. *Corrosion Science*, 44, 1669–1680.

Wan S, Zhang T, Chen H, Liao B, Guo X. (2022). Kapok leaves extract and synergistic iodide as novel effective corrosion inhibitors for Q235 carbon steel in H₂SO₄ medium. *Industrial Crops and Products*, 178, 114649.

Worldwide Corrosion Cost. <https://www.dynagard.info> (accessed on March 21, 2022).

Xianghong, L., Shuduan, D., Guanben, D., Xiaoguang, X. (2020). Synergistic inhibition effect of walnut green husk extract and sodium lignosulfonate on the corrosion of cold rolled steel in phosphoric acid solution. *Journal of the Taiwan Institute of Chemical Engineers*, 114, 263-283.

Xu Q, Ge K, Zhang S, Tan B. (2021). Understanding the adsorption and inhibitive properties of Nitrogen-Doped Carbon Dots for copper in 0.5 M H₂SO₄ solution. *Journal of the Taiwan Institute of Chemical Engineers*, 125, 23-34.

Yıldız, R., Dogru Mert, B. (2019). Theoretical and experimental investigations on corrosion control of mild steel in hydrochloric acid solution by 4-aminothiophenol. *Anti-Corrosion Methods and Materials*, 66-1, 127-137.

Zeng, W., Lia, W., Tan, B., Liu, J., Chen, J. (2021). A research combined theory with an experiment of 2-amino-6-(methylsulfonyl) benzothiazole as an excellent corrosion inhibitor for copper in an H₂SO₄ medium. *Journal of the Taiwan Institute of Chemical Engineers*, 128, 417-29.

Žbulj, K., Hrnčević, L., Bilić, G., Simon, K. (2022). Dandelion-Root Extract as Green Corrosion Inhibitor for Carbon Steel in CO₂-Saturated Brine Solution. *Energies*, 15, 3074.

Zhi, F., Jiang, L., Jin, M., Chen, L., Gu, Y. (2020) Inhibition effect and mechanism of polyacrylamide for steel corrosion in simulated concrete pore solution. *Construction Building Materyal*, 259, 120425.

Zhnag, C., Duan, H., Zhao, J. (2016). Synergistic inhibition effect of imidazoline derivatives and l-cysteine on carbon steel corrosion in a CO₂ saturated brine solution. *Corrosion Science*, 112, 160-169.

ÖZGEÇMİŞ

Kişisel Bilgiler	
Adı Soyadı	: Fatma KAYA
Doğum tarihi	: 03/01/1972
Doğum Yeri	: Bingöl
Uyruğu	: Turkish, British
Adres	: Recep Tayyip Erdoğan Mahallesi Üniversite Caddesi No: 39 Bingöl/ Merkez
Tel	: 05070541670
E-mail	: fzehrakaya@gmail.com
Eğitim	
Lise	: Bingöl Anadolu Kız Öğretmen Lisesi
Lisans	: 1.Fırat Üniversitesi Fen Edebiyat Fakültesi ➤ Kimya Bölümü 2.Bingöl Üniversitesi Fen Edebiyat Fakültesi ➤ İngiliz Dili ve Edebiyatı
Yüksek lisans	: 1.Fırat Üniversitesi Fen Bilimleri Enstitüsü ➤ Anorganik Kimya Ana Bilim Dalı 2.Brunel University West London ➤ Secondary Science Education (PGCE , QTS)
Doktora	: Bingöl Üniversitesi Fen Bilimleri Enstitüsü ➤ Fizikokimya Ana Bilim Dalı
Yabancı Dil Bilgisi	
English	: C2 Proficiency
German	: Beginner
Arabic	: Intermediate
Tezden Üretilmiş Yayınlar	
1. TÜRK DOĞA VE FEN DERGİSİ	
➤ Rheum Ribes (Işgın) Özütlerinin Asidik Ortamda Bakırın Korunması için Kullanılması	